Optimisation of Sliding Mode Controllers for Marine Applications: A study of methods and implementation issues

Euan William M^{c}Gookin

Department of Electronics and Electrical Engineering
University of Glasgow

A thesis submitted for the degree of
Doctor of Philosophy
to the University of Glasgow.

September 1997

Abstract

The optimisation of Sliding Mode controllers for marine vehicle guidance is presented in this thesis. This study is concerned with two optimisation methods which are based on natural processes. The first is Simulated Annealing which involves processes analogous to those involved in the cooling process in metallurgy. The second involves Genetic Algorithms which are based on the evolutionary process of species and genetics. These methods are evaluated through studying their application to the optimisation of controller parameters for particular marine vessels. Their performance is measured through simulation studies during the optimisation process. Existing literature in the fields of the two optimisation techniques, Sliding Mode control and marine control is surveyed. The theory of Simulated Annealing is presented in terms of the optimisation process and its convergence properties through Markov Chain analysis. A novel variation of this method, Segmented Simulated Annealing, is also outlined and evaluated in terms of its improved convergence properties. The theory of Genetic Algorithms is presented in terms of its process and convergence properties using Markov Chains and the Schema Theorem. The derivation of a decoupled Sliding Mode control theory is described and its well known stability robust properties are ensured by the choice of an appropriate set of design criteria. The elimination of the chattering phenomenon is achieved by soft switching which ensures performance robustness. The application of Sliding Mode controllers for governing the motion of three marine vehicles and their subsequent optimisation is presented. The first is the simulation of a linear mathematical representation of a military submarine. The second is the simulation of a non-linear mathematical representation of a super tanker. The third is an actual scale model of a supply ship which enables evaluation of the optimised controllers in a laboratory water basin facility. These applications allow aspects of the optimisation of Sliding Mode controllers through studies of simulation and post-optimisation implementation to a real system. Other aspects concerning optimisation are also addressed such as the prediction of how easy a problem is to optimise prior to optimisation. The conclusions of this work present the advantages and disadvantages of using these optimisation methods for controller optimisation. The Genetic Algorithm approach is shown in a favourable light. Suggestions for further work are also presented.

Acknowledgements

My sincere gratitude goes to my supervisors during this study. I would like to thank Prof. David Murray-Smith for his insight and guidance which has been invaluable in fulfilling this work and shaping this thesis. I would also like to thank Dr Yun Li for his expert knowledge of optimisation methods.

On a more personal note my deepest feelings of thanks goes to my fiancee, Frances and my mum and dad for their love and support during my studies. Also I'd like to thank my sister Adele for her help in obtaining greater insight into some aspects of this work. Particularly in providing contact with the Ministry of Defence (MOD), the Defence Evaluation and Research Agency (DERA) and the Royal Navy.

My deepest thanks goes to Prof. T.I. Fossen for his collaboration and for the use of the GNC laboratory. His knowledge and expertise has helped me extend my abilities in the marine control research field.

I would also like to thank Mr P.R. Curtis of DERA and Mr J. Lambert of the MOD for their information concerning submarine operations. In addition I would like to thank Commander Leatherby and the crew of HMS Sceptre for the visit to their Submarine. This allowed invaluable discussions regarding the practical operations of such a vessel.

In addition I would like to thank the staff and students of the Dept. of Electronics and Electrical Engineering and the Centre of Systems and Control for their help and advice. Particularly Dr Gary Gray for his help during the writing of this thesis.

In respect to funding I would like to thank the following organisations. Firstly the EPSRC for a studentship to carry out this research. Also the IEE Hudswell Bequest, the SIET and the British Research Council for travel grants so that collaboration with Norway could take place. Finally UKACC for funding part of my attendance at IFAC'96 in San Francisco.

Table of Contents

List of Figures

Chapter 3: Simulated Annealing

Chapter 4: Genetic Algorithms

Chapter 5: Decoupled Sliding Mode Control Theory

Chapter 6: Submarine Application

Chapter 7: Super Tanker Application

Chapter 8: Supply Ship Application

List of Tables

Chapter 1:
Introduction

1.1 Introduction

In recent decades the size and speed of all marine vehicles has increased, particularly in the case of vessels that carry cargo (e.g. oil and freight), many of which are now in excess of 500m in length and with a displacement of the order of 200,000 tonnes. The size of such vessels presents problems when manoeuvring them safely. Manoeuvring high performance vessels (e.g. submarines) is also a problem since the dynamic responses of this type of vessel move quickly and need to be accurately regulated. It is therefore apparent that there is a need for adequate regulation of the way in which these vessels move. Hence any system which will assist the helmsman to carry out this task more safely would be beneficial. A suitable way of achieving this is through the application of *control theory* [Franklin et al (1991), Slotine and Li (1991)].

The purpose of control theory is to formulate design strategies that allow a better understanding of systems and how to govern their behaviour. Generally speaking, it achieves this by designing a control system which is comprised of a governing mechanism, called a *controller*, and the process or system being controlled (e.g. a ship). These two elements are interconnected by actuators which directly influence the dynamic behaviour of the process by applying the control effort supplied by the controller (e.g. the rudder of a ship changes its heading).

The control effort is provided by the controller through the main building block of automatic control i.e. *feedback*. This concept is used to monitor the actual dynamic response of the system by feeding back measurements of the variables or states which define this behaviour. These actual responses are compared with the desired responses which define the required behaviour of the process. The difference between the two sets of responses is called the error and represents the divergence of the process from its required operating behaviour. This error is used by the controller to produce sufficient control effort that will enable the actual states of the process to follow the desired states and thus make the process behave in the way required by its operator. The relationship between the error and the control effort is called the *control law* [Franklin et al (1991)].

In this investigation a particular control law called *Sliding Mode* (SM) control is used [Utkin (1992), Slotine and Li (1991)]. This involves non-linear control theory due to the discontinuous operation of the controller. The way in which a SM controller works is through the *sliding surface*, which is a function of the error difference between the actual and desired states of the process system. The controller drives this error to zero by providing a control input which reduces the sliding surface to zero. Hence the actual states track the desired responses as required. This is achieved through the two components of this controller which are the *equivalent* term and the *switching* term. The equivalent term provides nominal control action and the switching term provides additional discontinuous signals to drive the surface to zero. This switching action allows the controller to be robust to changes in the process environment and provides potential advantages over more conventional linear forms of controller.

However the sliding mode approach does have potential disadvantages in terms of design. Each controller, independent of which control law is used, has to be designed in terms of the specific process system that it is being applied to, in this case marine vessels. As a result the key design parameters which define how a controller works have to be selected or tuned so that it operates in the way that is required of it. This design procedure can be a tedious and time consuming activity which varies with the level of expertise of the designer. Obviously if the designer is inexperienced with the controller type or the system, the time to obtain a satisfactory solution for the controller parameters will be longer than for someone with more experience. Thus there is an apparent need for automated methods for finding appropriate controller parameters.

Techniques for obtaining parameter values are called parameter *optimisation methods* and these explore possible permutations of parameter solutions by various different means. The surface defined by these permutations and how well they perform is called the *search space*. This space normally contains one or more acceptable solutions to the problem (these are called the *optimal solutions*). These parameter optimisation methods have been applied to numerous engineering applications (e.g. pattern recognition, signal processing) and interest in their use for controller parameter optimisation has grown in recent years [Li et al (1995), Ng et al (1995), Li et al (1996)]. The foundation of these optimisation methods lie in hill-climbing techniques which explore the search space to find an optimal solution through incremental improvements in the solution performance.

Other methods involve gradient searches where the search follows a localised gradient improvement in the solution performance. Such methods have shortcomings in that they frequently fail to find the best solution possible (called the *global* optimal solution).

Recently more advanced heuristics have been developed that are able to search for a global optimal solution in the search space. One group of methods that have become widely used are based on natural processes. Two such methods are considered in this work and are called *Simulated Annealing* (SA) and *Genetic Algorithms* (GAs). Both these methods are known for their unique methodology and improved search ability.

Simulated Annealing is a hill-climbing technique which is based on the cooling process in metallurgy [Metropolis et al (1953), Kirkpatrick et al (1983), Kirkpatrick (1984)]. As with conventional hill-climbing, SA changes the problem parameter values and accepts incrementally beneficial changes to the solution performance. However it varies the size of the parameter variation in terms of a temperature index which reduces as the search proceeds. One important feature of this algorithm is it has the ability to accept poorer solutions and thus enable the search to avoid locally optimal solutions. This helps in the location of the best possible global solution.

The Genetic Algorithm (GA) method is based on the natural selection process of species which is outlined in the Darwinian theory of *survival of the fittest* [Abercrombie et al (1985), Holland (1975), Goldberg (1989)]. This theory stated that a species evolves through its best genus in terms of adapting to its environment. This optimisation method applies evolutionary theory to parameter optimisation by establishing a population of parameter solutions in the search space then keeping the solutions which give the best performance and replacing the rest with other solutions. This allows the best to improve until a globally optimal solution is obtained.

Both these methods have the potential for optimising controller parameters. Their application in the marine controller field is investigated in this thesis. The behaviour of these methods is observed through the optimisation of sliding mode controllers for three different marine vehicles. The first application is the simulation of a submarine where controllers for the vehicles depth and heading are investigated. The second simulated vessel is an oil tanker and the motion that is controlled is the heading which in turn

affects the course. The third is a scale model of a supply ship used in oil platform support. Although these applications are marine specific they have allowed a comparison study of the SA and GA methods to be carried out which provides conclusions that can be applied to controller optimisation in general. This study will show which method(s) provides the best optimisation performance and illustrate the usefulness of such methods as design tools. Also it will provide a basis for conclusions regarding the effectiveness of Sliding Mode controllers for marine applications.

1.2 Outline of Thesis

The study of controller optimisation methods is carried out in this thesis as outlined below.

Chapter 2 discusses the existing research in the areas covered in this work. Firstly it provides an overview of parameter optimisation methods, particular the foundations of SA and GA methodology and their application to controller optimisation. The second field that is covered in this chapter is non-linear *Sliding Mode Control* which is the method used in this investigation. Finally the current progress in marine controller technology will be briefly discussed so that the apparent need in this area can be clearly seen.

In Chapter 3 the theory behind the SA method is developed from the metal annealing process upon which it is based. The ability of this method to obtain an optimal solution is called its *convergence* which is analysed by the well established *Markov Chain* (MC) theory [Laarhoven and Aarts (1987), Laarhoven (1988)]. This will illustrate that the basic SA method may not be able to obtain a desired solution from a random start. Therefore a novel variation on this method called *Segmented Simulated Annealing* (SSA) [Atkinson (1992)] is presented which is shown through MC analysis to have a better probability of converging than the basic SA method.

In Chapter 4 the theory of GAs is presented from its analogy to both the natural selection process of species and genetics. The mechanisms that comprise this algorithm are discussed and specific operating values are presented. The convergence ability of this method is described in terms of MCs and the *Schema Theorem* which illustrates

how GAs operate [Holland (1975), Goldberg (1989)]. This chapter shows theoretically that this method has a high probability of obtaining a globally optimal final solution for any problem it is applied to.

Chapter 5 provides the Sliding Mode control theory that is used in this study. It presents a decoupling process to allow systems with multiple inputs to be controlled by a separate controller for each input. This provides a controller structure that is then used in each of the marine vehicle applications studied in this thesis. The performance robustness of this method to model uncertainties and external influences is proven in this chapter. Finally the problem of highly oscillating controller signals (called *chattering*) is discussed and the established method of *soft switching* is presented as a solution to this problem [Burton and Zinober (1988), Slotine and Li (1991), Healey and Marco (1992), Healey and Lienard (1993), M^{c}Gookin (1993), Fossen (1994)].

The first of the marine vehicle applications is presented in Chapter 6. This is a depth and heading control problem for a submarine [M^{c}Gookin (1993), Dumlu and Istefanopulos (1995), Liceaga-Castro and van der Molen (1995(a)(b))]. The mathematical representation of this vessel is a linear model which is obtained from the operation of a generic submarine about a single operating condition. This particular model is used for three reasons: firstly to observe how the sliding mode controllers operate when applied to a linear system; secondly to see if any interaction between the depth and heading dynamics will degrade the performance of the controllers; and thirdly is to see how the three optimisation techniques operate when they are used to optimise controllers for such a linear system.

Chapter 7 illustrates the oil tanker case observed in this study. The tanker is represented by a non-linear model which describes the dynamic interaction of the vessel's motions and the depth of the water in which the vessel is operating. This is obviously a more complex model than the submarine and is more of a challenge for the controller and the optimisation strategies. In this case two different types of manoeuvres are used in the simulation and optimisation process. The first is called *course changing* where the heading is altered by commands form the helmsman (similar to the submarine heading case). The second is referred to as *course keeping* which uses the commands from an

autopilot to alter the heading of the vessel. Each has a Sliding Mode controller applied and the associated parameters are optimised using the three optimisation methods.

Chapter 8 presents the final marine vehicle that is investigated in this study which is an actual scale model of a supply ship. This model is used as an experimentation vessel in the Guidance Navigation and Control (GNC) laboratory at the Norwegian University of Science and Technology. These laboratory facilities allow controllers to be applied to an actual vessel in a realistic environment. Thus a physical response of the vessel to a controller can be obtained without the expense of actual sea trials. In this stage of the investigation a non-linear mathematical representation of the scale model is used to optimise a course or heading changing controller through simulation. The performance of the resulting optimised controllers is evaluated through further simulation studies and application to the real vessel in the GNC laboratory. This evaluation process provides crucial information on implementing optimised controllers directly from simulation. It also provides additional insight into the optimisation processes through application to a vessel with dissimilar dynamic responses compared to the previous two vessels.

Chapter 9 provides additional discussion about other aspects of the optimisation methods considered. It also provides a hypothesis for estimating the ease of optimising a problem from the dynamics of the system being considered.

Finally the thesis ends with chapter 10 which presents the conclusions drawn from this work and suggests additional work which could be used to further develop key aspects of this research.

1.3 Specific Originality

In general the specific original contributions of this work are the comparison and application studies of SA and GA methods to the optimisation of non-linear SM controller parameters. In particular the optimisation of the SM controllers outlined in Chapter 5. Also the application of these methods to the control of the marine vehicles in Chapters 6, 7 and 8 is particularly original. In the optimisation field itself, the study of the Segmented Simulated Annealing in Chapter 3 for this type of problem has never been carried out and is therefore highly original.

Chapter 2:

Background Literature Survey

2.1 Introduction

The research investigated in this thesis stems from three rapidly growing areas i.e. parameter optimisation, control theory and marine control applications. These fields cover many different areas and only specific aspects are addressed in this work.

This chapter presents a survey of relevant research in the following way. The first section (2.2) is concerned with the Simulated Annealing and Genetic Algorithm optimisation techniques. It illustrates the key points in the development of these techniques and their application to controller parameter optimisation. Section 2.3 presents some of the key literature in the field of Sliding Mode control theory and its application. Finally, in Section 2.4 a brief survey of the modelling and control of marine vessels is presented.

2.2 Optimisation Methods

Although many parameter optimisation methods are available only two particular techniques are studied here. These are methods which emulate natural processes in order to provide parameter values for problems. They have been chosen because they are known to perform well in complex problems in which traditional methods can present difficulties. The two particular methods considered here are Simulated Annealing (SA) and Genetic Algorithms (GAs). The SA method is considered to be the most advanced search technique based on conventional hill-climbing methods. GAs are evolutionary methods which are quite unique in terms of how they optimise parameters. Both these methods will provide a good comparison for these different heuristics

2.2.1 Simulated Annealing

The Simulated Annealing methodology is based on the algorithm defined by Metropolis et al (1959). That paper presents a variation on conventional hill-climbing techniques which is based on the energy contained within metal particles in the presence of

increased temperature. The method differs from conventional techniques in two ways. Firstly it is able to vary the size of the parameter perturbations as the search proceeds and thus is able to fine-tune the values as the search reaches its final solution. The second aspect is a probabilistic acceptance mechanism which allows poorer solutions to be accepted. This allows the search to come out of areas of locally optimum solutions. This is the major difference and advantage of this approach over basic hill-climbing heuristics.

Although proposed in 1959 this method is numerically intensive in terms of calculations and further development did not occur until the increase in processor power in the 1980s. This led to the next stage in SA history which is the work by Kirkpatrick et al (1983). In that 1983 paper the authors formally present the mechanism of SA and report numerous optimisation studies investigated using this method. The most noted of these is their solution for the standard optimisation benchmark, the 'travelling salesman problem'. This presents the problem of minimising the distance travelled by a salesman during visits to a number of prospective customers. The solution to this problem and the other case studied in that paper show the benefits of using this optimisation method. A further study by Kirkpatrick (1984) provides more quantitative evidence of the successful application of the SA method.

The further development of the theory and applications of this method are discussed in Laarhoven and Aarts (1987) and Laarhoven (1988). In these books the convergence theory of SA is developed in terms of *Markov Chain* analysis which lends itself well to such a stochastic process. The conclusion of these works is that the SA method converges to an optimal solution if an infinite chain is used. This is logical since an infinite chain will produce an exhaustive search of the problem search space. However this is also impractical as it requires an infinite amount of time to execute such a search. Therefore a finite search would limit the effectiveness of this method in terms of the range of values it can investigate.

Improvements in the convergence ability of this method have been reported. In Szu and Hartley (1987) the use of a Cauchey probability distribution to extend the perturbation range is suggested. This is supposed to help the resulting Markov chain to converge to an optimal solution.

Despite these reported drawbacks further papers describing successful application of the SA method have been presented in numerous fields. Bohachevsky et al (1986) illustrate the use of an SA to optimise functions. The work by Courat et al (1995) presents a novel approach to optimising the position of circuit components with respect to space on a printed circuit board. Successful application to signal processing problems are addressed in Sharman (1988) and Sharman and Esparcia-Alcazar (1993).

In the context of control, there has only been limited application of this method. Recently Whidborne and Postlethwaite (1996) have discussed the application of SA to the optimisation of weighting functions for H_∞ controllers. Also much success has been reported by M^{c}Gookin et al (1996(a)) in the application of the segmentation process for this method, as first presented by Atkinson (1992). This variation is applied to the optimisation of Sliding Mode controller parameters for submarine control. The limited literature on this method for control problems indicates the need for an investigation into this area.

2.2.2 Genetic Algorithm

The basis for Genetic Algorithms (GAs) is the Darwinian theory of *survival of the fittest* [Abercrombie et al (1985)]. This process of evolution inspired techniques which evolve parameters in a similar manner and GAs are one such method which also uses ideas from genetic reproduction theory to obtain solutions. The underlying principles of this method were developed by Holland in the 1960s and as a consequence a mathematical framework is formalised in his book [Holland (1975)].

From this start the algorithm received limited publicity because of its computational complexity. Use of GAs increased with the improvement in processor speed and availability in the late 1970s.

In the mid 1980s the investigation into this algorithm and its applications intensified. One of the most noted developments in the literature of this time is Grefenstette (1986) who provided a thorough study of the operational parameters of this method. This study illustrates the effect of varying these parameters on the convergence properties of the optimisation. It concludes that a GA with a rank based selection scheme out performs a

'simple' GA in terms of convergence. This is supported by Brooks et al (1996) where the comparison is extended to other optimisation methods (e.g. Taboo Searches).

The final key stage in the history of this method is the book by Goldberg (1989) which is felt to be instrumental in the recent increase in popularity of this method. This text provides discussion on GA theory and its application (e.g. the 'travelling salesman' problem). It also extends the *Schema Theorem* set out in Holland (1975) which provides a mathematical basis for the proof of convergence of this method. This book boosted the already growing research into this technique.

The popularity of this method is further attested by the existence of numerous GA conferences. These are the series of International Conferences on Genetic Algorithms in the 1980s and more recently the IEE Genetic Algorithms in Engineering Systems: Innovations and Applications (GALESIA) conferences in 1995 and 1997.

Literature concerning the theory of GAs has grown considerably since the publication of Goldberg's book in 1989. It has covered such aspects as convergence [Keane (1995)] and comparison with other methods [Brooks et al (1996), M^{c}Gookin et al (1997(d))]. Also hybrid techniques have been presented which allow GAs to be combined with other search heuristics [Adler (1993), Renders and Flasse (1996)]. These papers report improvements on the basic GA method through logical switching to the other methods in the latter stages of the search.

As well as theoretical advancements, the number of applications in different fields has increased dramatically. Areas that have been covered include signal processing [Sharman and Esparcia-Alcazar (1993), Brooks et al (1996)], system identification [Kristinsson and Dumont (1992), Renders and Flasse (1996)] and image processing [Suthaharan et al (1997)].

The use of this method has been most noticeable in the area of control. Here the use of GAs for the optimisation of linear control systems has been quite extensive [Li et al (1995),Jones and de Moura Oliveira (1996), Kawabe et al (1996)].

In non-linear sliding mode control there have been numerous successful applications [Li et al (1995), Li et al (1996), Ng et al (1995), Trebi-Ollennu and White (1996(a)), Goh et al (1996)]. These have shown the benefits of using this technique to optimise sliding mode controllers.

In the context of marine applications of sliding mode controller optimisation, literature is not as limited as in the case of the SA method. The majority of papers are concerned with the optimisation of controllers for submersibles [Trebi-Ollennu and White (1996(b)), M^{c}Gookin et al (1996(b), 1997(b)(d))]. The literature for surface vessels is mostly limited to the work in this thesis in respect to sliding mode control [M^{c}Gookin et al (1997(a)(c)(e)(f))]. However some work has been reported by Donha et al (1997) into H_{∞} controller optimisation.

This shows a clear shortfall in research in the area of marine vehicle controller optimisation using GAs.

However, the literature in this field reports the beneficial effects of using GAs for parameter optimisation. This good publicity continues to perpetuate this method as one of the most powerful modern optimisation methods. This and other aspects are investigated in this thesis.

2.3 Sliding Mode Control

The field of non-linear, variable structure Sliding Mode (SM) control has been in existence since the 1960s. However the basic formulation of the sliding mode theory is primarily due to the work by Utkin [Utkin (1972)]. This provided the definition of the slipping surface (which was later called the *sliding surface*) as the building block of this control theory. From this surface the *equivalent control* component is derived as "the mean value of control" for this theory.

The work by Utkin has been further developed by Utkin and Yang (1978) where the linear state space derivation is extended to encompass the non-linear switching term that ensures robustness in this theory. This work is based on state feedback equivalent control which can be visualised quite easily. Also this work presents the use of

Lyapunov functions to guarantee the robust properties of this control theory and thus illustrates the benefit of this type of control theory over conventional linear methods.

The application of this methodology is carried out and illustrated in Slotine (1984). This work shows, through derivation, the applicability of SM control to systems without linearised simplifications. Hence the SM control theory could be applied to any system. However the numerical complexity of this non-linear approach limited the general use of this approach.

The majority of the theory after this time deals with the unwanted oscillating phenomenon called *chattering*. The work by Burton and Zinober (1988) illustrated the need to smooth out the hard discontinuous switching term and thus eliminate chattering. This develops into the *soft switching* schemes that have become popular [Healey and Marco (1992), Healey and Lienard (1993), M^{c}Gookin (1993), Fossen (1994)].

These and other aspects of SM control theory are formally covered in the book by Slotine and Li (1991) on non-linear control. As well as addressing the Single Input, Single Output (SISO) control case, this work also presented a Multi-Input, Multi-Output (MIMO) strategy. This and other MIMO methods [Fossen and Foss (1991), Corradini and Orlando (1997)], although numerically complete in their derivation, have a tendency to be difficult to implement.

Implementation problems are largely avoided by using a decoupling process to produce a single controller for specific SISO dynamics of the system being controlled [Healey and Marco (1992), Healey and Lienard (1993), M^{c}Gookin (1993), Fossen (1994)]. These have been proven to work well in various applications since cross-coupling between dynamics are accounted for by the robust switching action of these controllers.

The successful applications of SM controllers in simulation studies for the aerospace field has shown their potential benefits for vehicle control [Fossard (1993), Mudge and Patton (1988(a)(b))]. This has also been reflected in the marine field [Fossen (1994)] particularly in the case of submersibles [Healey and Marco (1992), Healey and Lienard (1993), M^{c}Gookin (1993), Trebi-Ollennu and White (1996(b)), M^{c}Gookin et al (1996(a)(b),1997(b)(d)), Corradini and Orlando (1997)]. However a general application

study in the marine field particular in the context of controller performance optimisation has not been undertaken.

2.4 Marine Vehicle Control Applications

Although the increased size and abilities of marine vehicles has called for research into automatic control, this area has not been exploited to the same extent as areas such as the aerospace field [Fossard (1993), Mudge and Patton (1988(a)(b))]. However investigations have been undertaken into mathematical modelling [Norrbin (1970), Berlekom and Goddard (1972), Price and Bishop (1974), Astrom and Kallstrom (1976), Gill (1979), Kallstrom (1979)] and control [Zuidweg (1970), Kallstrom (1979), Kallstrom et al (1979), Miliken (1984), Dove and Wright (1991), Franklin et al (1991)]. This broad area of literature has provided a good basis for marine vehicle applications.

This area of research has been consolidated by the two major texts by Fossen (1994) and Burcher and Rydell (1993). Both provide excellent insight into the dynamics and control of all types of marine vehicles by bringing together a wealth of knowledge formulated over the last couple of decades.

Although these studies illustrate the benefits of using automatic control for governing the motion of marine vessels, their application in practice has been limited due to the reluctance of the shipping industry to use such methods.

The most significant application has been in the use of Autonomous Underwater Vehicles (AUVs) such as Remotely Operated Vehicles (ROVs) [Healey and Marco (1992), Healey and Lienard (1993), Fossen (1994), Corradini and Orlando (1997), Trebi-Ollennu and White (1996(b))]. Other submarine studies have involved simulation and control of military vehicles [Miliken (1984), M^{c}Gookin (1993), Liceago-Castro and van der Molen (1995(a)(b)), Dumlu and Istefanopulos (1995), M^{c}Gookin et al (1996(a)(b), 1997(b)(d))]. However these studies have not been exploited in practice since more conventional operation methods are well established in the control of these vessels.

With surface ships the simulation studies of control systems are more extensive [Zuidweg (1970), Kallstrom (1979), Kallstrom and Astrom (1979), Fossen (1994), Vik and Fossen (1997), M^{c}Gookin et al (1997(a)(c)(e)(f))]. Again resistance to applying these control systems has also occurred in this area. Thus the need for study and application of these in-situ instead of through simulation is felt to be paramount for this area of research.

In the context of marine control, system parameter optimisation research has been very limited. Only recently has it been a topic for significant investigation by this author [M^{c}Gookin et al (1996(a)(b),1997(b)(d)), M^{c}Gookin et al (1997(a)(c)(e)(f))] and a few others [Trebi-Ollennu and White (1996(a)(b)), Donha et al (1997)]. Therefore the need for investigation in this field is clear. The work of this thesis will help fulfil this shortfall in the area of marine vehicle controller optimisation.

Chapter 3:

Simulated Annealing

3.1 Introduction

The optimisation processes considered in this study are based on processes which occur in nature. The first of these is called *Simulated Annealing* (SA) which is a probabilistic hill-climbing technique based on the annealing/cooling process of metals [Metropolis et al (1953), Kirkpatrick et al (1983)]. Annealing is defined as the heating of a metal to the point at which it becomes molten. When the metal has reached this stage it is allowed to cool by regulation of the temperature. At each temperature level the energy of the metal particles reduces and the metal itself becomes more rigid. This continues until the metal temperature has reached the surrounding ambient temperature and the energy has been minimised to its lowest value. At this final temperature stage the metal is completely solid.

SA emulates this process by adapting a hill-climbing search to follow an adaptive perturbation mechanism which is based on a cooling regime (i.e. an *Annealing Schedule*) [Kirkpatrick et al (1983), Sharman (1988), Sharman and Esparcia-Alcazar (1993)]. Hill-climbing itself is an optimisation technique which searches for a solution by a piece-wise increment of the parameters that are being optimised. Obtained solutions are only accepted if they are considered to be better than the previous best. Since it has no way of accepting a worse solution the search process has a tendency to get stuck at local optimum solutions which are not as good as the global solution. SA avoids this by a probabilistic aspect of its heuristic. Another aspect of the SA algorithm considered here is the reduction of the possible step size for each stage in the annealing schedule. This enables the search to fine tune an optimal solution in the later stages of the search.

Although this technique is superior to the basic hill-climbing heuristics, it does have its limitations as a global optimisation technique [M^{c}Gookin et al (1996(a))]. This is addressed in this chapter and a solution is presented in the form of the technique called *Segmented Simulated Annealing* (SSA) [Atkinson (1992), M^{c}Gookin et al (1996(a))]. The segmentation process improves the performance of the original SA algorithm.

This chapter describes both these algorithms in the following stages. Firstly the mechanism of the SA used in this study is described in detail. In Section 3.3 the convergence properties of this technique are illustrated in terms of Markov Chain analysis [Laarhoven and Aarts (1987), Laarhoven (1988)] and the disadvantage of this technique shown. The SSA algorithm is then given in Section 3.4 and an analysis of its convergence properties given in Section 3.5. Finally the conclusions about these techniques are given in Section 3.6.

3.2 Simulated Annealing Algorithm

As the name suggests, SA emulates the annealing process in order to obtain an optimum solution [Metropolis et al (1953), Kirkpatrick et al (1983), Kirkpatrick (1984), Sharman (1988), Sharman and Esparcia-Alcazar (1993)]. It achieves this by firstly generating possible parameters at random which are then substituted into the problem and their effect on the system is obtained through simulation (see Figure 3.1). The applications studied here concern the optimisation of controllers for marine vehicles which are simulated in the time domain. These simulated responses are compared with the desired responses and a value of their relative cost C (usually called the *energy*) is obtained. This cost value is used by the SA algorithm to determine how good the response provided by the parameters is (i.e. ideally a low cost). These initial parameters are used as the starting point for the SA search.

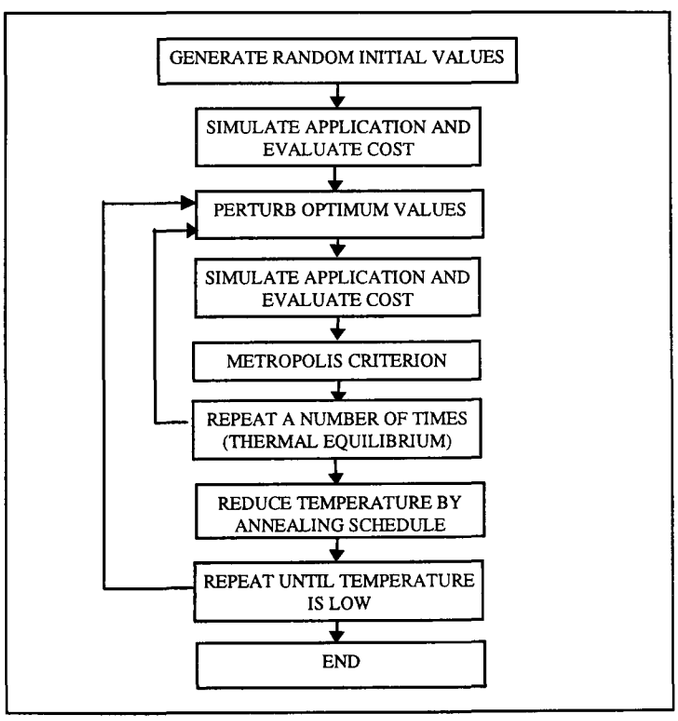

Figure 3.1: SA Flow Diagram

The next step is to obtain new parameters by perturbing the current values by amounts related to the value of a temperature index, T. These new parameters are then evaluated through simulation and a value for their cost is obtained. This new cost is compared with the initial cost in order to see which set of parameters is better. As with hill-climbing, if the new cost is lower than the previous cost then the new parameters are regarded as being better and replace the previous parameters as the current optimum solution. If the cost is higher they are subjected to probability tests called the *Metropolis Criterion* [Metropolis et al (1953), Kirkpatrick et al (1983), Kirkpatrick (1984)], which allows solutions with worse cost values to replace better solutions. This enables the SA to jump out of a local minimum in the search space and thus move towards the overall global minimum.

In this study the above operations (perturbation, simulation/evaluation and acceptance) are repeated a set number of times (20 in the applications described in this work) at each temperature level. This repetition is called *Thermal Equilibrium* (see Figure 3.1) [Kirkpatrick et al (1983), Laarhoven and Aarts (1987), Laarhoven (1988)] and increases the number of points investigated by the SA. This is analogous to letting the metal stabilise every time the temperature is reduced.

Once the thermal equilibrium has been executed the temperature index T is reduced in a way similar to that of the actual temperature in an annealing process. This systematic reduction in temperature is called the *Annealing Schedule* [Metropolis et al (1953), Kirkpatrick et al (1983), Laarhoven and Aarts (1987), Laarhoven (1988), Sharman (1988), Sharman and Esparcia-Alcazar (1993)] and determines how the perturbation range changes as the search proceeds. Since the perturbations are related to the temperature this schedule allows large steps at the beginning and smaller steps to fine tune the solutions as the search nears its conclusion.

The whole process is repeated until either the best cost has reached a minimum level or the temperature value has become too small to significantly affect the parameters (see Figure 3.1). If the cost has reached the minimum level the SA should have obtained the optimum parameter values. However, if the temperature is too small the results may not be optimal. This can happen if the search does not start near the optimum region since

SA has only one starting point which limits the range of the search [M^{c}Gookin et al (1996(a))].

3.2.1 Parameter Perturbation Mechanism

The mechanism for changing the parameter values perturbs each one by an amount *pert(T)* which is found from the following relationship [Sharman and Esparcia-Alcazar (1993), M^{c}Gookin et al (1996(a))]

$$pert(T)=p_{const}(T)\times p_{rand}= k\times T\times \tanh(\lambda) \tag{3.1}$$

where k is a scaling constant (selected as k = 0.1 in this study) and λ is an angle generated at random (in the range from -2π to 2π) in a uniform distribution. Subsequently the tanh function will yield a value between -1 and 1 as shown in Figure 3.2. This will scale the $p_{const}(T)$ value so that the perturbations vary in magnitude and sign.

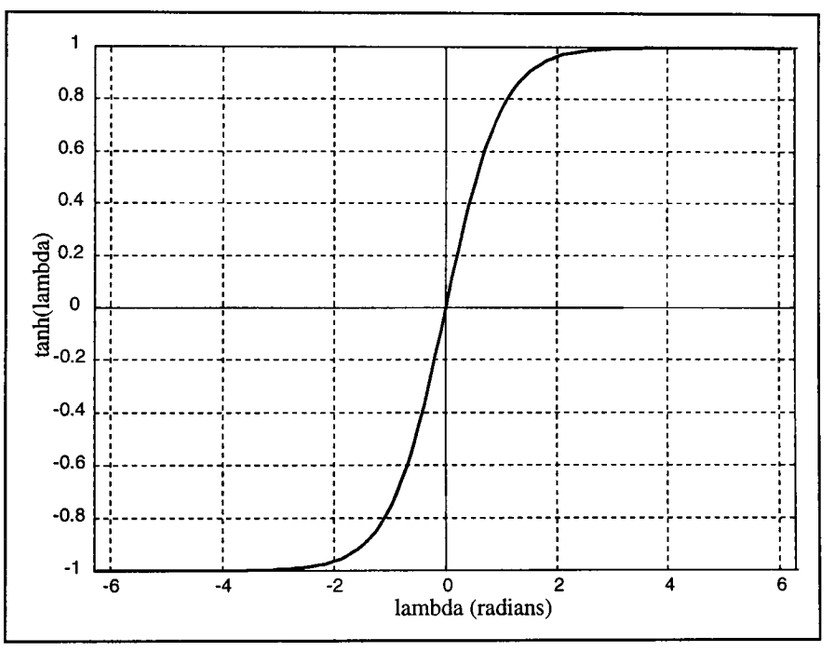

Figure 3.2: Perturbation tanh Function

It can be seen that the perturbation range reduces with temperature thus ensuring fine tuning of the parameters towards the end of the schedule. This should hopefully occur as the search nears the optimum. A fixed step length would not allow this fine tuning action and would restrict the usefulness of this method by removing the flexibility that a variable perturbation size provides.

3.2.2 Annealing Schedule

As mentioned previously, the temperature is reduced by the annealing schedule [Metropolis et al (1953), Kirkpatrick et al (1983), Laarhoven and Aarts (1987), Laarhoven (1988), Sharman (1988), Sharman and Esparcia-Alcazar (1993)]. Although there are various suggestions of how to implement this, the schedule chosen for this study is simply the reduction of the previous temperature by a set percentage (e.g. approximately 3% in this case). This is achieved by the following relationship

$$AS(T)=T_n=\gamma^n T_o \tag{3.2}$$

where T_o is the initial temperature (i.e. is chosen as 100 here), γ is the reduction constant (e.g. 0.9664 in this case) and T_n is the current temperature. This is represented graphically in Figure 3.3.

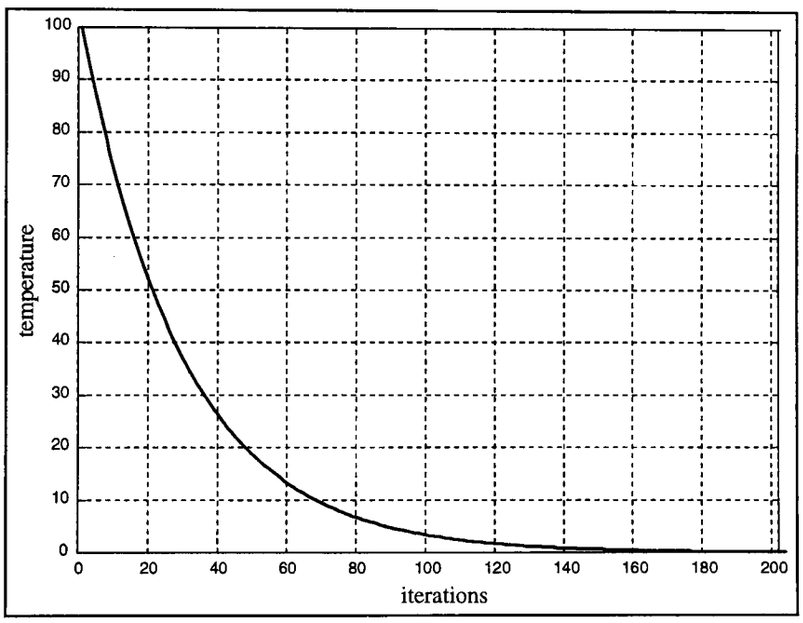

Figure 3.3: Annealing Schedule

The final cut off temperature T_{final} has been chosen in order to ensure a reasonably long schedule (e.g. 0.1 in this case). These values of T_o and T_{final} give the following total number of temperature changes n.

$$n=\frac{\log\left(T_{final}/T_o\right)}{\log(\gamma)}=\frac{\log(0.1/100)}{\log(0.9664)}\approx 202 \text{ changes} \tag{3.3}$$

When thermal equilibrium is considered the total number of iterations of the SA algorithm becomes

$$n_{total} = 202 \times 20 = 4040 \text{ iterations} \tag{3.4}$$

Which should be sufficient to observe the behaviour of this method.

3.2.3 Metropolis Criterion

The selection of parameters as optimal candidates has been discussed previously. But to reiterate, this method uses a cost probability check in order that suboptimal solutions are allowed to replace parameters that have better cost values. This is called the *Metropolis Criterion* which behaves in the following manner [Metropolis et al (1953), Kirkpatrick et al (1983), Kirkpatrick (1984)]. If the cost associated with the newly generated parameters (C_{new}) is lower then the new parameters replace the previous optimum parameters (as in conventional hill-climbing). However, if the new cost is not lower, the new parameters are not necessarily discarded. Instead, they may still be accepted if the cost passes a probability check (see Figure 3.4).

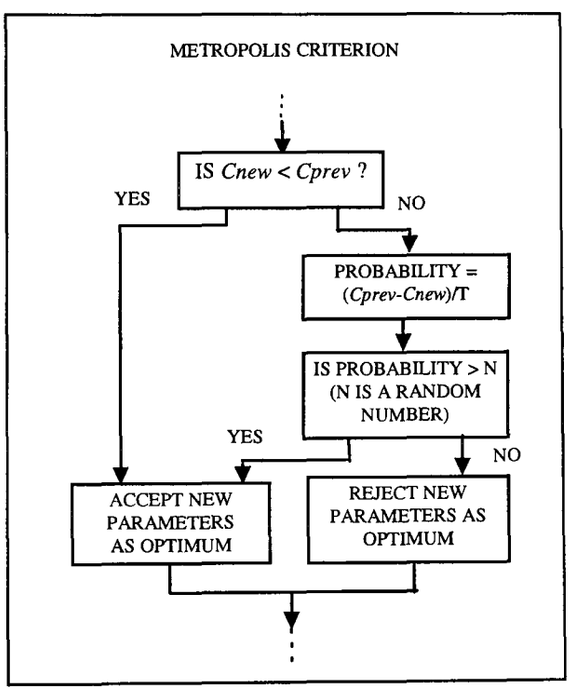

Figure 3.4: Metropolis Criterion

By analogy with the physical process of annealing the probability, P, of the new parameters cost relative to the previous optimum cost (C_{prev}) is calculated using Boltzmann's equation [Kirkpatrick et al (1983), Sharman (1988), Sharman and Esparcia-Alcazar (1993)] i.e.

$$P = \exp\left(\frac{C_{prev} - C_{new}}{T}\right) \tag{3.5}$$

P is then compared with a randomly generated number, N (which is generated uniformly in the range from 0 to 1). If $P > N$ then the new parameters are accepted as if $C_{new} < C_{prev}$. However, the new parameters are rejected if the $P < N$ (see Figure 3.4). As intended, this allows the search to move out of areas with local minima where it could get stuck. This ability enables the SA to reach the global optimum much better than conventional hill-climbing or gradient search method which would remain in a locally optimum region.

3.3 SA Convergence Analysis

3.3.1 Markov Chain Theory

The application of Markov Chain (MC) theory to Simulated Annealing is not new [Laarhoven and Aarts (1987), Laarhoven (1988)] as the convergence properties have been successfully established. However, a derivation of the range of the chain will be given here. In this section the foundations of the probability theory for MCs are defined and used to outline the formulation of a range theory.

MC theory fits into the SA process by considering each perturbation as a possible link from the present position (see Figure 3.5).

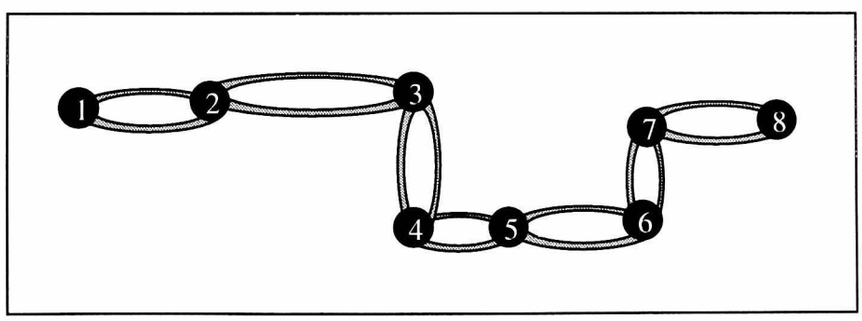

Figure 3.5: Markov Chain Representation

The probability of a link j having evolved from a link i of a homogenous[1] Markov Chain is given by the following equation [Laarhoven and Aarts (1987), Laarhoven (1988)]

[1] This chain is homogeneous because of the discontinuous nature of thermal equilibrium at each stage of the annealing schedule.

$$P_{ij}(T)=\begin{cases} G_{ij}(T)A_{ij}(T) & \forall j \neq i \\ 1-\sum_{l=1,l\neq i}^{|\Re|} G_{il}(T)A_{il}(T) & j=i \end{cases} \tag{3.6}$$

Each probability value is called a *transition probability* and they constitute the components of the *transition matrix* which describes the probabilistic history of every possible link that could be made. In equation (3.6) $G_{ij}(T)$ is the probability that the ith link is generated and is therefore called the *generating probability* [Laarhoven et al (1987), Laarhoven (1988)]. A_{ij} is the *acceptance probability* which determines whether this link is accepted as the next optimum solution. This is defined by the Metropolis criterion [Metropolis et al (1953), Kirkpatrick et al (1983), Kirkpatrick (1984)] which uses Boltzmann's equation [Kirkpatrick et al (1983), Sharman (1988), Sharman and Esparcia-Alcazar (1993)] from (3.5) i.e.

$$A_{ij}(T)=\begin{cases} 1 & C_{new} \leq C_{prev} \\ \exp\left(\dfrac{C_{prev}-C_{new}}{T}\right) & C_{new} > C_{prev} \end{cases} \tag{3.7}$$

The overall probability equals one if a new link is accepted by the above conditions or if the new link cannot be generated or accepted from the current solution. Numerous links are formed in thermal equilibrium but only the improved candidates form permanent links in the chain. This process continues until the MC has reached a final solution. If thermal equilibrium is not present the resulting MC would be inhomogeneous. However the links formed during the constant temperature plateaux of thermal equilibrium results in this MC being homogeneous [Laarhoven et al (1987), Laarhoven (1988)].

A criterion for the MC to converge to an optimum solution is that the annealing schedule must drive the temperature T to zero as the number of iterations tends to infinity (converge to zero asymptotically). From equation (3.2) it can be seen that as the number of iterations becomes very large the temperature does converge to zero for this Annealing Schedule i.e.

$$\begin{gathered} \lim_{n\to\infty} AS(T)=\gamma^{\infty}T_o=0 \\ \therefore\ as\ \lim_{n\to\infty} AS(T)\to 0 \quad T_\infty \to 0 \end{gathered} \tag{3.8}$$

Therefore this condition for convergence is satisfied and indicates that both the acceptance and generating probabilities change as $T_\infty \to 0$. The behaviour of each of these probabilities and hence the SA process itself can be obtained from this result. Firstly, the acceptance probability changes to

$$A_{ij}(T_\infty \to 0) = \begin{cases} 1 & C_{new} \le C_{prev} \\ 0 & C_{new} > C_{prev} \end{cases} \tag{3.9}$$

Which shows that only improved solutions will be accepted and the probability check becomes obsolete (i.e. this reverts to a basic hill-climbing technique).

From this the generating probability alters because it is related to the perturbation mechanism which in turn is related to the temperature in this application. Therefore, if $T_\infty \to 0$ then the perturbation mechanism will not change the current optimum parameters and thus no new candidates will be produced. This indicates that the generating probability will become zero i.e.

$$G_{ij}(T_\infty \to 0) = 0 \tag{3.10}$$

Therefore, from equation (3.4), the transition probabilities become

$$P_{ij}(T_\infty \to 0) = \begin{cases} 0 & \forall j \neq i \\ 1 & j = i \end{cases} \tag{3.11}$$

Hence, the SA process will converge to a final value. This will be an optimum if the chain is infinitely long (i.e. an exhaustive search of the given search space) [Laarhoven et al (1987), Laarhoven (1988)]. However, this is impractical as an infinite number of runs will never end and will not yield a final solution. Therefore, a finite homogeneous Markov Chain will have a limited range due to the parameter perturbation mechanism and this is one of the factors that defines the chains' ability to converge.

3.3.2 SA Markov Chain Range

The *range* of a MC generated by a SA process is a measure of the possible distance from the initial search point that the search can reach. This is determined by both the Annealing Schedule (see equation (3.2)) and the perturbation mechanism (see equation

(3.1)). Hence the maximum range of this MC (R_{MAX}) can be determined by the constant part of the perturbation mechanism, the annealing schedule and the number of thermal equilibrium points, ε, i.e.

$$\begin{aligned} R_{MAX} &= \sum_{i=1}^{l} \varepsilon \times p_{const}(T_i) \\ &= \sum_{i=1}^{l} \varepsilon \times k \times T_i \\ &= \sum_{i=1}^{l} \varepsilon k \gamma^i T_o \end{aligned} \tag{3.12}$$

Or generally,

$$R_{MAX} = \varepsilon \sum_{i=1}^{l} p_{const}(AS(T_i)) \tag{3.13}$$

However the range of any MC (R_{MC}) is less than this value due to the distribution of the random part of the perturbation mechanism (see equation (3.1))i.e.

$$\forall i \in \Re_{MC} \quad : \quad R_i \leq R_{MAX} \tag{3.14}$$

where $\Re_{MC}$ is the set of all possible MCs for this process and the given maximum range it can reach.

If the set $\Re_{OPT}$ is the set of all possible MCs leading to final solutions and is within $\Re_{MC}$ then the probability of this SA converging to an optimal solution is higher than average i.e.

$$P_i \geq P_{AVEOPT} \tag{3.15}$$

and is therefore more likely to converge to an optimum solution. However, if $\Re_{OPT}$ is not a subset of $\Re_{MC}$ then convergence is highly improbable.

Whether or not the chain has a large enough range depends on where the initial parameters lie. If they lie close to the optimal region (e.g. within the optimal region) then the chain will converge to an optimal solution. If the initial values are too far from the optimum then the chain will fail to converge.

Since *a-priori* knowledge of the location of the optimal region is usually not available, this search method cannot be relied upon as a global optimisation technique.

3.4 Segmented Simulated Annealing

The limited coverage of a search space is the main drawback with SA. This restriction means that SA is not a good global search method and may not converge to an optimum if the initial parameter values are not near this region. The development of the Segmented Simulated Annealing (SSA) algorithm [Atkinson (1992), M^{c}Gookin et al (1996(a))] means that this is no longer a problem. SSA consists of a number (in this case 20) of consecutively executed single SA runs (without thermal equilibrium) (see Figure 3.6 for illustration of concept). Each one starts at a different point in the search space with a wide range of possible initial values. This segments the search space into smaller regions and allows the SSA to initially cover more of the search space than the conventional SA process.

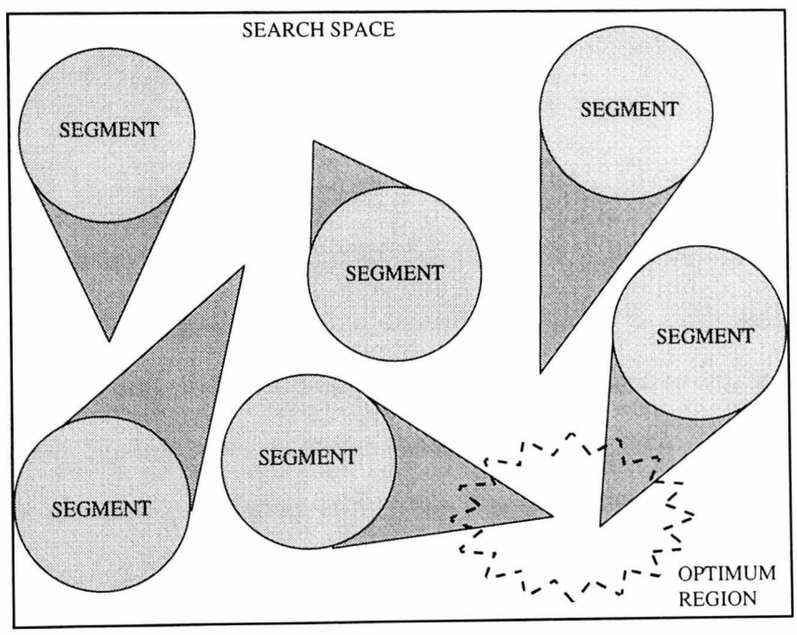

Figure 3.6: SSA Illustration

The final cost values from each of the 20 runs are bubble sorted into ascending order (see Figure 3.7 for algorithm) and the cost in first place (i.e. the smallest) is taken to be the optimum with its corresponding parameters providing an optimal result. SSA is therefore a much better search method than the conventional SA because of its wider exploration of the search space particularly in the initial stages.

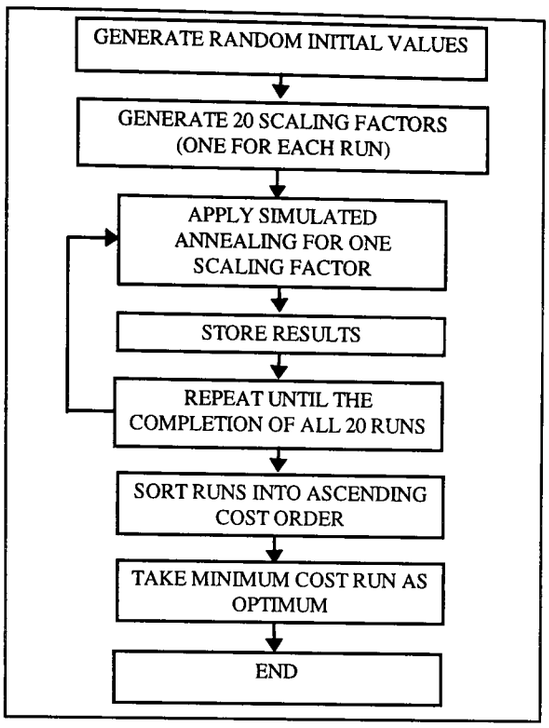

Figure 3.7: SSA Flow Diagram

3.5 SSA Markov Chain Convergence

With a Segmented Simulated Annealing (SSA) [Atkinson (1992), M^{c}Gookin et al (1996(a))] process involving χ runs, the initial values are represented as $INIT_i$, $i = 1..\chi$. By segmenting the search space, greater initial coverage is achieved. Therefore the probability of a MC of one of the runs having sufficient range is higher than for a single SA run. Since the SSA covers χ times more of the search space than the SA the probability of one run being initiated within the range of the optimum is higher than for a single run SA which will be called mc_1 i.e.

$$\begin{aligned} &\forall INIT_i, \quad 1 \le i \le \chi : mc(i) \in \Re_{MC} \\ &P(mc(i) \in \Re_{OPT}) > P(mc_1 \in \Re_{OPT}) \end{aligned} \tag{3.16}$$

where $mc(i)$ is a given MC and $\Re_{OPT}$ is the subset of $\Re_{MC}$ which leads to an optimal solution. In fact SSA is χ time more likely to start a run near the optimum than a single SA run with MC.

$$P(mc(i) \in \Re_{OPT}) \approx \chi \times P(mc_1 \in \Re_{OPT}) \tag{3.17}$$

For uniform coverage the probability of the MC of a particular run being within range of the optimum is greater than the average probability of all MC being within range (P_{AVEOPT}) i.e.

$$P(mc(i) \in \Re_{OPT}) >> P_{AVEOPT} \tag{3.18}$$

Therefore by (3.15) it follows that the *i*th MC run will be highly likely to start near the optimum region and end in the set of all optimal solutions i.e.

$$mc(i) \in \Re_{MC} \in \Re_{OPT} \tag{3.19}$$

which implies convergence. Hence the segmentation of the search space will increase the probability of the SSA process being able to find a globally optimal solution for a given problem.

3.6 Summary

In this chapter the mechanics of the Simulated Annealing algorithm has been shown. Also, through Markov Chain analysis, the limitations of this search process have been illustrated. The main limitation is the need for *a-priori* knowledge in order to ensure convergence to an optimal global solution. Hence it is indicated that SA performs well as a localised search method but is not reliable as a global search method.

In order to rectify this weakness in the SA method, a segmentation process has been described and shown to improve the probability of the search starting within sufficient range of the optimum to converge to it. This is self evident since localising the search method to smaller segments of the search space will allow this method to converge. Therefore it can be concluded that the Segmented Simulated Annealing should act well as a global search method and reliably furnish optimal solutions on each execution.

Verification of these conclusions may be found through the applications considered in future chapters. For each control system investigated both SA and SSA are applied to the parametric optimisation. For SA, the initial parameter values is positioned both near and reasonably far from the expected optimal regions, hence verifying the range theory illustrated in Section 3.3.2.

Chapter 4:

Genetic Algorithms

4.1 Introduction

The Genetic Algorithm (GA) [Holland (1975), Goldberg (1989), Grefenstette (1986)] optimisation technique is a relatively new method for parameter optimisation. Although the theory has existed for a number of decades, the computational effort needed to execute it has until recently exceeded the capabilities of most processors. Only now can the potential of this method be fully realised in applications involving dynamic systems and control.

The method is based on Charles Darwin's *Natural Selection* process [Abercrombie et al (1985)]. This asserts that the evolution of a particular species is on the basis of *survival of the fittest* whereby the best genus of a species will evolve and dominate other variations of the same species. In this context best means the strongest, healthiest and most intelligent genus which is able to adapt to its hostile surrounding by applying and developing its abilities. This degree of optimality for each genus is graded by some *survival value* i.e. the higher the value the more likely the genus is to survive.

As evolution progresses, the strongest elements develop thus becoming more prevalent and the weaker variants are eventually eliminated. Taking this to its natural conclusion would indicate that the species will evolve to a natural optimum and produce an almost *super-genus* which is far superior to its earlier predecessors. An example of this is the evolution of modern man from the primitive origin of the species [Abercrombie et al (1985)]. At an early stage numerous genus variations developed from the same origin but only one branch survived. This link was the genus called *homo-habilus* which survived due to its unique ability to use tools and weapons. This gave it an advantage over the other genus variations. From this key evolutionary point *homo-erectus* evolved to *homo-sapien* and subsequently modern man. This illustrates that beneficial abilities can swing the balance in determining which genus survives and which fades into history.

Direct parallels between evolution and optimisation can be drawn from this theory and are utilised by the GA method. The GA theory and how it is used for parameter optimisation is outlined in this chapter in the following way. Section 4.2 describes the mechanism of the GA by means of its component parts through use of genetic and evolutionary terminology. The convergence of this method is analysed in Section 4.3 by consideration of the Markov Chain (MC) [Laarhoven and Aarts (1987), Laarhoven (1988) and the Schema Theorem [Holland (1975), Goldberg (1989)]. Finally the theoretical conclusions of this analysis are given in Section 4.4.

4.2 Genetic Algorithm

The GA emulates the evolutionary process of species in the following way. In order to search the problem solution space the GA uses a number of integer strings called *chromosomes* as a representation of the parameters to be optimised [Holland (1975), Goldberg (1989)]. This group of strings is called the *population* and the number of constituent chromosomes is called the *population size*. The initial population is generated at random. These chromosomes are decoded into the corresponding parameters which are then applied to the optimisation problem and the resulting system is then simulated. A measure of how good the results of this simulation are is calculated using a cost function as in the SA methods in the previous chapter. Conventionally a fitness function is used to determine the degree of optimality of a chromosome solution [Goldberg (1989), Sharman and Esparcia-Alcazar (1993)]. This is usually a function of the reciprocal of the cost and is maximised in order to obtain a globally optimal final solution. In this application the cost (or *raw fitness* as it is sometimes called) is used so that the criteria for optimisation remain the same when comparing this method with the SA methods. Therefore the GA will try to minimise the cost.

Once the cost values for the entire population are obtained they are then subjected to the operation of *Reproduction* where some of the chromosomes are selected for the next generation. After reproduction the chromosomes that are not selected are replaced by new chromosome obtained through the two other operations *Crossover* and *Mutation* (see Figure 4.1) which provide different points within the search space for analysis [Holland (1975), Goldberg (1989)].

The processes of decoding, application/evaluation and chromosome manipulation are repeated for a set number of iterations by which time the GA should have reached an optimal solution (see Figure 4.1). This number of iterations is called the *generation size* where each iteration is called a *generation*.

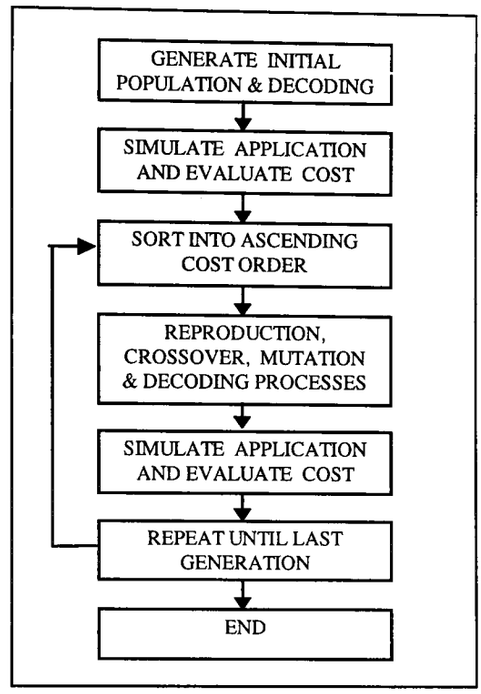

Figure 4.1: GA Flow Diagram

The major components of the GA i.e. decoding, reproduction, crossover and mutation, are now discussed in detail. This should give an insight into the methods used in this investigation.

4.2.1 Decoding

Although the parameters considered here are real numbers, the representation used in this technique is integer. In fact the real number parameters can be decoded from this representation which is used in the operations of this method. The decoding process is described below.

As mentioned previously the chromosomes consist of integers which represent the optimisation parameters. Each integer position is called a *gene* and the integer value is called an *allele*. This terminology stems from the genetic theory upon which this technique is based [Abercrombie et al (1985), Holland (1975), Goldberg (1989)]. Most early applications of GAs had a binary allele system which caused the chromosomes to

be large and hence memory intensive. A more compact numerical system is decimal which has ten possible allele values (i.e. from 0 to 9) and therefore results in smaller chromosomes.

The decoding scheme used here has five genes to represent a single parameter and therefore the size of the chromosome depends on the number of parameters. The value allocation of each gene is shown Figure 4.2.

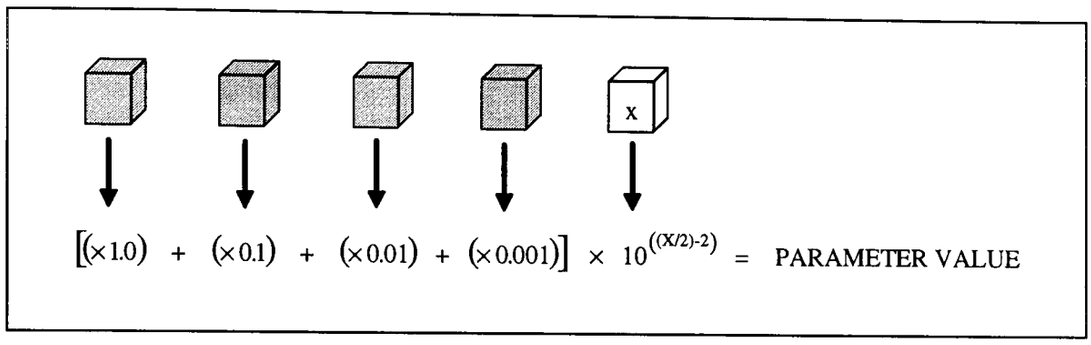

Figure 4.2: Gene Decoding

In this illustration it can be seen that the first four digits form a real number which is made up from the scaled sum of the alleles. This sum is then multiplied by an exponent of 10 which is obtained by scaling the fifth gene between 3 and -2. The resulting range that is achieved by this scheme is from 9.999×10^{3} to 0.001×10^{-2} which is chosen so that all possible values that the parameters could conceivably take are available (i.e. 10^{5} possible variations for each parameter). No sign is needed in this study since the parameter values are of a known sign condition. However, if sign became an issue it could easily become incorporated into the chromosome by adding a binary gene for each parameter. A suitable convention could be 0 is positive and 1 is negative.

It should be noted that a similar binary representation for the parameters would require twenty genes per parameter to achieve the same range. This would increase the chromosome size and resulting memory use by a factor of four compared with the decimal approach.

4.2.2 Reproduction

Once the cost values of the chromosomes are obtained from the simulation results, they are subjected to the first major operation of this method. This is the reproduction

operation that determines which members of the present generation progress on to the next generation.

There are numerous routines to perform this reproduction stage which differ in the way they select the candidates for the next generation. Three of the most popular are described below.

Roulette Wheel is a probabilistic selection process where chromosomes are assigned cost dependent acceptance probability values. The higher the cost the better the chromosome's chances of being accepted. It also allows sub-optimal solutions to have a chance of being accepted and ensures a reasonable mix of good and bad solutions to progress on to subsequent generations. This increases the average cost of the population and hence prevents premature convergence. However the price for this is a slow convergence rate.

Tournament Selection involves the random selection of small groups of chromosomes which are ranked in terms of cost. The best are kept and the worst are rejected. This is repeated until all the chromosomes have been considered. It allows the selection of suboptimal candidates and avoids premature convergence.

Elitist Selection is similar to tournament in that it is a cost rank based scheme but in this method the entire population is ranked instead of small groups. Once they are ranked a fixed percentage of the top chromosomes are selected for the next generation and the remainder are rejected. However this may cause premature convergence to a local optimum since too many local solutions may occupy the higher echelons of the population. This can be rectified by using a high mutation rate (see section 4.2.4).

In this study only elitist selection is considered due to its fast convergent properties. The resulting GA is called an *elite GA* because only the best chromosomes survive from generation to generation [Brooks et al (1996)].

The remainder of the chromosomes that are not selected are replaced by new chromosomes that are produced by the crossover and mutation operations [Holland (1975), Goldberg (1989)].

4.2.3 Crossover

The Crossover operation produces new chromosomes to replace those rejected by reproduction. It achieves this by firstly selecting any two chromosomes from the present generation which are called the *parents*. A number of the genes of one of the parents is swapped with the same number and positioned genes of the other parent. Usually this is achieved by selecting a single gene within a parent and swapping all genes that follow on from this point in the chromosome. This is called single point crossover (see Figure 4.3).

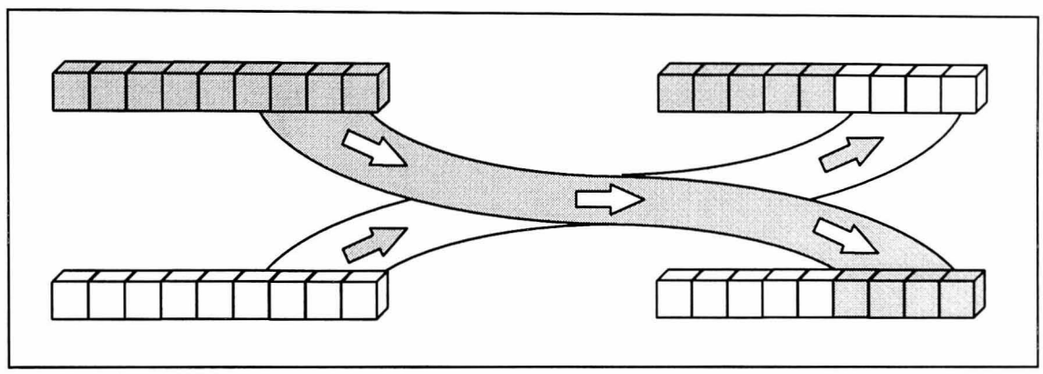

Figure 4.3: Single Point Crossover

However, in this study *two point crossover* is used where two gene positions are selected at random and all genes between these points are swapped (see Figure 4.4). This results in a greater amount of variation in the new chromosomes that are produced. The subsequent chromosomes that are produced by this operation are called the *children*. These inherit properties from both parents which may improve or degrade their performance.

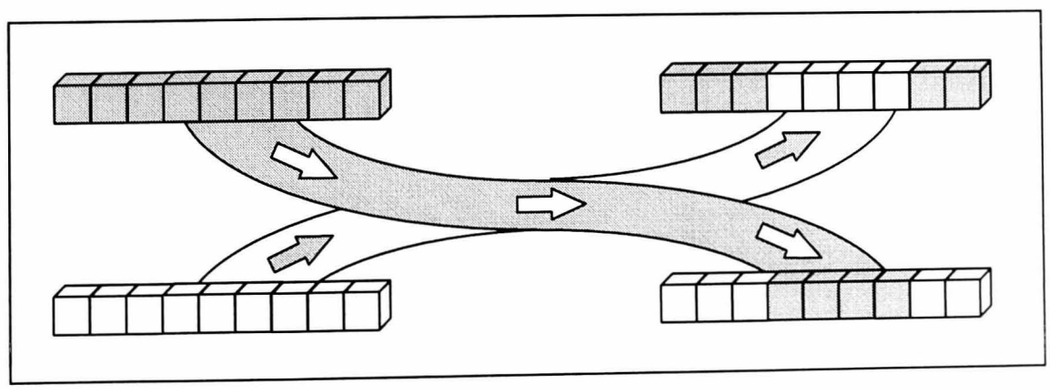

Figure 4.4: Two Point Crossover

The crossover process is repeated until there are enough children to replace the chromosomes rejected in reproduction. These children form the basis for the next generation.

4.2.4 Mutation

In nature, mutation is the sudden randomly occurring change in chromosomal properties. This can be due to adverse environmental changes (e.g. chemical or radiation effects on a species). In the context of GAs, the mutation operation is simply the random selection of a percentage of the children's genes and the random change of their corresponding alleles. The number of mutated genes (g_m) relative to the total number of genes (g_{total}) is the *mutation rate* (m) which can be represented as [M^{c}Gookin et al (1997(b))]

$$m = \frac{g_m}{g_{total}} \tag{4.1}$$

This is usually represented as a percentage. For elite GAs the mutation rate has to be higher than Goldberg's suggested value of 0.1%. This increase prevents premature convergence to a local optimum and ensures that the global optimum is attained. Therefore a suitable range has been found to be 1 - 5%.

4.2.5 Numerical Values

In order to maintain compatibility in the investigations carried out into this method, the values for the key operational parameters remain constant for all applications considered here. These are selection percentage, crossover percentage, mutation rate percentage, population and generation sizes. The values chosen for this study are shown in Table 4.1.

Selection	Crossover	Mutation	Population Size	Generation Size
20%	80%	5%	50	100

Table 4.1: GA Parameters

The last two values are chosen in order that the behaviour of this technique can be studied. It is suggested by Ng et al (1995) that the population size should be approximately equal to the number of genes in each chromosome and that the generation size should be double this. Since there are three applications considered here the one with the largest number of parameters is used to determine these parameters. This is the submarine which will be shown to have nine parameters The values shown above will give the following number of iterations of the optimisation problem.

$$\text{number of iterations} = [(100 \times 0.8) + 1] \times 50 = 4050 \qquad (4.2)$$

4.3 GA Convergence

4.3.1 Markov Chain theory

The concept of Markov Chains for GAs is slightly different from that considered when applying this methodology to SA [Laarhoven and Aarts (1987), Laarhoven (1988)]. Since the crossover operation depends on two chromosomes of the previous generation there is some link dependency on more than one previous link. This forms a connecting effect of two or more links which produces *Markov Chain-Mail* rather than a single chain (see Figure 4.5).

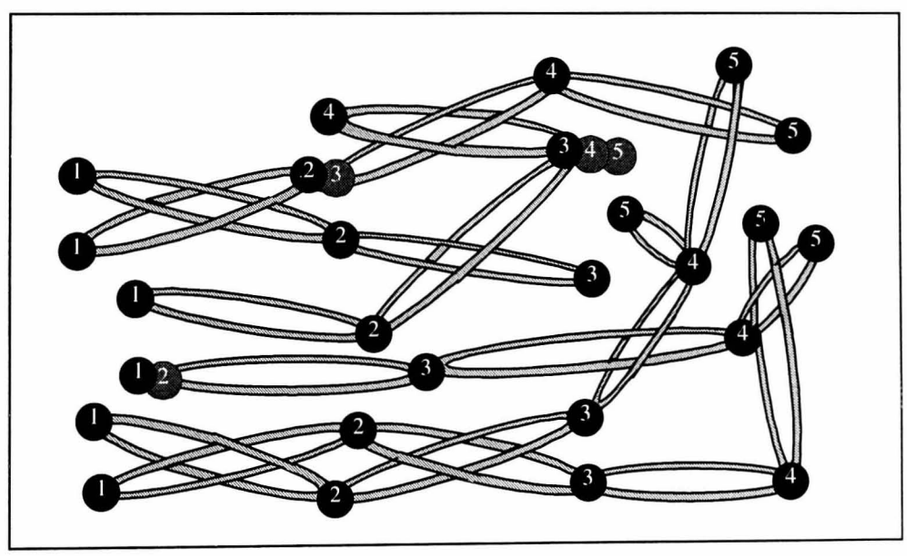

Figure 4.5: GA Markov "Chain-mail" Representation

Although the representation is slightly different, GA MC theory itself follows the same process as the SA case. The probability of each link in a Genetic Algorithm (GA) is also represented by equation (3.6) in the previous chapter i.e.

$$P_{ij}(T) = \begin{cases} G_{ij}(T)A_{ij}(T) & \forall j \neq i \\ 1 - \sum_{l=1, l\neq i}^{|\Re|} G_{il}(T)A_{il}(T) & j = i \end{cases} \tag{4.3}$$

However the constituent parts of these probabilities depend on the reproduction, crossover and mutation operations which are outlined below.

When considering GAs the generating probability is divided into two operations: crossover and mutation i.e.

$$G_i = G_C G_M \tag{4.4}$$

Crossover depends on the random selection of two parents and the relevant genes to swap i.e.

$$G_C = S_{CP} S_{CG} \tag{4.5}$$

where the parent chromosomes are selected with probability S_{CP}. As mentioned in section 4.2.3, the gene selection process (both in terms of position and number) involves selecting two genes at random and swapping them and all others in between. This has the following probability function.

$$S_{CG} = S_{PT1} S_{PT2} \tag{4.6}$$

Here S_{PT1} is the selection of the first gene and S_{PT2} is the conditional selection probability of the second gene given that the first gene has already been selected.

Mutation is the random selection of a percentage of the total number of genes where m is the mutation rate defined from equation (4.1). It is represented by the following equation.

$$G_M = S_{MG} M \tag{4.7}$$

Here S_{MG} is the selection of genes in the chromosome and M is the change of the gene to another value (which has a uniform probability in this case). The selection process has two parts

$$S_{MG} = S_T S_C \tag{4.8}$$

where S_T is the selection of a gene in the total gene population (i.e. the mutation rate) and S_C is the probability of this gene being in the chromosome in question.

The acceptance probability is dependent on the cost value of the chromosome relative to the other chromosomes' values. If the chromosome is within a certain cost limit it is accepted for the next generation (elitist). This limit is a set percentage of the population (e.g. $a\%$) and is associated with a limiting cost value ($C_{a\%}$) which is calculated for each generation. Therefore the acceptance probability becomes

$$A_i = \begin{cases} 1 & C_i \leq C_{a\%} \\ 0 & C_i > C_{a\%} \end{cases} \tag{4.9}$$

Hence only improved solutions are accepted and incremental improvements occur in each generation. However, this does not guarantee that the improved solutions are optimal. This will only occur when the majority of the optimised solutions progress to a form which is considered optimal. The natural progression of chromosomes to become this form comes from the *Schema Theorem*. This theorem will show that the top elements of the final generations are similar and optimal.

4.3.2 Schema Theorem

The Schema Theorem, as defined by Holland (1975) and Goldberg (1989), is based on the similarity between genes of certain chromosomes. These similar gene patterns are called *schemata* and chromosomes that exhibit the same *schema* have the same alleles in the same positions. The theorem of how these schemata behave is applied to the convergence of GAs by observing the probabilistic nature of the three operations of reproduction, crossover and mutation. Each of these operations affects the number of chromosomes with the same schema and alters the growth rate of prominent schemata that give optimal solutions. The effect of each of these on the growth of a schema is studied below.

Reproduction in this case is the elitist rank based selection process where only the top $a\%$ of the chromosomes are retained for the next generation. This means that the cost values fall into two categories i.e. those above the $a\%$ cost limit and those below (see equation (4.9)) which helps to define the probability of an individual or a particular

schema being accepted. Since the cost is used instead of fitness the derivation is slightly different. Let H represent a particular schema and $sch = sch(H,t)$ represent the number of examples of schema H at time t. The reproductive schema growth equation becomes

$$sch(H,t+1) = sch(H,t)\frac{C_{a\%}}{C(H)} \tag{4.10}$$

where $C(H)$ is the average cost of the chromosomes representing schema H. Therefore schema with small $C(H)$ will have a higher likelihood of increasing in number.

Crossover in this case is more involved than the conventional single process. Here a block of genes is subjected to this process and are defined by the genes at the beginning and end of the chosen block (see equations (4.5) and (4.6)). The following argument refers to the conditions illustrated in Figure 4.6.

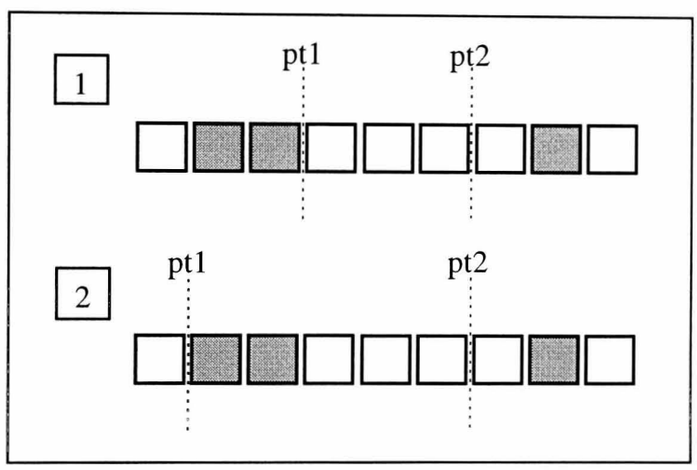

Figure 4.6: Crossover Cases

For the schema represented by the shaded blocks there are two different sets of crossover points represented by the two dashed lines. The only difference in both cases is the position of the initial point (pt1) relative to the section to be crossed over. The probability of either of these initial points being selected and destroying the schema by dividing the schema members is the same. The probability of this occurring is given by

$$p_{d1} = \frac{d(H)}{(l_g\text{-}1)} \tag{4.11}$$

where $d(H)$ is the *defining length* of the schema (i.e. the greatest number of selection points between two elements of the schema) and l_g is the number of genes in the

chromosomes. Only when you consider the conditional probability of the second point destroying the schema is there a difference in the cases.

In case one, where the initial point is inside the crossover region, the only way the schema can be affected is if the second point is outside this region. Therefore the destruction probability is defined as

$$p_{d21} = \frac{e(H)}{(l_g - n_1\text{-}1)} \tag{4.12}$$

where $e(H)$ is the number of selection points between the end of the crossover region and the end of the chromosome and n_1 is the position of pt1.

However, if the initial point is outside then the second point has to fall inside the crossover region to destroy the schema. This gives the following probability.

$$p_{d22} = \frac{d(H)}{(l_g - n_1\text{-}1)} \tag{4.13}$$

Thus resulting in two distinct probability cases. The overall probability of destroying the schema will be

$$p_d = p_{d1}(p_{d21} + p_{d22}) \tag{4.14}$$

and therefore the probability of survival becomes

$$p_s \geq 1\text{-}S_{CP}p_d = 1 - S_{CP}p_{d1}(p_{d21} + p_{d22}) \tag{4.15}$$

where S_{CP} is the parent selection probability of equation (4.5). Taking equation (4.15) into account will affect the number of a particular schema occurring in subsequent generations and thus alter equation (4.10) thus

$$sch(H,t+1) \geq sch(H,t)\frac{C_{a\%}}{C(H)}\left(1 - S_{CP}p_{d1}(p_{d21} + p_{d22})\right) \tag{4.16}$$

The final operator to affect the schema growth equation is mutation. As equation (4.7) shows that the mutation generation probability is G_M. In order for a schema to survive, individual components of the schema must survive the mutation process. Hence the probability of a schema surviving mutation is (1- G_M). Since this has to apply to all the

components of the schema it is multiplied by itself $o(H)$ times. Here $o(H)$ is the order of the schema and is the number of fixed gene positions in the schema. Hence the mutation survival probability is

$$p_m = (1 - G_M)^{o(H)} \tag{4.17}$$

Since the probability G_M is reasonably small, equation (4.17) can be approximated by the following series expansion [Goldberg (1989)]

$$p_m \approx 1 - G_M o(H) \tag{4.18}$$

where higher order terms are negligibly small. Hence equation (4.16) becomes

$$sch(H,t+1) \geq sch(H,t)\frac{C_{a\%}}{C(H)}\left(1 - S_{CP}p_{d1}\left(p_{d21} + p_{d22}\right)\right)\left(1 - G_M o(H)\right) \tag{4.19}$$

Which can be simplified if small cross-products are ignored after multiplying out the brackets i.e.

$$sch(H,t+1) \geq sch(H,t)\frac{C_{a\%}}{C(H)}\left(1 - S_{CP}p_{d1}(p_{d21} + p_{d22}) - G_M o(H)\right) \tag{4.20}$$

By analysing this equation it can be concluded that schema with average cost values below the selection threshold will increase in number. Also if the defining length of the schema is short then it is more likely to survive crossover. Hence the same conclusions can be drawn that are stated in Goldberg (1989) i.e. that the final solutions tend to be optimal due to the steady growth of optimal schema. Taking this argument to its logical conclusion it can be seen that any improvement in the cost value will lead to an increase in the number of members of that schema and as time goes on the schema with an optimal solution will tend to populate more of the top $a\%$ of the population. Thus a *saturation* effect occurs in the final generations.

4.3.3 Genetic Algorithm Convergence

The Schema Theorem has shown that as GAs approach the optimal region the chromosomes with the fittest cost values tend to duplicate and a saturation effect occurs. Therefore chromosomes with this schema will occupy the top $a\%$ of the population. Hence these schema will tend to re-occur since crossover will not affect the schema

(since individuals are similar) and mutation only incrementally improves these solutions (since detrimental mutation will result in rejection). Hence the optimal solutions will be similar and only solutions with the optimal schema will have an acceptance probability of 1. Since these optimal individuals are similar, their generation probability will converge to 1. Once the top $a\%$ is totally occupied with chromosomes of the same optimal schema, the selection cost limit $C_{a\%}$ asymptotically tends towards a value which is close to the optimal value of cost. Therefore the probability of incremental improvements to the optimal schema (due mostly to mutation) becomes very small and will finally become zero when no further improvement is possible. At this point the acceptance probability becomes zero for all new chromosomes since they give suboptimal solutions and one for the existing members of the top $a\%$. This will effect the probability elements of the transition matrix in the following way:-

$$P_{ij} = \begin{cases} 0 & \forall j \neq i \\ 1 & j=i \end{cases} \tag{4.21}$$

Therefore no new candidates are accepted which indicates that the GA has reached a final optimum. This is likely to be the global optimum since only optimal schema will occupy the top $a\%$ in the final generations. Hence GA convergence is suggested.

4.4 Summary

The mechanism of GAs has been demonstrated in this chapter and the convergence of this method has been illustrated through Markov Chain and Schema Theorem analysis. It has been shown mathematically that GAs are able to converge to an optimal solution without *a-priori* knowledge of where the optimal region lies.

For elite GAs the convergence is quicker and is assured globally by an increase in mutation rate. This high mutation will initiate the variation that is inherent in other selection processes without the drawback of slow convergence.

Hence the theory of elite GAs has proved that this method is potentially very powerful as a global optimisation technique. The actual application of this method to marine vehicle controller optimisation will verify this theory.

Chapter 5:

Decoupled Sliding Mode Control Theory

5.1 Introduction

In general, control is considered to be the process of automatically governing a system's behaviour in some desired manner. This is achieved by designing a controller which provides the required inputs for a system so that it will perform as required. In the context of this work control is used to govern the motion of marine vehicles. The control law used here to obtain controllers for this purpose is the non-linear, robust *Sliding Mode* (SM) form of control [Utkin (1992), Slotine and Li (1991), Mudge and Patton (1988(a)(b)), Healey and Marco (1992), Healey and Lienard (1993), Burton and Zinober (1988)]. Such robust techniques are considered to be better than a conventional linear PID controller in that they can handle changes in the plant and external disturbances without as much performance degradation [Fossen (1994)]. However, these types of controllers have always been thought to be difficult to design due to their mathematical complexity [Healey and Marco (1992), Healey and Lienard (1993), Fossen (1994), Fossen and Foss (1991)].

This chapter illustrates a simple method for designing and implementing single input sliding mode controllers for controlling decoupled dynamics of a system [Healey and Marco (1992), Healey and Lienard (1993), Fossen (1994)]. The decoupling process takes the full representation of the system and isolates the dominant dynamics of the vessel. Each set of dynamics forms a subsystem which represents a specific motion of the vessel. In this case each subsystem has a single input which governs the respective motion. This process is a widely used method for controlling multi input systems [Franklin et al (1991)].

An introduction to the fundamental theory behind SM control is given in Section 5.2. The derivation of the resulting control law is given in Sections 5.3 and 5.4 of this chapter. In Sections 5.3 and 5.5 the stability of this method of control is obtained from Lyapunov's Stability Theorem [Utkin and Yang (1978), Utkin (1992), Slotine and Li (1991)]. From this foundation, the controller equation for a subsystem is derived and a suitable criterion for stability is also obtained. A discussion about performance is

supplied in Section 5.6 which indicates that since stability is satisfied these controllers are robust to disturbances caused by changes in the system or external sources. Finally Sections 5.7 and 5.8 deal with the practical aspects of this type of controller. In particular, the problems encountered in terms of the phenomenon of chattering and steps to be taken to eliminate chattering without affecting the stability of the controller are considered [Healey and Marco (1992), Healey and Lienard (1993), Burton and Zinober (1988), Fossen (1994)].

5.2 Basic Theory

The purpose of sliding mode control studied here, as with many other control laws, is to make the states of a system ($\mathbf{x}$) follow some desired state response ($\mathbf{x}_d$) [Franklin et al (1991), Fossen (1994)]. This is achieved by reducing the state error ($\hat{\mathbf{x}} = \mathbf{x} - \mathbf{x}_d$) to zero by the use of something called the *sliding surface* $(\sigma(\hat{\mathbf{x}}))$ [Utkin (1972), Utkin and Yang (1978), Utkin (1992), Slotine and Li (1991), Mudge and Patton (1988(a)(b)), Healey and Marco (1992), Healey and Lienard (1993), Burton and Zinober (1988)] which is a function of the state error. The controller derived from SM theory tries to drive the state error to zero by driving the sliding surface to zero. It does this by providing a control input, for the system, which depends on state variables (to determine the state at present) and the desired state variables (to determine what the state should be). Once this control action is on the zero sliding surface the controller is said to be in the *Sliding Mode*. The controller defined from SM Theory has two components, the equivalent control (u_{eq}) and the switching term (u_{sw}) [Utkin and Yang (1978), Utkin (1992), Slotine and Li (1991), Mudge and Patton (1988(a)(b)] i.e.

$$u = u_{eq} + u_{sw} \tag{5.1}$$

The equivalent control law provides the main control action and the switching term provides additional control action in order to compensate for any change in the nominal operating point that the equivalent controller is designed around. This combined control effort ensures that the system tracks the state error to zero irrespective of changes in its operating conditions.

Systems usually have more than one input that has to be controlled and this is true for the applications studied in this thesis. However, the type of SM controllers used for this

work only allows for a single [Healey and Marco (1992), Healey and Lienard (1993), M^{c}Gookin (1993), Fossen (1994), Slotine and Li (1991), Mudge and Patton (1988(a)(b))]. Therefore, the number of controllers has to be the same as the number of controlled variables. In order to implement these controllers the system is decoupled (or divided) into a number of single input subsystems which govern particular modes of motion of the system [Healey and Marco (1992), Healey and Lienard (1993), Fossen (1994), Slotine and Li (1991), M^{c}Gookin (1993)]. Then the controller is designed using each subsystem as an independent system. The inputs which are obtained from these controllers are then applied simultaneously to the original, undivided system. Since the design of the decoupled controllers depends on the states of the system there is feedback present in the overall set-up [Healey and Marco (1992), Healey and Lienard (1993), Fossen (1994), M^{c}Gookin (1993)]. This is an accepted and widely used method of controller design and implementation.

5.3 Sliding Surface

The main premise behind why sliding mode controllers are considered non-linear is the switching control action. This is designed round the sliding surface, $\sigma(\hat{\mathbf{x}})$ which is derived so that as the surface value tends to and becomes zero the state error tends towards zero (see Figure 5.1).

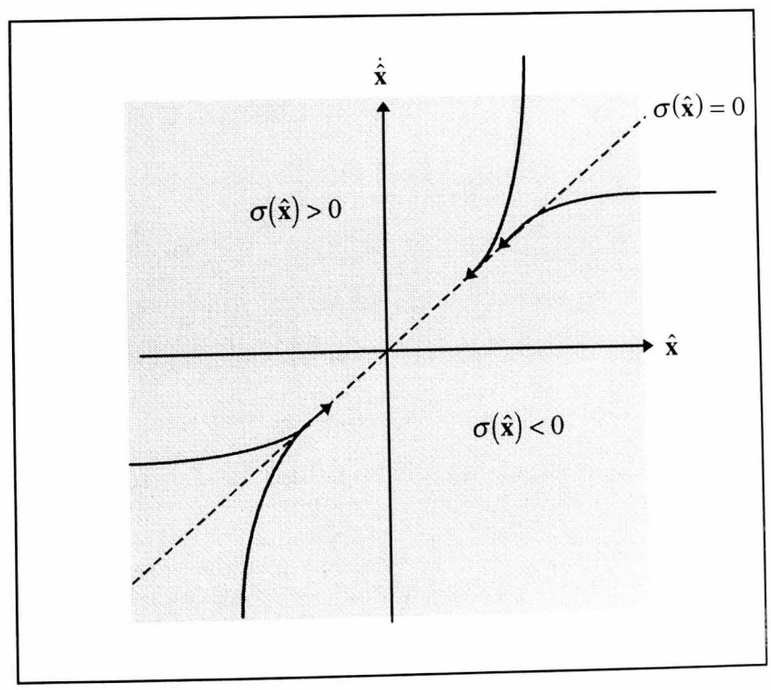

Figure 5.1: Sliding Surface in State-Space

Hence the actual state converges to the desired state as in the model reference type of control system. The surface chosen for this application is defined by the following equation [Healey and Marco (1992), Healey and Lienard (1993), M^{c}Gookin (1993)],

$$\sigma(\hat{\mathbf{x}}) = \mathbf{h}^T\hat{\mathbf{x}} = \mathbf{h}^T(\mathbf{x} - \mathbf{x}_d) \tag{5.2}$$

where $\mathbf{h}$ is the right eigenvector of the desired closed loop system matrix $\mathbf{A}_c$ (see section 5.4 for reasoning behind the selection of this vector). In order for the state error to converge to zero, global asymptotic convergence of the surface to a stable equilibrium position should be ensured. This is done by choosing a suitable Lyapunov function $V(\sigma)$ such that Lyapunov's Stability Theorem for time-invariant systems is satisfied [Slotine and Li (1991), Fossen (1994), M^{c}Gookin (1993)] i.e.

Theorem 5.1 : *("Lyapunov's Global Stability Theorem") If a scalar function* $V(\sigma)$ *of a variable* σ *has continuous first order derivatives and satisfies the following conditions*

1. $V(\sigma)$ *is positive definite i.e.* $\quad \forall\sigma \in \Re,\ V(\sigma) \in \Re^+$
2. $\dot{V}(\sigma)$ *is negatively definite i.e.* $\quad \forall\sigma \in \Re,\ \dot{V}(\sigma) \in \Re^-$
3. $V(\sigma) \to \infty$ *as* $\|\sigma\| \to \infty$

then the equilibrium at the origin of this function is globally asymptotically stable.

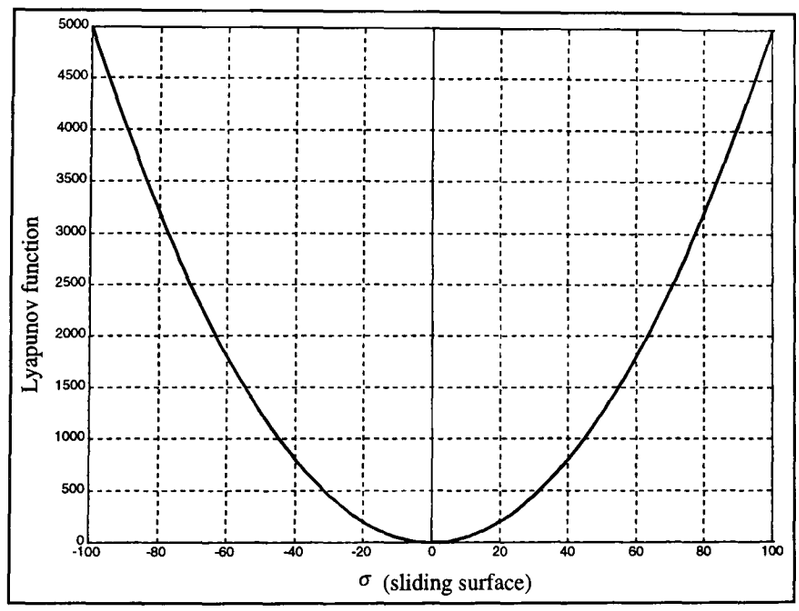

Figure 5.2: Lyapunov Function from equation (5.3) against sliding surface

For this investigation the standard Lyapunov function below is chosen because of its similarity to the equation of kinetic energy and since it provides the 'bowl' like shape needed for such a function [Slotine and Li (1991)].

$$V(\sigma) = \tfrac{1}{2}\sigma^2 \tag{5.3}$$

This gives the curve shown in Figure 5.2. This function satisfies both the first and third convergence conditions of the Theorem 5.1. The first is satisfied since the σ^2 term always give a non-negative value and hence $V(\sigma)$ is lower bounded as required. The third is also easily seen to be satisfied. If the sliding surface is allowed to tend to an infinite value, the value of σ^2 will also tend to infinity. Hence the value of $V(\sigma)$ will tend to infinity as required and the third condition is satisfied.

The remaining condition (i.e. the second) provides a necessary design criterion in order for convergence to occur i.e.

$$\dot{V}(\sigma) = \frac{dV(\sigma)}{dt} = \frac{\partial V(\sigma)}{\partial \sigma}\frac{\partial \sigma}{\partial t} = \frac{\partial\left(\tfrac{1}{2}\sigma^2\right)}{\partial \sigma}\frac{\partial \sigma}{\partial t} = \sigma\frac{d\sigma}{dt} = \sigma\dot{\sigma} < 0 \tag{5.4}$$

Convergence will occur only as long as this is satisfied since a negative gradient will naturally drive the function to the zero sliding surface irrespective of the initial value of V, σ and $\hat{\mathbf{x}}$.

Since all three conditions are met then the origin of the Lyapunov function is considered stable and will converge to that point as time tends to infinity i.e.

$$V(\sigma) \rightarrow 0 \quad \text{as} \quad t \rightarrow \infty \tag{5.5}$$

Therefore,

$$\tfrac{1}{2}\sigma^2 \rightarrow 0 \qquad \Rightarrow \qquad \sigma \rightarrow 0 \quad \text{as} \quad t \rightarrow \infty \tag{5.6}$$

Hence it follows from equation (5.2) that as σ tends to zero the state error will also converge to zero and the states will follow the desired state responses. Therefore, any controller designed round such a sliding surface will converge to a specified desired response. Hence the assurance of stability will allow a controller to guarantee the overall robustness of the system in terms of performance.

5.4 Controller Derivation

The controller is derived from the definition of the linear state space equation of the decoupled dynamics that are being controlled. In order to decouple a system in standard state space form [Healey and Marco (1992), Healey and Lienard (1993), M^{c}Gookin (1993), Fossen (1994), Mudge and Patton (1988(a)(b))]. i.e.

$$\dot{\mathbf{x}} = \mathbf{A}\mathbf{x} + \mathbf{B}\mathbf{u} + \mathbf{f}(\mathbf{x}) \tag{5.7}$$

careful selection of the states to be included in the decoupled subsystem is needed. Here $\mathbf{x}$ is the state vector, $\mathbf{A}$ is the system matrix, $\mathbf{B}$ is the input matrix, $\mathbf{u}$ represents the inputs of the system and $\mathbf{f}(\mathbf{x})$ describes any deviations that would cause the system to deviate from its equilibrium point e.g. nonlinearities, unmodelled dynamics or external disturbances. Unfortunately, such unknown quantities are usually omitted from a linear model of this type and this term is only included here for completeness. The subsystem's states are selected in such a way that the dominant dynamics of the manoeuvre that is being controlled are decoupled from the dynamics that have very little influence on the manoeuvre. This changes the Multi-Input, Multi-State (MIMS) system into as many Single Input, Multi-State (SIMS) systems as are required to be controlled [M^{c}Gookin (1993), Fossen (1994)]. Consider an m state system with n inputs. If this is partitioned into a subsystem with p states and a single input the order of the system and input matrices would be reduced. This would give $\mathbf{A}_s \subset \mathbf{A}$, $\mathbf{b}_s \subset \mathbf{B}$ and $\mathbf{f}_s \subset \mathbf{f}$ as the subsystem equivalent forms of the above state space equation. In turn these would define the subsystem in the following state space form.

$$\dot{\mathbf{x}}_s = \mathbf{A}_s\mathbf{x}_s + \mathbf{b}_s u_s + \mathbf{f}_s(\mathbf{x}_s) \tag{5.8}$$

where $\mathbf{x}_s$ represents the subsystem states and u_s is the single input that governs the subsystem motion.

With most systems the control action is provided via the input to the system which in the SIMS subsystem above is u_s. This control input for a subsystem is provided by equation (5.1) which becomes

$$u_s = u_{eq} + u_{sw} \tag{5.9}$$

Here the nominal equivalent control part is chosen as a state feedback gain controller of the following form [Mudge and Patton (1988(a)(b)), Slotine and Li (1991), M^{c}Gookin (1993), Fossen (1994)].

$$u_{eq} = -\mathbf{k}_s{}^T \mathbf{x}_s \tag{5.10}$$

where $\mathbf{k}_s$ is a feedback gain obtained from pole placement theory. This theory is regarded as robust pole placement theory since it avoids the numerical uncertainties associated with Ackermann's work when applied to systems of higher order than 6 or 7 [Franklin et al (1991)]. Therefore to avoid any such uncertainty the method proposed by Kautsky et al (1985) is used to obtain the feedback gain by minimising the sensitivity of the assigned poles to disturbances within the plant. Since this feedback control law is designed around a nominal linear plant it would not necessarily work well for all the operating conditions of the vessel. Therefore it requires additional control action in order to compensate for variation in the vessel's operating conditions. This additional control is provided by the non-linear switching term of equation (5.9) which is derived from the sliding surface in equation (5.2) i.e.

$$\sigma_s(\hat{\mathbf{x}}) = \mathbf{h}_s{}^T \hat{\mathbf{x}}_s = \mathbf{h}_s{}^T \left(\mathbf{x}_s - \mathbf{x}_{sd} \right) \tag{5.11}$$

On differentiating this equation with respect to time the following is obtained.

$$\dot{\sigma}_s(\hat{\mathbf{x}}) = \mathbf{h}_s{}^T \dot{\hat{\mathbf{x}}}_s = \mathbf{h}_s{}^T \left(\dot{\mathbf{x}}_s - \dot{\mathbf{x}}_{sd} \right) \tag{5.12}$$

Substituting equation (5.8) for $\dot{\mathbf{x}}_s$ in the above equation gives

$$\dot{\sigma}_s(\hat{\mathbf{x}}) = \mathbf{h}_s{}^T \left(\mathbf{A}_s \mathbf{x}_s + \mathbf{b}_s u_s + \mathbf{f}_s(\mathbf{x}_s) - \dot{\mathbf{x}}_{sd} \right) \tag{5.13}$$

and substituting for u_s results in the following equation.

$$\dot{\sigma}_s(\hat{\mathbf{x}}) = \mathbf{h}_s{}^T \left(\mathbf{A}_s \mathbf{x}_s + \mathbf{b}_s u_{eq} + \mathbf{b}_s u_{sw} + \mathbf{f}_s(\mathbf{x}_s) - \dot{\mathbf{x}}_{sd} \right) \tag{5.14}$$

If equation (5.10) is used to replace u_{eq} then the above equation becomes

$$\begin{aligned} \dot{\sigma}_s(\hat{\mathbf{x}}) &= \mathbf{h}_s{}^T \left(\mathbf{A}_s \mathbf{x}_s - \mathbf{b}_s \mathbf{k}_s{}^T \mathbf{x}_s + \mathbf{b}_s u_{sw} + \mathbf{f}_s(\mathbf{x}_s) - \dot{\mathbf{x}}_{sd} \right) \\ &= \mathbf{h}_s{}^T \left(\mathbf{A}_{cs} \mathbf{x}_s + \mathbf{b}_s u_{sw} + \mathbf{f}_s(\mathbf{x}_s) - \dot{\mathbf{x}}_{sd} \right) \end{aligned} \tag{5.15}$$

where

$$\mathbf{A}_{cs} = \mathbf{A}_s - \mathbf{b}_s \mathbf{k}_s^T \tag{5.16}$$

is the closed loop system matrix created by the feedback gain. Hence the eigenvectors of $\mathbf{A}_{cs}$ can be defined in terms of the feedback gain vector. Rearranging (5.15) yields

$$u_{sw} = \left(\mathbf{h}_s^T \mathbf{b}_s\right)^{-1} \left(\mathbf{h}_s^T \dot{\mathbf{x}}_{sd} - \mathbf{h}_s^T \mathbf{A}_{cs} \mathbf{x}_s - \mathbf{h}_s^T \mathbf{f}_s(\mathbf{x}_s) - \dot{\sigma}_s(\hat{\mathbf{x}})\right) \tag{5.17}$$

This assumes that $\mathbf{h}_s^T \mathbf{b}_s$ is nonzero. Since $\mathbf{h}_s^T$ is chosen as the right eigenvector of $\mathbf{A}_{cs}$ it therefore corresponds to an eigenvalue of zero of this matrix. Hence it provides the following relationship

$$\mathbf{h}_s^T \mathbf{A}_{cs} = \left(\mathbf{A}_{cs}^T \mathbf{h}_s\right)^T = 0 \tag{5.18}$$

Therefore (5.17) becomes

$$u_{sw} = \left(\mathbf{h}_s^T \mathbf{b}_s\right)^{-1} \left(\mathbf{h}_s^T \dot{\mathbf{x}}_{sd} - \mathbf{h}_s^T \mathbf{f}_s(\mathbf{x}_s) - \dot{\sigma}_s(\hat{\mathbf{x}})\right) \tag{5.19}$$

From Healey and Marco (1992) and Healey and Lienard (1993) $\dot{\sigma}$ is defined as

$$\dot{\sigma}(\hat{\mathbf{x}}_s) = \mathbf{h}_s^T \Delta \mathbf{f}_s(\mathbf{x}_s) - \eta_s \operatorname{sgn}\left(\sigma(\hat{\mathbf{x}}_s)\right) \tag{5.20}$$

Here $\Delta \mathbf{f}_s(\mathbf{x}_s)$ is the difference between the actual system deviations ($\mathbf{f}_s(\mathbf{x}_s)$) and the estimate made of this function ($\hat{\mathbf{f}}_s(\mathbf{x}_s)$) i.e. $\Delta \mathbf{f}_s(\mathbf{x}_s) = \mathbf{f}_s(\mathbf{x}_s) - \hat{\mathbf{f}}_s(\mathbf{x}_s)$, and η_s is the switching gain which determines the amount of switching control action which characterises this kind of control. The switching action itself is provided by the signum function which simply indicates the sign of the sliding surface [Fossen (1994)] i.e.

$$\operatorname{sgn}\left(\sigma(\mathbf{x}_s)\right) = \begin{cases} 1 & \text{if } \sigma \geq 0 \\ 0 & \text{if } \sigma = 0 \\ -1 & \text{if } \sigma < 0 \end{cases} \tag{5.21}$$

This determines which way the control effort should be applied in order to drive σ and ultimately $\hat{\mathbf{x}}_s$ to zero. The size of this switching action depends on the magnitude of the switching gain.

When (5.20) is applied to (5.19) the following is obtained

$$\begin{aligned} u_{sw} &= \left(\mathbf{h}_s{}^T\mathbf{b}_s\right)^{-1}\left(\mathbf{h}_s{}^T\dot{\mathbf{x}}_{sd} - \mathbf{h}_s{}^T\mathbf{f}_s(\mathbf{x}_s) - \mathbf{h}_s{}^T\Delta\mathbf{f}_s(\mathbf{x}_s) - \eta_s\,\mathrm{sgn}\left(\sigma_s\left(\hat{\mathbf{x}}_s\right)\right)\right) \\ &= \left(\mathbf{h}_s{}^T\mathbf{b}_s\right)^{-1}\left(\mathbf{h}_s{}^T\dot{\mathbf{x}}_{sd} - \mathbf{h}_s{}^T\hat{\mathbf{f}}_s(\mathbf{x}_s) - \eta_s\,\mathrm{sgn}\left(\sigma_s\left(\hat{\mathbf{x}}_s\right)\right)\right) \end{aligned} \tag{5.22}$$

When (5.10) and (5.22) are combined in (5.9) the total controller equation becomes

$$u_s = -\mathbf{k}_s{}^T\mathbf{x}_s + \left(\mathbf{h}_s{}^T\mathbf{b}_s\right)^{-1}\left(\mathbf{h}_s{}^T\dot{\mathbf{x}}_{sd} - \mathbf{h}_s{}^T\hat{\mathbf{f}}_s(\mathbf{x}_s) - \eta_s\,\mathrm{sgn}\left(\sigma_s\left(\hat{\mathbf{x}}_s\right)\right)\right) \tag{5.23}$$

This is not the form of the controller used in this study since the unknown dynamics are either not estimated or the values of $\hat{\mathbf{f}}_s(\mathbf{x}_s)$ are constant. In the latter case, the addition of this term in the controller equation provides a constant bias that allows the controller to have a sufficiently high operating point so as to compensate for the occurrence of unknown dynamic effects. Either way this value is negligible and can be compensated for by making the switching gain sufficiently high. Therefore the form of controller used in this work is [Fossen (1994), M^{c}Gookin (1993), Healey and Marco (1992), Healey and Lienard (1993)]

$$u_s = -\mathbf{k}_s{}^T\mathbf{x}_s + \left(\mathbf{h}_s{}^T\mathbf{b}_s\right)^{-1}\left(\mathbf{h}_s{}^T\dot{\mathbf{x}}_{sd} - \eta_s\,\mathrm{sgn}\left(\sigma_s\left(\hat{\mathbf{x}}_s\right)\right)\right) \tag{5.24}$$

where the switching component compensates for the unknown dynamics of the system without the need for biasing provided by the $\hat{\mathbf{f}}_s(\mathbf{x}_s)$ value.

5.5 Stability Criterion

It was shown in Section 5.3 that by the application of Lyapunov's Theorem the controller will converge to a sliding surface which is stable about the origin equilibrium point. This would indicate that the controller will exhibit stability robustness to changes in the plant or external changes in the system's operating environment. The only condition for global asymptotic stability and convergence to the equilibrium point that has not already been satisfied by the selection of a suitable Lyapunov function is condition 2 i.e.

$$\forall\sigma \in \Re, \quad \dot{V}(\sigma) \in \Re^- \tag{5.25}$$

For this particular study this derivative is represented by equation (5.4). When (5.20) is substituted into this equation the following results.

$$\begin{aligned}\dot{V}(\sigma_s) = \sigma_s\dot{\sigma}_s &= \sigma_s\left(\mathbf{h}_s{}^T\Delta\mathbf{f}(\mathbf{x}_s) - \eta_s\,\mathrm{sgn}(\sigma_s)\right)\\ &= \sigma_s\mathbf{h}_s{}^T\Delta\mathbf{f}(\mathbf{x}_s) - \eta_s\sigma_s\,\mathrm{sgn}(\sigma_s)\\ &= \sigma_s\mathbf{h}_s{}^T\Delta\mathbf{f}(\mathbf{x}_s) - \eta_s|\sigma_s|\end{aligned} \tag{5.26}$$

This equation should satisfy the stability condition.

$$\dot{V}(\sigma_s) = \sigma_s\mathbf{h}_s{}^T\Delta\mathbf{f}(\mathbf{x}_s) - \eta_s|\sigma_s| < 0 \tag{5.27}$$

On rearranging we get

$$\eta_s > \mathbf{h}_s{}^T \cdot \Delta\mathbf{f}(\mathbf{x}_s) \tag{5.28}$$

Since the switching action has to operate in opposition to the sliding surface, the switching gain must be positive. Therefore the above equation becomes:

$$\eta_s > \left\|\mathbf{h}_s{}^T\right\| \cdot \left\|\Delta\mathbf{f}(\mathbf{x}_s)\right\| \tag{5.29}$$

which will ensure that condition 2 is satisfied and stability occurs. Therefore, in order to insure that this type of Sliding Mode controller is stable and robust to changes, the switching gain must be greater than this value i.e. large enough to handle any deviations from the plant's nominal operating point.

5.6 Desired State Tracking

The previous section shows that the decoupled SM controllers used in this investigation are able to meet Lyapunov's three criteria for stability and robustness. From this it can be deduced that the equilibrium point for the chosen Lyapunov function is when the sliding surface is zero. Hence

$$\sigma_s \to 0 \quad \text{as} \quad t \to \infty \tag{5.30}$$

and consequently

$$\hat{\mathbf{x}}_s \to 0 \quad \text{as} \quad t \to \infty \tag{5.31}$$

This indicates that the system's states track to the desired states' responses as $t \rightarrow \infty$ which is the required behaviour of the control system.

Therefore, as long as the design criterion for η_s is satisfied in order to ensure global asymptotic convergence, then perfect tracking of the desired state responses is achieved. Hence the controller will behave as a model reference controller [Landau (1974)].

5.7 Chattering

A problem arises from the need to make the switching large enough to satisfy the robustness criteria. Due to the nature of the signum function, the switching action may cause the control input to start oscillating about the zero sliding surface. This phenomena is called *chattering* and it's presence can cause unwanted wear and tear in the input actuators of the system [Burton and Zinober (1988), Slotine and Li (1991), Healey and Marco (1992), Healey and Lienard (1993), Fossen (1994), M^{c}Gookin (1993)]. It may also cause the system to become unstable if the amplitude of the chatter is large. In either instance chattering causes the system's performance to deteriorate until it no longer tracks the desired state response.

The way to remove this behaviour is to smooth out the switching term as the sliding surface approaches zero. This is done by replacing the signum function with a saturation function [Healey and Marco (1992), Healey and Lienard (1993), Fossen (1994), M^{c}Gookin (1993)] i.e.

$$\text{sat}\left(\frac{\sigma_s(\mathbf{x}_s)}{\phi_s}\right) = \begin{cases} \text{sgn}\left(\sigma(\mathbf{x}_s)\right) & \text{if } \dfrac{\sigma_s}{\phi_s} \geq 1 \\ \dfrac{\sigma_s}{\phi_s} & \text{otherwise} \end{cases} \tag{5.32}$$

Here ϕ_s is called the boundary layer thickness and defines the range about the zero sliding surface where the switching term transition is smoothed. This term acts like a low pass filter and is the reason that this is called *soft switching*.

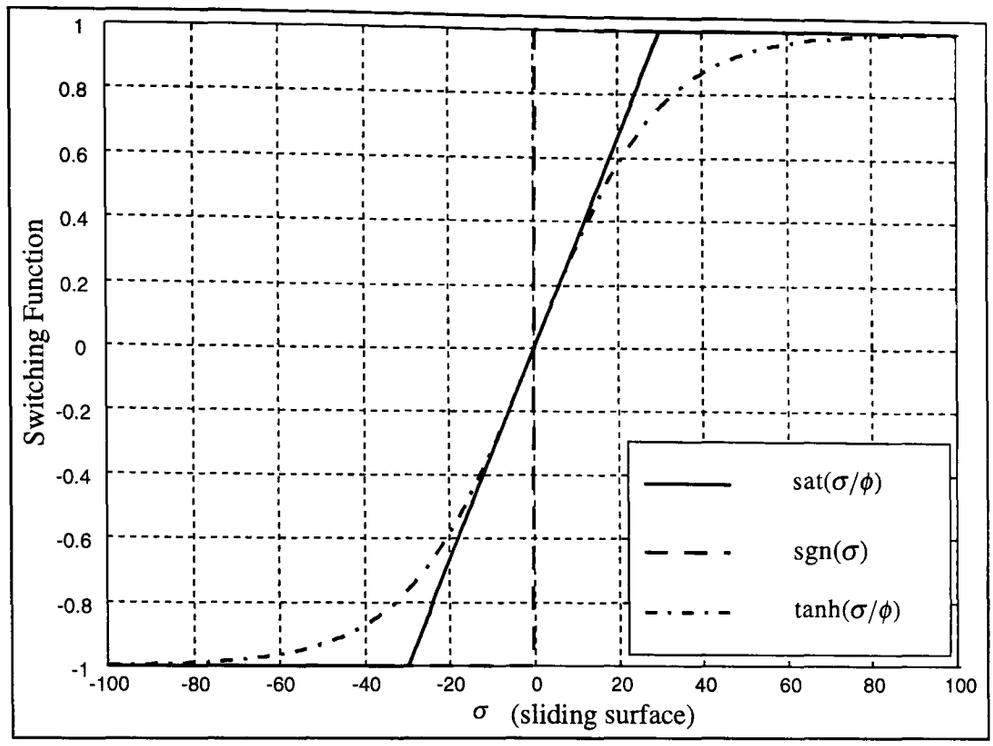

Figure 5.3: Switching Functions with Boundary Layer Thickness $\phi = 30$

Alternatively, the continuous tanh function provides the same type of switching transition without having any of the discontinuities of the saturation function. The behaviour of all three switching functions is illustrated in Figure 5.3 [Healey and Marco (1992), Healey and Lienard (1993), Fossen (1994), M^{c}Gookin (1993)]. The similarity between the saturation and hyperbolic tan functions should be noted. Hence the controller equation becomes

$$u_s = -\mathbf{k}_s{}^{\mathrm{T}}\mathbf{x}_s + \left(\mathbf{h}_s{}^{\mathrm{T}}\mathbf{b}_s\right)^{-1}\left(\mathbf{h}_s{}^{\mathrm{T}}\dot{\mathbf{x}}_{sd} - \eta_s \tanh\left(\sigma_s\left(\hat{\mathbf{x}}_s\right)/\phi_s\right)\right) \tag{5.33}$$

This form of controller equation is used in the investigation. The use of the tanh function removes chattering if the boundary layer thickness is sufficiently large to counteract the large switching action.

5.8 Stability in the Boundary Layer

It is self evident that if the controller reaches the boundary layer robustness is guaranteed since the switching area outside this region is effectively the signum function which is globally asymptotically stable. However the boundary layer should also be shown to be stable and robust.

If the saturation function is considered then the boundary layer can be examined clearly. This is more difficult with the tanh function due to the transition between the boundary layer and the hard switching region. However the following argument holds equally well for the continuous tanh function.

Outside the boundary layer the saturation function equals the hard switching signum function and therefore the previous stability criterion is applied in this region (see Section 5.5).

Inside the boundary layer the saturation function equals the sliding surface divided by the boundary layer thickness i.e.

$$\text{sat}\left(\sigma_s / \phi_s\right) = \frac{\sigma_s}{\phi_s} \tag{5.34}$$

Therefore to prove stability in this region we use the same strategy as in Section 5.5.

$$\begin{aligned}\dot{V}(\sigma_s) = \sigma_s\dot{\sigma}_s &= \sigma_s\left(\mathbf{h}_s{}^T\Delta\mathbf{f}(\mathbf{x}_s) - \eta_s\frac{\sigma_s}{\phi_s}\right)\\ &= \sigma_s\mathbf{h}_s{}^T\Delta\mathbf{f}(\mathbf{x}_s) - \eta_{sbl}\sigma_s\frac{\sigma_s}{\phi_s}\\ &= \sigma_s\mathbf{h}_s{}^T\Delta\mathbf{f}(\mathbf{x}_s) - \eta_{sbl}\frac{\sigma_s{}^2}{\phi_s}\end{aligned}$$

This means that in order to ensure that stability is satisfied

$$\begin{aligned}\eta_{sbl}\frac{\sigma^2}{\phi} &> \sigma\mathbf{h}^T\Delta\mathbf{f}(\mathbf{x}_s)\\ \eta_{sbl} &> \frac{\phi}{\sigma}\mathbf{h}^T\Delta\mathbf{f}(\mathbf{x}_s)\end{aligned} \tag{5.35}$$

Since $\sigma \le \phi$ in the boundary layer and $\phi/\sigma \ge 1$

$$\eta_{sbl} \ge \eta_s \tag{5.36}$$

where η_s is the switching gain outside the boundary layer. Therefore, if the stability condition outside the boundary layer is met sufficiently well the condition inside is automatically satisfied since it is within the required range of the switching gain in this region. However, if it is not, the system still remains stable since the confining area outside the boundary layer is stable and will therefore drive the state error towards zero. That means that the outside condition satisfies Lyapunov stability globally. Hence the

boundary layer does not affect the stability of the sliding mode controller. If anything the boundary layer ensures convergence onto the $\sigma = 0$ surface which in turn ensures perfect tracking and stability in the steady state.

The above holds for the case where the saturation function is replaced by the hyperbolic tan function (tanh). This removes the discontinuities which are inherent in the sat and sgn functions without jeopardising the stability of the controller.

5.9 Summary

The decoupled controller form derived in this chapter (equation (5.33)) is used in the applications studied in the remainder of this investigation. It has been proven that this control law is globally asymptotically stable throughout the state space. Therefore if it is global then the controller is said to be robust since it will return to an asymptotic steady state at the origin, no matter what the initial conditions of the states are or what perturbations the states may encounter. Hence this will be the case as long as the stability criteria of equation (5.29) is satisfied.

This controller is implemented in the three marine applications considered in the following chapters (i.e. submarine, tanker and ship). These are used as the optimisation subjects for the remainder of this thesis.

Chapter 6:

Submarine Application

6.1 Introduction

The first application used to study both the sliding mode control law and the optimisation techniques is a linear mathematical model of a military submarine. This type of vehicle can move in three dimensions and has motion in six degrees of freedom (i.e. both lateral and rotational for each dimension) [Burcher and Rydell (1993)].

The mathematical representation of the vessel used in this study describes the motion of a generic 'cigar shaped' submarine [Miliken (1984)] which is approximately 100 metres in length and designed to be highly manoeuvrable. It has similar operational statistics to the Los Angeles, Trafalgar and Swiftsure classes that are in service at present [Richardson et al (1991)]. These high speed submarines perform as 'hunter-killers' in that their role is to seek and destroy adversarial vessels. The need for adequate control of these vessels is crucial, particularly at high speeds, so that they can execute their manoeuvres without causing damage to the crew or any innocent party. This is of particular importance during a war situation when accuracy and stealth are needed in order that the vessel and crew can carry out their mission without detection or destruction. In this study the manoeuvres considered are relatively slow compared to the capability of such a vessel and are therefore considered to be carried out under coercive conditions.

Although these vessels are used for defence, the principals used in this investigation can be equally applied to commercial submersibles and Remotely Operated Vehicles (ROVs) since they have characteristics broadly similar to the above [Healey and Marco (1992), Healey and Lienard (1993), Trebi-Ollennu and White (1996 (a)(b)), Corradini and Orlando (1997)].

The model used here is linearised about a single operating point of 20kts forward speed. The representation is a linear state space model which simplifies the dynamics of the system. This simplified model can be easily applied to the sliding mode (SM) control law in Chapter 5 and as a result of its relatively fast dynamic responses is a good

candidate for testing the optimisation methods (Chapters 3 and 4). It also provides a six-degrees of freedom system which can be easily split into two subsystems to be controlled i.e. depth changing and heading changing. Hence two controllers (one for depth and one for heading) have to be designed and then optimised. This will allow the effect of the controller decoupling action to be observed in the context of dynamic cross-coupling.

This chapter deals with the application of these controllers and the parameter optimisation process that follows. In Section 6.2 , the derivation of this model is briefly given from the equations of motion to its linear state space representation. The decoupling process and application of the sliding mode control law of the previous chapter is detailed in Section 6.3, thus giving the two controller structures necessary for this study. Section 6.4 gives the results of the study of this system by firstly providing a manually tuned set of parameter solutions as a benchmark for comparison. The remainder of that section illustrates the results obtained from the various optimisation methods. Conclusions regarding the comparison of the results obtained from this optimisation study are summarised in Section 6.5.

6.2 Submarine Model in State Space Form

6.2.1 Submarine Dynamics

The linear state space model form used to represent this submarine is derived from the equations of motion of the vessel. These are obtained by considering the motion of the submarine relative to body-fixed axes and to some inertially fixed reference frame (i.e. the earth). These motions are defined in terms of the velocities illustrated in Figure 6.1 where the dynamics are split into linear and angular for both the body and earth fixed reference frames [Fossen (1994), M^{c}Gookin (1993)]. It should be noted that this representation is defined in deep water and the ballast system is not modelled. Therefore the resulting model should not be used for simulations near to the surface of the sea where the ballast dynamics would effect the motion of the vessel. Also, effects from the depth of water beneath the vessel are neglected.

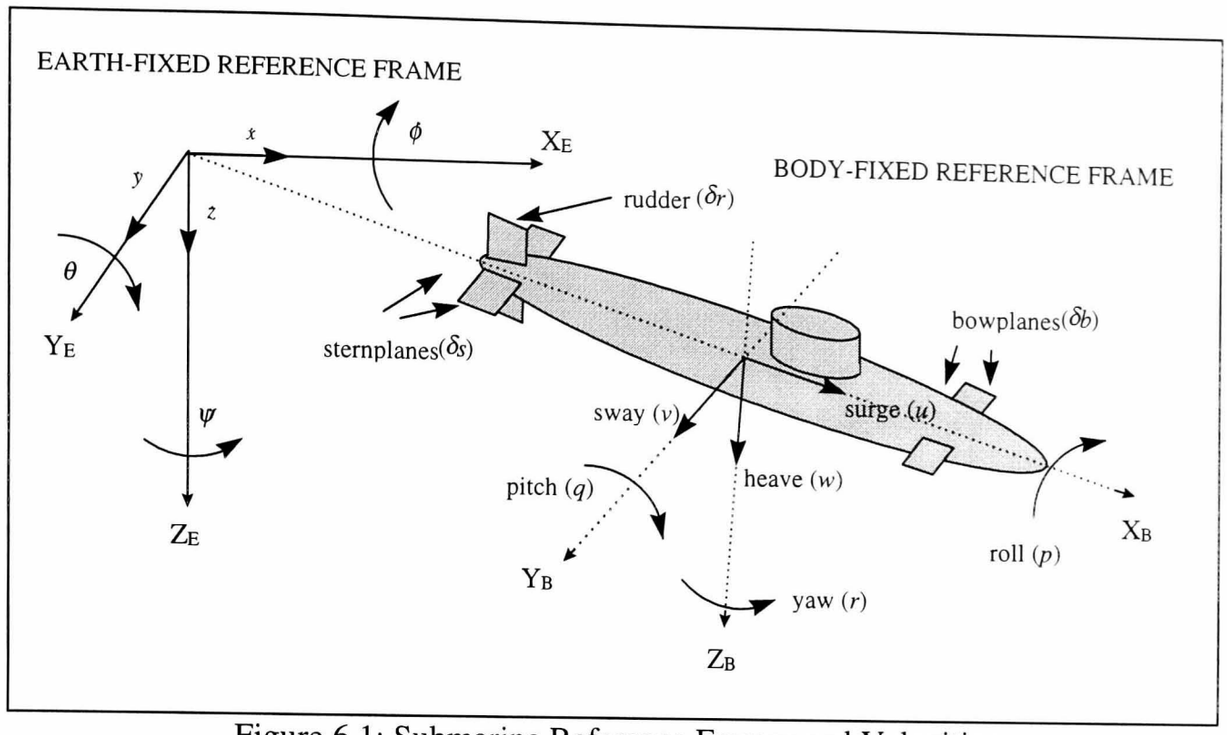

Figure 6.1: Submarine Reference Frames and Velocities

The relative velocities and inputs illustrated above are outlined in the table below. In this study the aft hydroplanes are referred to as the *sternplanes* and the fore hydroplanes are called the *bowplanes*.

Table 6.1: Submarine States and Inputs

STATES		INPUTS	
u	surge velocity	δb	bowplane deflection
v	sway velocity	δs_P	port sternplane deflection
w	heave velocity	δs_S	starboard sternplane
p	roll rate	δr	rudder deflection
q	pitch rate		
r	yaw rate		
ϕ	roll angle		
θ	pitch angle		
ψ	yaw (heading) angle		
z	diving depth		

The reference frames provide two separate sets of equations which describe their relative dynamics. These are the *kinetic* and *kinematic* equations. The kinetic equations define the hydrodynamics of the vessel in the body-fixed reference frame and are represented by the following matrix equation [Fossen (1994)].

$$\mathbf{M}\dot{\boldsymbol{\nu}} + \mathbf{C}(\boldsymbol{\nu})\boldsymbol{\nu} + \mathbf{D}(\boldsymbol{\nu})\boldsymbol{\nu} + \mathbf{G}(\boldsymbol{\eta})\boldsymbol{\eta} = \mathbf{B}'\mathbf{u} \tag{6.1}$$

Here **M** is the mass and inertia matrix, **C** contains the Coriolis terms, **D** is the damping matrix, **G** is gravitational and buoyancy components and **B′** relates the inputs to the system. The vector $\boldsymbol{\nu}$ represents the body-fixed velocities (i.e. $\boldsymbol{\nu} = [u, v, w, p, q, r]^T$), $\boldsymbol{\eta}$ represents the earth-fixed states (i.e. $\boldsymbol{\eta} = [x, y, z, \phi, \theta, \psi]^T$) and **u** is the input vector (i.e. $\mathbf{u} = [\delta r, \delta s, \delta b,]^T$) [Miliken (1984), Fossen (1994), M^{c}Gookin (1993), Burcher and Rydell (1993)]. From Table 6.1 it can be seen that the only earth-fixed distance modelled here is the diving depth, z (i.e. x and y are not considered). Hence the resulting model will be a tenth order system representation instead of twelfth order [Miliken (1984), M^{c}Gookin (1993), M^{c}Gookin et al (1996(a)(b), 1997(b)(d))].

The kinematic equations define the geometrical relationship of the motion of the vessel relative to the earth-fixed frame of reference. These are represented by the following equation:

$$\dot{\boldsymbol{\eta}} = \mathbf{J}(\boldsymbol{\eta})\boldsymbol{\nu} \tag{6.2}$$

Where **J** represents the Euler relationships between the two reference frames [Fossen (1994), M^{c}Gookin (1993)].

In order to obtain a linear representation from these equations they are linearised around a nominal operating condition. This treats each state as a relatively small perturbation about an equilibrium operating point. The linearisation process outlined in M^{c}Gookin (1993) yields the following linear equations.

$$\mathbf{M}\dot{\boldsymbol{\nu}} + (\mathbf{C}' + \mathbf{D}')\boldsymbol{\nu} + \mathbf{G}'\boldsymbol{\eta} = \mathbf{B}'\mathbf{u} \tag{6.3}$$

$$\dot{\boldsymbol{\eta}} = \mathbf{J}_1'\boldsymbol{\nu} + \mathbf{J}_2'\boldsymbol{\eta} \tag{6.4}$$

The equilibrium operating point chosen is a surge velocity of 20kts with all other states set to zero. Rearranging (6.3) yields

$$\dot{\boldsymbol{\nu}} = -\mathbf{M}^{-1}(\mathbf{C}' + \mathbf{D}')\boldsymbol{\nu} - \mathbf{M}^{-1}\mathbf{G}'\boldsymbol{\eta} + \mathbf{M}^{-1}\mathbf{B}'\mathbf{u} \tag{6.5}$$

When equations (6.4) and (6.5) are combined together the following matrix form is produced

$$\begin{bmatrix} \dot{\boldsymbol{\nu}} \\ \dot{\boldsymbol{\eta}} \end{bmatrix} = \begin{bmatrix} -\mathbf{M}^{-1}(\mathbf{C}' + \mathbf{D}') & -\mathbf{M}^{-1}\mathbf{G}' \\ \mathbf{J}_1 & \mathbf{J}_2 \end{bmatrix} \begin{bmatrix} \boldsymbol{\nu} \\ \boldsymbol{\eta} \end{bmatrix} + \begin{bmatrix} \mathbf{M}^{-1}\mathbf{B}' \\ \mathbf{0} \end{bmatrix} \mathbf{u} \tag{6.6}$$

This is easily seen to be the standard state space form similar to that described in equation (5.8) i.e.

$$\dot{\mathbf{x}} = \mathbf{A}\mathbf{x} + \mathbf{B}\mathbf{u} \tag{6.7}$$

A more detailed derivation of these equations can be found in McGookin (1993) and Fossen (1994) (see Appendix A.1 for model definition).

6.2.2 Input Actuator Dynamics

As well as the dynamics of the submarine which come from the hydrodynamics of the vessel, the input actuator dynamics are also defined. These apply physical rate and amplitude limits to all the input actuators which represent the limits on the hydroplanes due to their actual driving mechanisms. Firstly the rate limit is defined as the angle that the input can move through in one second. The input amplitude limit is the maximum angular deflection of that actuator. Values for both these constraints were obtained from Curtis (1996) and Lambert (1996). The values obtained for each of the actuators are show in Table 6.2 and represent typical figures which would apply to real submarines.

Table 6.2: Actuator Limit Values

ACTUATOR	RATE LIMIT (°/sec)	MAGNITUDE LIMIT (°)
RUDDER	5	35
STERNPLANE	5	25
BOWPLANE	5	20

These limits are used in this simulation study for limits on the corresponding actuators and add nonlinearities to the system in the form of actuator saturation.

6.3 Decoupled Subsystems

As mentioned in the previous chapter, the sliding mode controllers used in the investigation are applied to SIMS systems [Fossen (1994)]. This calls for decoupling MIMO into the appropriate form that was illustrated in Section 5.4. In this application the submarine system is decoupled into two subsystems (i.e. diving and heading) which are the only controllable dynamics that are considered here.

The third major dynamic is the roll motion of the vessel which is not usually controlled due to the position of the centres of gravity and buoyancy relative to each other [Burcher and Rydell (1993)]. Although these vessels are neutrally buoyant (i.e. the centres of gravity and buoyancy occupy the same point in the x-axis, $x_g = x_b$) their positions in the Z_B axis are not equal. In fact $z_b > z_g$ and the centre of buoyancy is above the centre of gravity. This is shown in Figure 6.2. It can be seen that if the centre of buoyancy moves relative to a fixed inertial reference during a manoeuvre (i.e. the vessel rolls), the centre of mass will force the centre of buoyancy back to an equilibrium point directly above it thus causing this motion to be stable about a zero roll. Hence this motion is self correcting and does not need to be controlled.

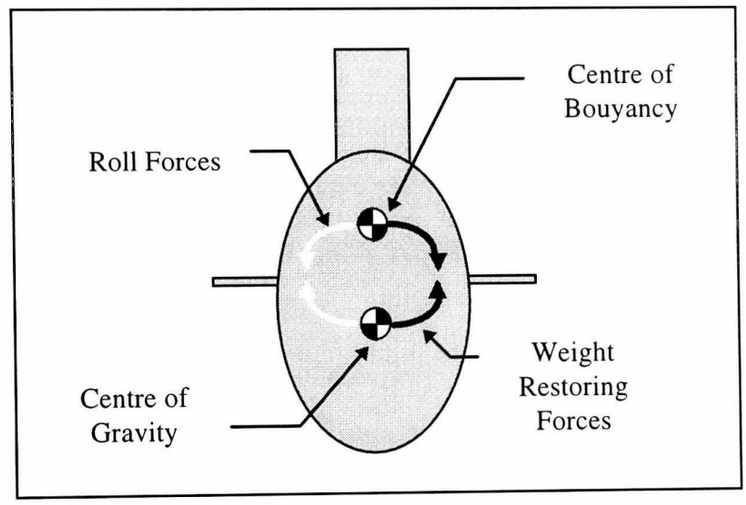

Figure 6.2: Roll Motion Stabilisation

The decoupling process for each of the two subsystems is described below.

6.3.1 Diving Subsystem

As the name suggests, the diving subsystem describes the depth motion of the submarine which is only concerned with the dynamics in the X_B-Z_B plane in deep water (see Figure 6.3). This diagram shows that only four states comprise this subsystem and therefore it is a fourth order system reduced from the original tenth order submarine representation. These states are w, q, θ and z. Table 6.1 shows that this motion can be controlled by two input actuators (i.e. sternplanes or bowplanes). However, in practical situations when submarines of this type operate at high speed, depth is governed by the sternplanes. The bowplanes are kept in the *fixed stick* position (i.e. at a deflection of zero degrees) [Burcher and Rydell (1993)].

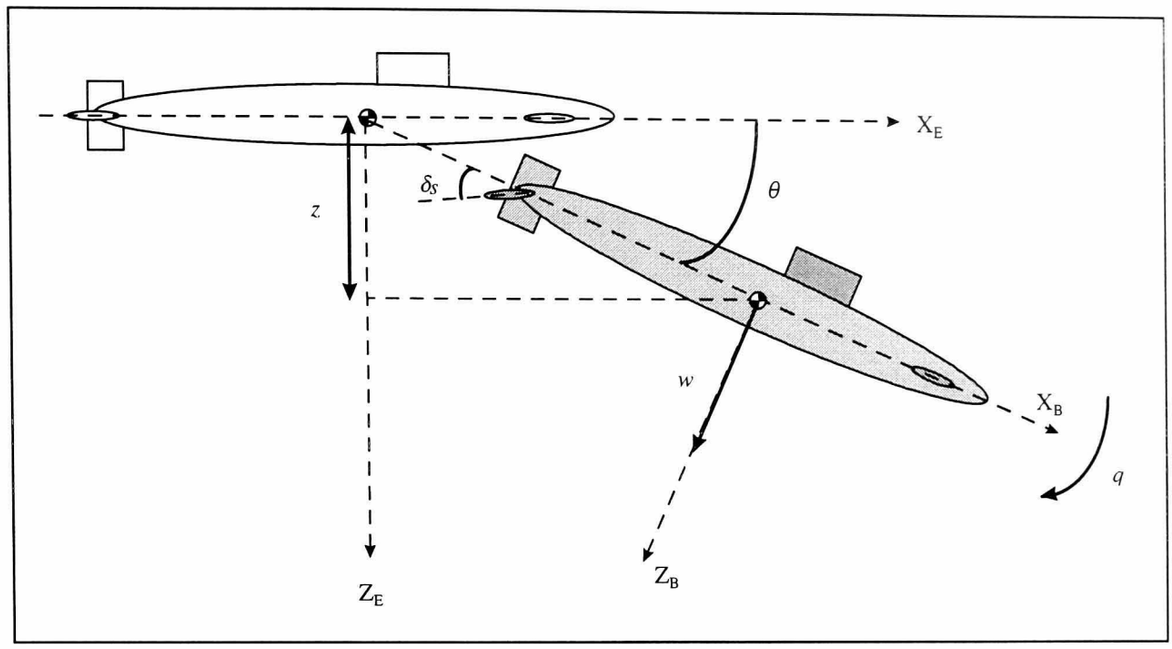

Figure 6.3: Diving Manoeuvre

However, in this representation of a submarine the sternplanes can be moved differentially as well as together. The differential motion is used to regulate the roll of the vessel which is not controlled in this application. Therefore the sternplanes are solely used for this diving manoeuvre. Since there are two sternplane deflections associated with the port and starboard actuators (i.e. δs_P and δs_S), the corresponding control effort is split between them. This means that the sum of the two input signals becomes the single input for this subsystem [M^{c}Gookin (1993)]. Hence, decoupling this motion gives the following state-space equation for this subsystem.

$$\dot{\mathbf{x}}_D = \mathbf{A}_D\mathbf{x}_D + \mathbf{b}_D\left(\delta s_P + \delta s_S\right)$$
$$\dot{\mathbf{x}}_D = \mathbf{A}_D\mathbf{x}_D + \mathbf{b}_D u_D \tag{6.8}$$

where $\mathbf{x}_D = [w,\ q,\ \theta,\ z]^T$ and u_D is the resulting input. Since the sternplanes work together in this manoeuvre, the value of the port sternplane deflection is equal to the deflection of the starboard sternplane and thus

$$u_D = \delta s_P + \delta s_S = 2\delta s \tag{6.9}$$

where δs is the sternplane deflection. This implies that the control effort should be divided equally between the two inputs and enables this subsystem to be treated as a SISO system. Hence a decoupled sliding mode controller of the form outlined in the previous chapter (equation (5.33)) can be applied thus giving the following equation.

$$u_D = -\mathbf{k}_D{}^{\mathrm{T}}\mathbf{x}_D + \left(\mathbf{h}_D{}^{\mathrm{T}}\mathbf{b}_D\right)^{-1}\left(\mathbf{h}_D{}^{\mathrm{T}}\dot{\mathbf{x}}_{D\mathrm{d}} - \eta_D \tanh\left(\sigma_D(\hat{\mathbf{x}}_D)/\phi_D\right)\right) \tag{6.10}$$

The desired states ($\mathbf{x}_{Dd}$) are obtained from a second order response for the major dynamics. In this case that is the depth response. The simulation of this system is illustrated in more detail in M^{c}Gookin (1993).

In order to ensure that this controller is performance robust, the condition set out in equation (5.29) is applied. Since the system representation used in this investigation does not illustrate any non-linear uncertainties the switching gain condition becomes

$$\eta_D > 0 \tag{6.11}$$

Therefore as long as the gain is positive definite the controller will be considered robust. This is easily incorporated into the optimisation techniques by confining their search to positive values. If estimates of nonlinearities became available these could also be incorporated in the optimisation process by limiting the search to values greater than these estimates.

6.3.2 Heading Subsystem

The heading subsystems describes the motion in the X_B-Y_B plane (see Figure 6.4) and represents the directional motion of the submarine. The control of this motion is more generally called *course changing* and comes from the regulation of the heading angle, ψ, by manipulation of the rudder actuator deflection, δr. This subsystem decouples to a third order system with v, r and ψ as the states.

Decoupling this motion from the rest of the submarine dynamics gives a SISO system with the rudder deflection, δr, as the input. This has the following state space form

$$\dot{\mathbf{x}}_H = \mathbf{A}_H\mathbf{x}_H + \mathbf{b}_H\delta r \tag{6.12}$$

where the state vector, $\mathbf{x}_H = [v,\ v,\ \psi]^{\mathrm{T}}$. From this representation of the subsystem a similar controller equation to the diving manoeuvre can be formed thus.

$$\delta r = -\mathbf{k}_H{}^{\mathrm{T}}\mathbf{x}_H + \left(\mathbf{h}_H{}^{\mathrm{T}}\mathbf{b}_H\right)^{-1}\left(\mathbf{h}_H{}^{\mathrm{T}}\dot{\mathbf{x}}_{H\mathrm{d}} - \eta_H \tanh\left(\sigma_H(\hat{\mathbf{x}}_H)/\phi_H\right)\right) \tag{6.13}$$

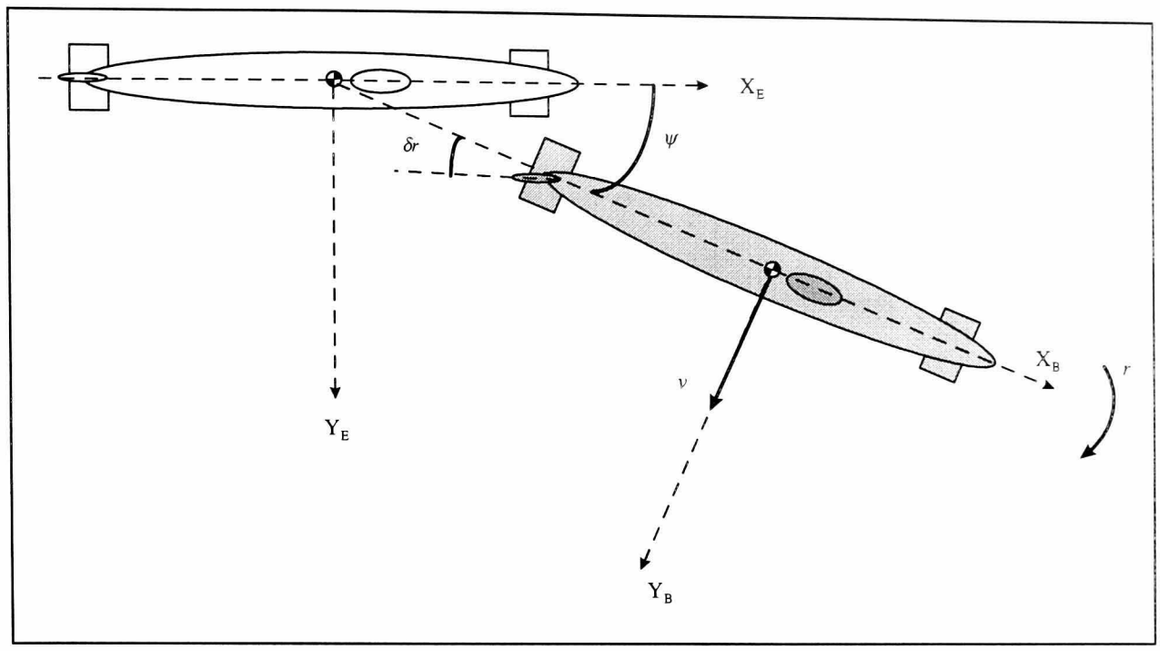

Figure 6.4: Course Changing Manoeuvre

Again the desired states are formed so that the controller will attempt to follow a second order response. Hence the course changing manoeuvre is controlled by regulation of the heading angle by means of the rudder actuator.

Since uncertainties are also not modelled in this subsystem, the same condition for robustness as in the diving subsystem can be applied i.e.

$$\eta_H > 0 \tag{6.14}$$

This is fulfilled during optimisation by confining the search to positive gain values.

6.3.3 Decoupled Controller Application to the Main System

As the previous sections illustrated, the input signals to the actuators of the submarine model are calculated separately for each of the manoeuvres considered here. These provide inputs for the rudder and the sternplanes when the bowplane deflection is zeroed at the fixed stick position [Burcher and Rydell (1993)]. Although these commanded actuator inputs are obtained for their relative subsystems, they are combined as elements of the input vector, **u**, for the full representation of the submarine system (see Figure 6.5). However, before these commanded signals are applied to the model, they are passed through rate and amplitude limit checks which implement the

actuator limits shown in Table 6.2. These slow the response of the inputs to a realistic level and add a non-linear aspect to the system.

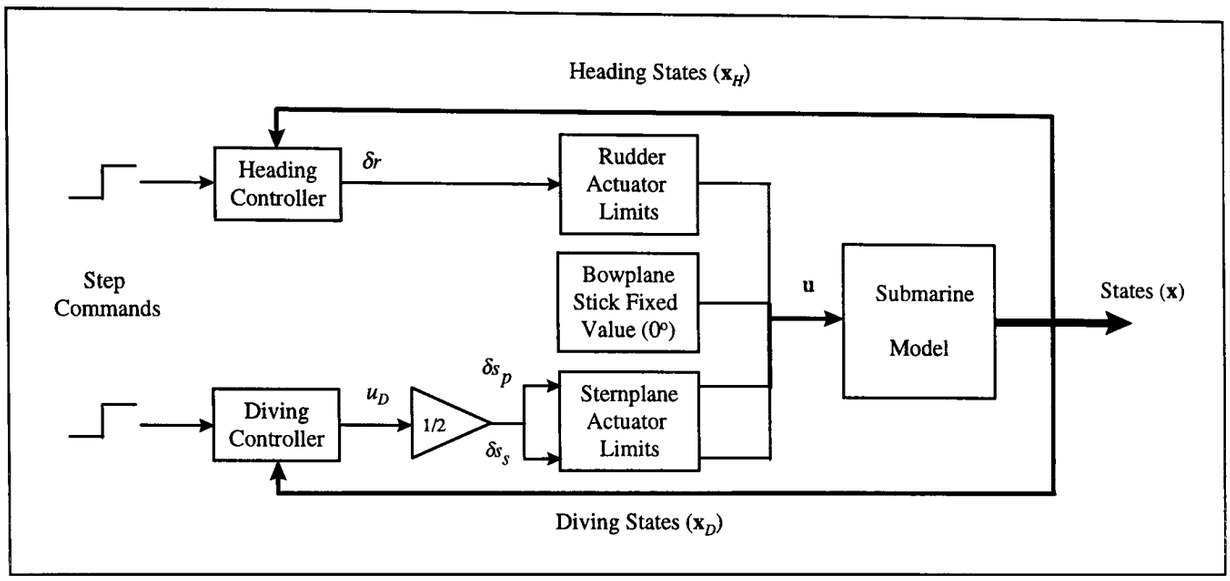

Figure 6.5: Submarine Model and Controller Configuration

This configuration is used as a schematic for simulating this system. In the resulting simulations the states are obtained from the state space equation by Euler's numerical integration method [Cheney and Kincaid (1985)]. This is used because of its speed of execution. If the step size is chosen so that it satisfies the time constant of the fastest of the two motions, no simulation instability should occur [Fossen (1994)]. However, if during the optimisation process such instability occurs then there is the chance that the control action is moving too fast for the system and may cause problems in a practical situation.

6.4 Optimisation Process and Results

This section outlines the aspects of the optimisation process used to investigate the diving and heading controllers for the submarine which are the same irrespective of the method used. These elements are specific to the optimisation subject and not the individual techniques and include controller parameters which are chosen for optimisation, the cost functions and desired responses that are used as the optimisation manoeuvres.

The remainder of this section is concerned with the presentation of typical optimised results obtained from this investigation. The first set of controller parameters are from

manually tuned responses that have been obtained through engineering judgement and a certain amount of trial and error [M^{c}Gookin (1993)]. This set is used as a benchmark against which the optimised results can be compared. Typical optimised results from SA, SSA and GA searches are presented and discussed in terms of controller performance, search convergence and optimal cost values.

6.4.1 Controller Parameters

The first aspect that needs to be defined is the particular set of controller parameters which are to be optimised by the methods investigated here. These parameters are altered until the two controllers provide the control action desired of them. In this case the nine associated parameters shown in Table 6.3 are used [M^{c}Gookin (1993), Fossen (1994), Healey and Marco (1992), Healey and Lienard (1993)].

Table 6.3: Submarine Controller Parameters to be optimised

Diving Parameters		Heading Parameters	
First Closed loop pole	*pd1*	First Closed loop pole	*ph1*
Second Closed loop pole	*pd2*	Second Closed loop pole	*ph2*
Third Closed loop pole	*pd3*		
Switching Gain	η_D	Switching Gain	η_H
Boundary Layer Thickness	ϕ_D	Boundary Layer Thickness	ϕ_H

As this table indicates, parameters *pd1..pd3* are three of the desired closed loop poles of the diving subsystem and *ph1* and *ph2* are two of the desired closed loop poles of the heading subsystem. Each subsystem has another pole positioned at the origin [M^{c}Gookin (1993)]. These poles are used to define the closed loop system matrix for each subsystem (i.e. $\mathbf{A}_C$). Once this matrix is defined, key vectors (i.e. **k** and **h**) can be obtained which are crucial to the controller definitions given in equations (6.10) and (6.13).

The other two sets of parameters are the switching gains and boundary layer thickness for each SM controller [Slotine and Li (1991), Healey and Marco (1992), Healey and Lienard (1993)]. As already mentioned the switching gains define the amplitude of the switching action provided by these controllers and the boundary layer thickness ensure smooth transition as the zero sliding surface is approached (see Chapter 5).

All these parameters are crucial to the optimisation as they provide values for all the constituent parts of the controllers.

6.4.2 Cost Function and Desired Responses

The most important aspect of any optimisation process is the criterion upon which the search is to be based. In practical applications this can be quite difficult to quantify mathematically and can sometimes be represented erroneously thus causing the search method to optimise to an incorrect criterion. In this investigation the optimisation criteria are represented in a single *cost function* which provides a single objective for the optimisation processes. The value of the cost varies with the parameters values and thus defines the problem *search space*. The search space represents the terrain for the optimisation to explore and contains the global optimum solution for the problem. Therefore the cost function choice not only defines the specifications to which the problem is optimised, but it also determines how difficult the problem is to optimise (i.e. if the cost criteria vary randomly the search space will be rough and hence more difficult to optimise than a smoother search space). After careful consideration, the particular cost function used here is a well established autopilot cost function used in the marine field [Dove and Wright (1991)] which is minimised to achieve an optimal system. This function is fundamentally a discrete version of the integral least squares criterion i.e.

$$C = \sum_{i=1}^{tot} \left[(\Delta y_i)^2 + (u_i)^2 \right] \tag{6.15}$$

Here *tot* is the total number of iterations, Δy_i is the ith output error between the desired and obtained outputs (in this case the outputs are either z (depth) or ψ (heading angle)), u_i is the ith input to the submarine (which is either sternplane deflection, δs , or rudder deflection, δr). It should be noted that a separate cost function is required to optimise each subsystem. The reasons for using Δy and u in the cost function are as follows. The quantity Δy (output error) gives an indication of how close the actual output is to the desired output, therefore showing how well the controllers are working. The component u (input to the system) is used to keep controller actuator movement and control effort to a minimum. This is of particular importance when the submarine is trying to execute covert manoeuvres. In these circumstances the actuator motion has to be kept to a

minimum in order to reduce cavitation noise which would make the submarine easy to detect. However restricted actuator usage results in large rise times in the output response since the movement is limited. Another reason for keeping the inputs small is to prevent the SM controllers from chattering (see Section 5.7). This is undesirable due to the high level of actuator activity which results in undue wear and tear [Burton and Zinober (1988), Slotine and Li (1991), M^{c}Gookin (1993), Healey and Marco (1992)].

In addition to the definition of the cost function the optimisation must be given a desired output response for the controllers to track. These are used as the desired states for the controller and to calculate the state errors (see Chapter 5). A consequence of this is that the output errors are obtained and used as a design criterion in the above cost function.

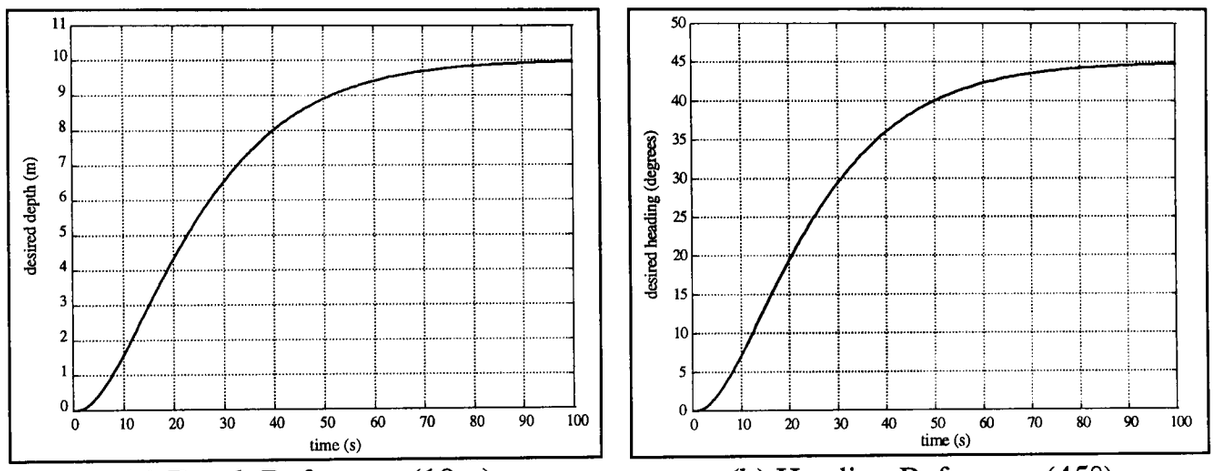

(a) Depth Reference (10m) (b) Heading Reference (45°)

Figure 6.6: Submarine Desired Responses

The chosen desired responses for depth and heading are critically damped steps with sufficient rise times so that the required inputs are well within the operational limits of the actuators involved (see Table 6.2). The amplitudes of the step for depth is chosen as 10m for this study (see Figure 6.6(a)) and the heading change is selected to be a 45° turn (see Figure 6.6(b)) [M^{c}Gookin (1993)].

Both reference steps are considered to be sufficient to test the performance of the SM controllers for large manoeuvres. Also these amplitudes are within the limits of the linearisation for this model and therefore the simulation results of this study are likely to be a good representation of the actual dynamics of such a submarine.

6.4.3 Manually Tuned Results

The initial step in this study of the optimisation of controllers for the submarine is to obtain an acceptable solution through manually tuning the controller parameters in Table 6.3. This gives the parameter values shown in Table 6.4 which are obtained from M^{c}Gookin (1993). In order to provide further comparison equation (6.13) is used to calculate the cost of each subsystem and these are also shown in the table.

Table 6.4: Manually Tuned Submarine Controller Parameters

Diving Parameters		Heading Parameters	
pd1	-0.3	*ph1*	-0.3
pd2	-0.2	*ph2*	-0.2
pd3	-0.1		
η_D	0.1	η_H	0.1
ϕ_D	0.1	ϕ_H	0.1
C_{dive}	175.5	C_{head}	971.8

When the manually tuned parameters are implemented in the submarine controllers the simulated output, output error and input responses in Figure 6.7 are obtained. The desired responses are represented by the dashed lines.

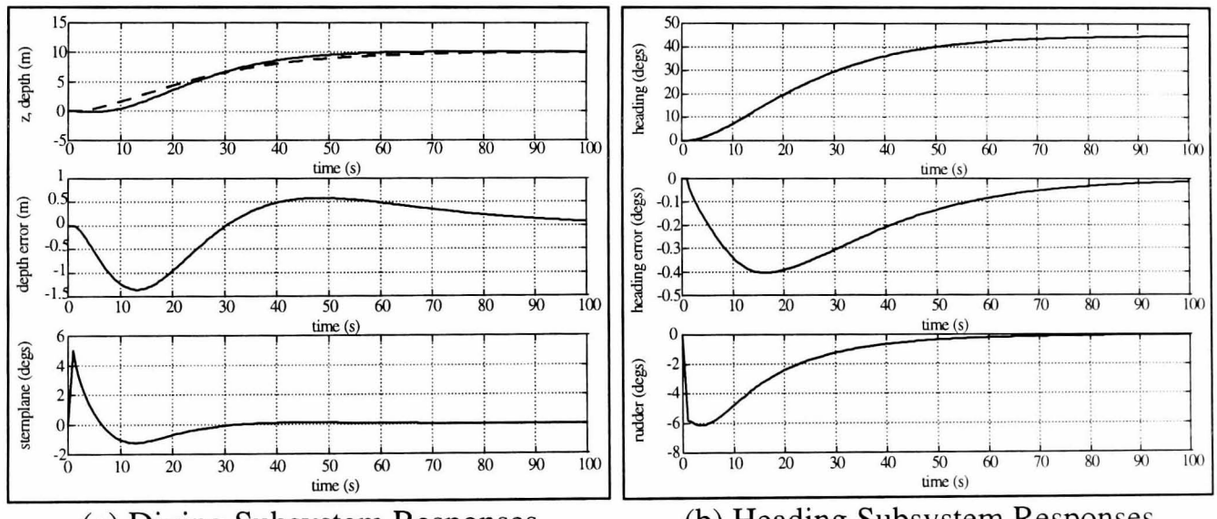

(a) Diving Subsystem Responses (b) Heading Subsystem Responses

Figure 6.7: Manually Tuned Submarine Responses

These responses are considered to be good inasmuch as the input signals operate well within recommended actuator amplitude limits (i.e. ±35° for rudder and ±25° for sternplane), thus allowing approximately 20° to be available if additional control is required to compensate for disturbances [Eda (1972), Price and Bishop (1974), Fossen

(1994)]. Also both the output errors converge to zero, thus indicating that the controllers manipulate the outputs so that they track the desired response. Hence both SM controllers are operating as required. It should be noted that the duration of the manoeuvres is sufficiently long as to reduce the amount of resistance to the commanded motions and thus limit the amount of cavitation created by the hull. It can therefore be said that this design is considered to be a good benchmark for the optimisation results to be compared with and can be taken as an optimum region for the search space in this problem.

Unfortunately, manual tuning is not a reliable process for finding optimal parameter values in that it often relies on luck as well as sound engineering judgement. It also involves a large number of designer hours to obtain an optimum result which can be tedious. Due to designer inexperience it took 80 design hours to obtain this solution.

6.4.4 SA Results

The parameter values in Table 6.5 are representative of those obtained from the controller optimisation using Simulated Annealing which starts its optimisation at a randomly generated point which is far from the optimum region (called SA(f)). Here the optimum region is defined as the manually tuned values. It should be noted that each subsystem is optimised separately through their individual costs.

Table 6.5: SA(f) Optimised Submarine Controller Parameters

Diving Parameters		Heading Parameters	
pd1	-8.0735	*ph1*	-14.2700
pd2	-9.3336	*ph2*	-0.1531
pd3	-35.0190		
η_D	0.0001	η_H	4.0768
ϕ_D	8.9988	ϕ_H	50.3473
C_{dive}	160143.01	C_{head}	3154.34

When these values are compared with the manually tuned values it can be clearly seen that they are not within the optimum region. This does not necessarily mean that they provide a suboptimal solution until the corresponding costs are considered. These show that the costs are considerably larger than the manually tuned calculation thus indicating that the solutions are not optimal. Another way to determine this is by observing the

performance of the controllers through the outputs, output errors and inputs shown in Figure 6.8. Again the desired responses are represented by dashed lines.

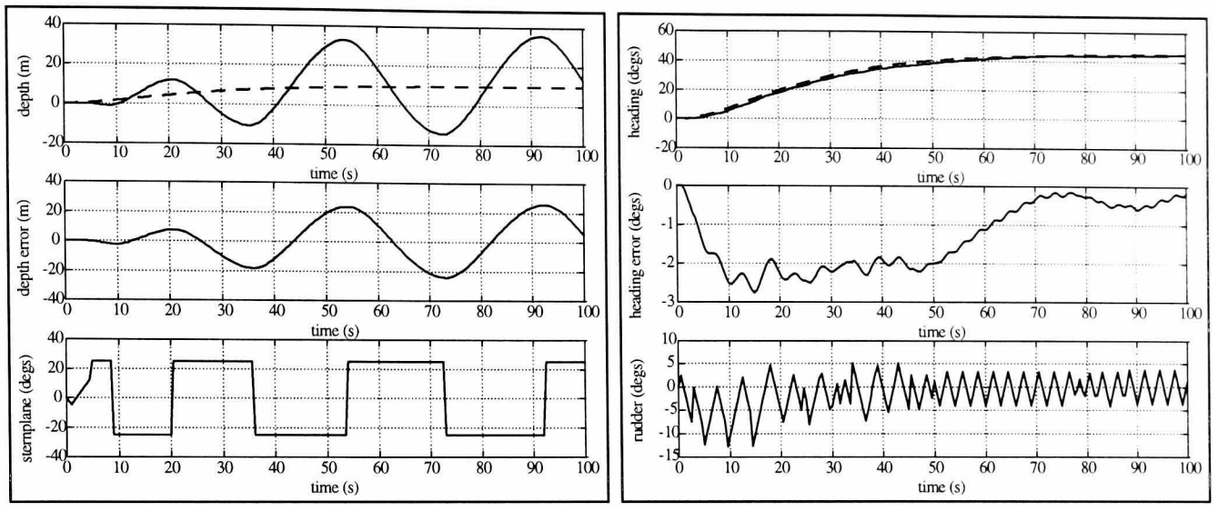

(a) Diving Subsystem Responses (b) Heading Subsystem Responses

Figure 6.8: SA(f) Optimised Submarine Responses

As expected by the cost values and the SA theory presented in Chapter 3 these responses are suboptimal. They are unsatisfactory since the cost function design criteria for both subsystems are not met. In fact the control systems provide oscillatory inputs for both subsystems and as a result the outputs do not follow the desired responses thus giving a large varying error. This is most noticeable in the diving subsystem, whereas the heading controller has tracked the desired response well. However the rudder deflections are undesirable due to oscillations. Therefore it can be said that the SA(f) method has designed final controller parameters which do not provide optimum responses and may cause the system to become unstable. This verifies that this method would not converge to an optimal solution if the starting point is too far from the optimal region.

Table 6.6: SA(n) Optimised Submarine Controller Parameters

Diving Parameters		Heading Parameters	
pd1	-0.4378	*ph1*	-0.2183
pd2	-0.1397	*ph2*	-0.5097
pd3	-0.0829		
η_D	2.3434	η_H	2.9419
ϕ_D	2.5478	ϕ_H	5.4568
C_{dive}	177.46	C_{head}	971.76

When the SA is given the manually tuned parameters as its starting points (called SA(n)) the optimised values in Table 6.6 are typical of those obtained. The cost values are also given. These parameter values and costs are very similar to the manually tuned values thus indicating that the SA(n) remains within the optimum region. This is further evaluated by examining the same set of responses as observed previously (see Figure 6.9).

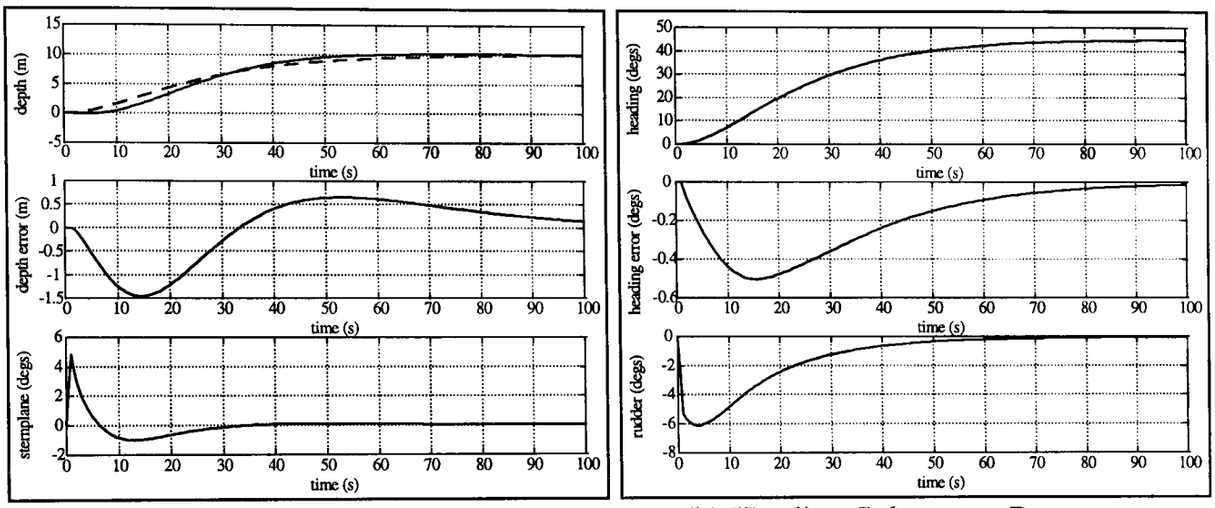

(a) Diving Subsystem Responses (b) Heading Subsystem Responses

Figure 6.9: SA(n) Optimised Submarine Responses

These responses are considered to be good in that they are similar to the manually tuned responses of Figure 6.7. However, there are slight differences between the two sets of results. Firstly the control action of both inputs are not as large and generally smoother in the context of a reduced initial duration where exceeding the rate limit. It can also be seen that the peak error is slightly larger in both subsystems. This indicates that the SA obtained a solution which has a smooth input response at the expense of desired output tracking. Either way the solution is still close to the optimum as comparison with the manually tuned cost shows (see Table 6.6). However, the major variation in the parameters are in both switching gains and boundary layer thickness. It can be seen that the SA values are much larger which would indicate that the optimisation method is insensitive to direct variation in these parameters. However, when the ratio of η/ϕ is considered it is found to be approximately unity for both. This is the same as the manually tuned case and would indicate that the ratio is being optimised rather than the individual parameters.

It is clear that this method requires *a-priori* knowledge of the location of the optimum region in order to obtain final results which are optimal. This indicates that the basic SA method needs to start its search in the optimal region so that it can be successful as an optimisation technique. Unfortunately, prior knowledge of where the optimum region lies can never be guaranteed and thus SA is an unreliable global search method. However, it performs well as a local method which could be used to fine tune solutions which have been obtained globally (e.g. by manual tuning).

6.4.5 SSA Results

With the SSA search the initial solutions are generated randomly throughout the search space. The final parameter values in Table 6.7 are obtained from a typical run of this method.

Table 6.7: SSA Optimised Submarine Controller Parameters

Diving Parameters		Heading Parameters	
pd1	-0.2641	*ph1*	-0.2295
pd2	-0.1694	*ph2*	-0.7755
pd3	-0.0820		
η_D	0.1594	η_H	3.1493
ϕ_D	0.1978	ϕ_H	19.8663
C_{dive}	174.23	C_{head}	973.54

These optimal values and their associated costs are very similar to both the manually tuned and SA(n) values. However the increased value of *ph2* has been compensated for by an increase in the boundary layer. On inspection of the responses that correspond to these parameters it is found that the obtained solution is optimal for the same reasons that the manually tuned responses are good (see Appendix B.1 for time histories). It should be noted that the cost values are of a similar magnitude to the manually tuned costs. Therefore this solution can be said to be in the optimal region for this problem.

In order to support that this is an optimal solution, the cost convergence of the run considered here should be considered. This is achieved by observing the response of the sum of the two subsystems costs, in particular the median cost value of all the SA runs (see Figure 6.10(a)) and the best SA run (see Figure 6.10(b)) of the optimisation.

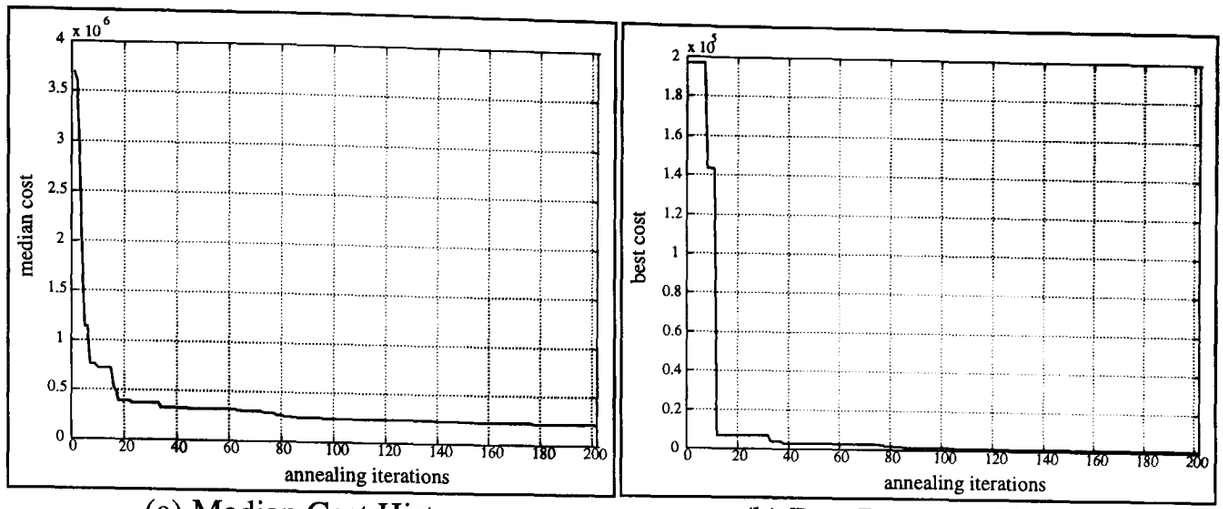

(a) Median Cost History (b) Best Run Cost History

Figure 6.10: SSA Cost Convergence Responses

It can be seen from the median cost that as the optimisation progresses the cost of the solutions found converge to a smaller value, thus indicating that a region of small cost (i.e. an optimum region) is found. However, the best cost history shows that the search converged to the optimum region within 36 iterations of this run. Since this particular run is the third to be executed, there are only 440 iterations to obtain this solution. Although this is a small number it cannot be guaranteed to be as small as this every time since the convergence depends on how close the initial solution is to the optimal region which is determined randomly. Therefore there is equal likelihood that the last run as well as the first will start near the optimum and hence provide the best run. It follows that every run of the SSA must be executed in order to obtain a globally optimal final solution.

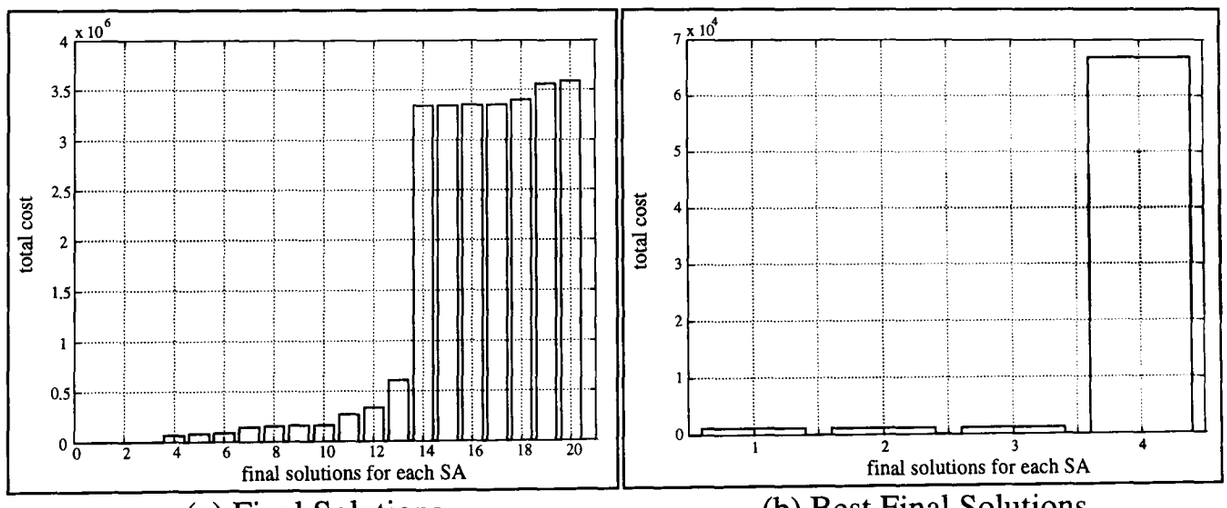

(a) Final Solutions (b) Best Final Solutions

Figure 6.11: SSA Final Solution Costs

Another way of determining how efficient this method is at obtaining the optimal region is the number of final solutions that each SA run provides that is similar to the best in terms of parameter values and cost. This clustering effect is called *Saturation* and would naturally occur if numerous runs start near the optimal region. The saturation of this SSA is represented by the histogram shown in Figure 6.11 where the sum of the subsystems' cost values are ranked in descending order.

Figure 6.11(a) shows that there is a wide variation in cost values and that only a few can be considered optimally small. Figure 6.11(b) shows the first 4 runs and only 3 of these are within the optimal region (i.e. 15% of the solutions). This is further verified by the corresponding parameter values which are similar to the best solution. These saturated solutions provide confidence in the best solution being close to the global optimum. If there is no saturation then there would be no way to determine if this a local solution and not the best that can be achieved.

This analysis has shown that even though the convergence rate for this method cannot always be guaranteed to be small, it can obtain an optimal final solution with considerable confidence. This is considered to be the major advantage of using SSA, when compared with SA, in that it does not need *a-priori* knowledge of the optimum region in order to obtain an optimal final solution. Thus the results provided here lend support to the theory in Chapter 3 that this is a much better global search method than SA.

6.4.6 GA Results

The final set of results are obtained from GA optimisation. Typical parameters values and associated costs obtained from an optimisation using this method are presented in Table 6.8. This search method varies from the SSA methods in that it used the sum of the two subsystems' costs to optimise the controllers instead of dealing with them individually.

Again these parameters are similar to the optimal solutions obtained by the previous methods and give similar responses (see Appendix B.2). It should be noted that the cost values are slightly smaller than previous solutions (particularly the heading subsystem).

Table 6.8: GA Optimised Submarine Controller Parameters

Diving Parameters		Heading Parameters	
pd1	-0.1844	*ph1*	-0.3070
pd2	-0.0755	*ph2*	-0.1805
pd3	-0.3173		
η_D	32.2100	η_H	1.8006
ϕ_D	26.1489	ϕ_H	1.6080
C_{dive}	172.68	C_{head}	970.62

Therefore the performance of this method as a global technique is shown to be very good.

This is further verified by observing the cost histories as in the SSA study. Again the median costs (Figure (6.12(a))) and the best costs (Figure (6.12(b))) for each generation are shown.

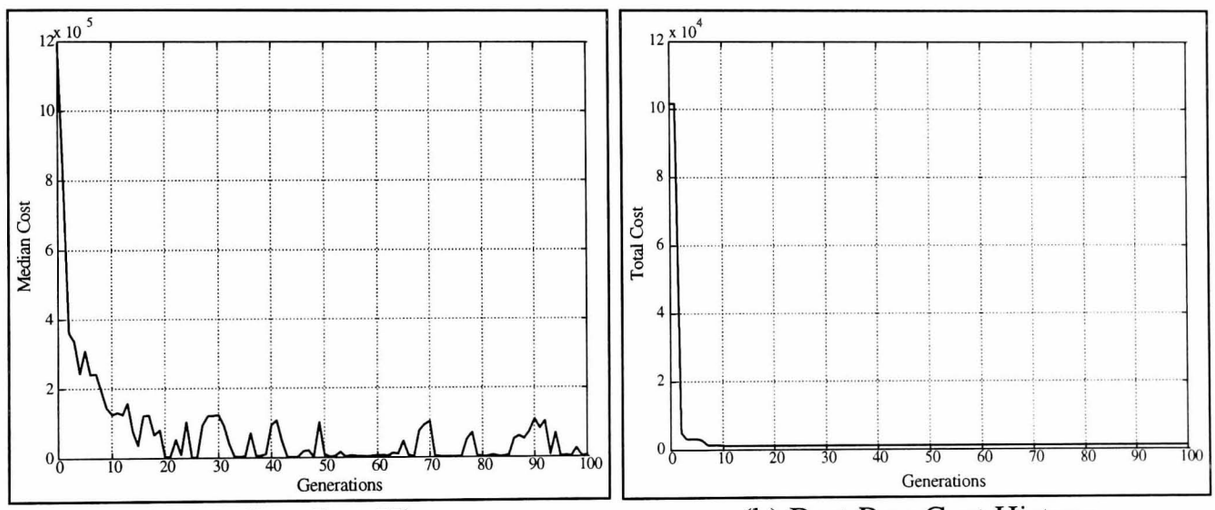

(a) Median Cost History (b) Best Run Cost History

Figure 6.12: GA Cost Convergence Responses

The median cost shows that this method converges to an optimal region within 20 generations even though the mutation rate is high for the method used here. Also the best cost shows that the GA converges to the optimum cost region within 7 generations. Since there are 40 iterations of the problem in each generation the number of iteration executed is 280. This is a typical value for this method when applied to this problem and does not require further iterations to ensure convergence. Therefore this method converges more quickly than the SSA method.

In order to continue the comparison the amount of saturation in the final generation is considered. This is illustrated by the histograms shown in Figure 6.13.

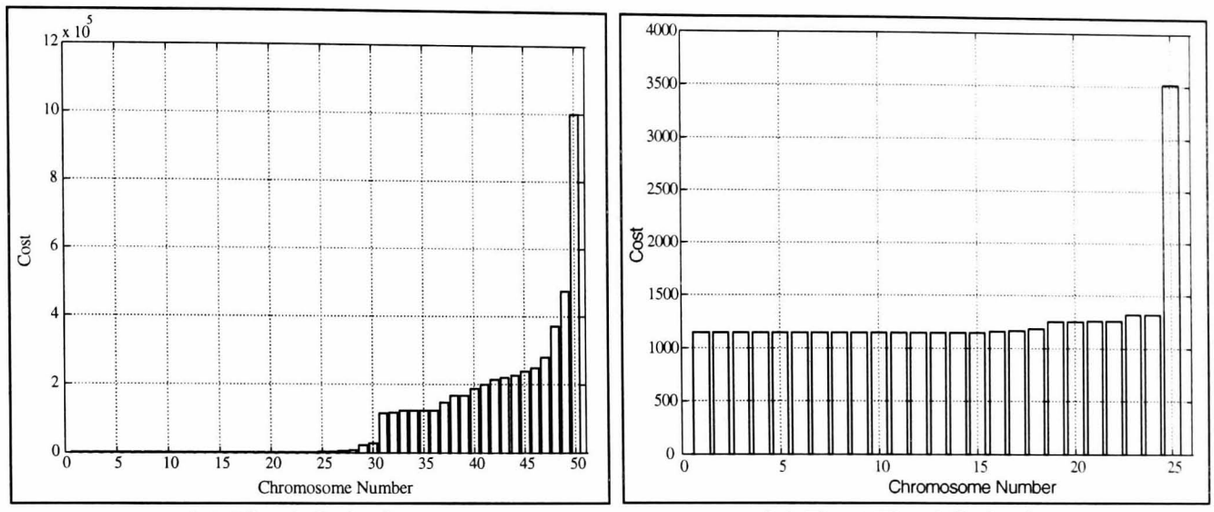

(a) Final Solutions (b) Best Final Solutions

Figure 6.13: GA Final Solution Costs

Again the wide variation in the generation costs can be seen in Figure 6.13(a) indicating that a sufficient search has been executed. The plot in Figure 6.13(b) shows the costs of the best individuals in the generation. It can be clearly seen that the amount of saturation (i.e. 15 individuals, 30% of the generation) is considerably more than in the SSA case. This provides even more confidence in the best solution being the global optimum.

6.4.7 Sliding Mode Boundary Layer Operation

Post-optimisation analysis of the optimal results obtained in this study show that the optimal controllers operate in the boundary layer alone rather than including the non-linear extremities of the switching term (see Figure 6.14 where the dashed line is the tanh switching function and the solid line is the operating region of the controllers).

In this region the switching term is proportional to the sliding surface i.e.

$$\tanh\left(\sigma/\phi\right) \approx \text{sat}\left(\sigma/\phi\right) = \sigma/\phi\Big|_{|\sigma|<\phi} \tag{6.16}$$

Thus, the controller structures become

$$u = -\mathbf{kx} + (\mathbf{h}^{\mathrm{T}}\mathbf{b})^{-1}\left[\mathbf{h}^{\mathrm{T}}\dot{\mathbf{x}}_{\mathrm{d}} - \eta\left(\sigma/\phi\right)\right] \tag{6.17}$$

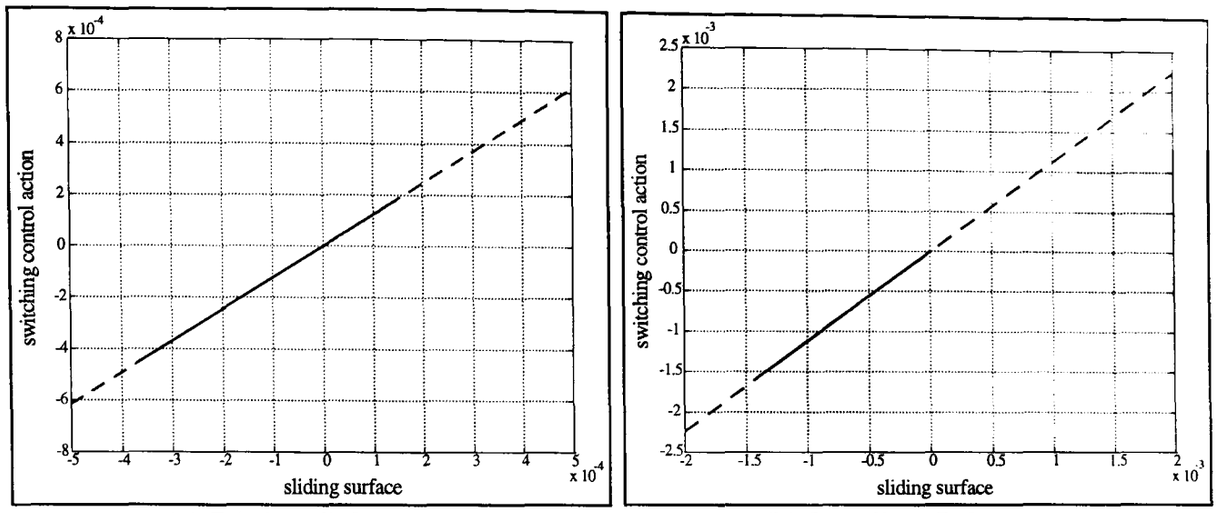

(a) Diving Subsystem (b) Heading Subsystem

Figure 6.14: Switching Operating Regions

Since the sliding surfaces are characterised by proportional and derivative (PD) error terms, the controllers become a hybrid of PD states and errors alone. Therefore, the controllers have linear PD properties rather than non-linear sliding mode switching terms in this region. Therefore, in order to ensure good performance the SM controllers operate in the boundary layer.

Although these controllers do have a PD structure, they retain the switching range which limits the controller action in the event of a large output error occurring. This could happen if the input is larger or if external disturbances (e.g. waves or water currents) are applied [Eda (1972), Price and Bishop (1974), Fossen (1994)]. Although the performance would be affected by this limiting factor, it improves the robustness of the controllers.

6.5 Summary

This chapter has presented the finding of a controller parameter optimisation study for a linear submarine model. In it the optimisation of two Sliding Mode controllers for the depth and heading control of the submarine was considered. These presented a good test for this type of model since cross-coupling between the two systems and the parametric complexity of the controllers are high for this system. The three optimisation methods used here are discussed below.

It has been illustrated that in this application Simulated Annealing only operates satisfactorily as a local optimisation method and requires *a-priori* knowledge of the optimal region in order to give satisfactory final responses. This, in a way, defeats the purpose of an global optimisation method as an optimal solution is already available. However it is suggested that this method could fine tune a solution which has already been obtained by other means.

The Segmented Simulated Annealing process has been shown to provide a fine tuned final solution without any knowledge of the optimal region within the problem search space. Therefore segmenting the search space improves the performance of the SA method. However the amount of saturation in the final solutions is small and provides limited confidence in the optimal solution that has been obtained. Nevertheless it is considered to be a good global optimisation method.

The Elite Genetic Algorithm studied here has been shown to be a good global search method which converges quickly to the optimum region. With regards to saturation this method provides adequate comparison within its final generation to give confidence in the optimal solution it provides.

It can be seen from the three methods considered that only two can be used for global searches (i.e. SSA and GA). This verifies the theories set out in Chapters 3 and 4. Moreover this comparison has indicated the advantages and disadvantages of using these methods for the optimisation problem considered here. These conclusions are also found to apply when these controllers are optimised in the presence of simulated sea current disturbances.

Since the same number of evaluations are executed by all the methods, it takes the same amount of time to optimise in each case. Coding these algorithms in MATLAB™ and running them on a 166MHz Pentium PC took approximately 3 hours. This is a considerable saving on the 80 design hours it took to manually tune the controllers. Therefore it can be said that the SSA and GA methods can obtain solutions more quickly than conventional design methods.

Chapter 7:

Super Tanker Application

7.1 Introduction

The second application considered in this work is the automatic control of a super tanker. These are large surface vessels that are used by the petroleum industry to transport crude oil [Berlekom and Goddard (1972)]. Although the resulting petroleum products affect nearly everything and everyone in modern life since the uses of oil are so widespread, they come with a hidden cost through the transportation of the crude oil [Crane (1973), Kallstrom et al (1979)]. Moving large quantities of oil inevitably involves risks to the environment and in the past few years safety issues have arisen concerning oil tanker navigation and control. These mostly arise from accidents such as the 'Sea Empress' disaster which had a considerable impact on the ecosystem of the local environment and will still have an effect for some time to come. As well as the environmental cost, it also presented a major cost to the oil company through loss of revenue, the effective loss of a ship and the subsequent clean up operation.

In order to avoid such incidences happening it is very important to find ways to control the motion of these vessels safely [Crane (1973), Kallstrom (1979), Kallstrom et al (1979), Astrom (1976), Zuidweg (1970)]. This is not an easy task due to the size of these tankers which in the case of super tankers can be in excess of 300m in length. Their bulk makes them very difficult to manoeuvre and this is not aided by the restricted proportions of the ships' main heading actuator (the rudder) [Crane (1973), Kallstrom et al (1979), Fossen (1994), M^{c}Gookin et al (1997 (a),(c),(e)]. However, the use of automatic control systems could help to provide an answer to the problem of diminished controllability. Such control systems have to be able to minimise the rudder effort as the ship is manoeuvred so that actuator saturation does not occur if additional effort is needed to counteract external disturbances [Eda (1972), Price and Bishop (1974), Fossen (1994)] or further changes in heading.

This chapter describes two automatic control systems for such a vessel. The first is a simple *course changing* control system which reacts to heading commands from a pilot in a similar way to the heading control system defined in the previous chapter [Fossen

(1994), M^{c}Gookin et al (1997(c),(e)), Kallstrom et al (1979), Zuidweg (1970)]. The second system considered here replaces the pilot/helmsman commands with the inputs from an autopilot and thus converts the system to a fully autonomous *course keeping* control system [Fossen (1994), M^{c}Gookin et al (1997(a),(e)]. This type of control system is not implemented in submarines as it requires GPS data to determine the heading which can only be obtained when the communications periscope is extended (i.e. near to the surface of the water).

This chapter deals with the above issues through the following structure. Section 7.2 describes the mathematical model of the tanker used in this optimisation study and outlines the problem of controlling these vessels in general. Section 7.3 describes both control systems used in this study. It will be shown that the same sliding mode controller for course changing can be used in the course keeping system while still maintaining the desired control effect. The penultimate section details the results obtained from the optimisation and the final section draws conclusions from these results.

7.2 Tanker Model in State Space Form

7.2.1 Tanker Dynamics

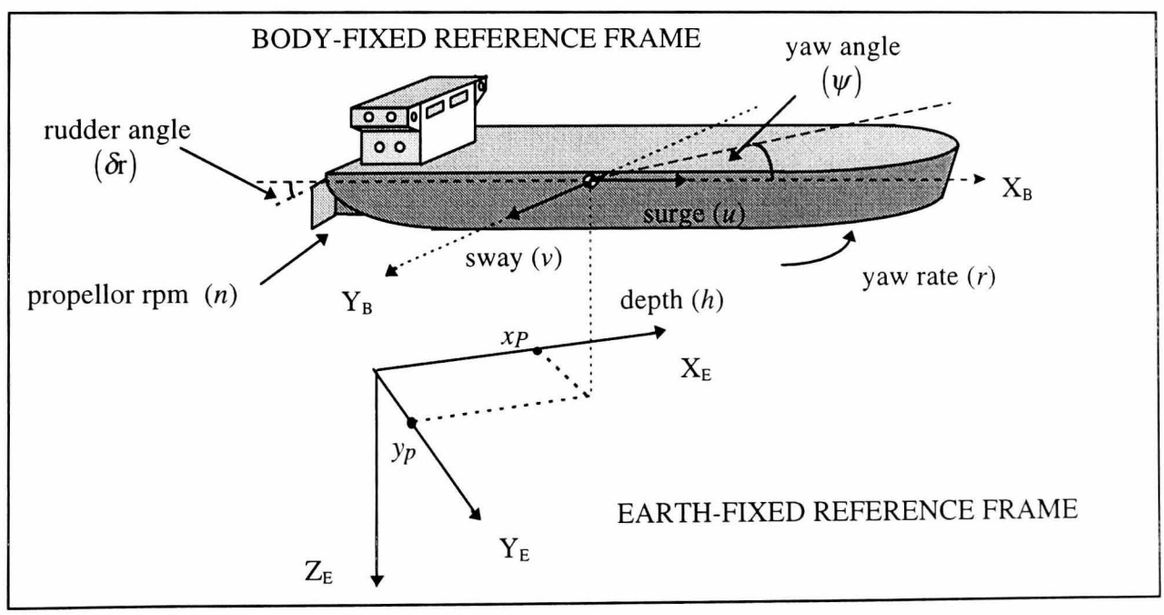

Figure 7.1: Tanker Reference Frames and Velocities

The mathematical representation used in this study models the heading and propulsion dynamics of a 190,000 dwt super tanker for transporting oil [Berlekom and Goddard 1972), Fossen (1994)]. The state variables of this representation are illustrated in Figure 7.1 as are the two reference frames. It can be clearly seen that the roll, pitch and heave dynamics are not considered here. This is usually the case when control systems for large surface vessels are simulated as they play a minimal role in the ship's motion.

The corresponding states and inputs for this vessel are outlined in Table 7.1.

Table 7.1: Tanker States and Inputs

STATES		INPUTS	
u	surge velocity	δr_c	commanded rudder
v	sway velocity	n_c	commanded propeller rpm
r	yaw rate	h	depth of water[1]
ψ	yaw (heading) angle		
x_p	x-position on earth		
y_p	y-position on earth		
δr	actual rudder deflection		
n	actual propeller rpm		

The model used here is non-linear and it exhibits cross-coupling between the main dynamics. Therefore this is a good example in which to apply the decoupling process for the design of a sliding mode controller and to verify its effectiveness on non-linear systems. An additional aspect of this model is that it changes its dynamics with the depth of water (h) it travels on [Berlekom and Goddard (1972), Norrbin (1970), Fossen (1994)]. Again this will test the performance of the sliding mode (SM) theory since the vessel dynamics will be continually changing.

As with the submarine, the dynamics of this vessel can be represented by the kinetic and kinematic equations. Due to the cross-coupling of the states and inputs, the kinetic equation exhibits extensive nonlinearities i.e.

$$\mathbf{M}(\mathbf{u})\dot{\boldsymbol{\nu}} + \mathbf{C}(\boldsymbol{\nu},\mathbf{u})\boldsymbol{\nu} + \mathbf{D}(\boldsymbol{\nu})\boldsymbol{\nu} + \mathbf{T}(\boldsymbol{\nu})\boldsymbol{\nu} = \mathbf{B}'(\boldsymbol{\nu},\mathbf{u})\mathbf{u} \tag{7.1}$$

Again **M**, **C** and **D** are the mass/inertia, Coriolis and damping matrices but in this case they are functions of the states and inputs. **T** represents the thrust dynamics of the propeller and **B′** relates the inputs to the system. It should be noted that there are no

[1] Water depth is a semi-controllable input since the pilot can direct the vessel into areas with suitable water depths. These depths are obtained from bathymetry charts of the voyage area.

gravitational or buoyancy terms (i.e. **G** is a zero vector). This is a result of Archimede's Principle [Fox and McDonald (1985)] which states that the buoyancy and weight of a floating body are equal and since roll and pitch are not modelled then the positions of the centres of buoyancy and gravity result in the vessel being neutrally buoyant [Fossen (1994)]. In this model the body-fixed velocities vector $\boldsymbol{\nu}$ reduces to $\boldsymbol{\nu} = [u, v, r]^T$ and $\boldsymbol{\eta}$ becomes $\boldsymbol{\eta} = [x_p, y_p, \psi]^T$. The input vector **u** has the commanded inputs for the rudder and the propeller rpm. It also involves the depth of water, h, as mentioned earlier (i.e. $\mathbf{u} = [\delta r_c, n_c, h]^T$). The interconnection of this input within the model causes a great deal of the dynamic cross-coupling and variation within this system (see Appendix A.2).

In addition to the states mentioned above, the model has two further states. These are the actual rudder deflection and propeller rpm after limits have been applied. This will be dealt with in the next section.

Although the kinetic equations differ from the standard form discussed in the previous chapter, the kinematic equations remain the same since the geometric relationships between the two references are the same i.e.

$$\dot{\boldsymbol{\eta}} = \mathbf{J}(\boldsymbol{\eta})\boldsymbol{\nu} \tag{7.2}$$

In this case **J** is reduced to the three states that are required since motion related to the Z_E axis is not possible.

To represent these equations in a standard state space form, (7.1) is rearranged to yield

$$\dot{\boldsymbol{\nu}} = -\mathbf{M}(\mathbf{u})^{-1}\left(\mathbf{C}(\boldsymbol{\nu},\mathbf{u}) + \mathbf{D}(\boldsymbol{\nu}) + \mathbf{T}(\boldsymbol{\nu})\right)\boldsymbol{\nu} + \mathbf{M}(\mathbf{u})^{-1}\mathbf{B}'(\boldsymbol{\nu},\mathbf{u})\mathbf{u} \tag{7.3}$$

When equations (7.2) and (7.3) are combined together the following matrix form is produced

$$\begin{bmatrix} \dot{\boldsymbol{\nu}} \\ \dot{\boldsymbol{\eta}} \end{bmatrix} = \begin{bmatrix} -\mathbf{M}(\mathbf{u})^{-1}\left(\mathbf{C}(\boldsymbol{\nu},\mathbf{u}) + \mathbf{D}(\boldsymbol{\nu}) + \mathbf{T}(\boldsymbol{\nu})\right) & \mathbf{0} \\ \mathbf{J}(\boldsymbol{\eta}) & \mathbf{0} \end{bmatrix} \begin{bmatrix} \boldsymbol{\nu} \\ \boldsymbol{\eta} \end{bmatrix} + \begin{bmatrix} \mathbf{M}(\mathbf{u})^{-1}\mathbf{B}'(\boldsymbol{\nu},\mathbf{u}) \\ \mathbf{0} \end{bmatrix} \mathbf{u} \tag{7.4}$$

This can be written as

$$\dot{\mathbf{x}} = \mathbf{A}(\mathbf{x},\mathbf{u})\mathbf{x} + \mathbf{B}(\mathbf{x},\mathbf{u})\mathbf{u} \tag{7.5}$$

Or more generally

$$\dot{\mathbf{x}} = \mathbf{f}(\mathbf{x}, \mathbf{u}) \tag{7.6}$$

which is the standard state-space form of a non-linear system (see Appendix A.2 for model).

7.2.2 Input Actuator Dynamics

As in the submarine case, the dynamics of the input actuators are modelled for the tanker. This obviously excludes the water depth input which is not a mechanical process. However the actual rudder and propeller rpm, after being subjected to rate and amplitude limits, are states of the system (see Table 7.1). Therefore the inputs are the commanded values which may be outside the physical operating range of the actuators. The rate and amplitude limit values for each of the actuators are show in Table 7.2 and represent standard values for this specific vessel.

Table 7.2: Actuator Limit Values

ACTUATOR	RATE LIMIT	MAGNITUDE
RUDDER	2.33 °/sec	30 °
PROPELLOR RPM		80 rpm

The rate limit for the propeller is not stated since the dynamics of its derivative is governed by a time constant, T_p i.e.

$$\dot{n}' = \frac{1}{T_p}(n - n_c).60 \tag{7.7}$$

where T_p = 50 and the values of n and n_c are in revolutions per second. The quantity n' has units of revolutions per minute.

7.2.3 Rudder Effectiveness

The main problem with controlling the heading of tankers is the limitations of the rudder actuator. In order to manoeuvre such a large vessel, a large turning moment is required to overcome the inertia. Generation of a turning moment of this size depends primarily on the localised flow over the rudder (i.e. the larger the flow the greater the turning moment) [Fossen (1994), M^{c}Gookin et al (1997(e)). Therefore the effectiveness

of the rudder to produce a large enough turning moment defines the rise time of the particular motion response of a vessel of the type considered here.

The localised flow over the rudder is represented in the model as the variable c which is obtained from the following equation [Fossen (1994)].

$$c = \sqrt{\left(c_{un}un + c_{nn}n^2\right)} \tag{7.8}$$

Here c_{un} and c_{nn} are constants [Fossen (1994)]. This illustrates that it is a function of the surge velocity, u, and the propeller rpm, n. This is due to the location of the rudder immediately aft of the propeller. Since the value of n is usually kept constant the dominant factor in the flow expression is the surge velocity. For a tanker this velocity is relatively small due to the size of the vessel. This coupled with the large inertia that has to be overcome to execute the manoeuvre makes the rudder less effective than the rudder of a smaller and faster vessel.

This deficiency indicates that in order to initiate a manoeuvre the rudder deflection must be large which runs the risk of saturating the actuator and rendering it ineffectual for any further commands during the motion. Therefore any automatic control system must be able to execute a commanded turn accurately while keeping the rudder deflection within its operational limits (see Table 7.2). Hence the trade off between accuracy and actuator saturation is the major problem that needs to be addressed in this application.

7.3 Decoupled Subsystems

Although there are two main dynamics in this model (i.e. propulsion and heading), only the heading motion has a sliding mode controller to govern the vehicle's course changing motion. The propulsion dynamics are usually controlled by simple step commands and the dynamics of the system self regulate the response (see equation (7.8)). Therefore, only the course changing subsystem needs to be decoupled from the main dynamics in order to control the heading of the vessel.

7.3.1 Course Changing Subsystem

The course changing subsystem describes the heading motion in the X_B-Y_B plane (see Figure 7.2) as in the submarine application. However the subsystem for obtaining the *course changing* controller differs in terms of the particular states used to represent it, even though the task of regulating the heading angle, ψ, by manipulation of the rudder actuator, δr, is the same. Due to practical economic considerations it is very unlikely that any additional expense will be allowed in obtaining the states for feedback. This is particularly the case with the sway velocity, v, where some commercial ships may not have a gyroscope to measure this variable whereas it would be available in the case of a military vessel (e.g. a submarine). Therefore, it is unreasonable to use this state in this application and the subsystem decouples to a third order system with states r, ψ and δr with the commanded rudder deflection δr_c as the input [Fossen (1994)].

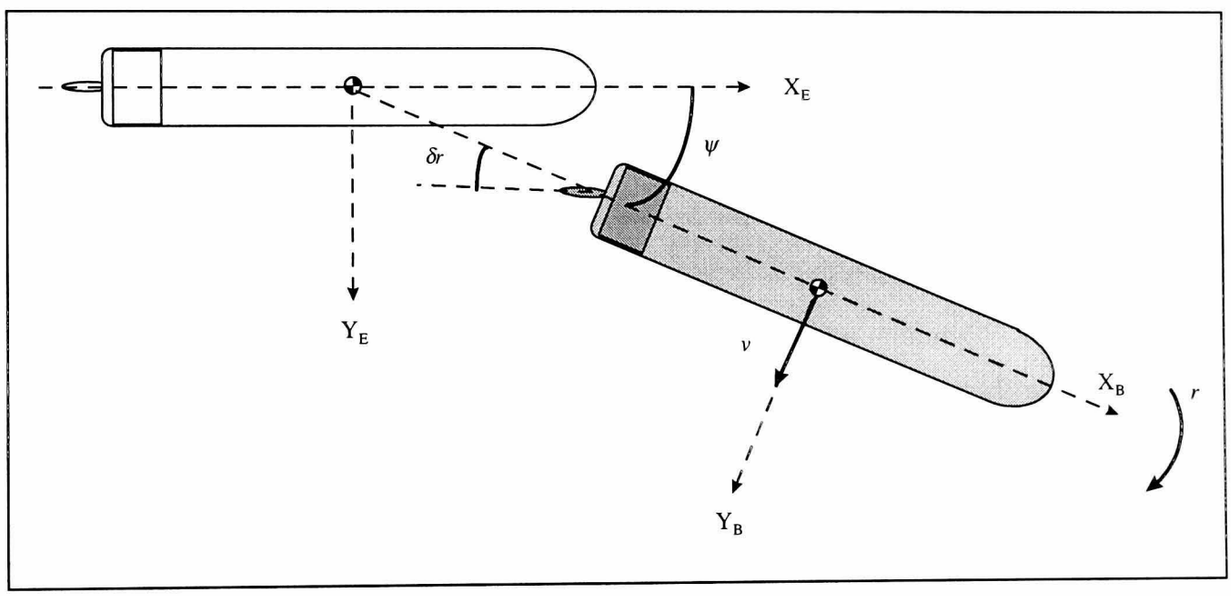

Figure 7.2: Course Changing Manoeuvre

Decoupling this motion results in a SISO system of the following state space form.

$$\dot{\mathbf{x}}_H = \mathbf{A}_H \mathbf{x}_H + \mathbf{b}_H \delta r_c \tag{7.9}$$

where the state vector, $\mathbf{x}_H = [r,\ \psi,\ \delta r]^T$. This representation of the subsystem allows the sliding mode theory of Chapter 5 to be applied (see section 5.4).

$$\delta r = -\mathbf{k}_H{}^T \mathbf{x}_H + \left(\mathbf{h}_H{}^T \mathbf{b}_H\right)^{-1} \left(\mathbf{h}_H{}^T \dot{\mathbf{x}}_{Hd} - \eta_H \tanh\left(\sigma_H\left(\hat{\mathbf{x}}_H\right)/\phi_H\right)\right) \tag{7.10}$$

The desired states are formed so that the controller will attempt to follow a second order response to a commanded step from a pilot. Thus the course changing manoeuvre is controlled in a similar way to that used by in the submarine case i.e. through governing the heading angle by mean of the rudder actuator.

Since the representation of the heading dynamics (equation (7.9)) does not have an estimate of the model uncertainties, the switching gain criterion for performance robustness (see Chapter 5) is taken to be

$$\eta_H > 0 \tag{7.11}$$

This is satisfied during the optimisation process by ensuring the parameter values for this gain are positive definite.

7.3.2 Decoupled Course Changing Controller Application to the Main System

In the course changing configuration of this model, the rudder actuator command for the tanker model is obtained from a sliding mode controller. The input for the propulsion system is a simple step and the water depth is defined externally to the model. These provide the inputs to the model's kinetic and kinematic equations (see Figure 7.3). As in the submarine system, before the commanded signals are applied to the model they are passed through rate and amplitude limit checks which implement the actuator limits shown in Table 7.2. These elements reduce the rate of response of the inputs and add a further non-linear element to the system.

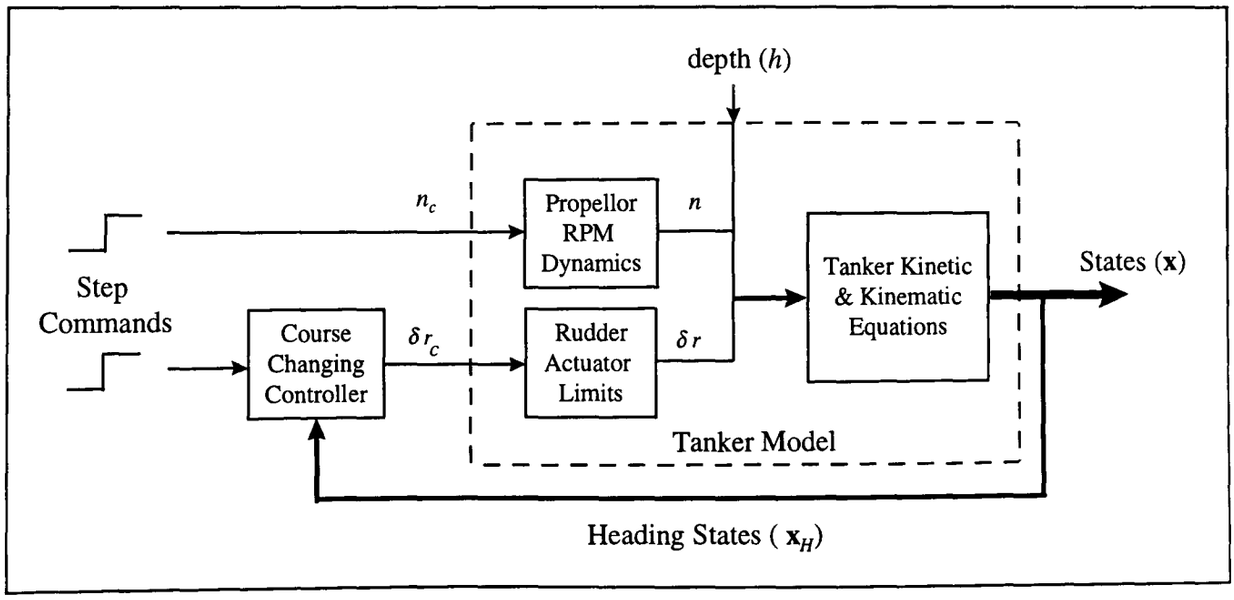

Figure 7.3: Tanker Model and Course Changing Controller Configuration

The simulation of this system in the course changing manoeuvre is based on Figure 7.3 and again the states are obtained from the state space equation by the Euler integration method [Cheney and Kincaid (1985)].

7.3.3 Course Keeping Subsystem

In course keeping the tanker control system is fully autonomous in that it automatically guides the vessel on a predetermined course without the necessity of a human operator. As long as the course is selected so that it avoids hazardous regions, such as shallow water, the passage of the tanker should be safe and uneventful. This system tracks a desired heading provided by an autopilot that determines course changes depending on the tanker's present position.

If this is compared with course changing it is easy to see that in course keeping the step commands from the pilot/helmsman are replaced by signals from the autopilot. Therefore there are two fundamental components to this control system i.e. an autopilot [Fossen (1994), Healey and Marco (1992), Healey and Lienard (1993)] and a course changing controller [Fossen (1994), M^{c}Gookin et al (1997(c),(e)), Kallstrom et al (1979), Zuidweg (1970)] which are configured to the tanker model in the way shown in Figure 7.4. The course changing controller has the structure shown in equation (7.10).

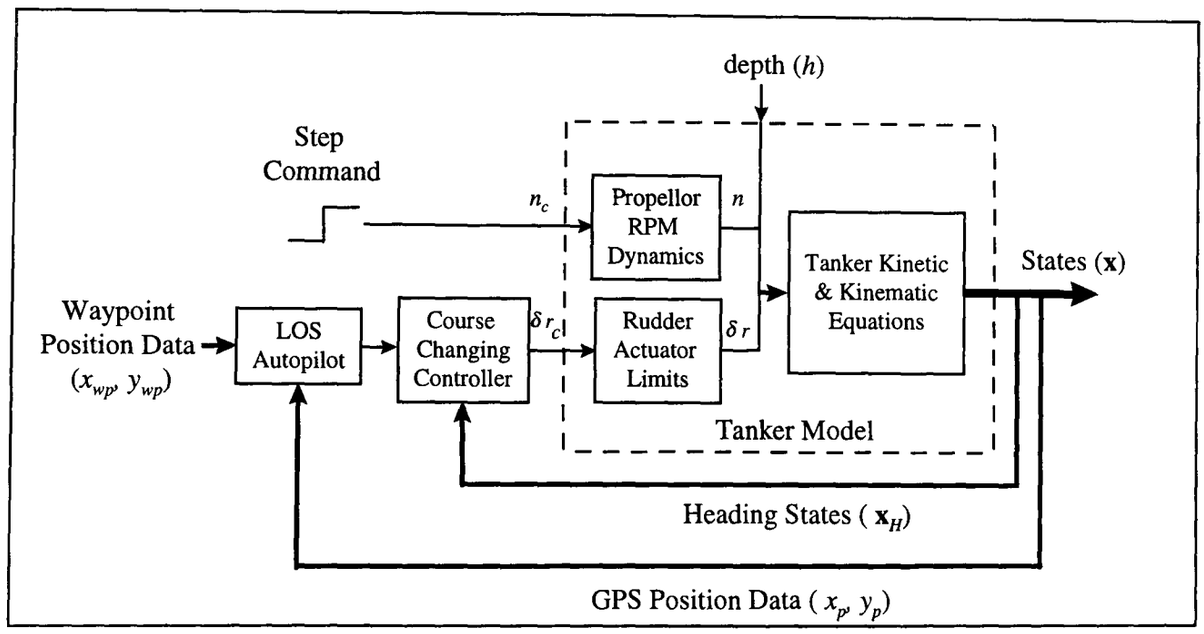

Figure 7.4: Course Keeping Control System and Tanker Model

This figure shows that the autopilot is integrated into the course changing controller/tanker system through the addition of an outer feedback loop which stabilises

the tanker position. The addition of an autopilot enables the tanker to keep course accurately which is of particular use in coastal or hazardous waters [Berlekom and Goddard (1972), Crane (1973), Fossen (1994)].

The particular type of autopilot used here is called a *Line Of Sight* (LOS) autopilot [Fossen (1994), Healey and Marco (1992), Healey and Lienard (1993)] since it provides a desired heading reference from a direct line between the tanker's current position and its destination. It achieves this by directing the tanker along a predetermined course which is set out prior to autopilot activation. This course is made up of points called *waypoints* [Fossen (1994), Healey and Marco (1992), Healey and Lienard (1993)] that are used to calculate the reference heading angle between the tanker's present position and the waypoint position (see Figure 7.5(a)). This heading angle ψ_{ref} is obtained from equation (7.12) [Fossen (1994), Healey and Marco (1992), Healey and Lienard (1993)]. The sign convention for this angle defines that positive angles ($0^O < \psi_{ref} \leq 180^O$) are to starboard and negative angles ($-180^O < \psi_{ref} < 0^O$) are to port.

$$\psi_{ref} = \tan^{-1}\left(\frac{y_{wp} - y_p}{x_{wp} - x_p}\right) \tag{7.12}$$

In this equation (x_p, y_p) are the current position co-ordinates of the tanker obtained from a Global Positioning System (GPS) and (x_{wp}, y_{wp}) are the waypoint co-ordinates. The reference heading is then used to obtain the desired heading response for the controller to track.

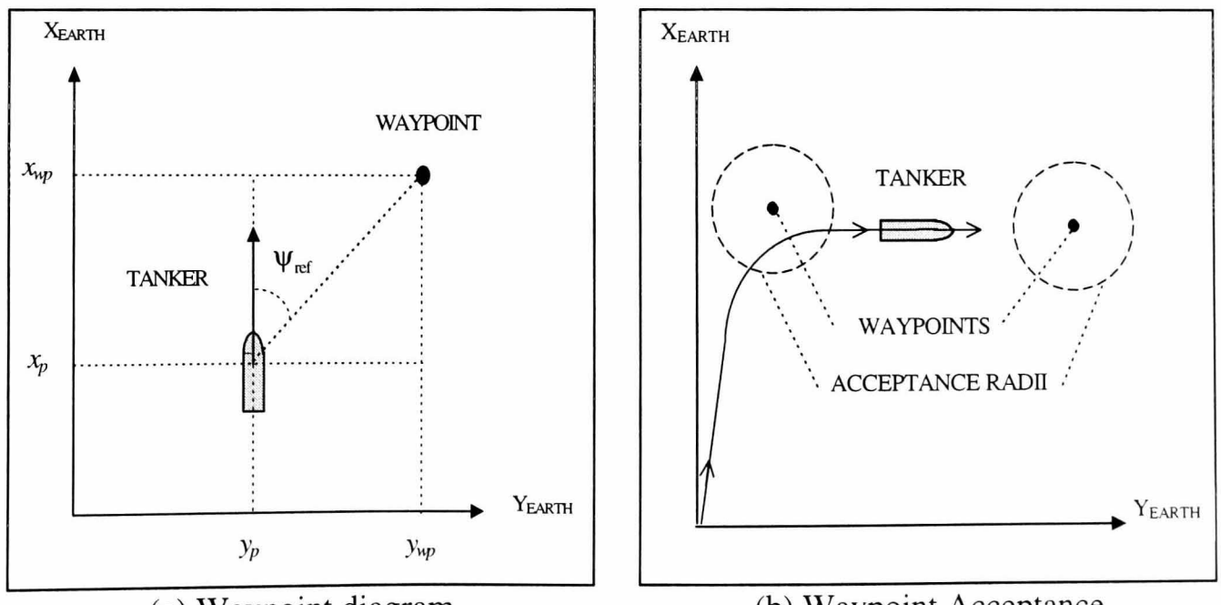

(a) Waypoint diagram (b) Waypoint Acceptance

Figure 7.5: Autopilot Illustrations

The autopilot guides the tanker from waypoint to waypoint in the following way. Once the tanker comes within a specified distance of the current waypoint, the autopilot acquires the next waypoint position and the tanker heads towards it (see Figure 7.5(b)). This distance is called the *acceptance radius* and is typically between one and three boat lengths. The acquisition process is repeated until the tanker reaches its final destination.

7.4 External Environment Considerations

In order to simulate both the course changing and course keeping tanker systems, an artificial external environment has been created which differs for each control system. This involves the water depth configuration but also the waypoint course used for the course keeping study.

7.4.1 Course Changing Depth Configuration

In course changing there was no need for an elaborate depth configuration but a suitable change of depth is required for this investigation. This is obtained from consideration of how the water depth (h) interacts with the other dynamics. Within the model a parameter ζ is used to relate the depth of water under the vessel (h) and its draft to the design waterline (D) in the following equation.

$$\zeta = \frac{D}{h - D} \tag{7.13}$$

This gives the graphical representation of ζ against h shown in Figure 7.6.

On this graph the draft is represented by a dashed line. Also shown is a transition point where the hydrodynamic coefficient $Y_{uv\zeta}$ changes value. It obeys the following conditional operation.

$$Y_{uv\zeta} = \begin{cases} 0 & \zeta < 0.8 \\ -0.85\left(1 - 0.8/\zeta\right) & \zeta \geq 0.8 \end{cases} \tag{7.14}$$

The result of this transition changes the dynamics of the sway equation by increasing the surge/sway coupling by an amount related to depth ratio ζ. Thus the ship starts to lose a certain degree of sway stability.

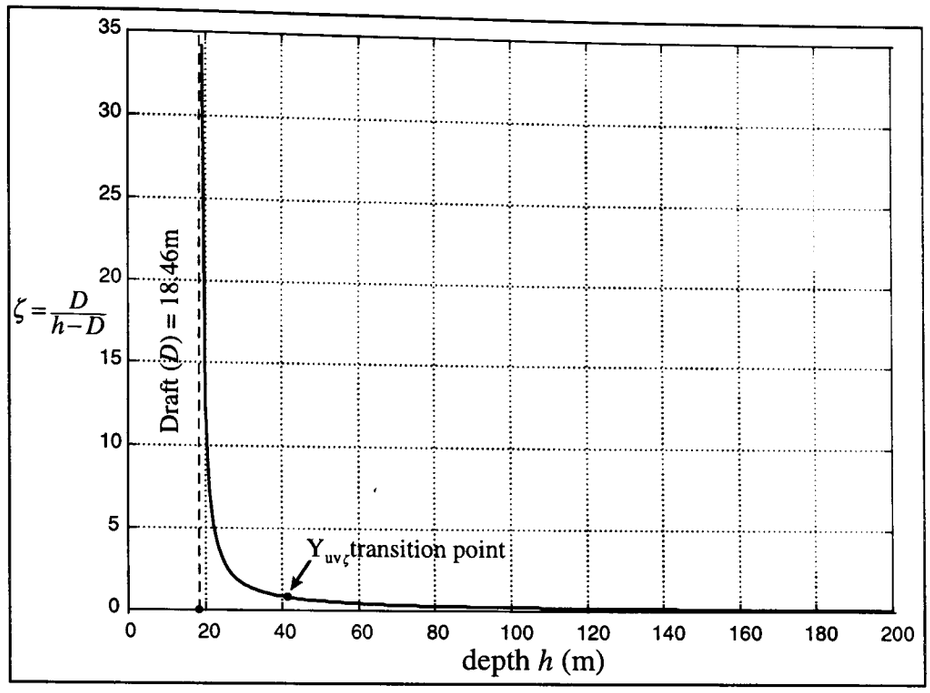

Figure 7.6: Depth Relationship

It can be clearly seen from Figure 7.6 that this relationship does not vary significantly for depths greater than 100m. Therefore, there are two distinct operating regions and a suitable choice would be to include a depth from both of them. However, it is normal practice for tankers to operate in water depths that are at least three times their draft which in this case is 55.38m [Crane (1973), Norrbin (1970)]. Therefore a depth of 200m has been used for the course changing study of this vessel. This should allow a suitably realistic operating environment for this vessel to be evaluated in the context of controller performance. It has been found that varying the depth does not effect the controller performance significantly [M^{c}Gookin (1997(e)]

7.4.2 Course Keeping Depth and Autopilot Waypoint Configurations

In the course keeping study, a slightly more sophisticated external environment is required because the tanker's inertially referenced position is required for the autopilot operation. This calls for a fixed bathymetry contour for the autopilot to guide the tanker through, thus enabling the autopilot waypoints to be placed within this depth configuration. The depth configuration used in this study allows full advantage to be taken of the tanker model dynamics. The configuration used is illustrated in Figure 7.7 and is created to represent a change in depth from deep water (500m) to shallow (25m).

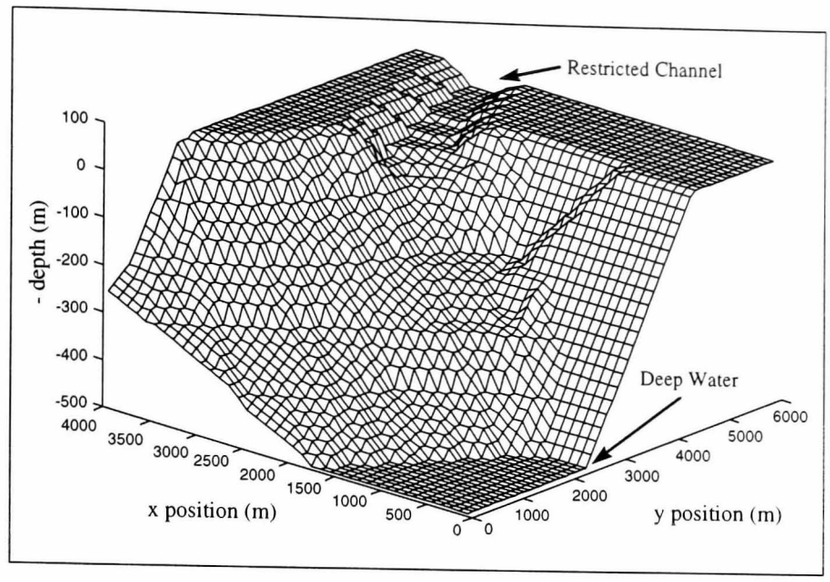

Figure 7.7: Water Depth Configuration

The deep water area is limited to this depth since further increase will not affect the tanker dynamics. Although the shallowest point is less than the recommended operating depth of about three times the draft [Crane (1973), Norrbin (1970)], it is used to investigate the controllability of the vessel if it got into trouble in shallow waters. The shallow waters are restricted by the banks of the channel which are used to limit the manoeuvrability of the tanker in this area. Unfortunately the banking effects encountered in such a narrow water channel are not incorporated into the model and could not be investigated here [Berlekom and Goddard (1972)].

The course laid out for the autopilot to follow must keep within the bounds of the depth configuration described above. In this case three points are used and their co-ordinates are illustrated in Figure 7.8.

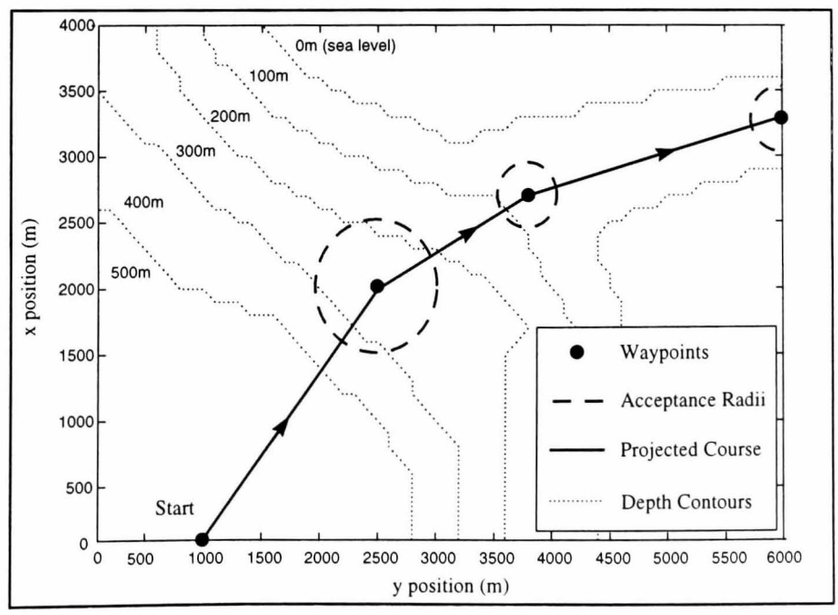

Figure 7.8: Waypoint Course

The acceptance radii, projected course and depth contours are also shown in this figure. It should be noted that the radii of the waypoints in the shallower waters are only one boat length whereas in deeper water it is taken as two boat lengths. The shallow water radii are smaller because of the bank constraints of the channel. This calls for greater acquisition accuracy on behalf of the autopilot due to the constrained manoeuvrability in this region. In the deeper water this is not a problem since there is more room to move.

7.5 Optimisation Process and Results

As with the previous optimisation study, this problem also has numerous design aspects which must be defined in order to proceed. This section defines the parameters that are to be optimised for both the course changing and keeping control systems. Also the cost functions used as the optimisation criteria are outlined. Although the cost function used for both optimisations are similar, the course keeping system has an additional penalty cost which is related to the autopilot waypoint acquisition. In order to implement these costs a desired heading response for each system has to be defined. The final sections will present the optimisation results of this study along with manually tuned solutions for comparison.

7.5.1 Controller Parameters

The key design parameters which have been chosen to be optimised for both control systems are shown in Table 7.3. It can be seen that these parameters are the same as those used in the submarine heading controller optimisation in Chapter 6.

Table 7.3: Tanker Controller Parameters to be optimised

1st Closed loop pole	*ph1*
2nd Closed loop pole	*ph2*
Switching gain	η_H
Boundary Layer Thickness	ϕ_H

The first two parameters (*ph1*, *ph2*) are two poles of the decoupled closed system (the third is a zero and corresponds to the yaw dynamics). These poles are used to obtain the feedback gain vector $\mathbf{k}_H$ and closed loop system right eigenvector $\mathbf{h}_H$ which are both constituent parts of the controller in equation (7.10). The final two design parameters are η_H and ϕ_H which are related to the switching action of this type of controller. As

mentioned previously the switching gain η_H determines the magnitude of the switch and ϕ_H defines the size of the boundary layer.

7.5.2 Cost Functions and Desired Responses

Again the optimisation design criterion is defined by the cost function. Since there are two systems which have different roles to fulfil, their individual cost functions must accommodate these differences. In addition to this each has a different desired response which the controller is required to track. Both these aspects are addressed separately for course changing and course keeping controllers.

7.5.2.1 Course Changing Cost Function and Desired Response

The cost function used as the design criterion in the course changing sections of this investigation is defined by equation (7.15) [Dove and Wright (1991)]. This function is similar to the integral least squares criterion used in the submarine optimisation i.e.

$$C_{PER} = \sum_{i=0}^{tot} \left[\lambda (\Delta\psi_i)^2 + (\delta r_i)^2 \right] \tag{7.15}$$

Here *tot* is the total number of iterations, λ is a scaling factor ($\lambda = 10$ in this case), $\Delta\psi_i$ is the ith heading angle error between the desired and obtained heading, δr_i is the ith rudder deflection [Dove and Wright (1991), McGookin et al (1997 (c),(e))]. Since the optimisation processes attempt to minimise the value of this function it is easy to see that both $\Delta\psi$ and δr will be minimised too. The selection of these elements follows the same reasoning as in the submarine study. However the elements are more specific for this heading controller whereas the submarine case was general in order to cover the diving and heading motions. Therefore following this train of thought, the quantity $\Delta\psi$ gives an indication of how well the controller is operating by showing the tracking between the actual and desired headings. The input component δr is used to keep rudder actuator movement to a minimum so that it can operate well within the actuator's operating limits. As well as this being of importance for SM controllers (i.e. to eliminate chatter) it is essential for this tanker application. It has been shown in Section 7.2.3 that large rudder deflections are required to manoeuvre such a vessel. This may cause problems since excessive control effort may be employed in order to reduce the

output error. As a consequence of this the rudder deflection will always be larger than the output error near the optimum and will thus dominate the cost values in this area. Hence the heading (output) error is scaled by the λ constant so that an equally balanced trade-off between these elements is obtained and thus avoid excessive rudder usage.

Another advantage of minimising the rudder deflection is the resulting savings in terms of fuel consumption since the resistance to the forward motion is minimised [Dove and Wright (1991)]. This results from the minimised rudder producing less drag since the amount of the hull which is in opposition to the turning manoeuvre is reduced. Hence more of the forward force goes to maintaining a relatively constant surge velocity and less fuel is used.

As with the submarine application a desired heading response is required for the optimisation process. So that this study can be compared with the submarine investigation the same heading manoeuvre is used here. This is a critically damped step response which represents a 45° turn as shown in Figure 7.9. Although both desired heading responses are similar in shape, the duration of this response is much larger to account for the reduced manoeuvring ability of the tanker.

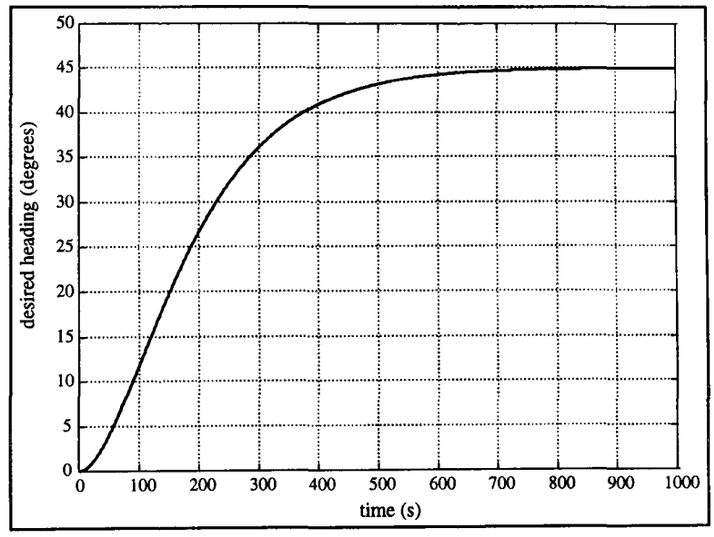

Figure 7.9: Desired Heading Response (45° manoeuvre)

This provides the desired heading states for the controller and thus enables the state error vector to be calculated. From these the value of the heading error can be obtained and used to calculate the cost (equation (7.15)) for each solution generated by the optimisation processes. Again this manoeuvre is considered to be a sufficient test for the course changing controller for this vessel.

7.5.2.2 Course Keeping Cost Function and Desired Response

The cost function for the Tanker's course keeping manoeuvre has an additional component compared with the course changing cost function in equation (7.15). As well as the heading and rudder performance provided by equation (7.15) an additional criterion is used to monitor the number of waypoints (n_{wp}) acquired by the autopilot. It is believed that in the time interval of the simulation only three waypoints should be acquired and therefore the following cost penalty function is used to calculate an addition cost value [Goldberg (1989)].

$$C_{PEN} = \kappa \left| n_{wp} - 3 \right| \tag{7.16}$$

Here κ is a large value used to penalise the cost and is taken as a value of 10000 in this study. The sum of this cost and the performance costs from equation (7.15) gives the following cost equation for course keeping.

$$\begin{aligned} C_{TOTAL} &= C_{PER} + C_{PEN} \\ &= \left[\sum_{i=0}^{tot} \left(\lambda (\Delta \psi_i)^2 + \delta r_i^{\,2} \right) \right] + \left[\kappa \left| n_{wp} - 3 \right| \right] \end{aligned} \tag{7.17}$$

The same value of λ (i.e. $\lambda = 10$) is also found to be sufficient for this part of the study. This total cost is used as the optimisation measure for course keeping in the same way as equation (7.15) alone is used for the course changing optimisations.

As with the previous cost functions a desired heading value is required to provide the heading error component. This desired heading is supplied by the autopilot as it follows the waypoint course illustrated in Figure 7.8 and does not need to be defined in the specific nature as in the course changing case. Therefore the reference provided by the autopilot is used to obtain the heading error.

7.5.3 Manually Tuned Results

The first step in this optimisation study is to obtain an acceptable solution through manually tuning the controller parameters in Table 7.3. This gives the parameter values shown in Table 7.4.

Table 7.4: Manually Tuned Tanker Controller Parameters

ph1	-0.2
ph2	-0.1
η_H	0.1
ϕ_H	0.1

The resulting controller is applied to both the course changing and course keeping problems.

7.5.3.1 Course Changing Responses

When the manually tuned parameters are implemented as the tanker course changing controller the simulated responses shown in Figure 7.10 are obtained. These are the output, output error and input responses which for this application are the heading angle, the heading error and the rudder deflection.

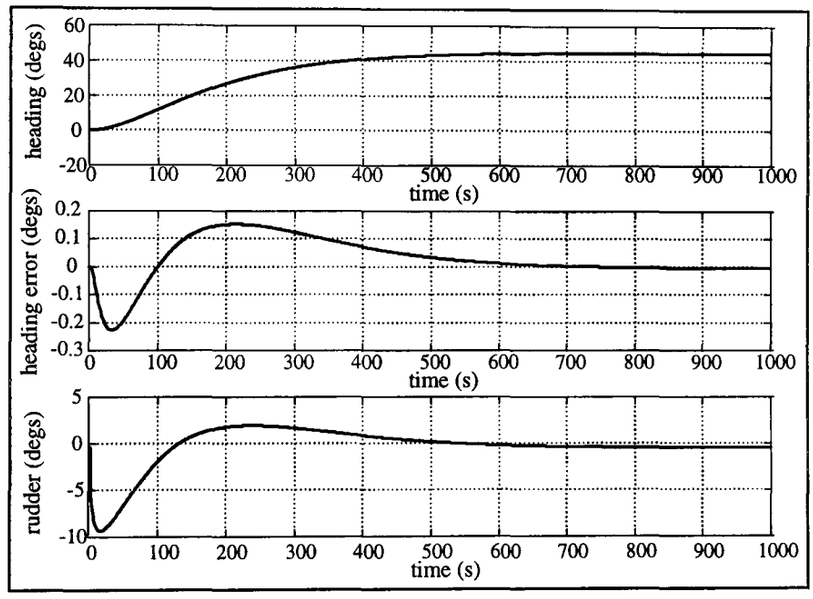

Figure 7.10: Manually Tuned Tanker Course Changing Responses

These responses are considered to be good in that the tanker control system performance satisfies the design criteria set out for this manoeuvre. This can be clearly seen in the responses above since the heading error peak is small (i.e. less than 0.5°) and tracks to zero. Also the rudder deflections are well within the actuators operational envelope (i.e. less than 30°). The peak is still larger than the peak in the submarine rudder response which indicates that the bulk of this vessel calls for increased control effort to make it turn (see Section 7.2.3). This solution is found to satisfy the design criteria set for the

cost function and will provide a good benchmark for the course changing part of this study.

The cost for this response is calculated using equation (7.15) which gives the following value.

$$C_{PER} = 5069.53 \tag{7.18}$$

This helps estimate the optimal region for the course changing control problem.

7.5.3.2 Course Keeping Responses

When the manually tuned parameters are implemented in the tanker course keeping configuration the following simulated responses are obtained. In Figure 7.11(a) the heading, heading error and rudder deflections are presented as in the course changing case. Figure 7.11(b) gives the position of the tanker with reference to the waypoint course and depth contours defined above.

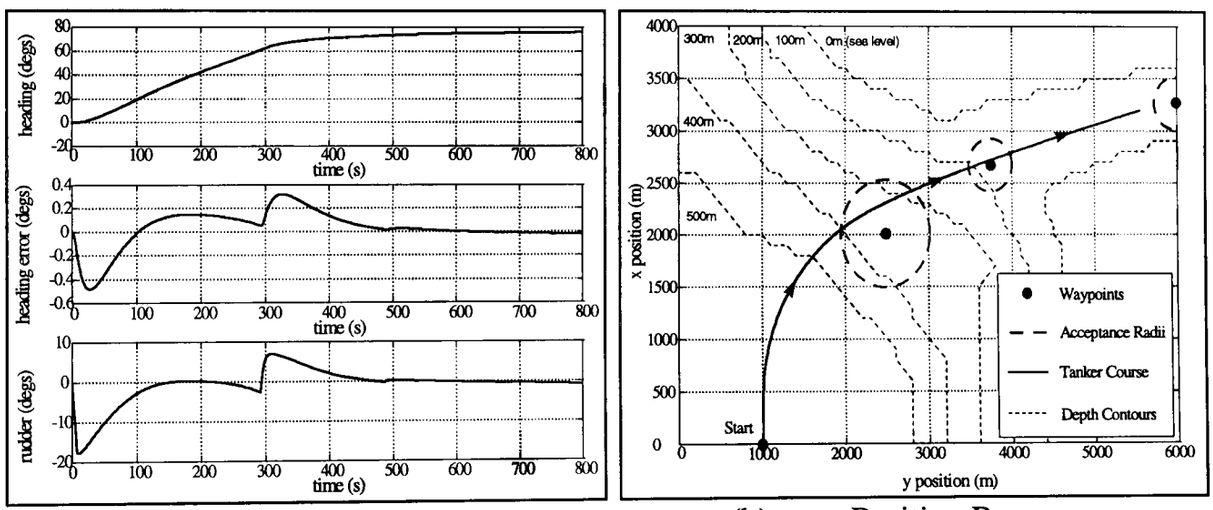

(a) Time History Responses (b) x_p-y_p Position Response

Figure 7.11: Manually Tuned Tanker Course Keeping Responses

These responses show that the tanker controller operates satisfactorily for course keeping since they satisfy the design criteria set out for this application. It can be clearly seen that the heading error peaks are sufficiently small and the response tracks to zero. Also the rudder usage is kept to a relative minimum and the largest peak value (i.e. 18°) is well within the amplitude limit for this actuator (i.e. 30°). In addition to these criteria the penalty cost is satisfied since the autopilot has acquired three waypoints as required. Since this control system has managed to manoeuvre the tanker through the

predetermined course with relatively minimal rudder movement, it is logical to say that this is a near optimal solution and a good benchmark for comparison with the results from the optimisation techniques.

In order to verify this further, the cost components for this solution are calculated using equation (7.17). This gives the cost values shown in Table 7.5.

Table 7.5: Tanker Course Keeping Cost Values

C_{PER}	15247.74
C_{PEN}	0.00
C_{TOTAL}	15247.74

It can be seen that the total cost for this solution is solely due to the performance measure and no penalty cost is applied since the autopilot has acquired the 3 waypoints. This total can be used as an estimate of the optimal region's cost value in the following investigation.

Again the manual tuning process has been found to be a tedious and somewhat difficult process. It took 20 design hours to find these parameters. Therefore there is an obvious need for automatic optimisation for this problem.

7.5.4 SA Results

The SA method is used in this section to optimise separate sliding mode controller parameters for both course changing and course keeping manoeuvres

7.5.4.1 Course Changing Responses

Table 7.6: SA(f) Tanker Course Changing Controller Parameters

ph1	-8.8033
ph2	-0.0497
η_H	6.6910
ϕ_H	47.4657
C_{PER}	119222.68

The parameter values and the related cost in Table 7.6 are obtained from the controller optimisation using Simulated Annealing which starts its optimisation at a randomly

generated point which is far from the optimum region (SA(f)). The optimum region is defined by the manually tuned values in Section 7.5.3.

These values vary considerably from the manually tuned set and the cost is considerably larger than the value shown in equation (7.18). This indicates that the obtained solution is suboptimal in comparison with the manually tuned solution for this problem. This is reflected by the responses illustrated in Figure 7.12.

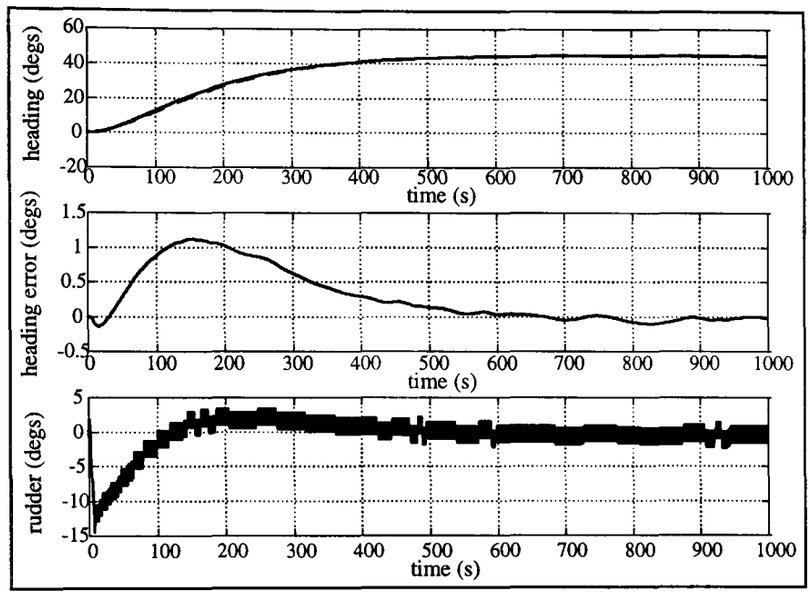

Figure 7.12: SA(f) Optimised Tanker Course Changing Responses

These responses indicate that the SA(f) method has not optimised the controller satisfactorily since it provides an oscillatory rudder response which would wear out this actuator. However the heading response tends to follow the desired heading as the small error shows and could be classed as an optimal solution. This is mainly due to the dynamics of the vessel acting like a low pass filter by not responding to the high frequency rudder signal. Nevertheless the SA method has designed final controller parameters which provide unacceptable rudder responses. This verifies the theory in Chapter 3 that this method would fail to converge if the starting point is too far from the optimal region.

The parameter and cost values in Table 7.7 are obtained from an SA run which is given the manually tuned parameters as its starting points (SA(n)). This is regarded as a near optimum start for the search.

Table 7.7: SA(n) Tanker Course Changing Controller Parameters

ph1	-0.1592
ph2	-0.1653
η_H	0.7659
ϕ_H	0.7189
C_{PER}	4996.01

The resulting pole positions are similar to the manually tuned ones which would suggest a similar solution. However the values for η_H and ϕ_H are different which could alter the response of the controller. When the ratio of these two parameters is compared with the ratio of the manually tuned pair they are found to be similar. This could indicate that this controller is operating in the boundary layer as was found in the submarine case. How this affects the response of the controller can only be found through observing the simulated time history for this solution (see Figure 7.13).

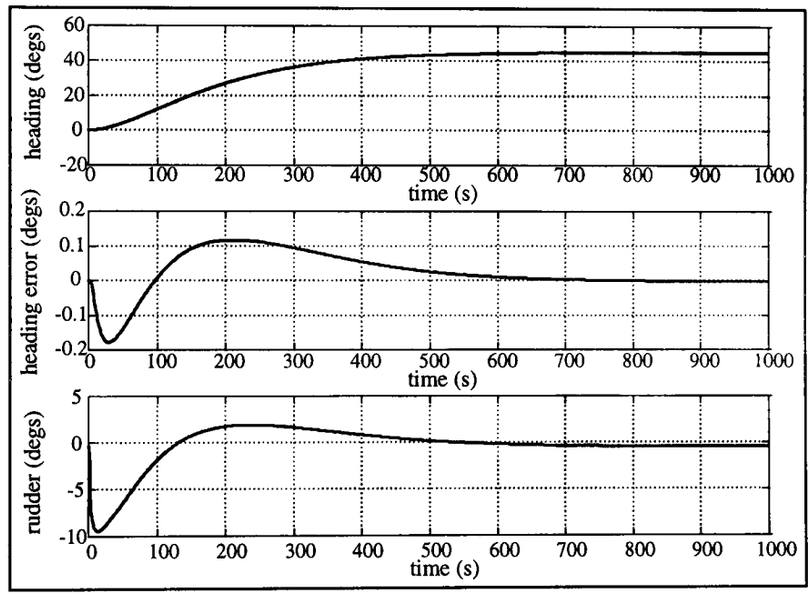

Figure 7.13: SA(n) Optimised Tanker Course Changing Responses

These responses are considered to be good in that they are similar to the manually tuned responses of Figure 7.10. The heading error peak is small and again tracks to zero in finite time. This suggests that the SM controller has obtained the zero sliding surface and performance robustness is guaranteed. In addition to this, the rudder deflection is well within its operating envelope to the same extent as in the manually tuned solution. The satisfaction of both these criteria indicates that the SA obtained a solution which is within the optimum region. However, it can be considered an improvement on the manual solutions when the respective cost values are considered since the value in Table 7.7 is smaller.

Again it is apparent that this method requires *a-priori* knowledge of the location of the optimum in order to optimise a given problem. Therefore SA is found to be a local search method as the theory in Chapter 3 and the results of the previous chapter testify.

7.5.4.2 Course Keeping Responses

The same analysis of the SA method is applied to the optimisation of a SM controller for course keeping. The results from SA(f) can be found in Table 7.8 below.

Table 7.8: SA(f) Tanker Course Keeping Controller Parameters

ph1	-15.8941	C_{PER}	499030801.28
ph2	-0.0006	C_{PEN}	0.00
η_H	40.4830	C_{TOTAL}	499030801.28
ϕ_H	20.7771		

As in the course changing application, the parameter values obtained by this method are found to differ from the manually tuned values. This solution is regarded as suboptimal since the cost values are large. Again this is made apparent when in the associated responses for this solution are considered (see Figure 7.14).

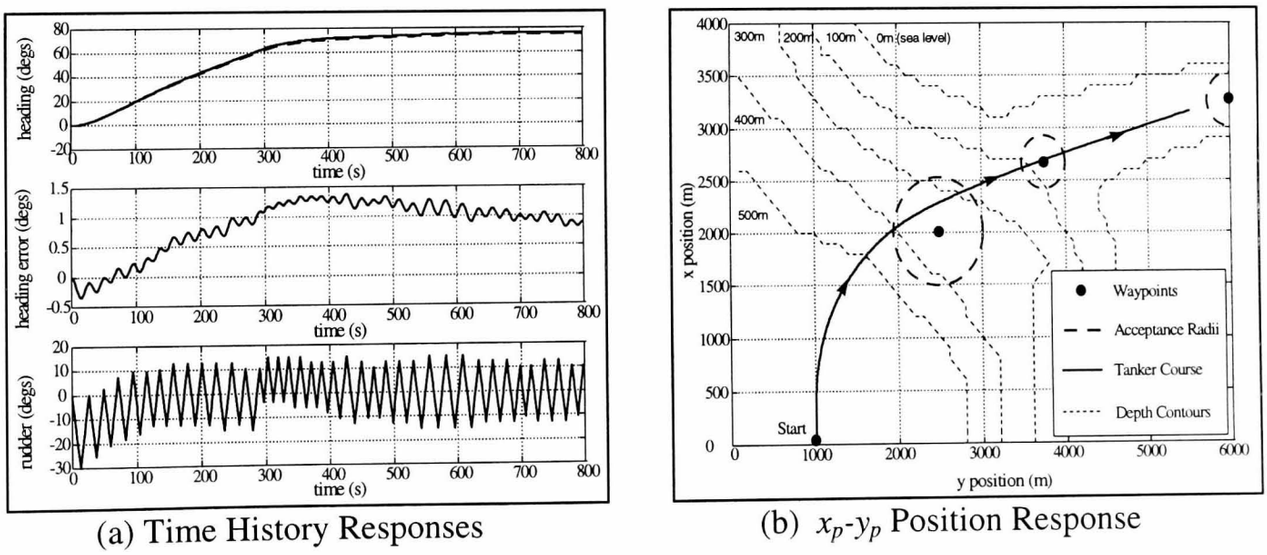

(a) Time History Responses (b) x_p-y_p Position Response

Figure 7.14: SA(f) Tanker Course Keeping Responses

These responses are unsatisfactory in a similar way to the course changing responses as the rudder signal is very oscillatory. Again the error response shows that the desired heading from the autopilot is tracked sufficiently well and the three waypoints are acquired. This shows that the tanker does not readily respond to quick rudder changes

and thus the rudder has limited effectiveness in changing course rapidly (see Section 7.2.3).

A typical SA(n) search which starts at the manually tuned values provides the values shown in Table 7.9.

Table 7.9: SA(n) Tanker Course Keeping Controller Parameters

ph1	-0.1377	C_{PER}	15072.95
ph2	-0.1318	C_{PEN}	0.00
η_H	1.6584	C_{TOTAL}	15072.95
ϕ_H	1.8209		

It can be clearly seen that the pole positions are close to the manually tuned values and that the switching ratio (η_H/ϕ_H) is approximately the same. From the cost values it is apparent that the performance of this solution is within the optimal region and the three waypoint course has been successfully negotiated by the tanker. This can be further verified by the responses in Figure 7.15.

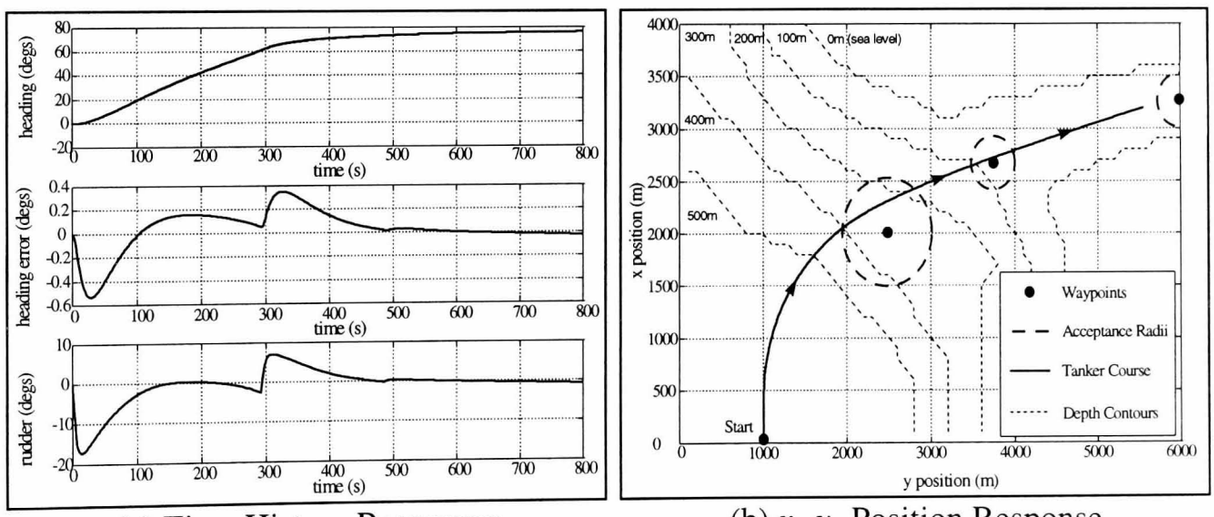

(a) Time History Responses (b) x_p-y_p Position Response

Figure 7.15: SA(n) Tanker Course Keeping Responses

These show that the solution is optimal due to its similarity to the manually tuned responses of Figure 7.11 (i.e. minimal rudder usage and small error which tracks to zero). Thus the SA(n) has optimised the parameters for this control system.

The results of this section add strength to the conclusion that SA is a local optimisation method which requires *a-priori* knowledge of the optimal region in order to optimise

globally [McGookin et al (1996(a))]. This is found to be the case for both the course changing and course keeping systems.

However the solutions obtained by the SA(n) method positions the poles in close proximity to each other. This indicates that the resulting feedback gains have been highly tuned by this method. Although this shows no detrimental effects in the simulations, it could cause problems when physically applied by possibly destabilising the tanker or causing the rudder to saturate.

7.5.5 SSA Results

As with the SA investigation both course changing and keeping controllers are optimised separately by the SSA method.

7.5.5.1 Course Changing Responses

An SSA search which starts at randomly generated points within the search space is used to optimise the course changing SM controller problem. Typical results from such an optimisation are shown in the table below.

Table 7.10: SSA Tanker Course Changing Controller Parameters

ph1	-0.1563
ph2	-0.1634
η_H	0.7325
ϕ_H	0.6387
C_{PER}	4997.28

The pole positions from this solution are similar to the previous optimal solutions obtained for this problem, particularly the SA(n) method. It can also be seen that the ratio of the switching gain to the boundary layer thickness is the same as in the previous near optimum solutions. Hence this solution is the same as the previous ones and is found to give similar responses (see Appendix C.1). This is confirmed by the performance cost value which is of optimal magnitude.

In order to verify that this method has converged to the optimum region an analysis of the median and best costs is required.

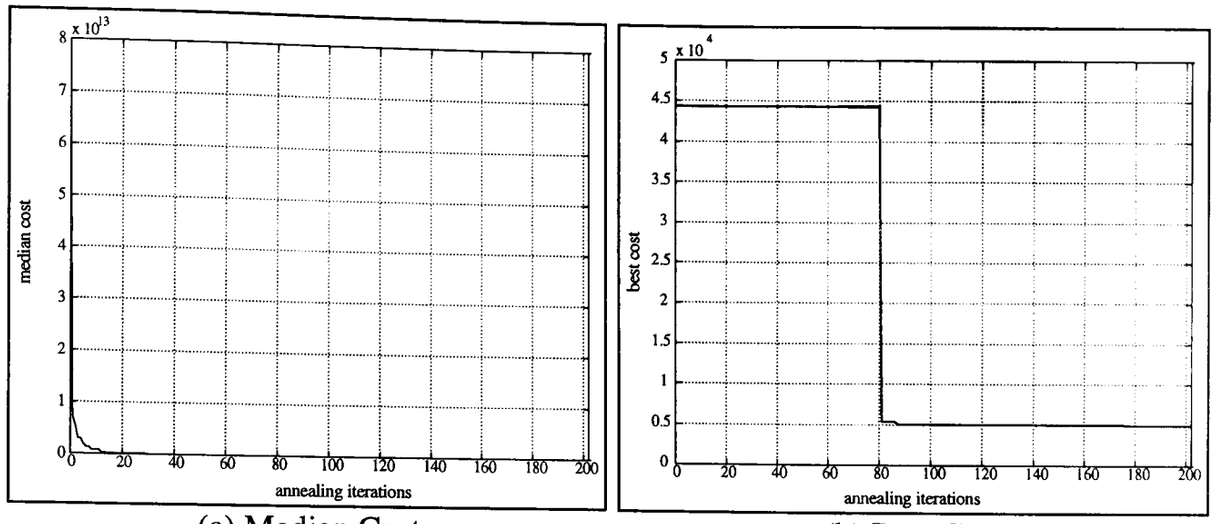

(a) Median Cost (b) Best Cost

Figure 7.16: SSA Course Changing Cost Responses

Figure 7.16(a) shows that the median cost of all the SA runs converges to a small value within 30 iterations. However the best cost plot illustrates that the run with the best final solution converges to within 10% of its final cost value in 86 iterations. As with the submarine case, this is not a true indication of the convergence since all the SA runs need to be executed to ensure the best possible solution is obtained.

To analyse this solution further, the amount of saturation in the final solutions is considered (see Figure 7.17).

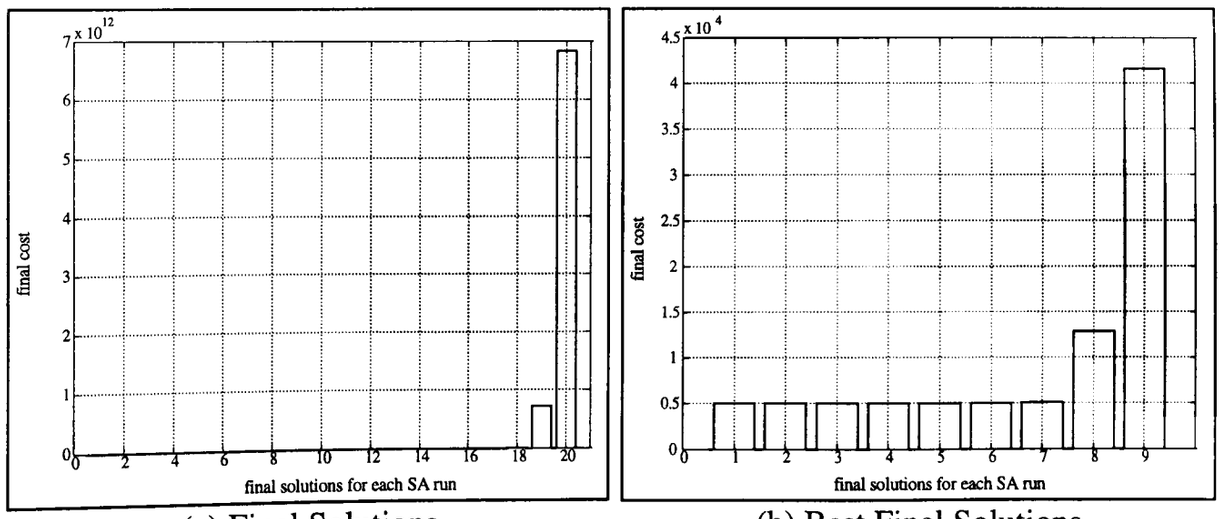

(a) Final Solutions (b) Best Final Solutions

Figure 7.17: SSA Course Changing Final Solution Costs

The histogram in Figure 7.17(a) shows the diversity of the final solutions in terms of performance cost. The best final solutions in Figure 7.17(b) illustrates that saturation has occurred. From this histogram it can be seen that 7 individual runs (i.e. 35% of the solutions) have provided similar near optimum solutions. This is more than in the submarine case which exhibited 15% saturation. One reason for this is the smaller number of parameters being optimised in this case (i.e. the fewer permutations of parameter solutions to explore in order to find the optimum).

Again it has been shown that the advantage of using SSA, compared with SA, is that it does not need *a-priori* knowledge in order to optimise this problem. Therefore this method is shown to be a good global method for optimising a tanker course changing controller.

7.5.5.2 Course Keeping Responses

When the SSA method is applied to the optimisation of a SM controller for the course keeping problem the following typical results are obtained.

Table 7.11: SSA Tanker Course Keeping Controller Parameters

ph1	-0.1569	C_{PER}	15084.23
ph2	-0.1164	C_{PEN}	0.00
η_H	0.3447	C_{TOTAL}	15084.23
ϕ_H	0.3841		

It should be noted that the pole positions are within the same region as the previous near optimum results. However the fine tuning action of this method has provided a solution with slightly higher feedback gains. As with the previous solutions, the switching ratio is approximately the same although the individual parameter values are different. This solution is considered to be a near optimal solution since the performance cost is of the same magnitude as previous solutions and the waypoint penalty cost is zero. When these values are considered in conjunction with the corresponding responses (see Appendix C.1) it is clear that this solution has satisfied the design criteria for this problem (i.e. small heading error, minimal rudder usage and three waypoints acquired).

The convergence of this method is illustrated through considering the median cost response (Figure 7.18(a)) and the best cost response (Figure 7.18(b)).

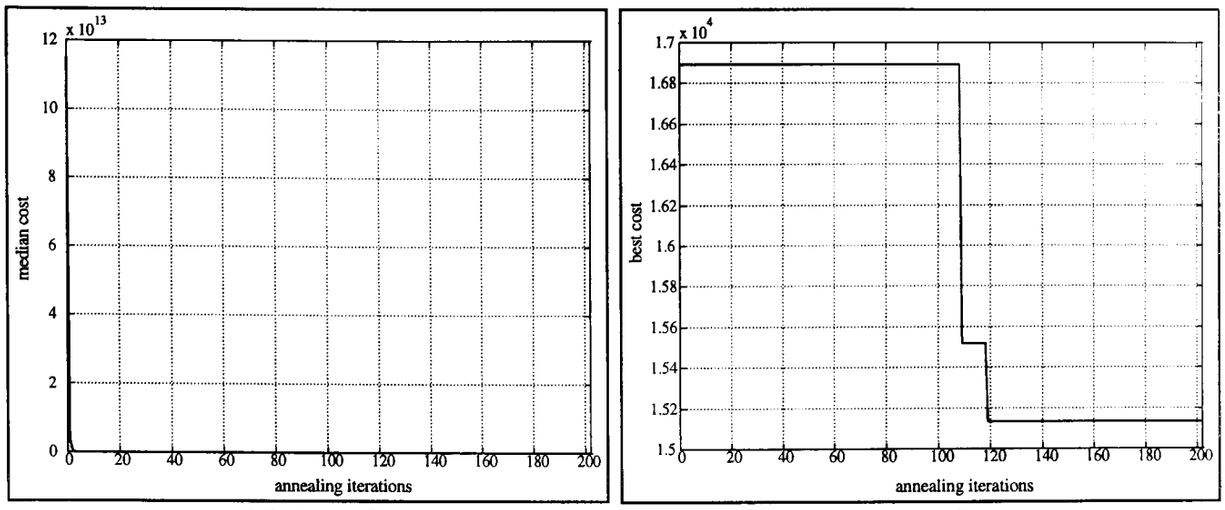

(a) Median Cost (b) Best Cost

Figure 7.18: SSA Course Keeping Cost Responses

The median cost of all the SA runs shows converging trend towards a small cost region within 7 iterations of the method. However the best cost response shows that this run starts its search within about 10% of the final cost value. Therefore it has started within the optimum region. This has happened through the random segmentation process and cannot be guaranteed every time.

To continue the analysis of this method the amount of saturation in the final solutions is illustrated by the following histograms.

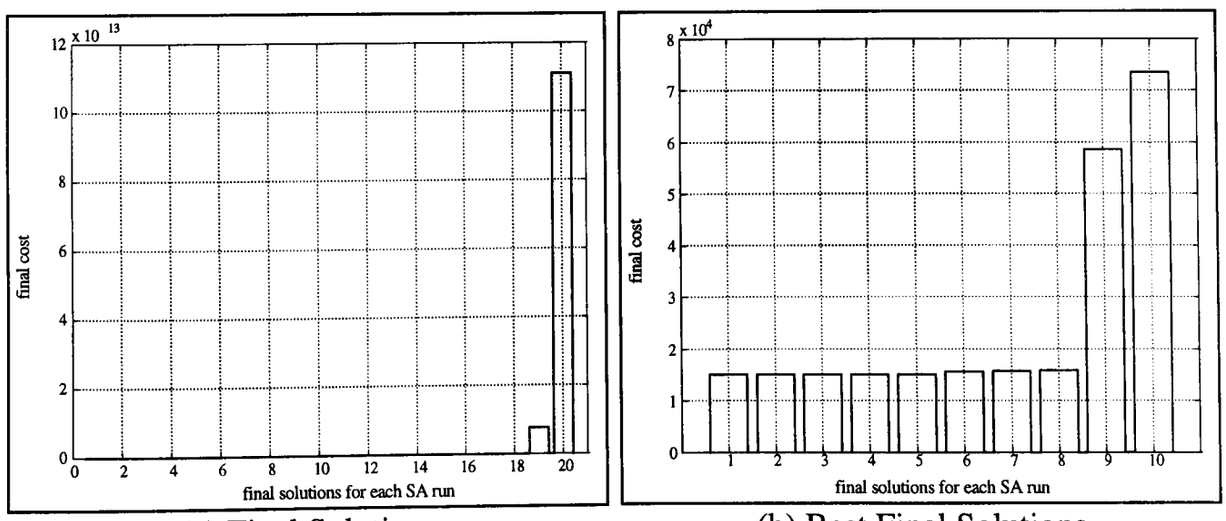

(a) Final Solutions (b) Best Final Solutions

Figure 7.19: SSA Course Keeping Final Solution Costs

Figure 7.19(a) shows a wide range of solution cost values. However saturation is seen to occur in the best solutions (see Figure 7.19(b)). In this case 8 individuals give similar

performance (i.e. 40% of the solutions) which is the about same amount as in the course changing case. This provides confidence that this a near optimum solution.

The above analysis of both the course changing and course keeping systems has shown that the SSA has performed very well as a global search technique for this problem. This strengthens its reputation as a better global search method than SA.

7.5.6 GA Results

Finally, the Elite GA method is used to optimise SM controller parameters for the tanker control problems discussed in this chapter.

7.5.6.1 Course Changing Responses

The parameter values shown in Table 7.12 are typical of those obtained by GA optimisation for the course changing problem.

Table 7.12: GA Tanker Course Changing Controller Parameters

$ph1$	-0.2167
$ph2$	-0.0990
η_H	1.2280
ϕ_H	0.9898
C_{PER}	3145.75

The pole positions for this solution are very similar to the manually tuned values and will therefore behave in a similar manner. Again the individual switching gain and boundary layer thickness values are larger than the manually tuned values. However the switching ratio is approximately unity which is the same value that has been found in the previous solutions. This would suggest that the responses for this solution are the same (see Appendix C.2 for plots) and are near optimal for this problem. When the cost value for this solution is compared with previous optimum values it is apparent that this controller solution performs better in satisfying the design criteria for this problem.

This is further confirmed by considering the convergence of the GA method through the median and best cost plots (see Figure 7.20).

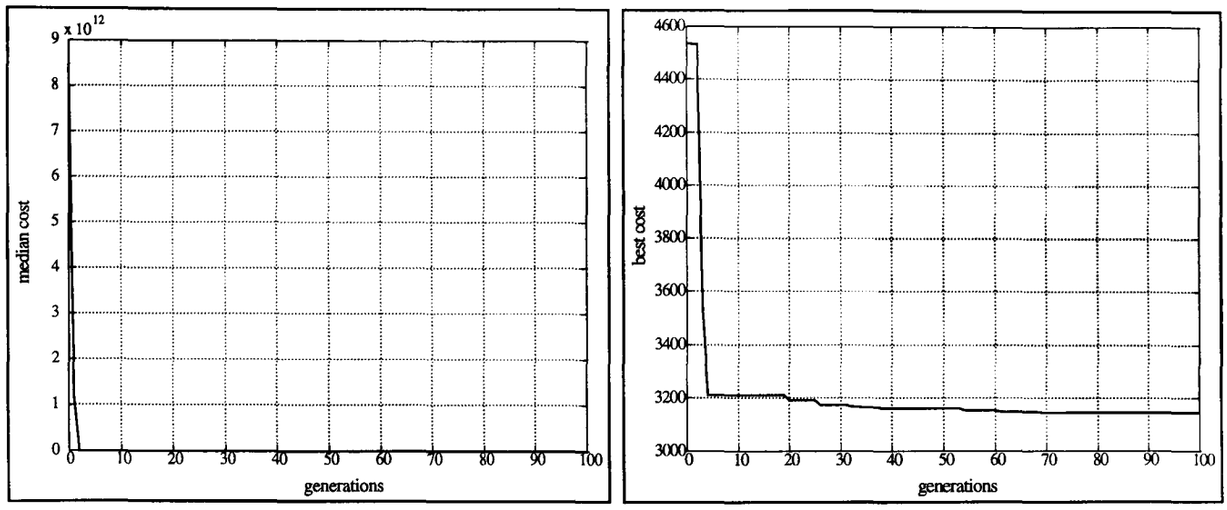

(a) Median Cost (b) Best Cost

Figure 7.20: GA Course Changing Cost Responses

In Figure 7.20(a) the median cost is shown to converge to a low cost region within 3 generations. This convergence is further illustrated by the best cost plot (Figure 7.20(b)). It can be seen from this plot that the search obtains a solution with a cost that is within 10% of the final cost value in the 4th generation. This indicates that the GA has converged very quickly and with minimal *a-priori* knowledge. Also, this is much faster than in the submarine case and is due to the smaller number of controller parameters being optimised in this application.

In order to extend the comparison, the amount of saturation in the final generation is considered (see Figure 7.21).

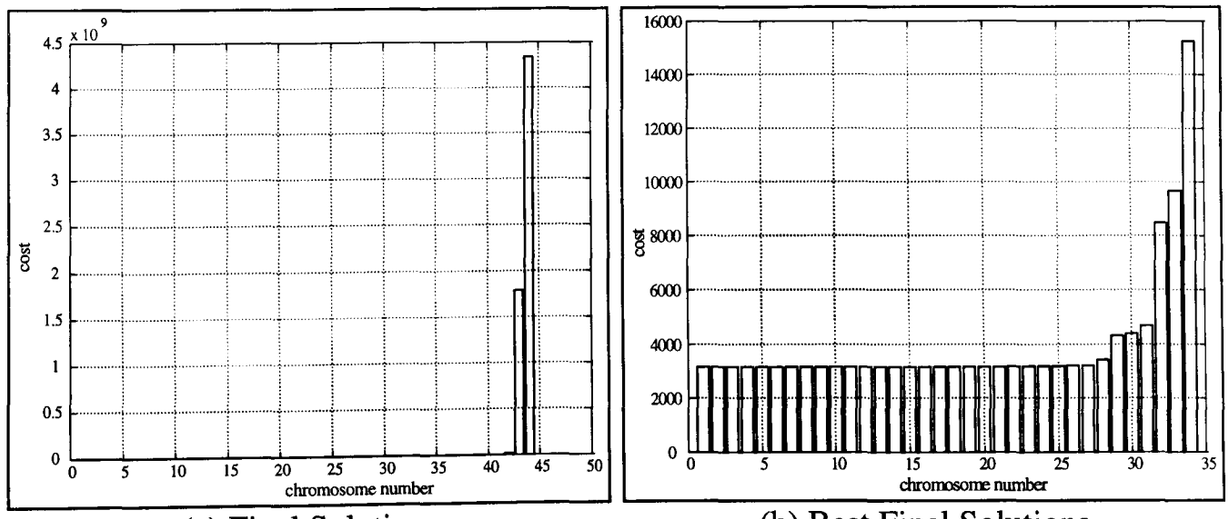

(a) Final Solutions (b) Best Final Solutions

Figure 7.21: GA Course Changing Final Solution Costs

As in the submarine case, the amount of saturation is high and provides confidence in the final solution being near optimal. It can be seen from Figure 7.21(b) that there are

21 individuals which are similar (i.e. 42% of the final generation). This level is higher than the 30% experienced in the submarine optimisation in the previous chapter. Again this is a result of the smaller number of controller parameters and fewer solution permutations for this problem.

7.5.6.2 Course Keeping Responses

When the course keeping control system is optimised using the GA method the values shown in Table 7.13 are typical of those obtained.

Table 7.13: GA Tuned Tanker Course Keeping Controller Parameters

ph1	-0.0995	C_{PER}	9471.16
ph2	-0.1515	C_{PEN}	0.00
η_H	0.4685	C_{TOTAL}	9471.16
ϕ_H	0.3894		

As with the previous solutions, the poles are located in the same area and can be considered near optimal. Also the switching ratio has been optimised to the unity value as in the previous cases. The optimality of this solution can be further illustrated by the response for this solution (see Appendix C.2). These are found to satisfy the performance and penalty cost criteria for this problem as the cost values testify.

The convergence of this search is verified by observing the cost profiles, as in previous analysis (see Figure 7.22).

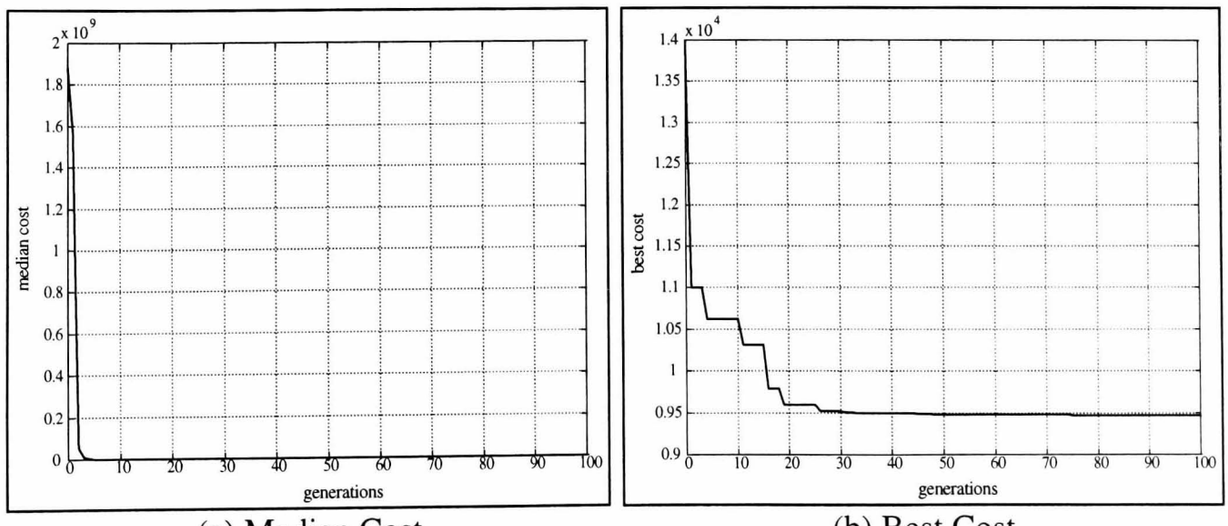

(a) Median Cost (b) Best Cost

Figure 7.22: GA Course Keeping Cost Responses

The median cost (Figure 7.22(a)) illustrates the trend of this search to reach an area of small cost solutions. It can be seen from Figure 7.22(b) that the GA considered here converges to within 10% of its final cost value in 10 generations. Therefore it can be said to be in the optimum region for this problem. This is similar to the convergence rate obtained from the course changing investigation discussed in the previous section. Again the relatively fast convergence is due to the small number of parameters being optimised.

When saturation is considered (see Figure 7.23) the number of similar individuals in the final solution is the same as in the course changing study (i.e. 21 individuals, 42% of the population).

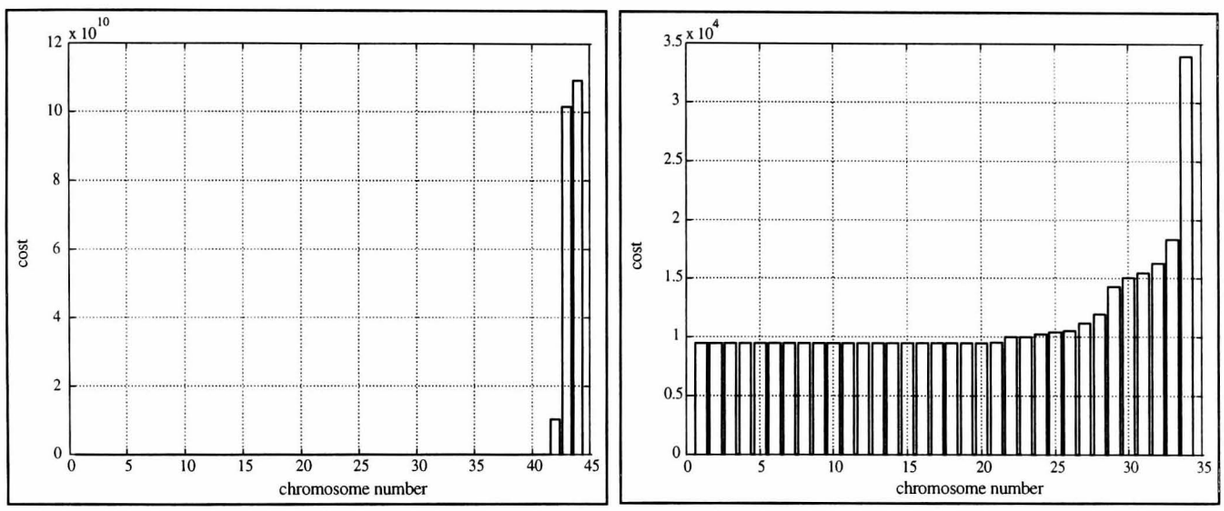

(a) Final Solutions (b) Best Final Solutions

Figure 7.23: GA Course Keeping Final Solution Costs

This would indicate that a similar search space is being explored for both control problems. Also since similar parameter values are obtained for both it can be said that the SM controller for the tanker is sufficiently robust to give good performance irrespective of the manoeuvre and control system configuration (i.e. course changing or course keeping) it is applied to.

7.5.7 Sliding Mode Boundary Layer Operation

As in the submarine case, the values for η_H and ϕ_H vary quite considerably through the optimisations considered here. Again the ratio of η_H/ϕ_H is seen to remain constant throughout thus indicating that in order to obtain good performance the sliding mode

controller must operate entirely within the boundary layer. However the existence of the hard limits at the extremities of the switching term guarantees robustness in the presence of large external disturbances (see Section 6.4.7 for detailed discussion).

7.6 Summary

This chapter has presented the findings of a comparison study between the optimisation methods and their application to control systems for a non-linear tanker model. The particular control systems are designed around two Sliding Mode controller applications which provide course changing and course keeping control capabilities for the tanker. The difference between these two systems is that course keeping provides a positional feedback loop which ensures that the vessel keeps to a predetermined course quite accurately. The course changing controller, on the other hand, only controls the heading of the vessel irrespective of the vessel's positional course. Both of these system configurations have been used as separate optimisation problems and the findings of the this application are discussed below.

It has been shown, for both applications studied here, that the Simulated Annealing method is only good as a local search technique and requires knowledge of the optimal region in order to find an optimal solution. This is also found to be the case in the submarine case where parallels can be drawn.

As expected from the theory set out in both Chapters 3 and 4, the Segmented Simulated Annealing and Elite Genetic Algorithm processes have performed well as global optimisation techniques. Both have obtained optimal solutions for course changing and course keeping configurations without *a-priori* knowledge of the optimal region. The convergence analysis provides evidence to support the Markov Chain analysis provided for both methods. These results strengthen the conclusions found in the submarine study and verify the theories set out in Chapters 3 and 4.

In the submarine study (Chapter 6) the SSA method is shown to have less saturation than the GA method and therefore did not handle that optimisation well. However the level of saturation in this case is shown to be the same for both methods. Therefore the performance of both is the same in this respect. There are two reasons for the difference

in performance in both these applications. Firstly the number of parameters being optimised in the tanker case is smaller and therefore fewer permutations. This makes the problem easier to optimise since less variation is possible. The second is the dynamic responses of the two vessels. The submarine manoeuvres quickly and responds readily to its inputs. This causes greater variation in the cost values for the solutions. The cost values for the tanker do not vary as much since the vessel does not respond readily to its rudder. This limited effectiveness of the rudder reduces the variation in the cost values in the search space and thus the optimum is more dominant for this problem. It is apparent from the results of these applications that the SSA method is more sensitive to the number of parameters being optimised and cost variation than the GA method which maintains a high level of performance throughout the investigation.

Since the same number of simulated evaluations are executed in each of the optimisations (i.e. 4050), it follows that each method takes the same amount of time to obtain a solution. In this case each optimisation took 8 hours on a 166 MHz Pentium running MATLAB™. This is a noticeable improvement on the manual tuning process.

It has also been noted that the controller parameters provide similar controllers for both course changing and course keeping manoeuvres. Thus a single SM controller should be robust enough to be used for both situations as long as its parameters are optimised well. This is logical since the SM discussed in Chapter 5 tracks a reference signal irrespective of how the signal is generated (i.e. human operator or autopilot).

Chapter 8:

Supply Ship Application

8.1 Introduction

The automatic control of a supply ship is chosen as the final optimisation subject for this study. Such ships are used for oil platform support (i.e. transporting supplies for crew and maintenance) and need to be highly manoeuvrable in order to carry out this role [Fossen (1994)]. As well as course changing manoeuvres this type of vessel has to maintain position accurately while loading and unloading is carried out. Such a manoeuvre is called *Dynamic Position Keeping* [Fossen (1994)] and can be difficult for a conventional propeller driven vessel to execute. In order to overcome this difficulty, the type of supply ship considered here uses a set of moveable thrusters to move the vessel in the required manner [Fossen (1994), M^{c}Gookin et al (1997(f))]. This means that there is a significant difference between this application and the oil tanker application considered in Chapter 7 in terms of ship dynamics. The supply vessel responds more quickly to input commands and has a faster time constant associated with the heading dynamics.

An additional advantage of investigating this vessel is the opportunity of testing the resulting optimised controllers in scale model trials. The scale model is called *CyberShip I* and is the test vehicle for the Guidance, Navigation and Control (GNC) Laboratory at the Department of Engineering Cybernetics, the Norwegian University of Science and Technology, Trondheim. This laboratory provides an excellent environment for implementing the sliding mode (SM) control system on a physical vessel without the cost of actual sea trials. Access to this facility has also allowed aspects concerning optimised controller implementation to be addressed [M^{c}Gookin et al (1997(f))].

The optimisation of course changing controllers for this scale model is carried out through simulation studies as in the submarine and oil tanker cases. Then the resulting controllers are evaluated through further simulation and physical trials using different manoeuvres. These tests will also provide a comparison of the non-linear mathematical

representation of this vessel and the actual scale model, thus determining whether this mathematical model is representative of the dynamics of the experimental vessel.

This investigation is concerned more with the implementation of optimised controllers than the techniques themselves. The majority of the study is to do with solutions obtained from the SSA and GA methods as they have already been shown to be global methods. This chapter covers this analysis in the following way. Section 8.2 derives the mathematical representation of this vehicle's dynamics and discusses the dynamics and configuration of the thrusters. Section 8.3 outlines the decoupled heading subsystem and the resulting course changing controller structure. The GNC laboratory facility and the model scaling factor are both described in Section 8.4. Penultimately, Section 8.5 displays the optimisation results and the response obtained from the simulation and physical trial evaluations. The final section summarises the conclusions for this part of the study.

8.2 Ship Model in State Space Form

8.2.1 Ship Dynamics

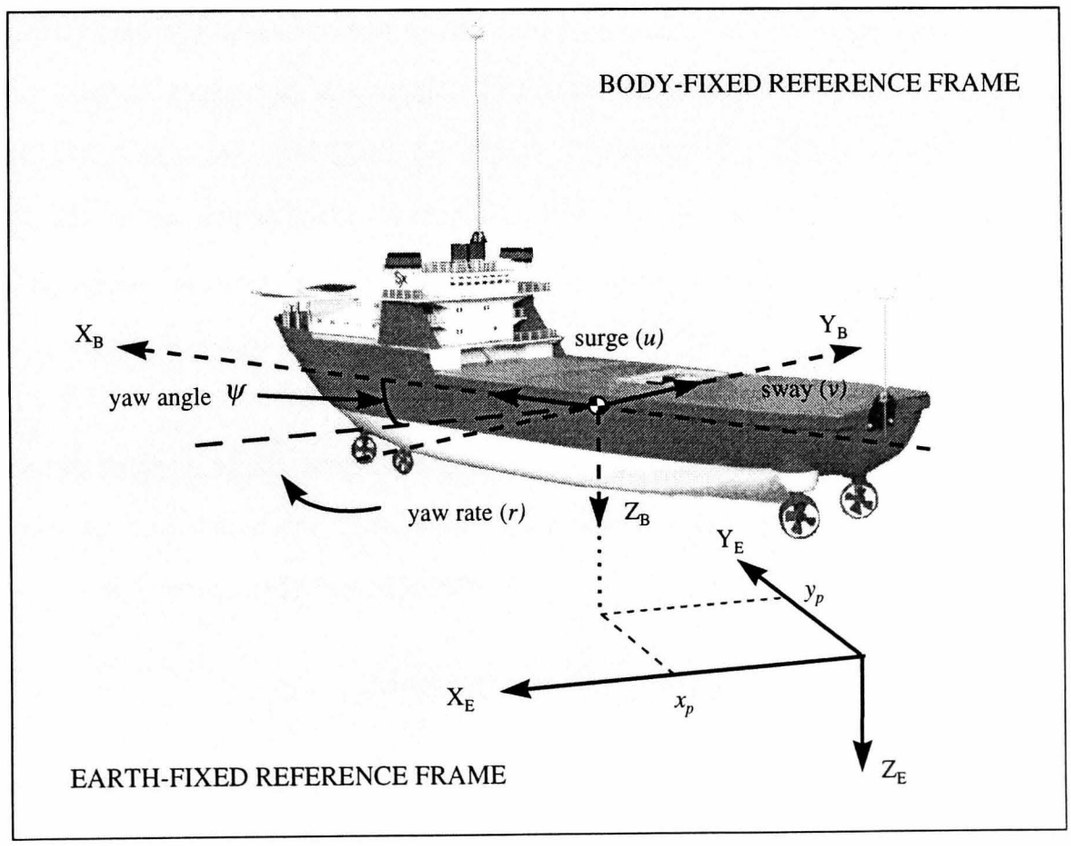

Figure 8.1: Ship Reference Frames and States

In order to explore this application the dynamics of the scale model must be represented by a set of mathematical equations. As with the previous applications, the dynamics are derived from the hydrodynamic equations of motion of such a surface vessel. Again they are obtained from the motion of the model relative to its body-fixed and earth-fixed reference frames (see Figure 8.1) [Fossen (1994), M^{c}Gookin (1993)]. The relative motions of the vessel are defined in terms of the linear and angular velocities [Fossen (1994), M^{c}Gookin (1993)].

The resulting states and inputs which stem from these reference frames are listed in Table 8.1.

Table 8.1: Ship States and Inputs

STATES		INPUTS	
u	surge velocity	τ_1	surge thrust force
v	sway velocity	τ_2	sway thrust force
r	yaw rate	τ_3	yaw thrust force
ψ	yaw (heading) angle		
x_p	x-position on earth		
y_p	y-position on earth		

It should be noted from this table that the propulsion of this type of supply vessel is provided by four thrusters instead of the propeller and rudder configurations used in the previous vessels studied in this work. These thrusters provide force vectors relative to the body fixed axes and constitute the inputs to this vessel. The resulting forces are the components of the input force vector (i.e. $\boldsymbol{\tau} = [\tau_1 \ , \tau_2 \ , \tau_3]^T$ given that τ_1 is the thrust vector along the X_B-axis, τ_2 is the thrust vector along the body fixed Y_B-axis and τ_3 is the thrust about the body fixed Z_B-axis).

As with the motion of all vessels, the dynamics of this scale model can be represented by its *kinetic* and *kinematic* equations. The kinetic equations are represented by the following matrix equation [Fossen (1994)].

$$\mathbf{M}\dot{\boldsymbol{v}} + \mathbf{C}(\boldsymbol{v})\boldsymbol{v} + \mathbf{D}\boldsymbol{v} = \boldsymbol{\tau} \tag{8.1}$$

Here **M, C**($\boldsymbol{v}$) and **D** are the mass/inertia, Coriolis and damping matrices respectively (see Appendix A.3 for values). The vector $\boldsymbol{v}$ represents the body-fixed velocities (i.e. $\boldsymbol{v} = [u \ , v \ , r]^T$) and $\boldsymbol{\tau}$ is the input force vector as defined above. When equation (8.1) is

compared with equation (6.3) it can be seen that the effects of gravity are counteracted by the buoyancy of the ship (i.e. it floats on the surface of the water). On re-arranging equation (8.1) the following is obtained.

$$\dot{\boldsymbol{\nu}} = -\mathbf{M}^{-1}(\mathbf{C}(\boldsymbol{\nu}) + \mathbf{D})\boldsymbol{\nu} + \mathbf{M}^{-1}\boldsymbol{\tau} \tag{8.2}$$

As with the previous applications, particularly the tanker, the kinematic equations are represented by the following matrix equation (see Appendix A.3 for details).

$$\dot{\boldsymbol{\eta}} = \mathbf{J}(\boldsymbol{\eta})\boldsymbol{\nu} \tag{8.3}$$

Again $\mathbf{J}$ is the Euler matrix and $\boldsymbol{\eta}$ represents the earth-fixed states (i.e. $\boldsymbol{\eta} = [\psi, x_p, y_p]^T$). The purpose of this equation is to define the geometric relationship between the vessel and the earth-fixed reference frame which is common to all vessels.

By combining equations (8.2) and (8.3) the following matrix form is produced

$$\begin{bmatrix} \dot{\boldsymbol{\nu}} \\ \dot{\boldsymbol{\eta}} \end{bmatrix} = \begin{bmatrix} -\mathbf{M}^{-1}(\mathbf{C}(\boldsymbol{\nu}) + \mathbf{D}) & \mathbf{0} \\ \mathbf{J}(\boldsymbol{\eta}) & \mathbf{0} \end{bmatrix} \begin{bmatrix} \boldsymbol{\nu} \\ \boldsymbol{\eta} \end{bmatrix} + \begin{bmatrix} \mathbf{M}^{-1} \\ \mathbf{0} \end{bmatrix} \boldsymbol{\tau} \tag{8.4}$$

This can be easy related to the following form of the state space equation

$$\dot{\mathbf{x}} = \mathbf{A}(\mathbf{x})\mathbf{x} + \mathbf{B}\boldsymbol{\tau} \tag{8.5}$$

where $\mathbf{x}$ is the state vector, $\mathbf{A}(\mathbf{x})$ is a non-linear system matrix which depends on the system's states and $\mathbf{B}$ is the input matrix. As indicated in equation (8.1) the input to this ship model is the thrusters' force vector. Hence equation (8.5) represents the dynamics of *CyberShip I* and is used to simulate this vessel in the following study.

8.2.2 Thruster Dynamics

As indicated previously, the purpose of the four thrusters is to propel *CyberShip I* in the direction commanded by the operator. The configuration of the thrusters is shown in Figure 8.2. It can be clearly seen from this figure that the position of the thrusters is given relative to the centre of gravity which is also defined as the origin for the body fixed reference frame. Each thruster is represented by the force it produces (i.e. $f_{1..4}$) and the azimuth angle defining its direction (i.e. $\alpha_{1..4}$) as shown in Figure 8.2.

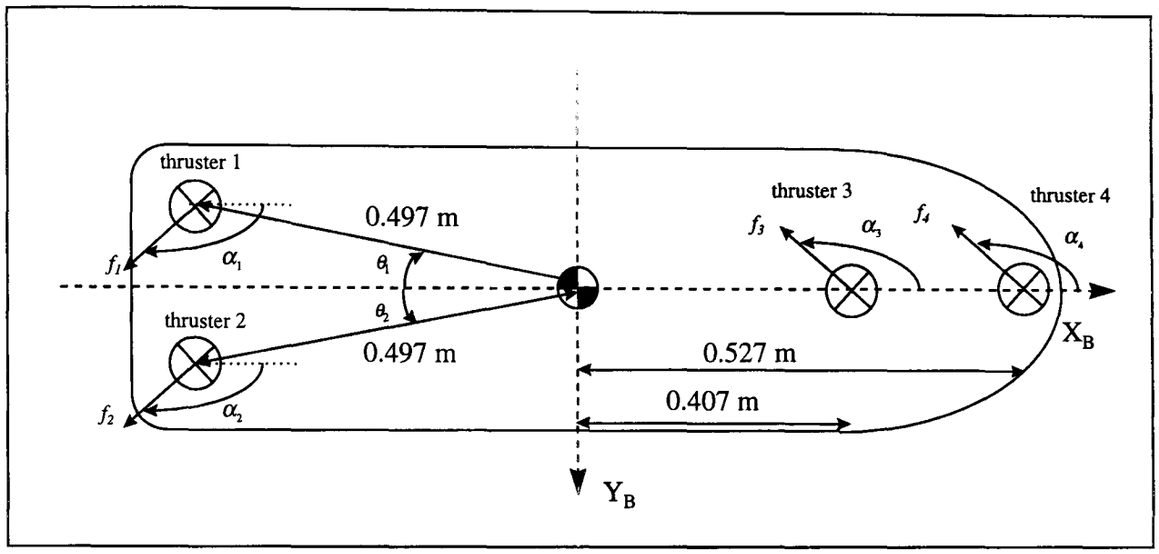

Figure 8.2: Thruster Configuration

In the actual scale model, α_1 and α_2 can be set independently of each other whereas α_3 and α_4 are always equal showing that their corresponding thrusters operate in the same direction. This convention is applied in the simulation of this vessel.

Each thruster has its own natural limits in terms of direction and the force it can produce. The estimates of these limits that are used here are shown Table 8.2 and it can be seen that since each thruster is identical they all have the same limitations.

Table 8.2: Thruster Magnitude Limits

forces $f_{1..4}$ (N)	angles $\alpha_{1..4}$ (radians)
± 0.9	$\pm \pi$

These limits set the operational envelope for the thrusters and subsequently the vessel. There are no rate limits given for this application since the forces occur almost instantaneously and the direction is chosen to be fixed. For this study the azimuth angles are chosen to be fixed at $\alpha_1 = \alpha_2 = \pi$ radians and $\alpha_3 = \alpha_4 = \pi/2$ radians. This indicates that the surge motion is governed by thrusters 1 and 2 at the stern and the sway/yaw motion is governed by thrusters 3 and 4. Although a more complex configuration can be implemented it is felt that this one was adequate for this investigation.

In order to relate the three input force components (τ) of equation (8.5) to the individual forces produced by the thrusters ($f_{1..4}$) the following trigonometric relationship is used [Fossen (1994)].

$$\tau = \mathbf{T}(\alpha)\mathbf{f} \tag{8.6}$$

where $\mathbf{f} = [f_1, f_2, f_3, f_4]^T$, $\boldsymbol{\alpha} = [\alpha_1, \alpha_2, \alpha_3, \alpha_4]^T$ and

$$\mathbf{T}(\alpha) = \begin{bmatrix} \cos\alpha_1 & \cos\alpha_2 & \cos\alpha_3 & \cos\alpha_3 \\ \sin\alpha_1 & \sin\alpha_2 & \sin\alpha_3 & \sin\alpha_3 \\ 0.497\sin(\alpha_1 - \theta_1) & 0.497\sin(\alpha_2 - \theta_2) & 0.407\sin\alpha_3 & 0.527\sin\alpha_3 \end{bmatrix} \tag{8.7}$$

Here the angles θ_1 and θ_2 present a phase shift in the yaw rate thrust allocation which is caused by the position of the thrusters relative to the centre of gravity (see Figure 8.2).

When the chosen azimuth angles are applied to equation (8.7) and small values are neglected, the following matrix is obtained.

$$\mathbf{T}(\alpha) = \begin{bmatrix} -1 & -1 & 0 & 0 \\ 0 & 0 & 1 & 1 \\ 0 & 0 & 0.407 & 0.527 \end{bmatrix} \tag{8.8}$$

This relationship is used to distribute the commanded thrust forces from the controller among the four thrusters of this model.

8.3 Decoupled Subsystems

As with the tanker (and most surface vessels) there are two main sets of dynamics for this model (i.e. surge propulsion and heading). This application is similar to the others in that only course changing manoeuvres are considered and a single sliding mode controller is used to govern this motion. The surge dynamics is directly controlled by step commands applied via the relevant thrust force (i.e. τ_1). Therefore, only the heading dynamics need to be decoupled from the mathematical representation of the ship in order to define the course changing subsystem for this vessel.

8.3.1 Course Changing Subsystem

The course changing subsystem defines the heading motion of the ship in the same way as the submarine and tanker applications (see Figure 8.3). However this subsystem differs from the previous two cases in that the governing input is a force vector rather

than a rudder deflection. Hence this is a direct manoeuvring force rather than the deflected control surface which in turn produces that force.

Another difference in comparison with the tanker study is that the sway velocity is available for feedback to the controller. Even though this model is a scale replica the sway velocity is also available in the actual vessel. The reason that this velocity is made available for this vessel and not for others is due to the role it fulfils. Since a supply vessel of this type provides support for oil platforms it must be able to maintain a constant position while loading and unloading takes place. This is called *dynamic position keeping* and requires full velocity information in order to operate effectively. Hence surge, sway and yaw rate are measured for this purpose. Thus the states for the course changing subsystem are the same as in the submarine case (i.e. v, r and ψ) and the commanded yaw thrust τ_3 is the input.

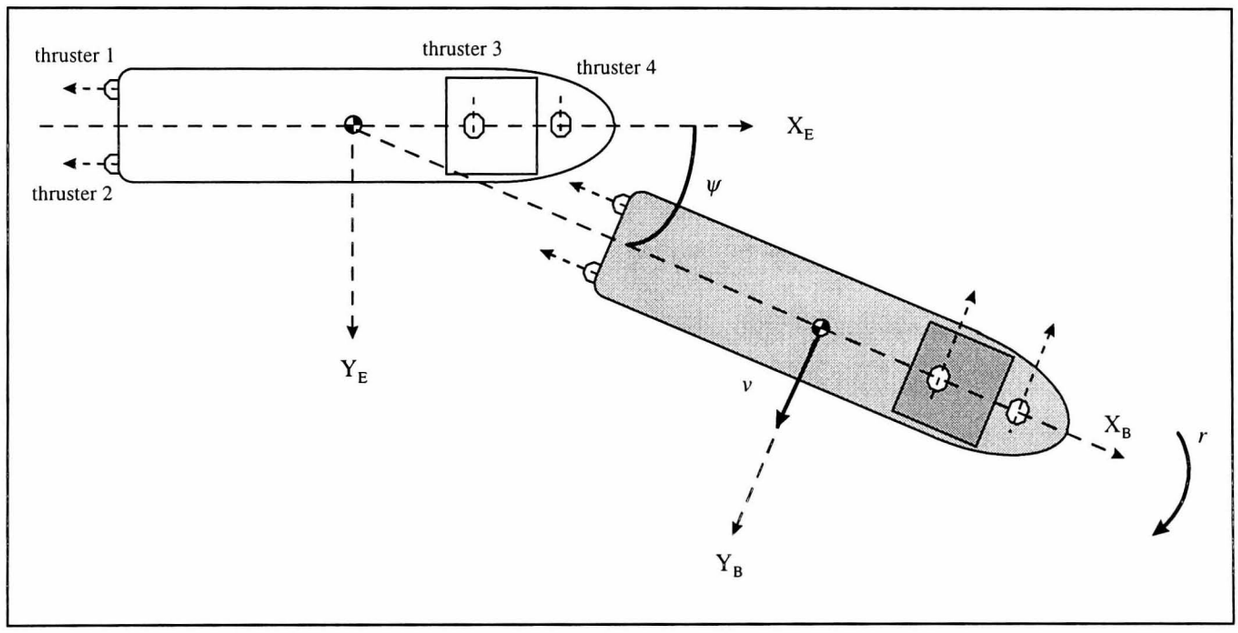

Figure 8.3: Ship Course Changing Manoeuvre

Once this subsystem is decoupled in the way described in Section 5.7, the following state space equation is formed.

$$\dot{\mathbf{x}}_H = \mathbf{A}_H \mathbf{x}_H + \mathbf{b}_H \tau_3 \tag{8.9}$$

In this equation the state vector is $\mathbf{x}_H = [v,\ r,\ \psi]^T$. This is then used as a basis for designing a sliding mode controller in the way described in Chapter 5. The resulting controller becomes.

$$\tau_3 = -\mathbf{k}_H{}^{\mathrm{T}}\mathbf{x}_H + \left(\mathbf{h}_H{}^{\mathrm{T}}\mathbf{b}_H\right)^{-1}\left(\mathbf{h}_H{}^{\mathrm{T}}\dot{\mathbf{x}}_{Hd} - \eta_H \tanh\left(\sigma_H\left(\hat{\mathbf{x}}_H\right)/\phi_H\right)\right) \qquad (8.10)$$

Again the desired heading response is defined as a critically damped second order response which is then used as the tracking reference for the controller.

As in the previous applications, the representation of the heading dynamics (equation (8.9)) does not have an estimate of the model uncertainties. Therefore the switching gain criterion for stability robustness (see Chapter 5) becomes

$$\eta_H > 0 \qquad (8.11)$$

This is satisfied during the optimisation process by ensuring the parameter values for this gain are positive definite as in the previous applications.

8.3.2 Decoupled Course Changing Controller Application to the Main System

For course changing manoeuvres *Cybership I* uses the commanded thrust force τ_3 from the sliding mode controller of equation (8.10). The surge motion is instigated by a τ_1 step command of +0.9 N and the sway thrust force, τ_2, is set to 0.0 N. These provide the inputs for the simulation of the model ship (see Figure 8.4). As with the previous simulations, these inputs are first passed through checks which implement the limits defined in Table 8.2. This confines the operation of the vessel simulation to within the limits set by the thrusters on the actual scale model. The simulation of this ship is based on the schematic shown in Figure 8.4 and again Euler integration [Cheney and Kincaid (1985)] is used to obtain the states from the state space equation.

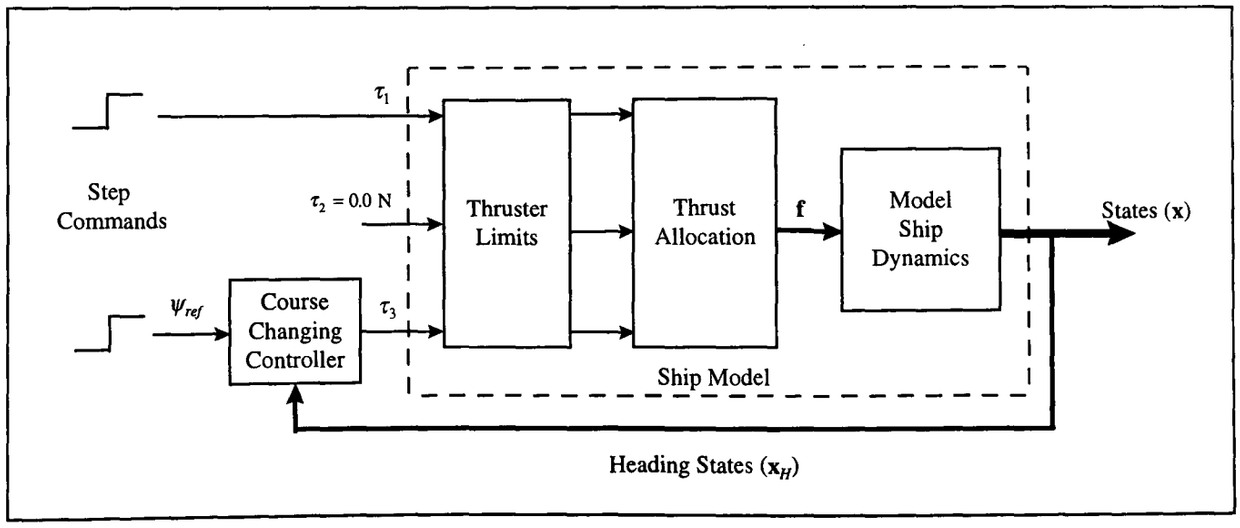

Figure 8.4: Ship Model and Course Changing Controller Configuration

This simulation is used by the optimisation processes to obtain sliding mode controller solutions for this model in course changing manoeuvres. The resulting controllers are then applied to the control of *CyberShip I* in the Guidance Navigation and Control (GNC) laboratory.

8.4 Laboratory Facility and Model Scaling

8.4.1 GNC Laboratory

The Guidance, Navigation and Control (GNC) Laboratory is a watertank facility at the Department of Engineering Cybernetics, Norwegian University of Science and Technology, Trondheim. Primarily this lab is used as a test-bed for the implementation of control systems for governing the motion of the *CyberShip I* model (1:70 scale compared to the actual vessel). The constituent parts of the GNC lab are illustrated in Figure 8.5.

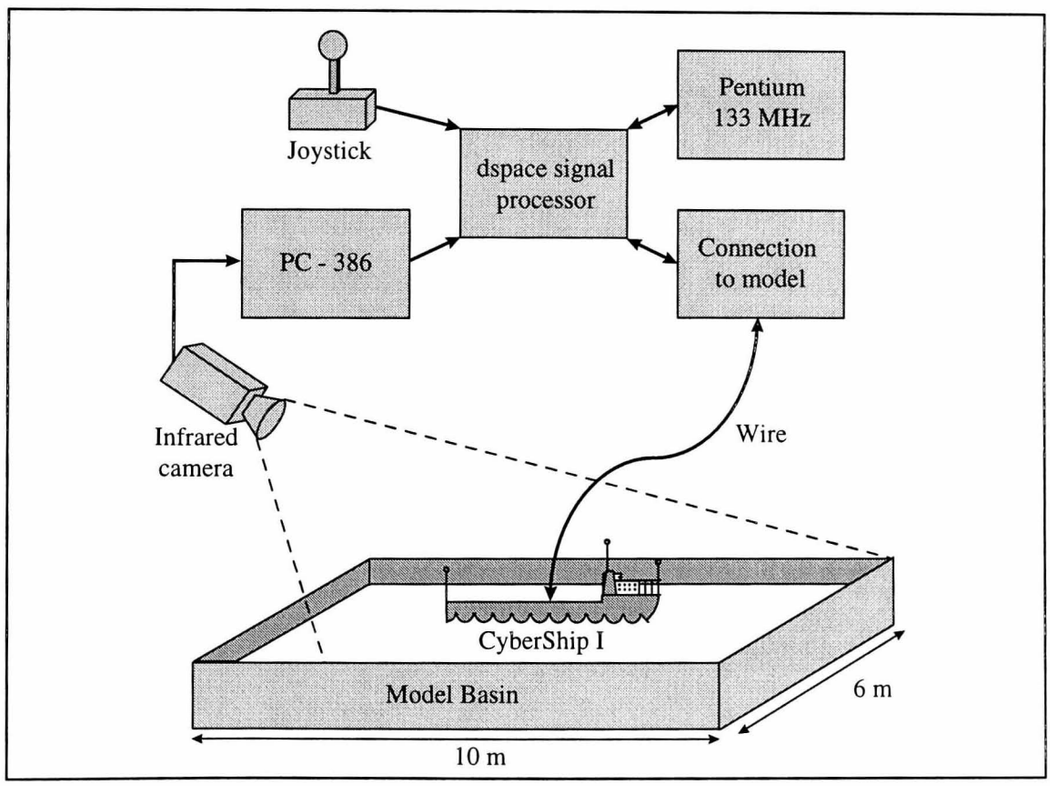

Figure 8.5: GNC Laboratory Schematic

The figure shows that the laboratory is centred around the *model basin* which provides the sailing environment for the ship. This basin defines operational limits of the vessel under investigation which have to be taken into account when simulating the vessel.

The other hardware components provide telemetry and control data for the ship as outlined below.

The *Infrared Camera* provides positional information for the ship in the basin. It achieves this by locating the position of the three masts on the model.

The *PC-386* computer receives the positional data from the camera and calculates the velocities and heading of the ship as well as its position in terms of tank co-ordinates (i.e. earth-fixed).

The *Pentium 133MHz* computer is used to implement the sliding mode control system (equation 8.10) in software. It does this by running MATLAB™ Simulink programs which use the telemetry data to provide commands that are intended to manoeuvre the ship.

The *Joystick* allows the operator to input commands to the system and hence manoeuvre the ship. It can also be used to operate the ship in open loop without the used of a control system.

The *Wire Connection to the Model* carries the commands to the ship thruster servos and carries the actual thruster motion back to the computer system. Although at present this is a wire connection, in future this will be carried out by a radio transmitter system.

The *dspace signal processor* is the hub of the whole system. It processes the data from the other hardware elements and sends out the control system signals to the ship. Hence it is a crucial part of the system. The dspace system can be matched well to the Matlab Simulink software to provide an easy to use block diagram environment for the operator.

The complete system gives an ideal test facility for trials of marine control systems that could execute various roles for this ship (e.g. course changing, dynamic position keeping). This laboratory is used to evaluate the controllers obtained through optimisation and determines how readily they can be applied to a physical system.

8.4.2 Model Velocity Scaling

Since the *CyberShip I* is a scale model of an actual type of supply vessel the velocities it produces are scaled proportionally. The amount of scaling depends on the *dimensionless parameter* used to determine the ratio between the model and the actual vessel [Fox and McDonald (1985)]. In this case the *Froude number* is used to represent the relationship between two similar vessels in the same fluid i.e.

$$Fr = \frac{V}{\sqrt{gL}} \tag{8.12}$$

where V is the velocity of the vessel, g is the acceleration due to gravity and L is the length of the vessel. In this context the dimensionless Froude number of the model (Fr_m) is equal to the Froude number of the actual vessel (Fr_a) i.e.

$$Fr_m = Fr_a$$
$$\frac{V_m}{\sqrt{gL_m}} = \frac{V_a}{\sqrt{gL_a}}$$

When this is rearranged the following velocity relationship is obtained

$$V_a = \sqrt{\frac{L_a}{L_m}} V_m \tag{8.13}$$

Since *CyberShip I* is a $1/70^{th}$ scale model, equation (8.12) becomes

$$V_a = \sqrt{\frac{70}{1}} V_m = 8.37 V_m \tag{8.14}$$

Therefore the linear velocities of the boat are approximately eight time larger than the corresponding velocities on the model.

The angular rates are handled in a similar manner. Since the angular rate Ω is effectively

$$\Omega = \frac{V}{L} \tag{8.15}$$

the relationship represented by equation (8.12) can be used i.e.

$$\Omega_a = \frac{V_a}{L_a} = \sqrt{\frac{L_a}{L_m}}\frac{V_m}{L_a} = \sqrt{\frac{L_a}{L_m}}\frac{L_m\Omega_m}{L_a} = \sqrt{\frac{L_m}{L_a}}\Omega_m \tag{8.16}$$

When the relevant scaling is applied this equation becomes

$$\Omega_a = \sqrt{\frac{1}{70}}\Omega_m = 0.12\Omega_m \tag{8.17}$$

Hence the opposite ratio applies for the angular velocities i.e. the model's angular velocities are eight time larger than the actual vessel's.

These ratios provide an insight into how the results shown in this study relate to the real vessel which is being modelled.

8.5 Optimisation Process and Results

As with the previous optimisation studies, this problem also has numerous design aspects to be defined in order to proceed. In this section the controller parameters that are to be optimised are defined along with the cost function used to represent the optimisation criteria. Similar to the previous cases a desired heading response has to be defined for the optimisation. This response is used as the optimisation case and the optimal results are outlined in the final subsections. However additional test data is used to evaluate the resulting controllers through other simulated manoeuvres and corresponding experiments in the GNC laboratory. This allows the global optimisation methods to be examined with respect to direct implementation issues.

8.5.1 Controller Parameters

Since this application is a course changing control system the four parameters used to optimise the controller which are shown in Table 8.3. Again these are the two poles of the decoupled closed system (the third is zero and corresponds to the yaw dynamics) and η_h and ϕ_h which are the switching gain and boundary layer thickness respectively.

These are manipulated by the optimisation techniques to produce an optimal controller for this application.

Table 8.3: Ship Controller Parameters to be optimised

1st Heading Closed loop pole	*ph1*
2nd Heading Closed loop pole	*ph2*
Heading switching gain	η_h
Heading Boundary Layer Thickness	ϕ_h

8.5.2 Cost Function

The cost function is effectively the same integral least squares criterion used in the previous chapters [Dove and Wright (1991)].

$$C = \sum_{i=0}^{tot} \left[(\Delta\psi_i)^2 + (\tau_{3i})^2 \right] \tag{8.18}$$

As in the previous cases *tot* is the total number of iterations and $\Delta\psi_i$ is the *i*th heading angle error. However the input in for this ship is τ_{3i} which is the *i*th thruster force value in yaw [Dove and Wright (1991), M^{c}Gookin et al (1997(c)(e)(f))]. Again the optimisation methods attempt to minimise the value of this function which in turn allows both $\Delta\psi_i$ and τ_{3i} to be minimised too. As with the submarine (Chapter 6) and tanker (Chapter 7) problems $\Delta\psi_i$ gives an indication of how well the controller is operating and τ_{3i} is used to keep the yaw thruster force value to a minimum to avoid operational limits (see Table 8.2) and chattering (see Section 5.7). This function allows the same trade off between heading tracking accuracy and input usage to be considered during the optimisation. Another advantage of minimising the thruster force is the saving in terms of fuel consumption since the resistance to the forward motion is minimised [Dove and Wright (1992)]. Since the thruster force is reduced, the hull produces less drag and hence more of the forward force goes to producing a larger surge velocity. This is similar to the tanker situation.

8.5.3 Desired Responses

In order to keep the optimisation conditions the same as the previous investigations, a desired heading response of 45° is chosen which gives the critically damped step shown in Figure 8.6. This response enables the desired states for the controller to be obtained and thus enables the state error vector to be calculated.

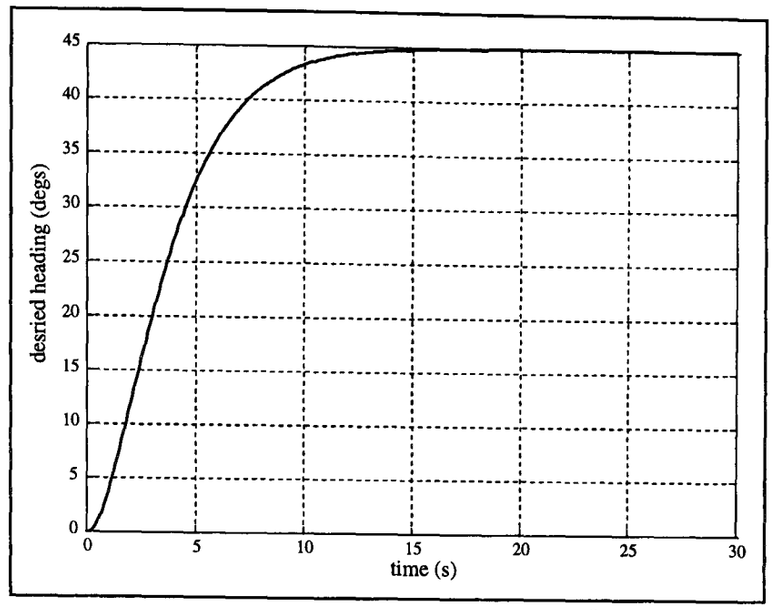

Figure 8.6: Desired Heading Response (45^{O} manoeuvre)

8.5.4 Optimised Controller Evaluation

In order to test the optimised controller further it is simulated using another manoeuvre. A $20^{O}/-20^{O}$ manoeuvre is chosen which gives the desired heading response shown in Figure 8.7 [M^{c}Gookin et al (1997(f)].

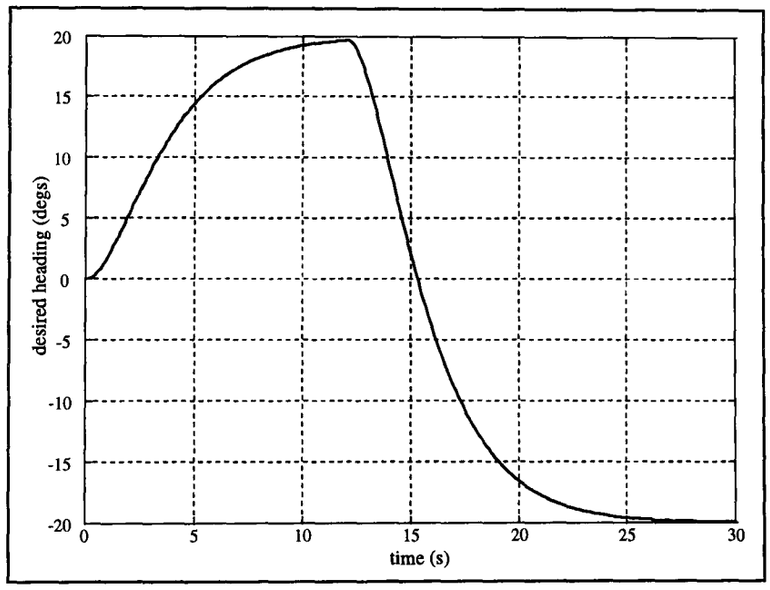

Figure 8.7: Desired Heading Response ($20^{O}/-20^{O}$ manoeuvre)

The above response provides a manoeuvre which will assess any asymmetry with in the motion of the vessel since it commands positive and negative turns. This will allow the controller to be evaluated for a different simulated turn from the one for which it was optimised. The same desired response is then used in the GNC when the controller is used to manoeuvre *CyberShip I.* This provides further evaluation in terms of applying an optimised controller directly to the system it is designed for.

8.5.5 SA Discussion

In the previous two chapters it has been shown that the SA method only operates well as a local optimisation technique. Although this is also found to be true in this case the purpose of this chapter is to investigate the practical implementation of globally optimised controllers in the GNC Laboratory. Therefore there is no need to reiterate what has already been proven in the previous part of this work.

8.5.6 SSA Results and Evaluation

The SSA method has been shown to work well for a global optimisation for the submarine and tanker problems. When this is applied to the supply ship problem the following set of results are typical of the results it obtains.

Table 8.4: SSA Optimised Controller Parameter

ph1	-3.7700
ph2	-0.2053
η_h	19.2135
ϕ_h	5.0369
C_{head}	6.0161

These give the simulated responses for the heading (ψ), the heading error ($\Delta\psi$) and the thrust commanded for this manoeuvre (τ_3) as shown in Figure 8.8.

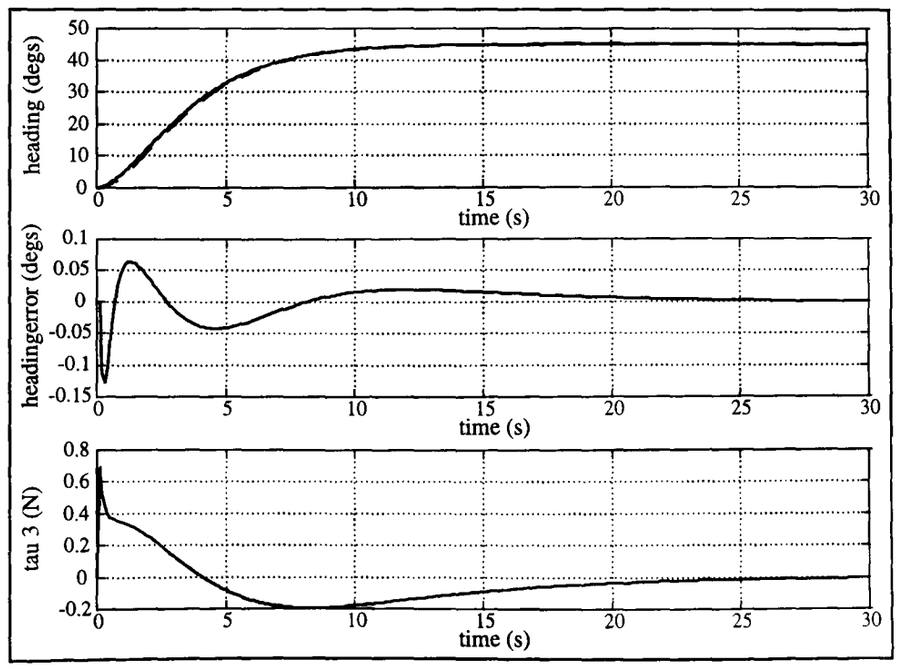

Figure 8.8: SSA Optimised Controller Simulation Responses (45° manoeuvre)

It can be seen that the results appear consistent with the design criteria that constitute the cost function since the peak error magnitude is very small (i.e. 0.1° which 0.2 % of the desired heading) and tracks to zero in the steady state. It is also apparent that the thrust magnitude is small and that the vessel executes this manoeuvre well within its operational envelope. However it should be noted that the initial thrust spike is quite large and may cause problems during implementation. From these results it can be deduced that the SSA has optimised the controller parameters to satisfy the design criteria and therefore the parameters and cost are within the optimal region. However these are simulated responses for a single manoeuvre and may not operate well for different simulated manoeuvres or when it is applied to the actual system.

In order to test the optimised controller further it is simulated for the 20^{o}/-20^{o} manoeuvre which was discussed above. The simulation gave the responses shown in Figure 8.9.

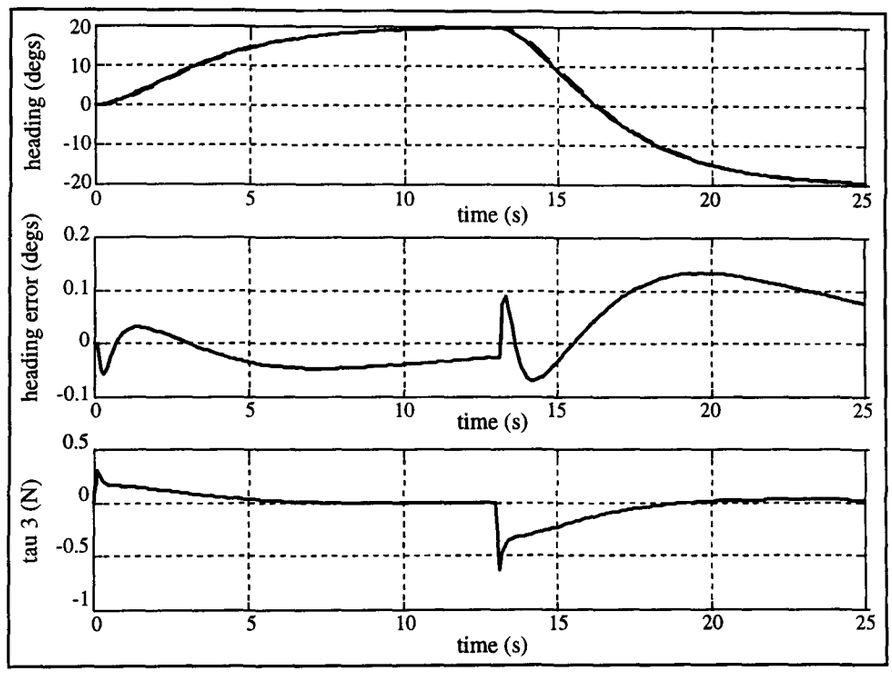

Figure 8.9: SSA Optimised Controller Simulation Responses (20°/-20° manoeuvre)

As with the optimised responses of Figure 8.8, the heading, heading error and thruster time histories are shown. Again the error is small which indicates that the heading tracks the desired response well. The thruster force peaks are reasonably large showing that this manoeuvre is quite demanding for this vessel. However, it still remains within the operational limits of the thrusters and therefore shows that the controller can handle course changing commands other than the single manoeuvre it is designed for. These

simulation results illustrate that the optimised controller could be used for general course changing manoeuvres.

The final test is the implementation of this controller for course changing on the GNC *CyberShip I* model. So that a comparison with the simulation results can be carried out, the responses for a 20°/-20° manoeuvre are given in Figure 8.10.

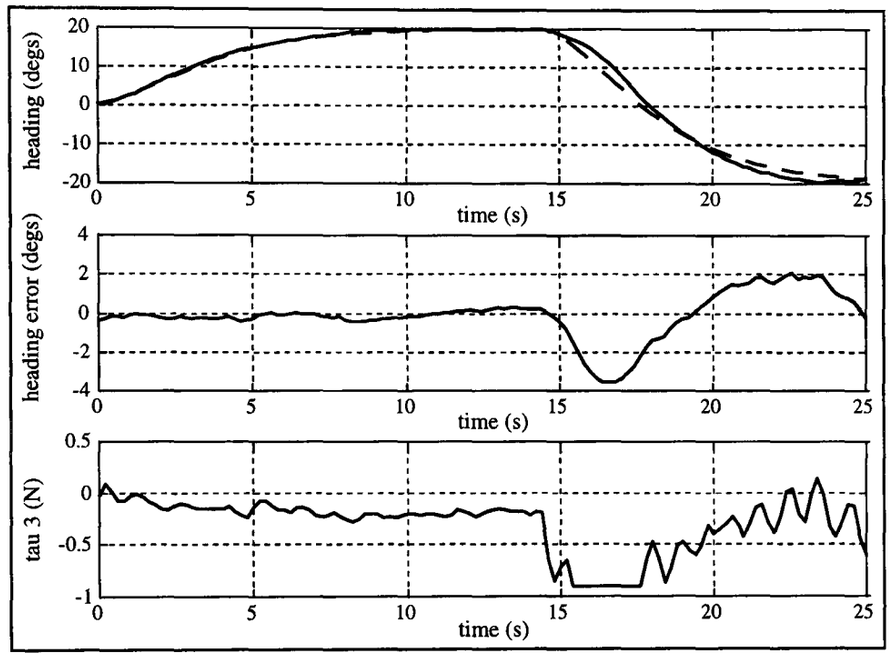

Figure 8.10: SSA Controller Model Basin Responses (20°/-20° manoeuvre)

These show a slight difference from the simulated responses for this manoeuvre. It can be clearly seen that both the peak heading error and thruster commands are larger than in the simulated case. There are three main reasons for this difference. Firstly it has been found that the mathematical representation of the model is not accurate and therefore gives slightly unrealistic responses in the simulation study. The second aspect is that very little consideration is given to the drag caused by the position of the thrusters. Since the bow thrusters are perpendicular to the flow over the hull they cause maximum drag and this affects the motion of the model. This could account for the slight offset in the thruster plot. Finally the roll motion and water disturbance effects are also not considered and can alter the motion of the model in the lab's model basin.

However the main drawback with this implementation is that during the largest part of the manoeuvre the thruster is seen to saturate. This would indicate that the controller gains are too highly tuned for this manoeuvre and that the optimised solution would

need further alteration to produce a satisfactory control system. Therefore the fine tuning action of this method can be a problem where implementation is concerned.

8.5.7 GA Results and Evaluation

The typical GA optimisation of this problem yields the values shown in Table 8.5.

Table 8.5: GA Optimised Parameter Values

ph1	-2.2092
ph2	-0.2059
η_h	8.1620
ϕ_h	1.2851
C_{head}	6.0387

Although there is variation in the parameter values, the cost is similar to the SSA optimised value. When these parameters are applied to the 45° manoeuvre simulation the responses in Figure 8.11 are obtained.

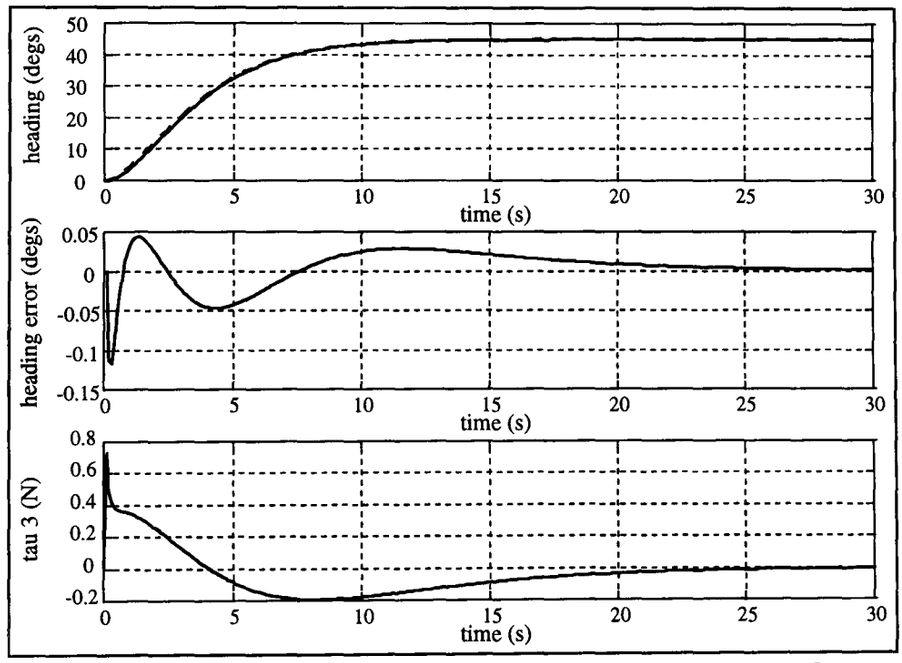

Figure 8.11: GA Optimised Controller Simulation Responses (45^{O} manoeuvre)

As in the SSA simulation the peak error magnitude is very small and is zero in the steady state. It should be noted that the thruster magnitude does not have as large an initial peak as in the SSA responses. However the switching gain is not as large as in the SSA case showing that this parameter is not as highly tuned. Nevertheless these

results show that the GA has optimised the parameters so that the controller performance satisfies the design criteria.

This controller solution is evaluated further using the same 20°/-20° manoeuvre as in the SSA case. These give the responses shown in Figure 8.12. From these responses it can be clearly seen that the error and thruster force peak values are relatively small and good heading tracking is achieved. It should be noted that the thrust is applied for a longer duration than in the SSA case. This shows that the control effort is more evenly divided throughout the manoeuvre with this solution. Nevertheless this controller can be applied to similar manoeuvres to the magnitudes shown here (approximately 45°) and can be used for general course changing operations within this limit.

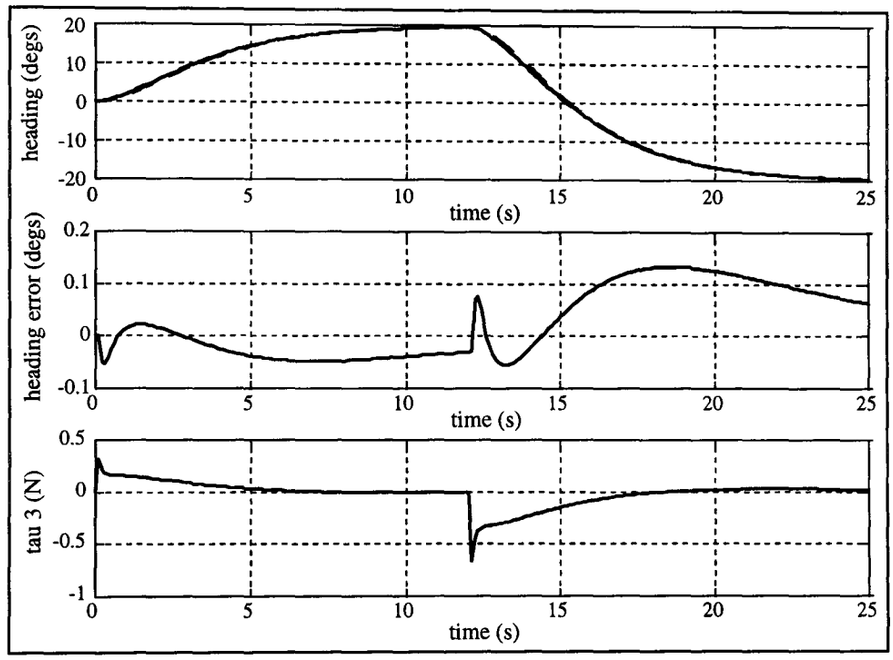

Figure 8.12: GA Optimised Controller Simulation Responses (20°/-20° manoeuvre)

Again the final test is the application of this optimised controller for a 20°/-20° manoeuvre in the GNC lab. It is found that *CyberShip I* responds to this controller in the way shown in Figure 8.13.

Again differences between these and the simulated responses are apparent for the same reasons as discussed in the previous section. Although these aspects could alter the motion, their influence does not substantially degrade the performance of the controller. It should be noted that this controller solution does not saturate. In fact the controller operates a lot better since the errors are relatively small and the thruster forces stay

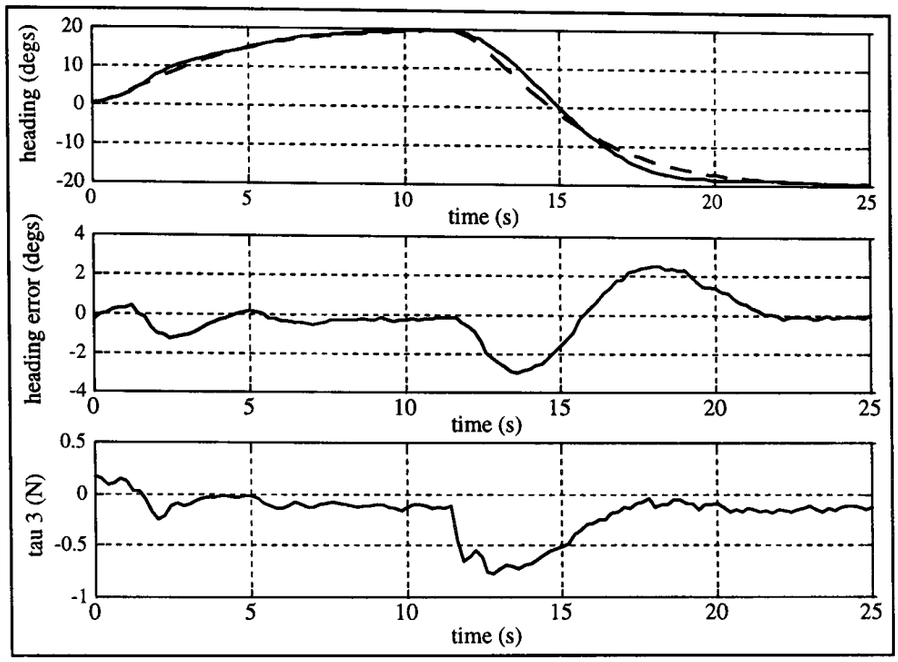

Figure 8.13: GA Controller Model Basin Responses (20°/-20° manoeuvre)

within their physical limits. From these responses it can be seen that the controller is still able to track the desired response adequately and a minor amount of further tuning could yield a slightly better solution. However the solution provided by the GA from simulated data has been shown to operate adequately when applied to the actual scale model.

8.6 Summary

In this chapter a study of controller parameter optimisation and evaluation for the actual scale ship model *CyberShip I* has been presented. Here a Sliding Mode controller has been optimised for a simulated course changing manoeuvre of 45°. The resulting controllers have also been evaluated for a simulated 20°/-20° manoeuvre and then applied in the GNC laboratory for the same manoeuvre. The optimisation study mainly considered the two global methods discussed in the previous applications (i.e. SSA and GA). Since the SA method has been shown to be a local optimisation method it was not considered here.

The results from the SSA method showed that the optimised controller performed well for simulated manoeuvres. This is to be expected since the same mathematical representation is used. When the controller is applied in the GNC laboratory the thruster force is found to saturate thus showing that the controller gains are too highly

tuned. This is a result of the fine tuning mechanism associated with this method which can cause any resulting optimised controller to require further tuning before implementation.

The GA optimised controller performed similarly for both simulated and actual responses. However no saturation occurs in the actual implementation in the GNC laboratory. This shows that the lack of fine tuning in the latter stages of this method can be advantageous since it does not run the risk of over tuning controller parameters as in the SSA case.

Therefore the main result of this chapter is that the broad optimisation provided by the GA can avoid over tuning solutions more readily than the SSA method. It is also more likely to provide a solution which can be implemented directly to the actual problem without further parameter tuning.

Chapter 9:

Optimisation Methods: Their Limitations and Refinement for Controller Design Problems

9.1 Introduction

The previous chapters of this work have been concerned with the comparison of specific evolutionary optimisation techniques such as simulated annealing (SA) and genetic algorithms (GAs). The systems under consideration have remained the same throughout and the study has thus enabled some more general observations to be made regarding optimisation methods. Variations of these optimisation methods have been examined and used to overcome some problems and potential disadvantages of standard optimisation tools that have been highlighted by this application oriented study. In this chapter these variations are discussed and each debated in separate sections.

The initial variants are presented to attempt to remove some of the limitations in the performance of the global search techniques (i.e. SSA and GA) in the light of problems which have arisen in the course of this work. These guide the search techniques to the optimum region by removing redundancy inherent in the standard search methods [M^{c}Gookin et al (1997(b))].

Other aspects concerning alternative search principles are also discussed. The first is the use of smaller *demetic* groups within GA populations to aid the search for problems with a large number of parameters. Although it is not directly applicable to the problems investigated here the approach is presented to show the relationship between this method and the segmentation process used in the SSA method. A second principle considered concerns the use of *multi-objective* optimisation [Fonseca and Fleming (1994), Whidborne and Postlethwaite (1996)] where instead of single cost functions which provide single objectives each design criterion is considered separately. *Pareto* optimality is presented for this optimisation theory and the differences between this method and the single objective criteria used in the previous chapters are discussed.

The final part of this chapter presents some discussion about the problem *search space*. This search space is the mathematical terrain which defines the variation and interaction

of the optimisation problem parameters in terms of the cost value for the possible solutions. Obviously the form of the terrain will determine how dominant the optimum region is within this space. This in turn determines how easy the problem will be to optimise. Therefore a method of determining the search space terrain prior to optimisation would be extremely useful. In this section such a method is presented for predicting how easy a controller problem is to optimise. This is based around the cost function definition and how the dynamics of the plant involved can influence the value of this function. Using definitions from control and marine vehicle theory a qualitative theory of optimisation prediction is evolved. From this and standard manoeuvrability tests a quantitative measure is presented [Nomoto and Norrbin (1969), Fossen (1994)] and used to determine the nature of the problem search space and suggest which optimisation methods should be used. Such an approach is of potential interest for control applications outside the marine field.

These aspects are addressed in this chapter in the following way. Improvements in the segmented simulated annealing (SSA) and the GA algorithms are outlined in Section 9.2. Section 9.3 describes the use of demetics to improve the GA technique when optimising large sets of parameters. This is compared with the segmentation process and parallels are drawn. Following this the multi-objective optimisation mechanism is described and compared with the single objective optimisation approach studied previously. Finally, the use of well established control definitions to determine optimisation ease is discussed in Section 9.4. This enables guidelines for a test to be used to determine which optimisation process should be used for a specific problem.

9.2 SSA and GA Improvements

Although both the SSA and GA methods have been shown to be good global optimisation techniques for the problems considered here, they also have drawbacks that have been discussed previously. These are detailed below.

The SSA method is limited by the number of final candidates which are near the optimum region i.e. saturation. This tends to reduce confidence in the best final solution being near the global optimum without a-priori knowledge of where that optimum lies. A process called *cloning* is presented for this method.

In the case of the elite GA method the amount of saturation in the final generation can be excessive and may cause convergence to a local optimum if the mutation rate is not high enough (see Chapter 4). In order to prevent premature convergence a minimisation process is discussed here which will lessen the amount of saturation by reducing the population size during the optimisation. Both these mechanisms are outlined below.

9.2.1 SSA Cloning Process

Segmented Simulated Annealing is found to be lacking in the sense that it does not give a concentrated number of similar optimum solutions. This means that the final optimal solution, although good, could not be compared or verified by similar optimal results and thus reduces confidence that this solution is globally optimal.

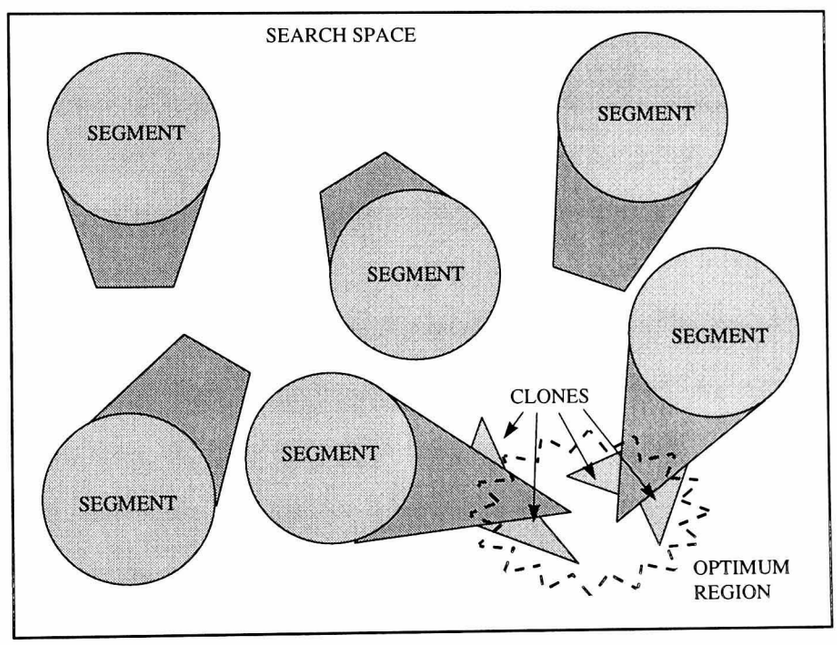

Figure 9.1: Cloning Process in the Search Space

To rectify this the SSA algorithm can be altered in the following manner. The process of SA is carried out for only half the annealing schedule at which point a *cloning* operation is instigated where the best $s\%$ (e.g. 10%) of the solutions are cloned (or copied) a number of times (e.g. nine times). This percentage is known as the *cloning percentage*. The resulting clones then replace the remaining (100-s)% (e.g. 90%) poorer solutions and are then used as the starting point for the remainder of the temperature changes (see Figure 9.1). This method directs the search into the optimum region and increases the number of final solutions within the optimum region. Consequently this adds validity to the final solutions being global optimums in a similar way to GA

saturation (see Sections 6.4.6 and 7.5.6). This is applied to the SSA method in the way shown in Figure 9.2 and has been found to operate in the desired manner.

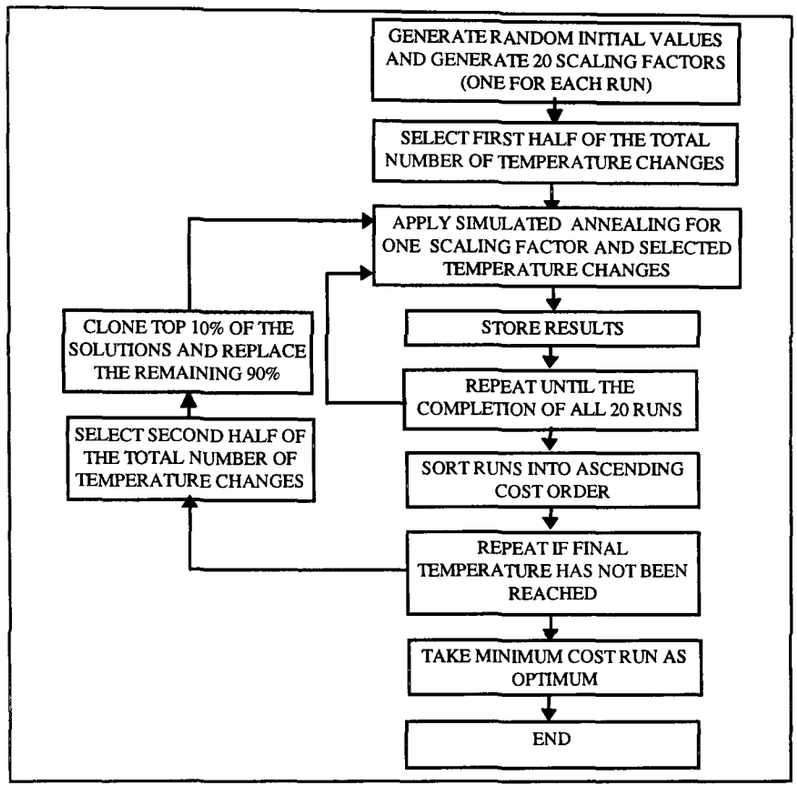

Figure 9.2: SSA with Cloning Flow Diagram

It should be noted that careful consideration must be given to the size of the cloning percentage. If this percentage is too small then the search will become too localised and the final solutions may not lie near the true optimal region. Therefore the cloning percentage should be chosen so that the amount of variation in the best *s%* is sufficiently wide to ensure diversity in the final solutions. This ensures that a reliable search has been carried out in the final stages of the annealing schedule.

9.2.2 GA Population Minimisation Process

Genetic Algorithms (GAs) [Goldberg (1989), Brooks et al (1996), M^{c}Gookin et al (1997(b))] have been found in this study to produce very similar individuals in the best members of the final generations. This phenomenon is called *saturation* and is mainly caused by the crossover operator. Since crossover between similar individuals will result in similar children and the mutation rate will only result in very slight incremental improvements in the solutions, the saturation effect is inevitable. Although this is considered to be a good aspect of this method, the amount of saturation can be slightly

excessive and can make certain population members redundant as they are already represented. These redundant elements cause the convergence rate to slow down since similar results are evaluated a number of times. This problem is particularly prevalent in elite GAs [Brooks et al (1996)] which through their rank based selection scheme can tend to saturate the final population quite heavily.

In order to reduce this redundancy and thus decrease the amount of saturation, numerous hybrid schemes have been implemented which use the GA in the initial part of the search and then another method when saturation occurs (e.g. Simulated Annealing [Adler (1993), Renders and Flasse (1996)]). Although these algorithms provide beneficial results they tend to stray from the evolutionary analogy used in GA theory. Therefore, in order to combat the saturation problem and still remain loyal to the fundamental basis of GAs, a form of *Minimising Genetic Algorithm* (MiGA) [M^{c}Gookin et al (1997(b))] is presented here. This reduces the population size as redundant saturation occurs and thus decreases the number of crossover operations. By slightly varying the approach to mutation the apparent mutation rate increases thus adding more variety to the individuals found by the search. This helps to avoid local minima and helps ensure the acquisition of the global optimum.

The GA saturation effect and the resulting reduction in convergence rate is analogous to there being too many tribe leaders and not enough minions to carry out constructive work. However it can be rectified by reducing the population size as saturation starts to occur [M^{c}Gookin et al (1997(b))]. This is achieved as detailed below.

9.2.2.1 Population Reduction Process

The process of reducing the population size is determined by monitoring the variation in the parameters and cost of the top k individuals of the population. The value of k is usually a certain percentage (b%) of the initial population size. This reduction should be chosen wisely so that the number individuals eliminated by this process does not reduce the population size too much. If the corresponding parameters and costs of these individuals are within a tolerance of 10% of each other then the population is reduced by d individuals. This is achieved by removing the bottom $d/2$ of the top k individuals and the worst $d/2$ individuals of the entire population so that a cost balance is maintained.

To continue the previous analogy, this is similar to some of the tribe leaders moving away to bigger and better things and taking the most easily influenced individuals in the tribe with them.

The value of d is apparently the major design parameter for this mechanism. It has been found that sensible guidelines for this value are

$$k/2 \leq d \leq k \tag{9.1}$$

Although both limits will give different reduction rates, the saturation rate will compensate so that they will give similar final population sizes (i.e. a smaller reduction rate will have its reduced parameters replaced more quickly and will therefore have to do more work to maintain the set number of saturated values). It has been found that the upper limit of this range (i.e. $d = k$) works sufficiently well. However, the number of individuals observed should be selected wisely in order to still retain a sufficient amount of saturation so that the final solution is confidently optimal. It should be noted that this process will still allow the final generation to contain some individuals which are similar to each other but they will be outside the specified tolerance.

9.2.2.2 Crossover Rate Change

Since the population size will reduce when saturation occurs and the percentage of children is kept constant (i.e. 80%), the resulting number of children will also reduce. Therefore the number of crossover processes executed will be reduced proportionally. This is proved below.

After saturation the population size (q) will reduce by d i.e.

$$\begin{aligned} q_{i+1} &= q_i - d \\ &= q_i - q_o \tfrac{b}{100} \end{aligned} \tag{9.2}$$

where q_o is the initial population size. Therefore the number of children (c) will be reduced to the nearest even integer to

$$\begin{aligned} c_{i+1} &= q_{i+1} \times 0.8 \\ &= (q_i - d) \times 0.8 \\ &= c_i - d \times 0.8 \end{aligned} \tag{9.3}$$

Since the number of crossover executions (x) is half of the number of children the number of these executions becomes

$$\begin{aligned} x_{i+1} &= \frac{c_{i+1}}{2} \\ &= \frac{c_i}{2} - \frac{d \times 0.8}{2} \\ &= x_i - \frac{d \times 0.8}{2} \end{aligned} \tag{9.4}$$

Hence crossover is reduced by half the amount that the number of children is reduced. This in turn is related to the population reduction rate.

9.2.2.3 Mutation Rate Change

Mutation is treated differently in this method. With a fixed population size GA the mutation rate (m) is kept constant and thus the number of genes mutated (g_m) is constant. However, in this method g_m remains constant and the mutation rate is allowed to vary. Given that the number of chromosomes is reduced by the minimisation process, it can be easily seen that the number of genes eligible for mutation (g_{total}) is decreased as well. Since the mutation rate can be defined by the following equation

$$m = \frac{g_m}{g_{total}} \tag{9.5}$$

where g_m is constant, it can be concluded that as g_{total} decreases the mutation rate m will increase. Therefore as the population size is minimised the mutation rate increases. This allows wider variation in the search and hence the ability to jump out of a local optimum in the later stages. It also enables an increase in incremental improvement in the final solutions which is in some way similar to the fine-tuning action of the SA and SSA.

9.2.2.4 Variation of Optimisation Execution Time

The major potential time saving is associated with reductions in the population size. If this number is reduced it follows that the number of evaluation simulations is reduced by the same amount. In control applications the execution time for a simulation is the main component of each iteration of the algorithm and it is logical to say that the

reduction in time is proportional to the population reduction. Hence a saving in execution time is achieved which is dependent on the saturation rate.

However, the amount of time saved is dependent on the amount of saturation. This is dependent on how quickly the search locates the optimal region which in turn is related to how close the initial population is to this region. Of course this is randomly determined when the initial population is created and cannot be accurately guaranteed without *a-priori* knowledge.

9.3 Segmentation and Demetics

The study of the SSA has indicated that the segmentation of the search space can help the localised Simulated Annealing (SA) search technique to operate as a global search mechanism. Although this has been shown to work well with SA, it can be equally well applied to other hill-climbing and gradient search techniques which might not have adequate range to optimise a problem globally.

In addition to helping local searches this segmentation process could also assist global search methods when the number of parameters is considered to be large (e.g. 20 parameters). This increases the dimensions of the search space and thus increases the number of permutations of parameter values available for evaluation. Therefore segmenting the search space allows numerous wide ranging localised searches and thus increases the likelihood that a globally optimal solution is obtained in this circumstance.

In the context of GAs a similar segmenting process already exists which is generally called *Demetics*. This isolates the population into smaller groups and evolves these groups separately (see Figure 9.3 for illustration). Each demetic population evolves through separate elite GAs by keeping the best of each group generation. In order to ensure variation in the populations and avoid local convergence, individuals are allowed to *migrate* to other populations at regular intervals (see Figure 9.3). The individuals and their corresponding destinations are selected at random thus making migration independent of the optimality of the individuals and groups considered.

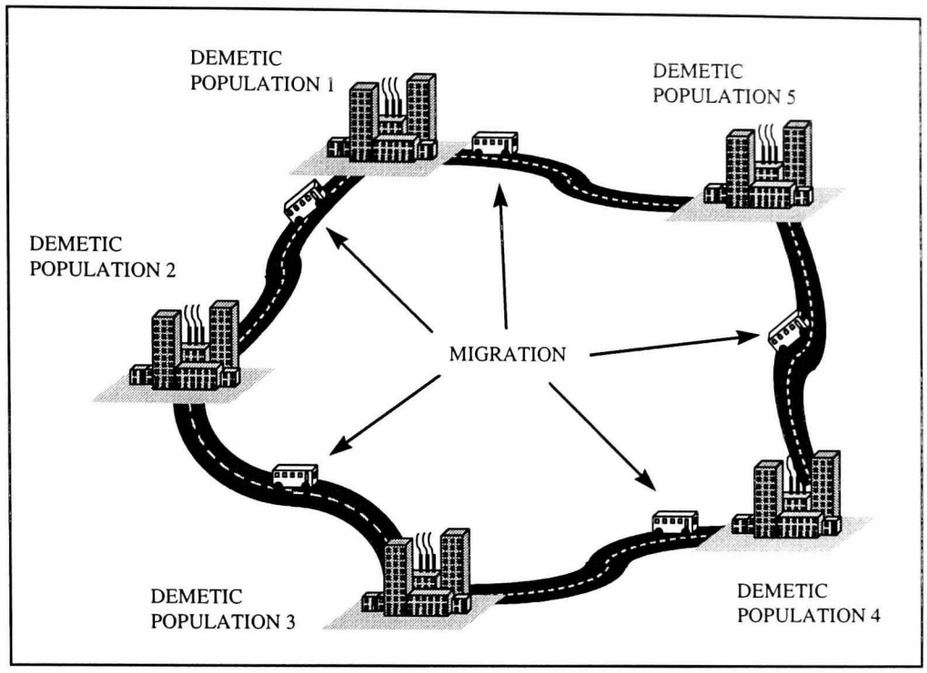

Figure 9.3: Demetic Illustration

This demetic action allows the separate populations to evolve in the different areas of the search space that their constituent chromosomes occupy. Hence smaller groups are allowed to search globally and segment the search space among the groups to allow a wider search. Hence demetic searches in GAs are analogous to segmentation and are considered to be a particular subsection of that methodology.

It should be noted that this process is found to be just as effective as a single population elite GA for the problems considered here. Therefore the number of parameters optimised in these investigations do not warrant a further segmentation of the search space through demetics.

9.4 Multi-objective Optimisation

Most optimisation problems have more than one equally valid optimisation criterion or objective to satisfy. Often these problems have no perfectly unique solution where all objectives are met and trade-offs must therefore occur in the final solutions. The control systems in this study have two design criteria to meet (i.e. minimisation of the controller input and of the resulting output error). However, these objectives have so far only been represented by a single cost function. Therefore the optimised solutions are the result of trade-offs between the two objectives for each controller.

If these objectives are considered separately the optimisation can result in non-dominated solutions where any improvement in one objective will result in the degradation in the other objective. These objective solutions belong to the Pareto-optimal set and thus a multi-objective regime can be used in these optimisations [Fonseca and Fleming (1994), Whidborne and Postlethwaite (1996)].

In order that these problems can be optimised in terms of these multi-objectives, the solutions are sorted by *Pareto ranking* (see Figure 9.4) [Fonseca and Fleming (1994)]. This is where each solution is considered in a f-dimension plane where f denotes the number of objectives to be optimised. Each solution is represented in this plane by the cost value for each objective. The case of two objectives is illustrated in Figure 9.4. Using this illustration as an example the process of Pareto ranking will be explained further.

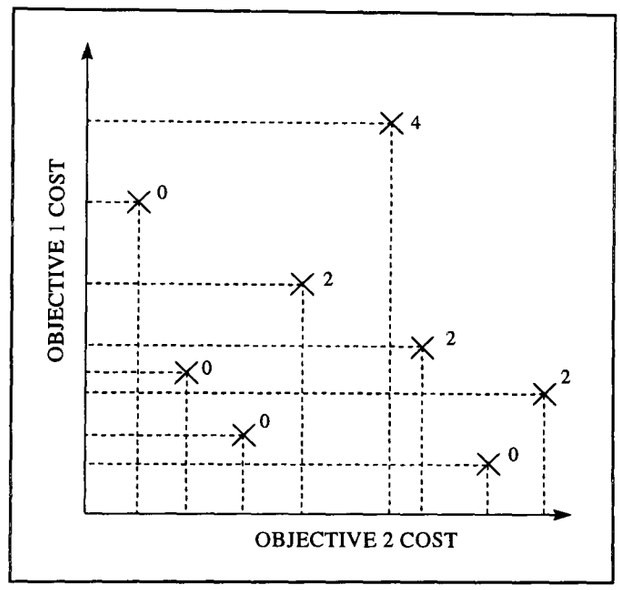

Figure 9.4: Pareto Ranking

When the solutions are plotted in the objective cost plane a measure of their *dominance* can be found. This dominance is determined for an individual by how many other solutions have better (i.e. smaller) cost values for all of their objectives. The number of solutions which dominate the considered individual is used as its Pareto ranking number. Obviously any non-dominated solutions will have a ranking number of zero and will thus be a member of the Pareto-optimal set of solutions [Fonseca and Fleming (1994)]. Those solutions evaluated with a zero ranking are kept as the current optimal values and remain for the next evaluated iteration (e.g. the next generation in a GA). As the optimisation progresses these zero ranked solutions converge to a *Pareto surface*

which graphically represents the trade-off between the objectives (see Figure 9.5). The elements of this surface are considered as the optimal non-dominated solutions for this problem and can vary quite widely in terms of the relative objective costs.

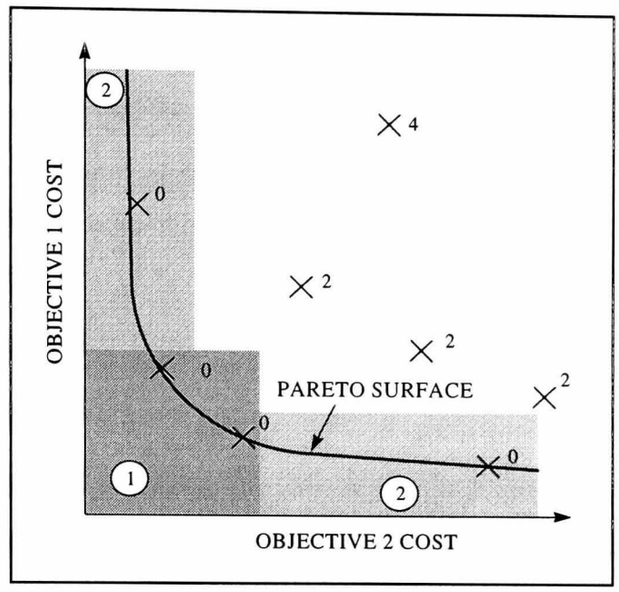

Figure 9.5: Pareto Surface

Unfortunately, this type of optimisation regime may not yield a sufficiently optimal final solution for implementation in the marine controller problems investigated in this study. Since objectives for these control problems are well defined as low input actuator usage and zero tracking error, any variation away from the direct trade-off region (region 1 in Figure 9.5) will result in an unacceptable final solution being presented as optimal. These suboptimal solutions fall in region 2 where one cost improves at the expense of the other.

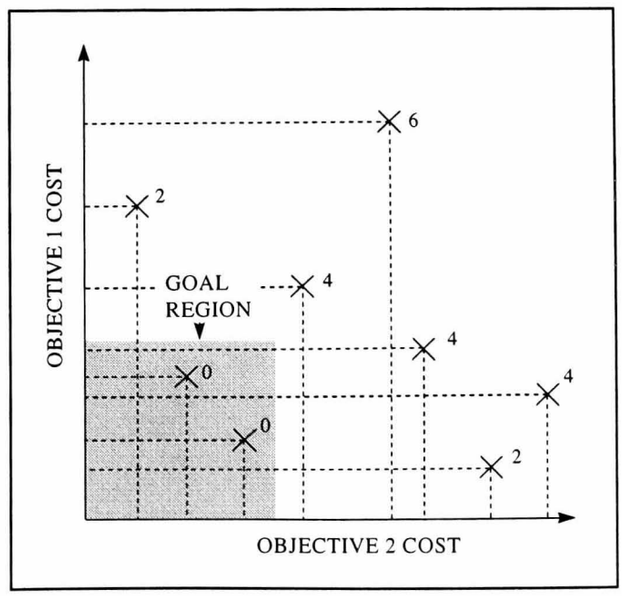

Figure 9.6: Pareto Ranking With Goal

One way to improve this method so that only solutions with small cost values for both objectives are found is to set a *goal* region for these desired solutions (see Figure 9.6). This alters the Pareto ranking in the following way. Firstly the solutions are ranked as described previously and the number of solutions which fall within the goal area is found. This number is then added to the ranking numbers of all those solutions which lie outside the goal region thus biasing then away from the Pareto-optimal set (see Figure 9.6). Hence only solutions which satisfy the goal and lie on the Pareto surface are considered optimal.

Unfortunately definition of a goal region calls for *a-priori* knowledge of the optimal cost values which may not be available prior to the optimisation. Hence multi-objective optimisation is not a viable prospect for the controller optimisations studied here since the optimisation objectives are closely linked to each other. Any prejudice to either objective would result in final solutions which would not be considered practically optimal. Therefore the use of a single objective multi-aspected cost function provides optimal final solutions much more readily than would be possible with a multi-objective regime.

9.5 Optimisation Ease Prediction

As indicated in the introduction to this chapter, the prediction of how easy a problem is to solve prior to optimisation would be very useful. The degree of optimisation difficulty is dependant on the search space which defines all possible permutations of the problem being studied in terms of cost value. This depends on the interaction of the constituent parts of the cost function which in turn defines the terrain of the search space. Since the majority of the solutions within the search space are suboptimal, the variation of the poorer solutions would help predict how difficult the given problem is to solve by estimating an extensive part of the search space terrain.

9.5.1 Search Space Terrain

If the search space is *rough* (i.e. the cost varies quite considerably with the optimisation parameters) it follows that the optimal region of the problem will be surrounded by terrain which will vary in amplitude and contain many local optima. This type of

problem will require an extensive search to obtain a globally optimal final solution. Conversely, a search space that is *smooth* (i.e. the cost variation is relatively small) will have a dominant global optimum which is much easier to detect. Therefore it follows that a less extensive search is required and the problem is easier to optimise.

In order to determine the ease of optimisation the search space terrain must be estimated. In the context of this study the terrain is defined in terms of the cost function elements which are the control inputs and the resulting output error. Thus the amount that these elements vary is very important to this definition. Therefore if the solution is near optimal this cost value will be minimal since the input usage is small and the output error is nearly zero. However a poor solution will give a large cost value since the input will not act in the way required and may oscillate wildly (e.g. in a type of limit cycle action). Since the majority of the search space contains such poor solutions the terrain can be determined by analysing the variation of these suboptimal results and the effect they have on the system being considered.

It is logical to say that the input to the system reflects the optimality of the controller being designed. This will vary with the parameter permutations and can provide oscillatory signals which are consider suboptimal. However this is only part of the cost function and will only define part of the terrain variation of the search space. The remainder of the cost reflects the output response of the system to the corresponding inputs. Although the cost function contains the output error, this value will be very large for the poorer solutions. For these solutions this error will almost be as large as the output itself and can be approximated by it. Therefore the terrain can be determined by the output and input interaction. This can be obtained by considering the *natural* or *open loop response* of the system [Franklin et al (1991)] which reflects how the output reacts to given inputs.

If the output follows the input readily and has a fast time constant, then both cost components will be of approximately the same magnitude. Therefore the poor cost values will be large and vary greatly with the optimality of all the possible solutions. Hence the search space will have a very rough terrain. However, if the system dynamics restrict the output response and it does not follow its inputs then the resulting cost values will be smaller and vary less. Hence the problem will have a smoother search

space. Hence the natural response of a system is the key to predicting the optimisation ease of a given problem. The natural response of the system is dependant on the pole positions of the open loop system matrix and is therefore related to the stability of the system [Franklin et al (1991)].

For marine vehicles the relationship between inputs and outputs defines their ability to execute specific manoeuvres. This capability of carrying out desired changes in motion is called *manoeuvrability* [Fossen (1994)]. This indicates how well a vessel is able to react to given inputs in order to give desired states which can be reflected by the natural response of the vessel [Franklin et al (1991)] and ultimately its stability. Hence by referring to the s-plane, this discussion can be extended (see Figure 9.7).

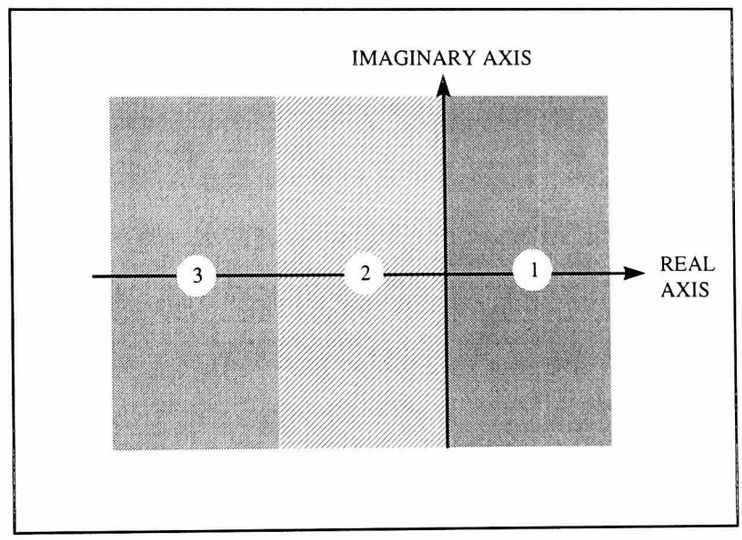

Figure 9.7: s-Plane Partition Diagram

From this diagram it can be seen that the s-plane can be regarded as three separate regions for marine vehicles [Franklin et al (1991)].

Region 1 is the right hand side of the s-plane which represents vessels which are inherently unstable. This instability means that the vessel is excessively manoeuvrable and requires extreme control effort in order to make the vessel move in the way required. This could cause the input actuators to saturate in certain cases. If the inputs are suboptimal the resulting output error will be extremely large. Hence both elements within the cost function vary with the optimality of the controller solution but the output error will vary much more than the input which causes it. Hence the search space for such vessels will vary greatly and it may be very difficult to obtain a satisfactory optimal controller.

Region 2 encompasses the first section of the left hand side of the s-plane, including the imaginary axis. In this area the systems are slightly and marginally stable and are therefore regarded as having very low manoeuvrability due to large time constants [Franklin et al (1991)]. These represent very large vessels which require extreme control effort to overcome their inertia. Therefore within the cost function the input element will dominate the output error since any change in the output requires a very large input. Hence such vessels will have small output error variation in terms of large input variations. Thus the search space will be relatively smooth since only one element of the cost function is varying significantly which results in the optimum being easy to locate since variation in the cost terrain is slight. It follows that such problems will be easy to optimise and a local optimisation method may be able to locate the global optimum.

Region 3 represents the area of the s-plane where vessels are extremely stable. These vessels are considered to be highly manoeuvrable since they have small time constants and thus react well to their inputs [Franklin et al (1991)]. Therefore they require minimal control to move. It follows that the elements of the cost function will vary proportionally since the output will follow the input. Therefore suboptimal controllers will result in output errors which vary in the same way as the inputs. Hence the search space for such vessels will vary considerably with many local optima to overcome. Thus a very good global optimisation technique is required to optimise such vessel's controllers.

These three regions show that the degree of manoeuvrability reflects the natural response of the system. Therefore a manoeuvrability measure would indicate how the output varies with large changes in the given input. This can then be used to estimate how much effort is required to optimise the problem in hand by estimating the search space terrain.

9.5.2 Manoeuvrability Test

The above discussion provides a qualitative definition of how to predict the ease of controller optimisation. In order to give a quantitative measure a suitable test is required to determine the manoeuvrability of the vessel in question. A standard test for

the manoeuvrability of marine vehicles is the Kempf 20°-20° zigzag test [Nomoto and Norrbin (1969), Fossen (1996)] for this purpose which was proposed to compare the manoeuvring and control characteristic of ships.

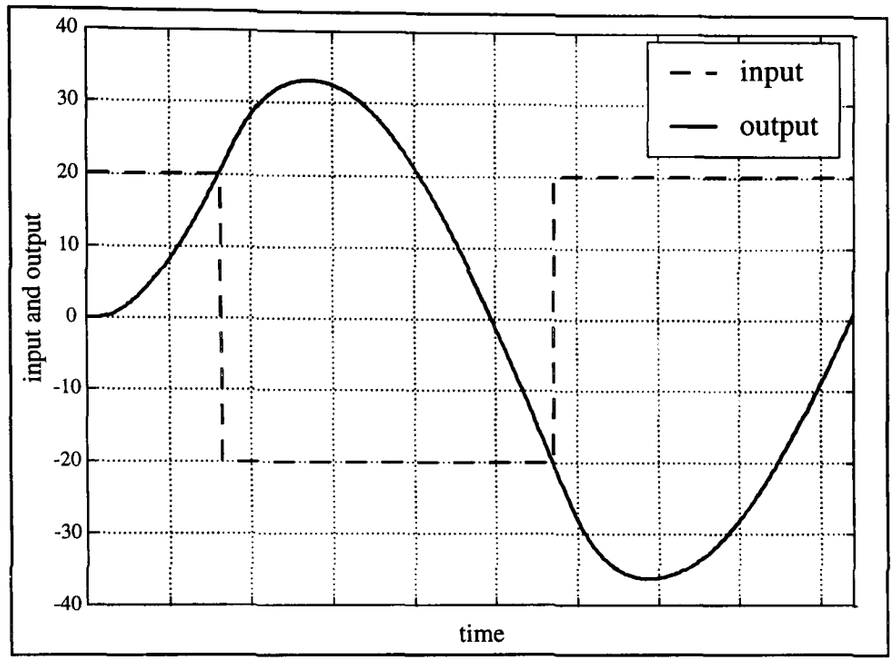

Figure 9.8: Zigzag Manoeuvre

Although this test is used to determine the heading motion of vessels it can be applied to any motion of a marine vehicle. The first stage is to set the input actuator to 20° and the relevant output is allowed to reach the same value (i.e. 20°)(see Figure 9.8). At this point the input is changed to -20° and the response of the vessel observed. This is repeated for a number of input changes and the results are analysed. These manoeuvres are quite rigorous as the inputs and required outputs are reasonably large. Although it is a very good test of how a vessel reacts to limited input commands (thus simulating the extremities of the search space) Kempf's test does not itself give a quantitative measure of the manoeuvrability. A suitable measure to use is the Norrbin Measure of Manoeuvrability [Nomoto and Norrbin (1969), Fossen (1994)] which is based on the ratio of the heading angle to the corresponding input. This results in the course changing quality number P_m i.e.

$$P_m = \frac{\psi}{\delta} \tag{9.6}$$

This measure can be applied to any motion and thus determines the manoeuvrability for that particular dynamic. It can therefore be generalised to the ratio of the output (Y) to the input which causes it (U) i.e.

$$P_m = \frac{Y}{U} \tag{9.7}$$

In order to establish how applicable this is to the problems studied in this investigation the models are simulated for a 20°-20° zigzag manoeuvre and the Norrbin Measure is calculated. In order to evaluate the vessels from their piece-wise continuous time histories for this manoeuvre the following variation of equation (9.7) is used.

$$P_m = \frac{1}{T_{final}} \left[\sum_{i=0}^{total} Y_i \Big/ \sum_{i=0}^{total} U_i \right] \tag{9.8}$$

Here *total* is the final iteration of the zigzag simulation. When this is applied to the submarine, tanker and surface ship problems the values shown in Table 9.1 are obtained. It should be noted that the submarine diving output is taken to be the pitch angle instead of the depth itself. However this angle is directly rated to the depth and is sufficient to represent the dynamics of this subsystem. Also the input for the ship (τ_3) is scaled so that its magnitude is equal to the other inputs (i.e. a value of 20).

Table 9.1: Manoeuvrability Measures

Application	Output	Input	Duration	P_m
Submarine (Diving)	θ	δs	47.0s	0.0074
Submarine (Heading)	ψ	δr	42.5s	0.0233
Tanker (Heading)	ψ	δr	470.0s	0.0009
Ship (Heading)	ψ	$33\tau_3$	9.9s	0.0018

It can be clearly seen that the submarine has larger values for both diving and heading subsystems (particularly the heading). This is to be expected since such vessels have to be highly manoeuvrable to execute their role as pursuit vehicles. Therefore it follows that the search space terrain for that application varies more and will need a global optimisation method to obtain a satisfactory solution.

The tanker on the other hand has a low value of P_m which is self evident since it is a large vessel and is not very manoeuvrable. Therefore the output will not vary much as the input changes and the search space terrain will be relatively smooth. Hence the global optimum will be easier to locate and the problem could be optimised by either a global or extended local search.

In the case of the ship model the measure of manoeuvrability is nearer to the tanker value than the submarine. This indicates that the model (and presumably the actual vessel it represents) is reasonably manoeuvrable. It follows that like the tanker this problem is relatively easy to optimise and does not require an excessively long search to obtain an optimal solution.

From these results it can be concluded that a manoeuvrability measure can be used to estimate how easy a controller problem will be to optimise. In fact a guidelines for the selection of an optimisation method for a specific problem can be formulated on this basis. Figure 9.9 is a table which provides an outline of the optimisation methods which could be used for different values of the manoeuvrability measure P_m.

$P_m << 1$	$P_m \approx 1$	$P_m >> 1$
Vessel is Marginally Stable, has low Manoeuvrability and needs excessive Control effort. Therefore output error will be very much smaller than the input which creates it. Thus the problem search space terrian will be smooth and the global optimum will dominate.	Vessel is Stable and Extremely Manoeuvrable. Therefore output error will follow the input which creates it. Thus the problem search space terrian will be moderately rough and need global search methods to optimise.	Vessel will tend to be Unstable and Excessively Manoeuvrable. Therefore output error will be very much larger than the input which creates it. Thus the problem search space terrian will be very rough and need an extensive global search in order to optimise.
Suggested Optimisation Method: GA, SSA, SA, Hill climbing, Gradient Search	Suggested Optimisation Method: GA, SSA (moderate segmentation), SA (with large annealing schedule)	Suggested Optimisation Method: Elite GA, Demetic GA, SSA (extensive segmentation), Exhaustive Search

Figure 9.9: Optimisation Method Suggestion based on Manoeuvrability

Although the discussion presented here is in terms of marine vessels, the theory can equally well apply to any system which possess an input that controls a desired output.

9.6 Summary

This chapter has provided a discussion on aspects of optimisation that have not been covered in the previous chapters. It has addressed areas which have been investigated during this research but are considered to diverge slightly from the main thread of the study. They are presented here for completeness and to give additional understanding of optimisation processes in general.

Firstly, improvements to the SSA and GA methods are described and discussed to indicate the benefits they provide over more standard methods investigated previously. Both the cloning process for SSA and the minimising GA compensate for drawbacks that were encountered during the main research and improve the performance of these methods.

The use of demetic grouping for GAs is shown to be similar to the segmentation mechanism presented for SSA. This indicates that reducing the search space into smaller areas or segments assists optimisation methods by increasing their ability to optimise difficult problems.

Also discussed in Section 9.4 is the theory of multi-objective cost optimisation. This is discussed in terms of its ability to obtain a globally optimal solution compared with the single objective cost functions used in the major part of this work. It is found that multi-objective optimisation only works satisfactorily if a cost goal region is defined and solutions that lie outside this area are penalised. This calls for *a-priori* knowledge of the desired optimal cost values which is not always possible. Therefore in this work multi-objective optimisation operates poorly compared with the single objective, multi-aspect optimisations studied here. It can be concluded that if the elements of the cost function are sufficiently well defined then multi-objective optimisation is redundant. This is the case for marine vehicle control system optimisation.

The final discussion of this chapter stems from observations made during this study. Since the stability and manoeuvrability aspects of a vessel determine its controllability, it follows that this will reflect the optimality of the optimisation solutions. This can be used to determine the amount of variation in the cost function and subsequently the terrain of the search space. It follows that this information gives some indication of how easy the problem is to optimise and can be used to determine the best optimisation technique for a given control problem.

All these aspects extend the discussion of optimisation and go some way to giving additional insight into this complex area of study.

Chapter 10:

Conclusions and Further Work

10.1 Conclusions

The general conclusion to be drawn from this work is that advanced optimisation methods are useful tools for obtaining controller parameters for specific applications with a minimal amount of *a-priori* knowledge of the optimal solution. It has been found that these techniques are able to optimise the performance of Sliding Mode controllers to specified design criteria. As long as these criteria are logically thought out and defined precisely, it is felt that these methods can be extended to the optimisation of any controller in any situation.

Evidence has been given that the best performance in optimisation is achieved by the Genetic Algorithm method since the conclusions of this comparison study show this method in a favourable light.

The particular conclusions regarding the optimisation techniques and controller type studied in this thesis are outlined below.

10.1.1 Simulated Annealing

The Simulated Annealing (SA) theory in Chapter 3 has shown that this method has a limited search range which could hamper its ability to find an optimal solution. This has been reinforced by the optimisation studies in Chapters 6 and 7. These have shown that SA searches fail to locate an optimal solution for a problem if the initial starting point is not near this optimum region. It follows that in order for this method to optimise a problem *a-priori* knowledge of a near optimum solution must be available. This in itself defeats the purpose of a global optimisation method which should require limited information about the optimal solution in order to obtain a suitable solution. Therefore SA is only useful as local optimisation method and this localisation is dependant on the range of the method which is defined by the annealing schedule. Hence the SA method could be used to fine tune an existing hand tuned solution but is not a reliable global method.

10.1.2 Segmented Simulated Annealing

The convergence analysis of the Segmented Simulated Annealing (SSA) method in Chapter 3 has been borne out by the application studies in Chapters 6, 7 and 8. These have shown that this method can provide globally optimal solutions for controller parameters. Therefore by segmenting the search space the SA method is improved in terms of global searches. However the diversity of the final set of solutions presented by this method is too vast to ensure confidence in the acquisition of the true global optimum.

Although the simulation results from this investigation have shown that this method provides final solutions which are finely tuned, the implementation of the controller for *CyberShip I* has indicated that the fine tuning process of this method may provide a controller with gains that are too high. This could result in control signals that saturate the actuator which they are attempting to govern. Therefore the SSA can obtain optimal simulated solutions which may need corrective tuning when implemented in the actual system.

10.1.3 Genetic Algorithms

The *Markov Chain* (MC) and *Schema Theorem* analysis in Chapter 4 suggests that the genetic algorithm (GA) method is a powerful optimisation technique which is guaranteed to find a globally optimal solution. This was verified by the simulation studies carried out for all three marine vehicles studied. These results show that the optimisation would satisfy well defined design criteria and provide satisfactory solutions. The amount of saturation in the final generation provided a high level of confidence in the solution. However this saturation should be monitored as it may cause premature convergence [M^{c}Gookin (1997(b))].

It has also been shown that the GA provides solutions which are similar in performance to manually tuned controllers and thus may be sufficient for implementation. When a GA tuned controller was applied to *CyberShip I* it was found to perform well and require no further tuning. This could be further improved if the mathematical representation of the actual vessel was more accurate. However due to the broad nature of the GA search the solution is not highly tuned and can therefore be readily applied to

a real system. So overall this method has been shown to have the best performance of the methods considered in this thesis.

10.1.4 Sliding Mode Controllers and Marine Vehicle Applications

A decoupled Sliding Mode (SM) controller has been developed in this thesis which can be classed as a non-linear model-following controller structure (see Chapter 5). This control law has been shown to be asymptotically stable and thus robust to changes in the system's operating conditions if the design criterion in Section 5.5 is satisfied.

This criterion ensures stability robustness by setting the switching gain magnitude sufficiently high to compensate for any model uncertainties and external disturbances to the system it is controlling. If this criterion is met the controller will operate on the zero sliding surface where the actual and desired states are equal (i.e. zero tracking error). Therefore the controller is guaranteed to make the system behave in the way required and thus performance robustness is ensured. Both robustness issues are unaffected by the use of a boundary layer to prevent chattering. In fact the presence of this layer helps the sliding surface approach its zero value by gradually reducing the effective switching amplitude of this control law.

The application of this type of controller to marine vehicles has been shown to perform well through simulation if suitable parameter values are chosen. The results from these simulations illustrate the performance robustness of this type of control methodology through its ability to track the desired output response for the system. This has been shown for application to both linear and non-linear systems. The stability robustness has been guaranteed in each case by satisfying the design criterion for the switching gain value (i.e. for the applications studied here the switching gain is positive definite to ensure robustness).

However the application of this method to *CyberShip I* shows that if there is a slight deviation in the mathematical representation the controller may not be implementable in the physical system. This part of the study illustrated the importance of good mathematical models in order for controllers to be designed sufficiently well. When the performance of the controllers for this system is considered it can be seen that with appropriate tuning this type of controller will be well suited to the control of marine

vehicles. It has been shown to track the desired heading well thus showing that the zero sliding surface discussed in Chapter 5 has been obtained. Hence the performance robustness of this type of controller is assured in this case.

Also from the *CyberShip I* study it is apparent that if the commanded input is too demanding the controller tracking deteriorates. This is to be expected since the controller is designed around a nominal representation of the vessel. However the performance of this controller has been found to outperform conventional PID controllers and thus be considered a better control law for application to marine vessels.

10.2 Further Work

The work presented in this thesis can be extended in many ways along the numerous lines of research that constitute its main structure. These are the optimisation methods, SM control techniques and the marine vehicle applications which are discussed below.

10.2.1 Optimisation Methods

The optimisation methods discussed in this work have only optimised parameters for a given controller structure. It is therefore suggested that these methods should be extended to develop the structure of a controller as well as its key parameters.

This would be easily done through variations in the GA method by allowing certain gene values represent controller building block elements which could be combined to form various controller structures. More flexibility could be provided by using the extension of the evolutionary programming concepts inherent in GAs to a more general approach called *Genetic Programming* (GP) [Koza (1992)]. This method forms symbolic expression trees which could represent controller functions. These variable length trees are constructed from a library of conventional mathematical functions and are then evaluated in a similar way to the GA method (i.e. through simulation).

In this way the structure of a controller could be evolved as well as the parameter values. However careful consideration concerning such things as stability and robustness is essential for the resulting controllers. This and the long execution time for such optimisation methods could cause practical problems.

Also, with respect to optimisation methods, it is felt that the hypothesis in Chapter 9 concerning predicting the optimisation ease should be developed. This should provide a general theory for predicting the optimisation ease of a problem prior to the optimisation process.

10.2.2 Sliding Mode Controller Design

Although multi-input versions of SM control theory exist [Slotine and Li (1991), Fossen and Foss (1991), Utkin (1992)], they are numerically complex which tends to prevent them from being implemented in practical situations. From a theoretical standpoint the method of decoupling the dynamics which are required for control is an acceptable process and in Chapter 5 it has shown that a single input SM controller can be easily designed with minimal numerical complexity. It has also been shown that these controllers can compensate for any matched uncertainties that it can directly influence by having a suitably large switching term. By extending this design framework to the multi-input case could make this control theory more readily used.

On a more practical side, the use of toolboxes for a package such as MATLAB would aid in the design of multi-input SM controllers. This would make the design of such controllers an easier process where the designer need not worry about an in-depth understanding of the control theory.

Both this and a more comprehensible design theory would allow this type of non-linear model-following control system to be more accepted on an industry wide basis.

10.2.3 Marine Vehicle Applications

The number of marine vehicle control applications are really limitless since the roles of ocean going vessels are so diverse. Each would require a system specific controller in order to meet the required performance specifications. Two applications of some importance are discussed below i.e. the control of military submarines at slow speeds and the dynamic position control of floating oil production barges. Both would provide ideal applications for testing non-linear control theory and optimisation techniques.

10.2.3.1 Submarine Control at Slow Speeds

In the study of the submarine carried out in Chapter 6 the vessel executed manoeuvres at high speeds (e.g. 20kts). This means that the hydroplanes operate in the way described in that chapter in that the sternplanes control the diving motion and the bowplanes are ineffectual and remain at zero displacement (see Figure 10.1).

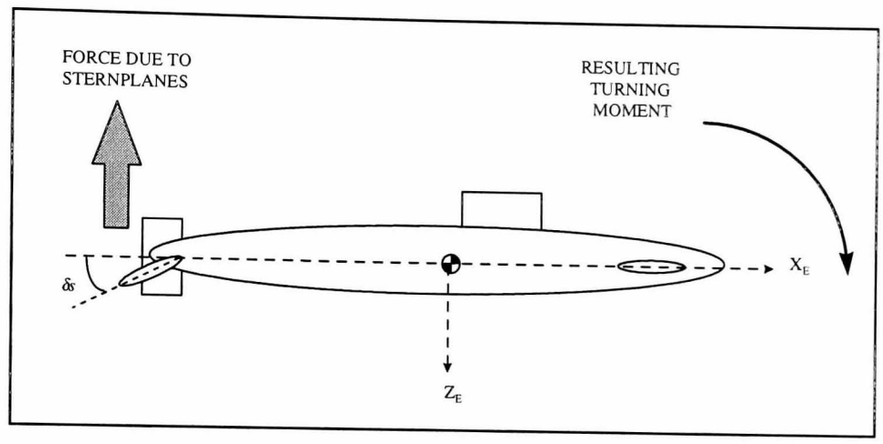

Figure 10.1: Hydroplane Action at High Speed

At slower speeds (i.e. < 2kts) the roles of the hydroplanes are in some ways reversed due to the reduced flow hydrodynamics of the vessel. This results in the bowplanes dominating the depth control and the sternplanes start to operate in the opposite direction compared with their high speed deflections (see Figure 10.2). This phenomenon is called *the Chinese Effect* [Burcher and Rydell (1993), Papoulias and Riedel (1994)] and is of particular importance when the submarine is trying to maintain periscope depth. It is clear that this is a particularly difficult control problem which requires a rigorous control system to compensate for this effect. This would therefore provide an ideal test application for both the SM control theory and the optimisation techniques.

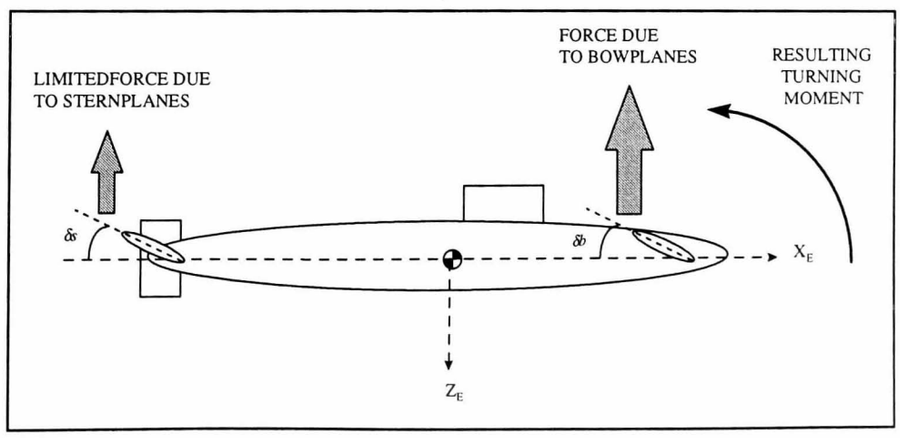

Figure 10.2: Hydroplane Action at Low Speeds (*Chinese Effect*)

10.2.3.2 Oil Production Barges

In recent years it has been noticed that reserves of easily accessible oil are starting to dwindle and that exploitation of sources located in deeper water has to be considered. These deeper oil fields cannot be drilled using conventional oil platforms since the expenditure would not yield a satisfactory return.

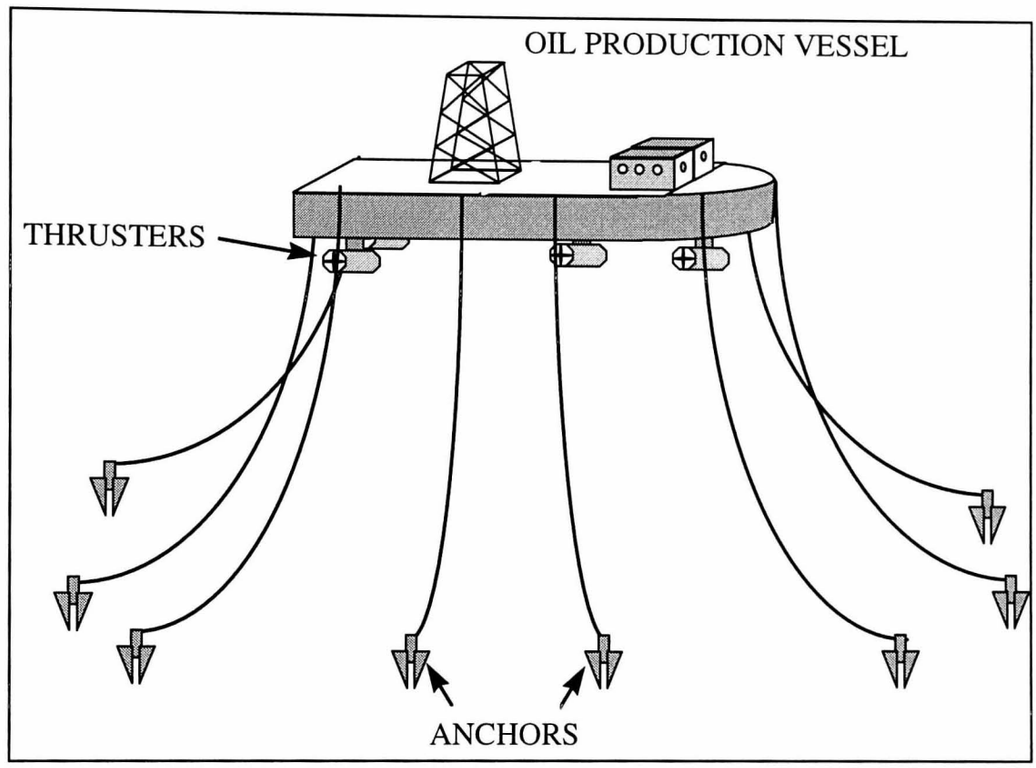

Figure 10.3: Oil Production Vessel Illustration

A proposed way of drilling these fields is by using *Oil Production Barges* which can be positioned over the field as required (see Figure 10.3). These vessels maintain position by a combination of thrusters and anchors. The anchors (e.g. ten in number) keep the general position of the barge within the confines of a few boat lengths. The thrusters are then used to keep the position of the barge constant with reference to GPS position data and operate in the same way as *CyberShip I.* Dynamically speaking this would present quite a difficult control problem as drift of the anchors' positions and the effects of severe sea conditions [Eda (1972), Price and Bishop (1974), McGookin (1993), Fossen (1994)] could drastically effect the vessel. Hence this problem would also provide an ideal test subject for the control and optimisation theories presented in this thesis.

Abercrombie, M., Hickman, C.J. and Johnson, M.L., (1985). "The Penguin Dictionary of Biology", Penguin Books Ltd., Aylesbury, UK.

Adler, D. (1993). "Genetic Algorithms and Simulated Annealing: A marriage proposal", IEEE Conference on Neural Networks, pp. 1104-1109.

Atkinson, A.C. (1992). "A segmented algorithm for simulated annealing", Statistics and Computing, 2, pp 221-230.

Astrom, K.J. and Kallstrom, C.G. (1976). "Identification of Ship Steering Dynamics", Automatica, Vol. 12, pp 9-22.

van Berlekom, W.B. and Goddard, T.A. (1972) "Maneuvering of Large Tankers", Transactions of the Society of Naval Architects and Marine Engineers, Vol. 80, pp 264-298.

Bohachevsky, I.O., Johnson, M.E. and Stein, M.L. (1986). "Generalized Simulated Annealing for Function Optimisation", Technometerics, Vol. 28, No. 3, pp 209-217.

Brooks, R.R., Iyengar, S.S. and Chen, J. (1996). "Automatic correlation and calibration of noisy sensor readings using elite genetic algorithms", Artificial Intelligence 84, pp 339-354.

Burcher, R. and Rydell, L. (1993). "Concepts of Submarine Design", Cambridge University Press, Chapter 8 : Dynamics and Control, pp 151-191.

Burton, J.A. and Zinober, A.S.I. (1988). "Continuous self-adaptive control using a smoothed variable structure controller", International Journal of Systems Science, Vol.19, No.8, pp 1515-1528.

Cheney, W. and Kincaid, D. (1985) "Numerical Mathematics and Computing", Brooks/Cole Publishing Company, Pacific Grove, California, USA.

Corradini, M.L. and Orlando, G. (1997) "A discrete Adaptive Variable-Structure Controller for MIMO Systems, and Its Application to an Underwater ROV", IEEE Transactions on Control Systems Technology, Vol.5, No.3.

Courat, J.P., Raynaud, G. and Siarry, P. (1995). "Extraction of the Topology of Equivalent circuits based on parameter statistical evolution driven by simulated annealing", International Journal of Electronics, Vol. 79, No. 1, pp 47-52.

Crane, C.L., (1973)."Maneuvering Safety of Large Tankers: Stopping, Turning and Speed Selection", Transactions of the Society of Naval Architects and Marine Engineers, Vol.81, pp 213-242.

Curtis, P.R. (1996). *Communication received from Submarine Hydrodynamics Dept., DERA Haslar, Gosport.*

Donha, D.C., Desanj, D.S. and Katebi, M.R. (1997). "Automatic Weight Selection for H_∞ Control Design", Second International Conference on Genetic Algorithms in Engineering Systems: Innovations and Applications, pp 50-55, Glasgow, UK.

Dove, M.J. and Wright, C.B. (1991) "Development of Marine Autopliots", Computer Methods in Marine and Offshore Engineering, Computational Mechanics Publications, Murphy, T.K.S. (Ed), Southampton, pp 259-272.

Dumlu, D. and Istefanopulos, Y. (1995). "Design of an Adaptive Controller for Submersibles via Multimodel Gain Scheduling", Ocean Engineering, Vol. 22, No. 6, pp 593-614.

Eda, H. (1972). "Directional Stability and Control of Ships in Waves", Journal of Ship Research, pp. 205-218.

Fogel, D.B. (1994) " An Introduction to Simulated Evolutionary Optimization", IEEE Transactions on Neural Networks, Vol. 5, No. 1, pp 3-13.

Fonseca, C.M. and Fleming, P.J. (1994) "Multiobjective Optimal Controller Design with Genetic Algorithms ", International Conference on Control '94, Coventry, UK, Vol.1, pp 745-749.

Fossard, A.J. (1993). "Helicopter control law based on sliding mode with model following", International Journal of Control, Vol. 57, No. 5,pp 1221-1235.

Fossen, T.I. (1994). "Guidance and Control of Ocean Vehicles", John Wiley & Sons Ltd, Chichester.

Fossen, T.I. and Foss, B.A. (1991) "Sliding control of MIMO nonlinear systems", Modeling, Identification and Control, Vol. 12, No. 3, pp 129-138.

Fox, R.W. and McDonald, A.T. (1985) "Introduction to Fluid Mechanics", John Wiley & Sons Ltd, Singapore.

Franklin, G.F., Powell, J.D. and Emami-Naeini, A. (1991) "Feedback Control of Dynamic Systems", Addison-Wesley, New York.

Gill, A.D. (1979) "Mathematical Modelling of Ship Manoeuvring", Mathematical Aspects of Marine Traffic, Academic Press, London, pp 193-227.

Goh, S.J., Gu, G.W. and Man, K.F. (1996) "Multi-Layer Genetic Algorithms in Robust Control System Design", Proceedings of the IEE International Conference on Control '96, Exeter, UK, Vol.1, pp 699-704.

Goldberg, D. (1989) "Genetic Algorithms in Searching, Optimisation and Machine Learning", Addison Wesley, Reading, MA.

Grefenstette, J.J. (1986) ".Optimisation of control parameters for genetic algorithms", IEEE Transactions on Systems, Man and Cybernetics, Vol. 16, No. 1, pp 122-128.

Healey, A.J. and Lienard, D. (1993) "Multivariable Sliding Mode Control for Autonomous Diving and Steering of Unmanned Underwater Vehicles", IEEE Journal of Oceanic Engineering, Vol. 18, No. 3, pp 327-339.

Healey, A.J. and Marco, D.B. (1992) "Slow Speed Flight Control of Autonomous Underwater Vehicles: Experimental Results with NPS AUV II", Proceedings of the Second International Offshore and Polar Engineering Conference, pp 523-532, San Francisco, USA.

Holland, J.H. (1975) "Adaptation in Natural and Artificial Systems", University of Michigan Press, Ann Arbor.

Jones, A.H. and de Moura Oliveira, P.B. (1996) "Auto-tuning of PI Smith Predictor Controller Using Genetic Algorithms", Proceedings of the IEE International Conference on Control '96, Exeter, UK, Vol.1, pp 454-459.

Kallstrom, C.G. (1979) "Identification and Adaptive Control Applied to Ship Steering", Ph.D. Thesis, Department of Automatic Control, Lund University of Technology, Sweden.

Kallstrom, C.G., Astrom, K.J., Thorell, N.E., Eriksson, J. and Sten, L. (1979) "Adaptive Autopilots for Tankers", Automatica, Vol. 15, pp 241-254.

Kautsky, J., Nichols, N.K. and Van Dooren, P. (1985). " Robust Pole Assignment in Linear State Feedback", International Journal of Control, Vol. 41, pp 1129-1155.

Kawabe, T., Tagami, T. and Katayama, T. (1996) "A Genetic Algorithm based minimax Optimal Design of Robust I-PD Controller", Proceedings of the IEE International Conference on Control '96, Exeter, UK, Vol.1, pp 436-441.

Keane, A.J. (1995) "Genetic Algorithm optimization of multi-peak problems: studies in convergence and robustness", Artificial Intelligence in Engineering, 9, pp 75-83.

Kirkpatrick, S. (1984). "Optimization by Simulated Annealing: Quantitative Studies", Journal of Statistical Physics, Vol. 34, Nos 5/6, pp 975-986.

Kirkpatrick, S., Gelatt, C.D. and Vecchi, M.P. (1983). "Optimization by Simulated Annealing", Science, Vol. 220, No. 4598, pp 671-680.

Kristinsson, K. and Dumont, G.A. (1992) "System Identification and Control Using Genetic Algorithms", IEEE Transactions on Systems, Man and Cybernetics, Vol. 22, No. 5, pp 1033-1046.

Koza, J. (1992). "Genetic Programming: On the programming of computers by means of natural selection", The MIT Press, Cambridge, Mass..

Laarhoven, P.J.M. van (1988). "Theoretical and computational aspects of simulated annealing", CWI Tract 51, Centre for Mathematics and Computer Science, Amsterdam.

Laarhoven, P.J.M. van and Aarts, E.H.L. (1987). "Simulated Annealing: Theory and Applications", Dordrecht, Lancaster.

Lambert, J. (1996). *Communication received from Director of Naval Architecture and Future Projects, MOD Abbey Wood, Bristol.*

Landau, I.D. (1974). " A Survey of Model Reference Adaptive Techniques - Theory and Applications", Automatica, Vol. 10, pp 353-379.

Li, Y., Ng, K.C., Tan, K.C., Gray, G.J., McGookin, E.W., Murray-Smith, D.J., and Sharman, K.C. (1995). "Automation of linear and nonlinear control systems design by evolutionary computation", Proceedings of the International Federation of Automatic Control Youth Automation Conference, Beijing, China, pp 53-58.

Li, Y., Ng, K. C., Murray-Smith, D. J., Gray, G. J. and Sharman, K. C. (1996). "Genetic Algorithm Automated approach to design of Sliding Mode Controller systems", International Journal of Control, 63(4), pp 721-739.

Liceaga-Castro, E. and van der Molen, G.M. (1995(a)). "Submarine H^{∞} Depth Control Under Wave Disturbances", IEEE Transactions on Control Systems Technology, Vol. 3, No. 3, pp 338-345.

Liceaga-Castro, E. and van der Molen, G.M. (1995(b)). "A submarine depth control system design", International Journal of Control, Vol. 61, No. 2, pp 279-308.

Metropolis, N., Rosenbluth, A.W., Rosenbluth, M.N., Teller, A.H. and Teller, E. (1953) "Equation of state calculation using fast computing machines", *Journal of Chemical Physics*, 21, pp 1087-1092.

M^{c}Gookin, E.W. (1993). "Sliding Mode Control of a Submarine", M.Eng. Thesis, Department of Electronics and Electrical Engineering, University of Glasgow.

M^{c}Gookin, E.W., Murray-Smith, D.J. and Li, Y. (1996(a)). "Segmented Simulated Annealing applied to Sliding Mode Controller Design", Proceedings of the 13th World Congress of IFAC, Vol. D, pp 333-338, San Francisco, USA.

M^{c}Gookin, E.W., Murray-Smith, D.J. and Li, Y. (1996(b)). "Submarine Sliding Mode Controller Optimisation using Genetic Algorithms", Proceedings of the IEE International Conference on Control '96, Exeter, UK, Vol.1, pp 424-429.

M^{c}Gookin, E.W., Murray-Smith, D.J., Li, Y and Fossen, T.I. (1997(a)). "Parameter Optimisation of a Non-linear Tanker Control System Using Genetic Algorithms", Second International Conference on Genetic Algorithms in Engineering Systems: Innovations and Applications, pp 37-42, Glasgow, UK.

M^{c}Gookin, E.W., Murray-Smith, D.J. and Li, Y. (1997(b)). "A Population Minimisation Process for Genetic Algorithms and its Application to Controller Optimisation", Second International Conference on Genetic Algorithms in Engineering Systems: Innovations and Applications, pp 79-84, Glasgow, UK.

M^{c}Gookin, E.W., Murray-Smith, D.J., Li, Y and Fossen, T.I. (1997(c)). "Non-linear Tanker Control System Parameter Optimisation Using Genetic Algorithms", Proceedings of OCEANS'97, Vol. 1, pp 17-22, Halifax, Nova Scotia, Canada.

M^{c}Gookin, E.W., Murray-Smith, D.J. and Li, Y. (1997(d)). "Simulated Annealing, Segmented Simulated Annealing And Genetic Algorithms : A Comparison Study In The Context Of Markov Chain Analysis And Non-Linear Controller Design", *Submitted to IEEE Transactions on Evolutionary Computing*.

M^{c}Gookin, E.W., Murray-Smith, D.J., Li, Y. and Fossen, T.I. (1997(e)). "Ship Steering Control System Optimisation Using Genetic Algorithms", *Submitted to IFAC Journal Control Engineering Practice*.

M^{c}Gookin, E.W., Murray-Smith, D.J., Li, Y. and Fossen, T.I. (1997(f)). "Supply Ship Autopilot Optimisation Using Genetic Algorithms", *Submitted to IEEE Journal of Oceanic Engineering*.

Miliken, L.G. (1984). "Multivariable control of an underwater vehicle", Engineers' Thesis, Massachusetts Institute of Technology.

Mudge, S.K. and Patton, R.J. (1988(a)). "Enhanced Assessment of Robustness for an Aircraft's Sliding Mode Controller", Journal of Guidance, Control and Dynamics, Vol. 11, No. 6, pp 500-507.

Mudge, S.K. and Patton, R.J. (1988(b)). "Variable Structure Control Laws for Aircraft Manoeuvres", ", Proceedings of the IEE International Conference on Control '88, Oxford, UK, pp 564-568.

Ng, K.C., Li, Y., Murray-smith, D.J. and Sharman, K.C. (1995). "Genetic Algorithm applied to Fuzzy Sliding Mode Controller design", First International Conference on Genetic Algorithms in Engineering Systems: Innovations and Applications, pp 220-225, Sheffield, UK.

Nomoto, K. and Norrbin, N.H. (1969). "Report of Manoeuvrability Committee", 12th International Towing Tank Conference, Rome, Italy.

Norrbin, N.H. (1970). "Theory and Observations on the use of a Mathematical Model for Ship Maneuvering in Deep and Confined Waters", Proceedings of the 8th Symposium on Naval Hydrodynamics, pp. 807-904, Pasadena, USA.

Papoulias, F.A. and Riedel, J.S. (1994) "Solution Branching and Dive plane Reversal of Submarines at Low Speeds", Journal of Ship Research, Vol. 38, No. 3, pp. 203-212.

Price, W.G. and Bishop R.E.D. (1974) "Probabilistic Theory of Ship Dynamics", Chapman and Hall, London.

Renders, J-M and Flasse, S.P. (1996) "Hybrid Methods Using Genetic Algorithms for Global Optimization", IEEE Transactions on Systems, Man and Cybernetics - Part B: Cybernetics, Vol. 26, No. 2, pp 243-258.

Richardson, D., Gunston, W. and Hogg, I. (1991). "High Tech Weapons of the Gulf War", Salamander Books Ltd., London.

Sharman, K.C. (1988). "Maximum Likelihood parameter estimation by Simulated Annealing", Proceedings of IEEE International Conference on Acoustics, Speech and Signal Processing, Vol. V, pp 2741-2744.

Sharman, K.C. and Esparcia-Alcazar, A.I. (1993). "Genetic Evolution of Symbolic Signal Models", Proceedings of 2nd IEE/IEEE Workshop on Natural Algorithms in Signal Processing, Vol. 2, paper 29, pp 1-11, Essex, UK.

Slotine, J.J.E. (1984). "Sliding controller design for non-linear systems", International Journal of Control, Vol. 40, No. 2, pp 421-434.

Slotine, J.J.E. and Li, W. (1991). "Applied Nonlinear Control", Prentice-Hall International Inc., New Jersey, USA.

Suthaharan, S., Zhang, Z. and Sathananthan, S. (1997). "An Improved Wiener Filter using Genetic Algorithms", Second International Conference on Genetic Algorithms in Engineering Systems: Innovations and Applications, pp 75-78, Glasgow, UK.

Szu, H. and Hartley, R. (1987). "Fast Simulated Annealing", Physics Letters A, Vol.122, No. 3.4, pp 157-162.

Trebi-Ollennu, A. and White, B.A. (1996(a)) "Multiobjective Fuzzy Genetic Algorithm Optimization approach to Nonlinear System Design", Proceedings of the IEE International Conference on Control '96, Exeter, UK, Vol.1, pp 460-466.

Trebi-Ollennu, A. and White, B.A. (1996(b)). "A Robust Nonlinear Control Design for Remotely Operated Vehicle Depth Control Systems", Proceedings of the IEE International Conference on Control '96, Exeter, UK, Vol.1, pp 993-997.

Utkin, V.I. (1972). "Equations of the Slipping Regime in Discontinuous Systems II", Automation and Remote Control, Vol. 2, pp 211-219.

Utkin, V.I. (1992). "Sliding Mode in control and optimization", Springer-Verlag, New York, USA.

Utkin, V.I. and Yang, K.D. (1978). "Methods for Constructing Discontinuity Planes in Multidimensional Variable Structure Systems", Automation and Remote Control, Vol. 39, pp 1466-1470.

Vik, B. and Fossen, T.I. (1997) "Semiglobal Exponential Output Feedback Control of Ships", IEEE Transactions on Control Systems Technology, Vol.5, No.3, pp 360-370.

Whidborne, J.F. and Postlethwaite, I. (1996) "Simulated Annealing for Multi-Objective Control Systems Design", Proceedings of the IEE International Conference on Control '96, Exeter, UK, Vol.1, pp 376-381.

Zinober, A.S.I. and Liu, P. (1996). "Robust Control of Nonlinear Uncertain Systems via Sliding Mode with Backstepping Design", Proceedings of the IEE International Conference on Control '96, Exeter, UK, Vol.1, pp 231-236.

Zuidweg, J.K. (1970). "Automatic Guidance of Ships as a Control Problem", Ph.D. Thesis, Delft University of Technology.

Appendix A:

Mathematical Representations of Vessels

A.1 Linear Submarine Model

The military submarine model discussed in Chapter 6 [Miliken (1984)] is represented by the following state space equation

$$\dot{\mathbf{x}} = \mathbf{A}\mathbf{x} + \mathbf{B}\mathbf{u} \tag{A.1}$$

where the state ($\mathbf{x}$) and input ($\mathbf{u}$) vectors are defined in the chapter and the system and input matrices are defined below.

System Matrix **A**:

$$\begin{bmatrix}
-3.82\times10^{-2} & -2.19\times10^{-2} & -2.77\times10^{-3} & -1.90\times10^{-2} & -2.94\times10^{-1} & 3.17\times10^{0} & 0.00\times10^{0} & -2.77\times10^{-3} & 0.00\times10^{0} & 0.00\times10^{0} \\
1.15\times10^{-3} & -1.59\times10^{-1} & -1.93\times10^{-3} & -1.15\times10^{0} & 1.13\times10^{-1} & -1.54\times10^{-1} & 1.30\times10^{-1} & -1.76\times10^{-3} & 0.00\times10^{0} & 0.00\times10^{0} \\
2.42\times10^{-5} & 4.65\times10^{-4} & -1.06\times10^{-1} & -1.60\times10^{0} & 1.21\times10^{1} & 8.02\times10^{-2} & 0.00\times10^{0} & 7.56\times10^{-3} & 0.00\times10^{0} & 0.00\times10^{0} \\
2.46\times10^{-4} & -1.17\times10^{-2} & -1.32\times10^{-3} & -4.34\times10^{-1} & -2.39\times10^{-1} & -7.18\times10^{-3} & -1.60\times10^{-1} & 2.16\times10^{-3} & 0.00\times10^{0} & 0.00\times10^{0} \\
-5.37\times10^{-6} & -1.86\times10^{-5} & 1.32\times10^{-3} & -1.14\times10^{-2} & -4.08\times10^{-1} & 1.01\times10^{-4} & 0.00\times10^{0} & -2.50\times10^{0} & 0.00\times10^{0} & 0.00\times10^{0} \\
-2.76\times10^{-5} & -2.03\times10^{-3} & 2.41\times10^{-5} & -8.10\times10^{-3} & 3.60\times10^{-3} & -3.82\times10^{-1} & 2.58\times10^{-4} & -3.50\times10^{-6} & 0.00\times10^{0} & 0.00\times10^{0} \\
0.00\times10^{0} & 0.00\times10^{0} & 0.00\times10^{0} & 1.00\times10^{0} & 0.00\times10^{0} & 0.00\times10^{0} & 0.00\times10^{0} & 0.00\times10^{0} & 0.00\times10^{0} & 0.00\times10^{0} \\
0.00\times10^{0} & 0.00\times10^{0} & 0.00\times10^{0} & 0.00\times10^{0} & 1.00\times10^{0} & 0.00\times10^{0} & 0.00\times10^{0} & 0.00\times10^{0} & 0.00\times10^{0} & 0.00\times10^{0} \\
0.00\times10^{0} & 0.00\times10^{0} & 0.00\times10^{0} & 0.00\times10^{0} & 0.00\times10^{0} & 1.00\times10^{0} & 0.00\times10^{0} & 0.00\times10^{0} & 0.00\times10^{0} & 0.00\times10^{0} \\
0.00\times10^{0} & 0.00\times10^{0} & 1.00\times10^{0} & 0.00\times10^{0} & 0.00\times10^{0} & 0.00\times10^{0} & 0.00\times10^{0} & -3.82\times10^{1} & 0.00\times10^{0} & 0.00\times10^{0}
\end{bmatrix}$$

Input Matrix **B**:

$$\begin{bmatrix}
-1.63\times10^{-3} & -5.84\times10^{-2} & 2.80\times10^{-3} & 2.80\times10^{-3} \\
0.00\times10^{0} & 2.31\times10^{0} & -1.70\times10^{-1} & 1.70\times10^{-1} \\
-1.44\times10^{0} & -1.48\times10^{-6} & -9.85\times10^{-1} & -9.85\times10^{-1} \\
0.00\times10^{0} & 4.26\times10^{-2} & 2.08\times10^{-1} & -2.08\times10^{-1} \\
1.39\times10^{-2} & 4.89\times10^{0} & -2.38\times10^{0} & -2.38\times10^{0} \\
0.00\times10^{0} & -5.86\times10^{-2} & -3.37\times10^{-4} & 3.37\times10^{-4} \\
0.00\times10^{0} & 0.00\times10^{0} & 0.00\times10^{0} & 0.00\times10^{0} \\
0.00\times10^{0} & 0.00\times10^{0} & 0.00\times10^{0} & 0.00\times10^{0} \\
0.00\times10^{0} & 0.00\times10^{0} & 0.00\times10^{0} & 0.00\times10^{0} \\
0.00\times10^{0} & 0.00\times10^{0} & 0.00\times10^{0} & 0.00\times10^{0}
\end{bmatrix}$$

A.2 Non-linear Super Tanker Model

The Super Tanker model discussed in Chapter 7 [Berlekom and Goddard (1972), Fossen (1994)] is represented by the following state space equation

$$\dot{\mathbf{x}} = \mathbf{f}(\mathbf{x},\mathbf{u}) \tag{A.2}$$

where the state ($\mathbf{x}$) and input ($\mathbf{u}$) vectors are defined in the chapter. The non-linear vector function $\mathbf{f}$ is comprised from the rigid body and kinematic equations for such a vessel i.e. (note: values for the non-dimensional coefficients used here can be obtained from Berlekom and Goddard (1972) and Fossen (1993))

$$\dot{u} = \frac{1}{(L(m_{11} - X_{\dot{u}\zeta}\zeta))}(X_{uu}u^2 + Ld_{11}vr + X_{vv}v^2 + X_{c|c|\delta r\delta r}|c|c\delta r^2$$
$$+ X_{c|c|\beta\delta r}|c|c\beta\delta r + Lg_T(1-t) + X_{uu\zeta}u^2\zeta + LX_{vr\zeta}vr\zeta + X_{vv\zeta\zeta}v^2\zeta^2)$$

$$\dot{v} = \frac{1}{(L(m_{22} - Y_{\dot{v}\zeta}\zeta))}(Y_{uv}uv + Y_{|v|v}|v|v + Y_{|c|c\delta r}|c|c\delta r + Ld_{22}ur + Y_{c|c|\beta|\beta||\delta|}|c|c|\beta|\beta|\delta r|$$
$$+ Y_T g_T L + LY_{ur\zeta}ur\zeta + Y_{uv\zeta}uv\zeta + Y_{|v|v\zeta}|v|v\zeta + Y_{c|c|\beta|\beta||\delta r|\zeta}|c|c|\beta|\beta|\delta r|\zeta)$$

$$\dot{r} = \frac{1}{(L^2(m_{33} - N_{\dot{r}\zeta}\zeta))}(N_{uv}uv + LN_{|v|r}|v|r + N_{c|c|\delta r}|c|c\delta r + Ld_{33}ur + N_{c|c|\beta|\beta|\delta r}|c|c|\beta|\beta|\delta r|$$
$$+ LN_T g_T + LN_{ur\zeta}ur\zeta + N_{uv\zeta}uv\zeta + LN_{|v|r\zeta}|v|r\zeta + N_{c|c|\beta|\beta||\delta r|\zeta}|c|c|\beta|\beta|\delta r|\zeta)$$

$$\dot{\psi} = r$$

$$\dot{x}_p = u\cos(\psi) - v\sin(\psi)$$

$$\dot{y}_p = u\sin(\psi) + v\cos(\psi)$$

$$\dot{\delta r} = (\delta r_c - \delta r)/\Delta t$$

$$\dot{n} = (n_c - n)/\Delta t$$

where

$$\beta = v/u, \qquad g_T = (1/L)T_{uu}u2 + T_{un}un + LT_{nn}|n|\,n$$

$$c = \sqrt{(c_{un}un + c_{nn}n^2)}$$

A.3 Non-linear Supply Ship Model

The mathematical model of *CyberShip I* discussed in Chapter 8 [Fossen (1994)] is represented by the kinetic and kinematic equations. The kinetic equation defines the rigid body dynamics thus

$$\mathbf{M}\dot{\boldsymbol{\nu}} + \mathbf{C}(\boldsymbol{\nu})\boldsymbol{\nu} + \mathbf{D}\boldsymbol{\nu} = \boldsymbol{\tau} \tag{A.3}$$

where $\boldsymbol{\nu} = [u, v, r]^{\mathrm{T}}$, $\boldsymbol{\tau} = [\tau_1, \tau_2, \tau_3]^{\mathrm{T}}$,

$$\mathbf{M} = \begin{bmatrix} m_{11} & 0 & 0 \\ 0 & m_{22} & m_{23} \\ 0 & m_{32}(=m_{23}) & m_{33} \end{bmatrix} = \begin{bmatrix} m - X_{\dot{u}} & 0 & 0 \\ 0 & m - Y_{\dot{v}} & mx_G - Y_{\dot{r}} \\ 0 & mx_G - N_{\dot{v}} & I_z - N_{\dot{r}} \end{bmatrix} = \begin{bmatrix} 19.0 & 0 & 0 \\ 0 & 35.2 & 0 \\ 0 & 0 & 2.0 \end{bmatrix}$$

$$\mathbf{C}(\nu) = \begin{bmatrix} 0 & 0 & -m_{22}v - m_{23}r \\ 0 & 0 & m_{11}u \\ m_{22}v + m_{23}r & -m_{11}u & 0 \end{bmatrix} = \begin{bmatrix} 0 & 0 & -35.2v \\ 0 & 0 & 19.0u \\ 35.2v & -19.0u & 0 \end{bmatrix}$$

$$\mathbf{D} = \begin{bmatrix} -X_u & 0 & 0 \\ 0 & -Y_v & 0 \\ 0 & 0 & -N_r \end{bmatrix} = \begin{bmatrix} m_{11}/T_1 & 0 & 0 \\ 0 & m_{22}/T_2 & 0 \\ 0 & 0 & m_{33}/T_3 \end{bmatrix} = \begin{bmatrix} 6.3 & 0 & 0 \\ 0 & 7.0 & 0 \\ 0 & 0 & 2.0 \end{bmatrix}$$

given that the time constants for surge, sway and yaw are T_1 = 3.0s, T_2 = 5.0s and T_3 = 1.0s respectively.

The kinematics equation is

$$\dot{\boldsymbol{\eta}} = \mathbf{J}(\boldsymbol{\eta})\boldsymbol{\nu} \tag{A.4}$$

where $\boldsymbol{\nu} = [u, v, r]^{\mathrm{T}}$, $\boldsymbol{\eta} = [x_p, y_p, \psi]^{\mathrm{T}}$ and

$$\mathbf{J}(\eta) = \begin{bmatrix} \cos\psi & -\sin\psi & 0 \\ \sin\psi & \cos\psi & 0 \\ 0 & 0 & r \end{bmatrix}$$

Appendix B:

Additional Optimisation Responses for Submarine Application

B.1 SSA Optimised Responses

The SSA optimisation responses discussed in Section 6.4.5 are presented below.

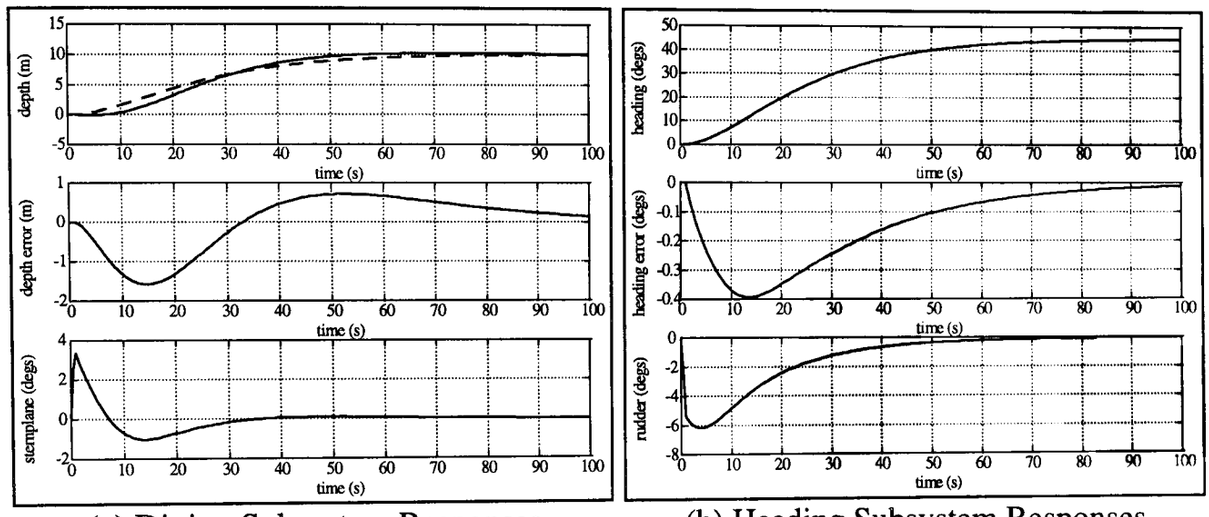

(a) Diving Subsystem Responses (b) Heading Subsystem Responses

Figure B.1: SSA Optimised Submarine Responses

B.2 GA Optimised Responses

The GA optimisation responses discussed in Section 6.4.6 are presented below.

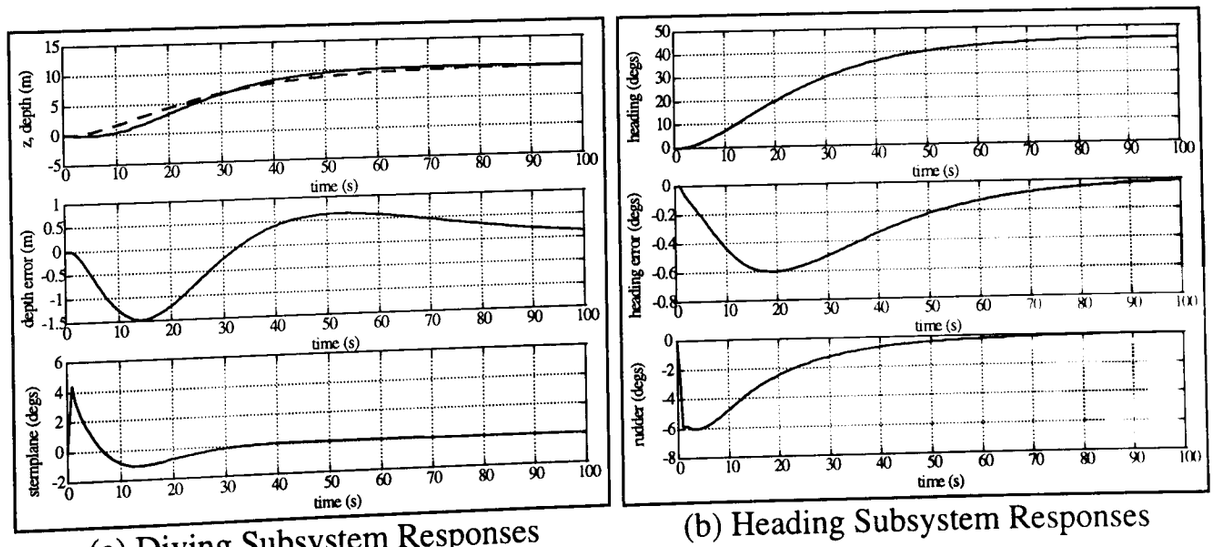

(a) Diving Subsystem Responses (b) Heading Subsystem Responses

Figure B.2: GA Optimised Submarine Responses

Appendix C:

Additional Optimisation Responses for Super Tanker Application

C.1 SSA Optimised Responses

The *Course Changing* responses discussed in Section 7.5.5.1 are presented below.

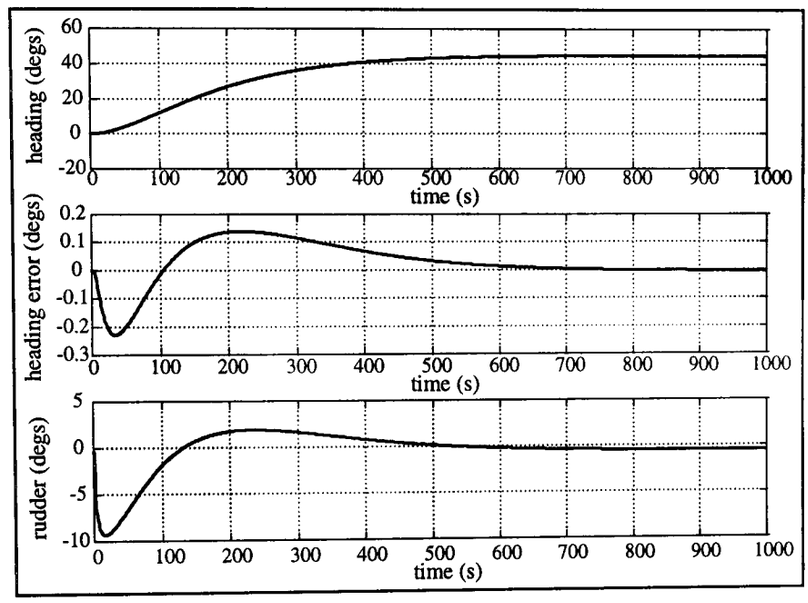

Figure C.1: SSA Optimised Tanker Course Changing Responses

The *Course Keeping* responses discussed in Section 7.5.5.2 are presented below.

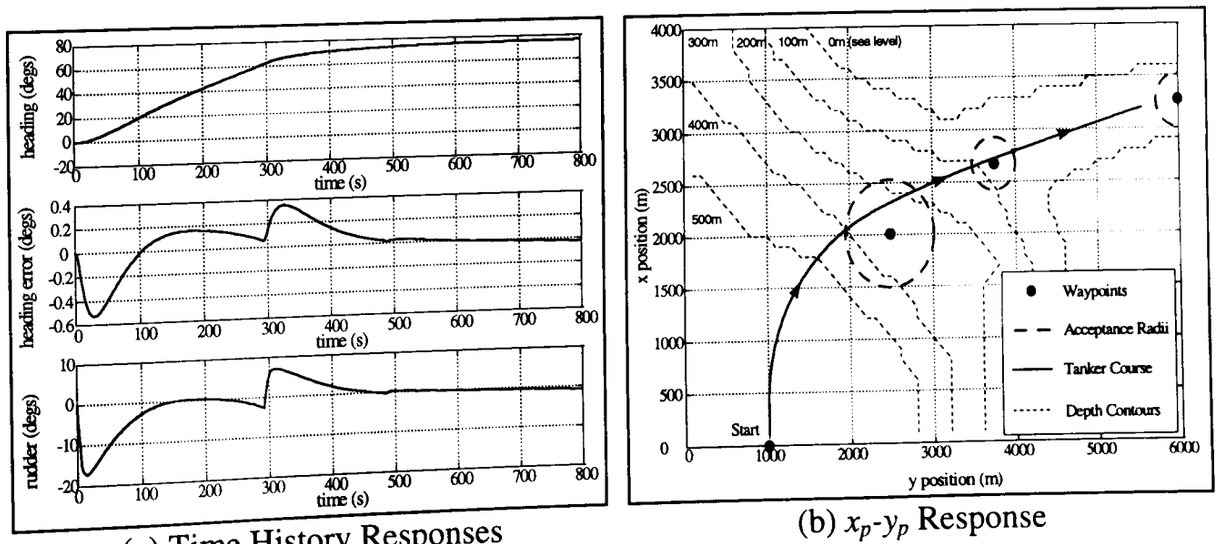

(a) Time History Responses (b) x_p-y_p Response

Figure C.2: SSA Optimised Tanker Course Keeping Responses

C.2 GA Optimised Responses

The *Course Changing* responses discussed in Section 7.5.6.1 are presented below.

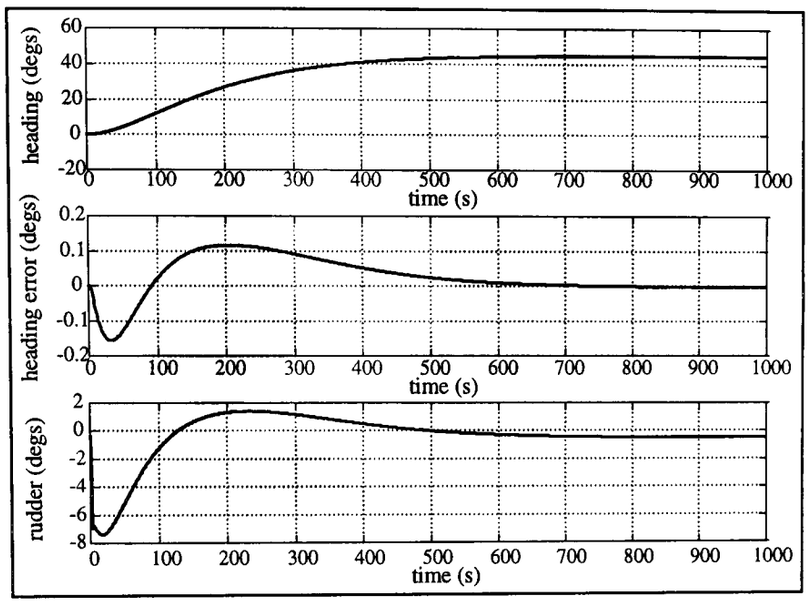

Figure C.3: GA Optimised Tanker Course Changing Responses

The *Course Keeping* responses discussed in Section 7.5.6.2 are presented below.

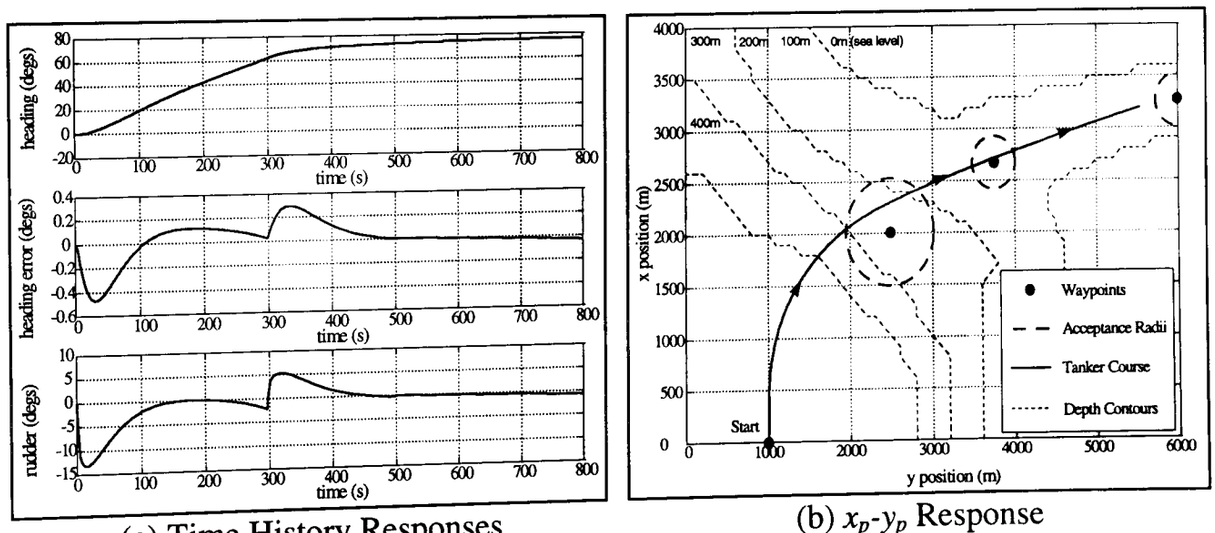

(a) Time History Responses (b) x_p-y_p Response

Figure C.4: GA Optimised Tanker Course Keeping Responses